



HAL
open science

Single synthetic cell microreactor for the fundamental understanding of NOS enzymatic activity and its implication in system biology

Louis Beauté

► **To cite this version:**

Louis Beauté. Single synthetic cell microreactor for the fundamental understanding of NOS enzymatic activity and its implication in system biology. Polymers. Université de Bordeaux, 2019. English. NNT : 2019BORD0069 . tel-02179366

HAL Id: tel-02179366

<https://theses.hal.science/tel-02179366>

Submitted on 10 Jul 2019

HAL is a multi-disciplinary open access archive for the deposit and dissemination of scientific research documents, whether they are published or not. The documents may come from teaching and research institutions in France or abroad, or from public or private research centers.

L'archive ouverte pluridisciplinaire **HAL**, est destinée au dépôt et à la diffusion de documents scientifiques de niveau recherche, publiés ou non, émanant des établissements d'enseignement et de recherche français ou étrangers, des laboratoires publics ou privés.

Thèse présentée
pour obtenir le grade de

DOCTEUR DE L'UNIVERSITÉ DE BORDEAUX

École Doctorale des Sciences Chimiques
Spécialité : Polymères

Par **Louis Beauté**

**Développement de cellule synthétique comme micro-réacteur pour l'étude
de l'activité enzymatique des NO-synthases et la compréhension de leur
fonctionnement en conditions physiologiques**

*Single synthetic cell microreactor for the fundamental understanding of NOS
enzymatic activity and its implication in system biology*

Directeurs de Thèse : Sébastien Lecommandoux, Nathan McClenaghan

Soutenue le 27/05/2019

Mme MARIE-BEGUE Emmanuelle
M. GUNNLAUGSSON Thorfinnur
Mme LI Min-Hui
Mme RAVAINÉ Valérie
M. MCCLENAGHAN Nathan
M. LECOMMANDOUX Sébastien

Chargée de Recherche, CNRS, ENS
Professeur, Trinity College Dublin
Directrice de Recherche, CNRS, Chimie Paris Tech
Professeur, Bordeaux INP
Directeur de Recherche, CNRS, ISM Bordeaux
Professeur, Bordeaux INP

Rapporteur
Rapporteur
Examinatrice
Examinatrice
Co-Directeur de thèse
Directeur de thèse

Président du Jury : Mme Valérie Ravaine

Remerciements

J'aimerais tout d'abord remercier l'Agence Nationale de Recherche qui a financé ces travaux de recherche et qui a rendu possible l'aboutissement de cette thèse.

Je voudrais ensuite remercier Sébastien Lecommandoux en tant que directeur du LCPO et Dario Bassani en tant que directeur du groupe NEO. Les conditions de travail au sein du LCPO et de l'ISM sont excellentes et c'est un réel plaisir de pouvoir travailler et évoluer dans ce laboratoire grâce aux moyens mis à notre disposition.

Je voudrais remercier toutes les personnes qui font en sorte que le LCPO fonctionne si bien : Catherine Roulinat, Dominique Richard, Séverine Saint Drenant, Corinne Goncalves, Claude Le Pierres, Rémi Cédric et Loïc Petrault. Merci pour toute l'aide que vous m'avez apporté durant ces 4 années au laboratoire et pour votre gentillesse. Merci Dominique pour la petite attention ramenée de Nouvelles Calédonie ! Je remercie également Pascale Godard et Clotilde Davies de s'occuper si bien du laboratoire et de son fonctionnement à l'ISM.

Je voudrais remercier ensuite Nathan McClenaghan et Sébastien Lecommandoux mes deux directeurs de thèse qui m'ont fait confiance pour me confier ce projet ambitieux et qui m'ont prodigué de nombreux conseils et montré les directions à prendre tout au long de ma thèse. J'ai beaucoup aimé chacune de nos réunions qui se déroulaient dans une ambiance très conviviale et agréable. Je ressortais de ces réunions avec encore plus de motivation qu'à l'arrivée. Merci de m'avoir encouragé quand les expériences fonctionnaient et de m'avoir reboosté quand elles marchaient moins bien. Grâce à vous j'ai également eu la chance de pouvoir présenter mes résultats dans de nombreux congrès. J'ai vraiment apprécié le voyage à la nouvelle Orléans dans le cadre du congrès des ACS en votre compagnie.

Merci Sébastien de m'avoir accepté en stage de fin d'étude et de m'avoir fait suffisamment confiance pour me proposer ensuite une thèse dans ton équipe. Tu t'es toujours rendu disponible si nécessaire, fait en sorte que j'aie dans la bonne direction et que je rencontre les bonnes personnes pour avancer. Merci pour les conseils pour le Mexique et le guide du routard !!

Merci Nathan de m'avoir accueilli dans le groupe NEO, et d'avoir fait toujours en sorte que je m'y sente le bienvenu, que j'ai une paillasse et un bureau de libre si besoin !! Merci pour ton temps et tous les cafés pris ensemble !

Merci à Mykhaylo Potopnyk, qui pendant les premiers mois de ma thèse m'a tout montré et guidé ! Merci à Arnaud Tron qui a pris de son temps pour m'aider à mesurer les quantum yield, une technique pas du tout évidente à maîtriser !! Merci à Ruben Rust d'avoir été un super stagiaire.

Je voudrais également remercier tous les permanents de l'équipe 3 du LPCO, Élisabeth, Jeff Christophe, Olivier, Bertrand et plus récemment Angela et Colin. Tous étant toujours très disponibles pour m'aider et partager leurs savoirs. Les discussions avec chacun d'entre eux m'ont beaucoup enrichies (entre autre le virus de la grippe qui produit du venin de cobra, la polymérisation ou comment ranger sa paillasse) et leurs conseils prodigués m'ont permis d'avancer de manière efficace dans mon projet de thèse.

Merci à tous les experts du LCPO Amélie Vax, Sylvain Bourasseau, Anne Laure Wirotus, Manu Ibarboure qui m'ont apporté leur savoir-faire et leur aide pour bien maîtriser les appareils et analyser les résultats. Manu merci pour toute ton aide et merci d'avoir montré à Ariane qui était le patron du confocal !

Merci à Ariane Boudier pour la collaboration dans le cadre des sondes à NO, les astuces et les protocoles qui m'ont beaucoup servi à manier le NO qui est une molécule capricieuse !!

Merci également à Jérôme Santolini d'avoir répondu à mes interrogations sur le NO, la NO synthase et de m'avoir montré la technique de l'hémoglobine !!

Merci à Stéphane Arbault, Pauline Lefrançois, Manu Suratini, et Jeremy. La collaboration avec le NSysa a toujours été vraiment intéressante. J'ai beaucoup aimé votre manière de travailler : pointue précise et efficace ! La dernière semaine de manipulations a été très intense et enrichissante ! Merci d'avoir pris de votre temps et de m'en avoir un peu plus appris sur l'électrochimie.

Merci à Jean Michel Guigner pour les superbes images de Cryo TEM obtenues sur les polymersomes !!

Amélie merci d'avoir été un tel soutien, d'avoir été aussi présente durant toute ma thèse. Merci d'avoir si souvent réussi à me faire penser à autre chose qu'à la thèse. Merci d'avoir partagé les bons et les moins bons moments, merci de me tirer toujours plus vers le haut.

Je voudrais ensuite remercier mes parents qui m'ont toujours poussé à donner le meilleur de moi-même et à me soutenir pour pouvoir faire ce qui me plaît ! Merci à mes frères, mes sœurs, Nounouk et Chillou, et toute ma famille pour leur soutien depuis toujours. Merci à ceux qui ont pu venir à Bordeaux et qui ont quand même écouté 3x45 min de la même présentation en 3 jours, merci d'avoir fait le déplacement !!

Merci également à toute la tribu Legoupil qui m'ont si bien accueilli chez eux ! Merci pour leur soutien, leur intérêt, et de s'être réjouis pour ma réussite autant que ma famille !

Merci les doudous d'avoir été des amis en OR !! Merci pour toutes les soirées, les sorties, les travaux, les délicieux repas, et les jeux de société !!

Aribooo, Gaugau le plus beau, la team Glagla merci à vous deux d'avoir été deux génialissimes collègues de bureau et amis qui m'ont fait passer 3 super années ! Merci pour votre soutien, votre aide, toutes les discussions aux pauses café, les marches digestives, le voyage à Berlin, la rué des fada, le nunchaku, et j'en passe ! Vous êtes de belles rencontres.

Merci à Quentin Zob zob de m'avoir donné les 50 couronnes, d'avoir toujours un jeu de mot pourri pour me faire rire, le 7 wonders duel, et pour toutes les boulangeries 24/24 que l'on a écumé !

Merci à tout le bureau N2-29 d'avoir été des super collègues et amis en particulier pendant la partie la moins fun de la thèse : la rédaction ! Vous allez me manquer !!!! Merci à Rima pour à la fois ton aide scientifique, et pour toutes nos discussions (de vieux et de moins vieux en passant par le pschitt à chien ou comment avoir un bon taux). Merci à Timtim et Martin pour toutes les anecdotes sur le tableau, de ne pas oublier les pauses café de 10h du midi et de 16h et de rendre ces pauses si agréables ! Merci à Clouclou Coco Coralie à la fois d'être une super collègue de bureau, j'aime beaucoup nos discussions et aussi d'être une doctorante aussi pro ! Grâce à toi les dernières manips ont super bien marché merci d'avoir pris autant de ton temps !! Merci Michmich d'avoir autant la patate et d'être aussi improbable !!! Juju the best merci à toi

d'avoir été le papa du bureau, si tu as encore besoin d'un coup de main pour un déménagement n'hésite pas ☺ !

Thank you Hang for our very interesting discussion about synthetic cells, for your time for the last minute experiments and to made me laugh so much with the invisible window during the gala dinner. We still have to break Tim! Thank you Tingting, Ye Machine, Vusala and Vangelis you are awesome coworkers I really enjoyed being in the same office!!!

Merci à toute l'équipe 3 Manon, Florian, Esra, Monica, Pedro, Chloé, Guillaume, Sophie, Laura, Gaëlle pour la super ambiance qu'il y a au sein de l'équipe c'est un plaisir de travailler tous ensemble !! Merci à Estelle Cardoso d'avoir été une super stagiaire !!

Merci au N1, N0 et B8 également pour l'ambiance au labo et à l'extérieur du labo : Lélé (coude coude) Arthur, Bakka (avec l'aloevera) Hélène, Martin C, Thomas, Guillaume C, David, QP, Lucie Cédric, PL, Alex, Geoffrey, Léa, Romain, Christopher Fiona, Jérémy, Nicolas, Camille, Antoine !

Merci à Titou !

Merci aussi à toutes les personnes qui m'ont aidé et que je n'ai pas citées !!!

1. Introduction	3
1.1. Project presentation	3
1.1.1. Nitric Oxide function in living organisms.....	3
1.1.2. NO synthase and its partially known mechanism.....	3
1.1.3. Microreactor	4
1.2. Light-activated delivery system	7
1.2.1. Molecular mechanisms of light-activated delivery system	8
1.2.1.1. Physical effects	8
1.2.1.1.1. General mechanism for conversion of light energy to heat	8
1.2.1.1.2. Design of nanoheaters for efficient light to heat energy transformation	9
1.2.1.1.3. Converting radiation: upconverting nanoparticles	11
1.2.1.2. Chemical effects	13
1.2.1.2.1. Photoinduced chemical cleavage.....	13
1.2.1.2.2. Isomerization and rearrangements	18
1.2.2. Release mechanisms	21
1.2.2.1. Light-induced structural changes inducing species carrier destabilization	21
1.2.2.1.1. Self-assembled nanoparticles	22
1.2.2.1.2. Giant polymersomes.....	26
1.2.2.1.3. Gels	27
1.2.2.2. Light-induced increase of diffusion speed (Heat generation / permeability modification)	30
1.2.2.2.1. Polymer / Gel shrinkage (solubility change)	30
1.2.2.2.2. Glass transition and melting induced release.....	33
1.2.3. Pore blocking / unblocking.....	35
1.3. Conclusion	39
2. Light-sensitive Nano-polymersomes	51
2.1. Introduction	51
2.2. Coumarin synthesis (a light-sensitive cleavable molecular synthon)	52
2.2.1. Light-sensitive amphiphilic block copolymer design.....	52
2.2.2. Synthesis.....	53
2.3. Polymer synthesis and chain-end modifications.....	56
2.3.1. TMC polymerization to obtain well-defined PTMC.....	56
2.3.1.1. Introduction to Ring Opening Polymerization	56
2.3.1.2. Initiator synthesis	56
2.3.1.3. Polymerization mechanism	57
2.3.1.4. Polymerization Kinetic and DP measurement	58
2.3.1.5. Unwanted diblock: possible mechanism of formation.....	60
2.3.1.5.1. Side reactions.....	61
2.3.1.5.2. O ₂ coupling.....	62
2.3.1.5.3. Post-functionalization.....	62
2.3.1.5.4. Reactant purity	63
2.3.1.6. PTMC end chain analysis, alcohol benzylic PTMC formation and IR spectra comparison	65
2.3.1. PEG ₄₅ -OH end chain modification	67
2.3.1.1. Tosylation	67
2.3.1.2. Azide formation	68
2.3.1.3. Amination	68

2.4. Polymer grafting on the light-sensitive coumarin linker	68
2.4.1. Amidation reaction.....	68
2.4.2. Copper-catalyzed Huisgen ("click") 1,3-cycloaddition.....	70
2.5. Self-assembly characterization	71
2.5.1. Study on PEG- <i>b</i> -PTMC Copolymer.....	71
2.5.1.1. Synthesis.....	71
2.5.1.2. Nanoprecipitation.....	72
2.5.1.3. Syringe pump to control particle sizes.....	74
2.5.1.4. Determination of the appropriate hydrophilic ratio to obtain polymersomes	74
2.5.1.5. TEM.....	76
2.5.1.6. Cryo-TEM	76
2.5.2. Self-assembly characterization of light-sensitive PEG ₄₅ -coumarin- <i>b</i> -PTMC ₈₁	78
2.5.2.1. Dynamic light scattering at 90°	78
2.5.2.2. Multi-angle light scattering (static and dynamic)	79
2.5.2.3. TEM.....	80
2.5.2.4. Cryo-TEM	80
2.6. Irradiation effects.....	81
2.6.1. Introduction.....	81
2.6.2. Irradiation effect at the molecular level.....	82
2.6.3. Effect of irradiation at the macromolecular level	83
2.6.4. Effect of the irradiation on the particles morphology.....	86
2.6.4.1. Multi-angle light scattering	86
2.6.4.2. Dynamic light scattering analysis at 90°	88
2.7. Conclusion.....	89
2.8. 2nd generation design of the light sensitive copolymer.....	90
2.8.1. New copolymer Strategy	90
2.8.2. Synthesis.....	93
2.8.2.1. Light-sensitive linker.....	93
2.8.2.2. PEG ₄₃ end chain modifications	94
2.8.2.3. PEG grafting on coumarin via amide bond formation	97
2.8.2.3.1. Test Reaction	97
2.8.2.3.2. PEG ₄₃ -HMDI grafting reaction on Coumarin	98
2.8.2.4. Copper-catalyzed Huisgen ("click") 1,3-cycloaddition	100
2.8.3. Self-assembly.....	101
2.8.4. Self-assembly characterization.....	104
2.8.4.1. Visual	104
2.8.4.2. Multi-angle light scattering	104
2.8.4.3. Cryo-TEM	105
2.8.5. Irradiation effects.....	106
2.8.5.1. Irradiation effect at the molecular level.....	106
2.8.5.2. Effect of Irradiation at the macromolecular level	107
2.8.6. Irradiation Effect on the particle stability	108
2.8.6.1. Light scattering analysis.....	108
2.8.6.1.1. Comparison between 1 st and 2 nd generation of copolymer.....	108
2.8.6.1.2. Buffer effect.....	109
2.8.6.2. Multi-angle light scattering (static and dynamic)	110
2.8.6.3. Cryo-TEM	111

2.9. Conclusion	112
3. GUV rupture through light-driven osmotic pressure increase	121
3.1. Introduction	121
3.2. Coumarin cleavable molecule	122
3.2.1. Synthesis.....	122
3.2.2. Irradiation study.....	124
3.2.2.1. Cleavage Mechanisms	124
3.2.2.2. Absorption and Fluorescence	125
3.2.2.3. Monitoring cleavage via NMR	126
3.2.2.4. Quantum yield	127
3.2.2.5. pH control.....	128
3.3. N-alkyl-4-picolinium	129
3.3.1. Introduction.....	129
3.3.2. Synthesis.....	130
3.3.2.1. Design	130
3.3.2.2. 1 st generation.....	130
3.3.2.3. Solubility properties	131
3.3.3. Irradiation study	132
3.3.3.1. Mechanisms.....	132
3.3.3.2. Quantum yield	133
3.4. Encapsulation in polymersome	134
3.4.1. Thioxanthone encapsulation method	135
3.4.2. Coumarin encapsulation method.....	136
3.5. Conclusion	138
4. Nitric Oxide detection.....	145
4.1. Introduction	145
4.2. NO production.....	145
4.2.1. NO quantification based on hemoglobin absorption	146
4.2.1.1. Principle of hemoglobin quantification	146
4.2.1.2. Hemoglobin preparation	146
4.2.1.3. Quantification method	147
4.2.2. S-Nitrosoglutathione	149
4.2.2.1. Synthesis of GSNO	149
4.2.2.2. Quantification of GSNO produced	149
4.2.2.3. NO Release from GSNO	150
4.2.3. NO production from NaNO ₂ and sulfuric acid	152
4.2.4. Nitric oxide from gas bottle.....	152
4.3. Nitric oxide fluorescent probes.....	153
4.3.1. Introduction on nitric oxide fluorescent probes	153
4.3.2. Synthesis of the hydrophilic and hydrophobic nitric oxide fluorescent probes	154
4.3.2.1. Hydrophobic probe synthesis	154
4.3.2.1.1. Naphthalene building block synthesis	154
4.3.2.1.2. Hydrophobic probe synthesis	155
4.3.2.2. Hydrophilic probe synthesis	156
4.3.2.2.1. Carboxylic acid protecting group	156

4.3.2.2.2. Carboxylic acid deprotection	157
4.3.3. Fluorescence properties of the nitric oxide probes	158
4.3.3.1. NO probe solution preparation method.....	158
4.3.3.2. Calibration of the NO probe with GSNO as a NO source	158
4.3.3.3. Calibration of the NO probe with NO from gas bottle as the NO source	159
4.3.4. Conclusion	160
4.4. Control of the NO production in situ via a molecular tool	161
4.4.1. Feedback strategy presentation.....	161
4.4.2. BAPTA-NOp and BAPTA-AZO synthesis	164
4.4.3. Calcium constant Measurement of BAPTA-NOp and BAPTA-AZO	167
4.4.4. Fluorescent properties	169
4.4.5. Conclusion	169
4.5. Conclusion	170
5. Investigation of species release in microreactors	177
5.1. Introduction	177
5.2. Controlled species release in space and time inside a microreactor	177
5.2.1. Controlled destabilization of nanopolymersomes inside a microreactor	177
5.2.1.1. Photosensitive polymersome encapsulation in a microreactor	177
5.2.1.2. Temporal control of nanopolymeromes destabilization in a microreactor.....	178
5.2.1.3. Spatial control of nanopolymerome destabilization in a microreactor.....	180
5.2.2. Species release inside the microreactor.....	181
5.2.2.1. Strategy	181
5.2.2.2. Fluorescein encapsulation method	182
5.2.2.3. Measurement of the amount of loaded fluorescein	182
5.2.2.4. Release inside a pseudo-microreactor	184
5.3. Enzyme activity inside a microreactor	185
5.3.1. Study of the horseradish peroxidase enzymatic reaction.	185
5.3.1.1. Calibration of the fluorescence under confocal microscopy	185
5.3.1.2. Encapsulation with emulsion centrifugation technique	186
5.4. Conclusion	188
6. General conclusion	193
7. Experimental Part	203

Résumé

Résumé

L'oxyde nitrique (NO) est un important messenger chimique dans l'organisme vivant. Le NO est impliqué dans un large éventail de mécanismes de défense immunitaire et de signalisation biologiques telles que la communication neuronale, l'activité antitumorale, la régulation de la tension artérielle et la défense immunitaire non spécifique. De plus, plusieurs études suggèrent que le NO pourrait jouer un rôle clé dans l'apparition et la propagation d'un large éventail de maladies telles que les maladies neurodégénératives, les maladies cardiovasculaires, le diabète et le cancer. Il est donc crucial de mieux comprendre les mécanismes impliqués dans la production de NO, et ainsi développer des pistes pour l'élaboration de nouveaux médicaments et traiter les maladies précédemment citées. Le NO est produit par la NO synthase, une enzyme pouvant avoir des fonctions biologiques opposées. Son fonctionnement n'est pas encore bien compris malgré les nombreuses études sur la NO synthase. L'utilisation de microréacteurs pour encapsuler et étudier l'enzyme permettrait d'obtenir un environnement confiné et contrôlé mimant celui de la cellule. Cependant, dans la plupart des microréacteurs qui ont été développés dans la littérature, les réactions biochimiques sont induites simplement par le mélange des différents composants ou dépendent des propriétés de diffusion à travers les membranes des microréacteurs. L'étude de la cinétique de ces réactions complexes est donc très difficile, voire impossible.

Dans ce contexte, trois enjeux majeurs ont été abordés dans cette thèse : le contrôle de la libération et de la concentration des espèces réactives à l'intérieur du microréacteur, la mesure de la réponse enzymatique par la détection du NO et la libération contrôlée dans l'espace et dans le temps d'espèces au sein des microréacteurs.

Pour résumer, nous avons décidé de développer un microréacteur compartimenté et sensible à la lumière pour étudier le comportement complexe du NOS (Figure 90).

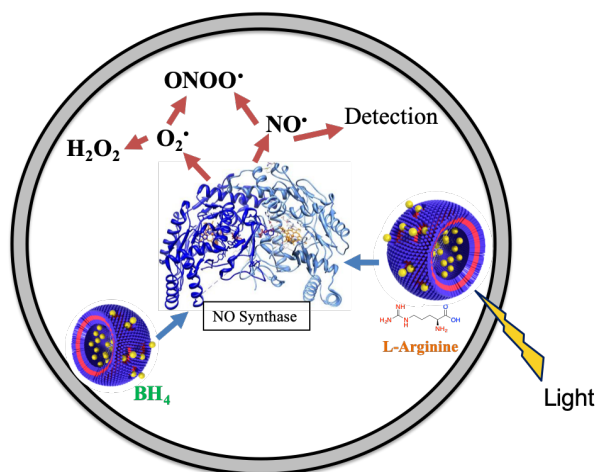


Figure 1: Représentation schématique de la cellule synthétique pour étudier l'activité de la NO synthase, basée sur l'encapsulation de nanopolymersomes photosensibles. La modulation des substrats enzymatiques et des cofacteurs (L-Arg, BH4) peut être contrôlée par photoactivation.

Le contrôle de la libération des espèces a été effectué par l'intermédiaire de nanopolymersomes photosensibles. Dans un premier temps, plusieurs PEG₄₅-*b*-PTMC avec différentes longueurs de poly(triméthylène carbonate) PTMC ont été synthétisés afin de trouver le rapport hydrophile/hydrophobe permettant de former des polymersomes stables. Le PEG₄₅-*b*-PTMC₈₁, avec un rapport hydrophile/hydrophobe de 19%, s'auto-assemble en polymersomes avec une polydispersité faible. Dans un second temps, une 1^{ère} génération d'un copolymère photosensible a été synthétisé : le PEG₄₃-coumarine-*b*-PTMC₈₁ dont la photosensibilité est basé sur une molécule de liaison : la coumarine photoclivable (Figure 9).

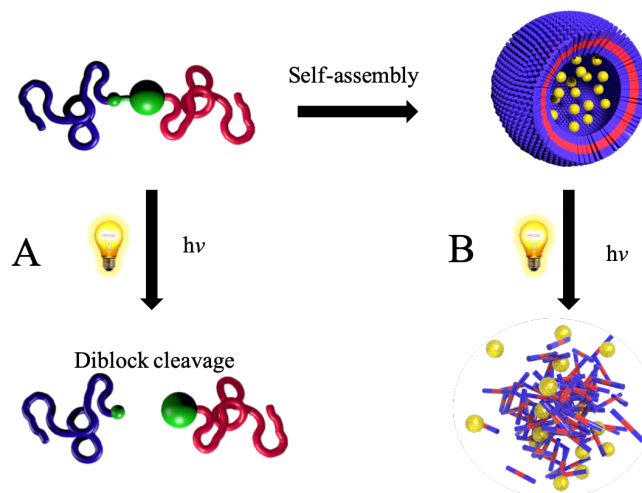


Figure 2: Stratégie utilisée pour contrôler la libération des réactifs dans le temps et dans l'espace par l'intermédiaire de polymersomes photosensibles (B), à l'aide des copolymères photodégradables (A).

La coumarine photosensible a d'abord été synthétisée avec un groupe acide carboxylique et un groupe alcyne aux deux extrémités, afin de pouvoir greffer un polymère hydrophile et un polymère hydrophobe. L'extrémité de la chaîne d'un PEG₄₃ a été modifiée en une amine afin de pouvoir le lier à l'acide carboxylique de la coumarine. Le bloc hydrophobe a été par la suite synthétisé. Le triméthylène carbonate (TMC) a été polymérisé pour former du PTMC avec une extrémité de chaîne azotée. Le paramètre clé pour obtenir une faible dispersité (1,05) était une purification poussée de l'initiateur 3-azido-1-propanol. PEG₄₃-NH₂ et PTMC₈₁-N₃ ont été greffés successivement sur la molécule de liaison coumarine pour donner le copolymère amphiphile photosensible de 1^{ère} génération PEG₄₅-coumarine-*b*-PTMC₈₁. Le copolymère a été obtenu avec une dispersité faible de 1,05.

Les mesures de diffusion de la lumière ont montré que le copolymère pouvait s'auto-assembler en particules bien définies avec un rayon hydrodynamique de 150 nm et une polydispersité faible (PDI \approx 0.1). La cryo TEM a montré que ces particules étaient des polymersomes.

Les polymersomes ont ensuite été irradiés sous UV (365 nm) n'entraînant pas de modification de leur morphologie ou de leur taille. La mesure de la diffusion de la lumière a montré que les particules étaient partiellement déstabilisées ou perdaient partiellement leur masse après irradiation (30% de perte de signal après 2,5 heures d'irradiation).

Cependant, la plupart des nanoparticules (70 %) n'ont pas été déstabilisées par l'irradiation. La stabilité des polymersomes pourrait s'expliquer par la dimérisation de la coumarine, elle-même favorisée par l'auto-assemblage empêchant la libération du PEG. Afin d'améliorer l'efficacité de déstabilisation des nanoparticules, un nouveau copolymère a été synthétisée et analysée.

La première génération de particules photosensibles n'était pas complètement déstabilisée et il a été supposé que la dimérisation, empêchant la libération du PEG, améliorerait la stabilité des particules. Afin de favoriser la libération du PEG, la conception du copolymère a été modifiée de deux façons différentes. L'efficacité du clivage a été améliorée en changeant le groupe partant. Le rendement quantique obtenu par irradiation à 365 nm (0,012) était supérieur à celui de la 1^{ère} génération (0,0034). Le PEG est libéré plus efficacement avant de dimériser. La deuxième modification était la position des polymères sur la coumarine. En effet, avec le deuxième copolymère, seul le PEG est libéré au lieu du PEG-coumarine induisant une libération plus efficace du PEG.

Afin de synthétiser la 2^{ème} génération de PEG₄₃-coumarine-*b*-PTMC₈₁, la coumarine photosensible a été synthétisée avec un groupe hydroxyle et un groupe alcyne aux deux extrémités, afin de pouvoir greffer un polymère hydrophile et un polymère hydrophobe. L'extrémité de la chaîne PEG₄₃ a ensuite été modifiée en isocyanate afin de pouvoir le lier au

groupe hydroxyle de la coumarine. PEG₄₃-NCO et PTMC₈₁-N₃ ont été greffés successivement sur la molécule de liaison coumarine pour donner le copolymère amphiphile photosensible de 2^{ème} génération PEG₄₃-coumarine-*b*-PTMC₈₁ (Figure 3).

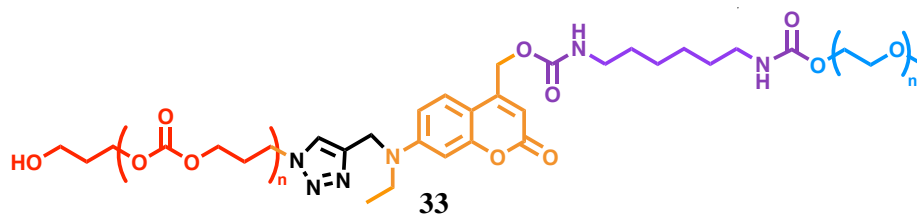


Figure 3 : Structure chimique du copolymère PEG₄₃-coumarine-*b*-PTMC₈₁ photosensible.

Le copolymère a été obtenu avec une dispersité faible de 1,04. Les mesures de diffusion de la lumière ont montré que le copolymère pouvait s'auto-assembler en particules bien définies avec un rayon hydrodynamique de 150 nm et une polydispersité faible (PDI \approx 0.1). Les observations par cryo-TEM ont montré des polymersomes et des agrégats de polymersomes. L'irradiation des polymersomes a induit un changement de leur morphologie. Après irradiation, le rapport Rg/Rh des particules restantes a diminué, ce qui suggère une densification des particules. La solution de polymersomes a été irradiée pendant 150 minutes et l'intensité de la lumière diffusée a diminué de 71%, suggérant une déstabilisation et une agrégation des particules. Les mesures de diffusion de la lumière ont été confirmées par cryo-TEM. Les images obtenues ont montré une majorité d'agrégats indéfinis après irradiation des polymersomes. Cette partie a présenté la synthèse d'un copolymère photosensible, son auto-assemblage en polymersomes, et la photosensibilité des particules formées par irradiation UV.

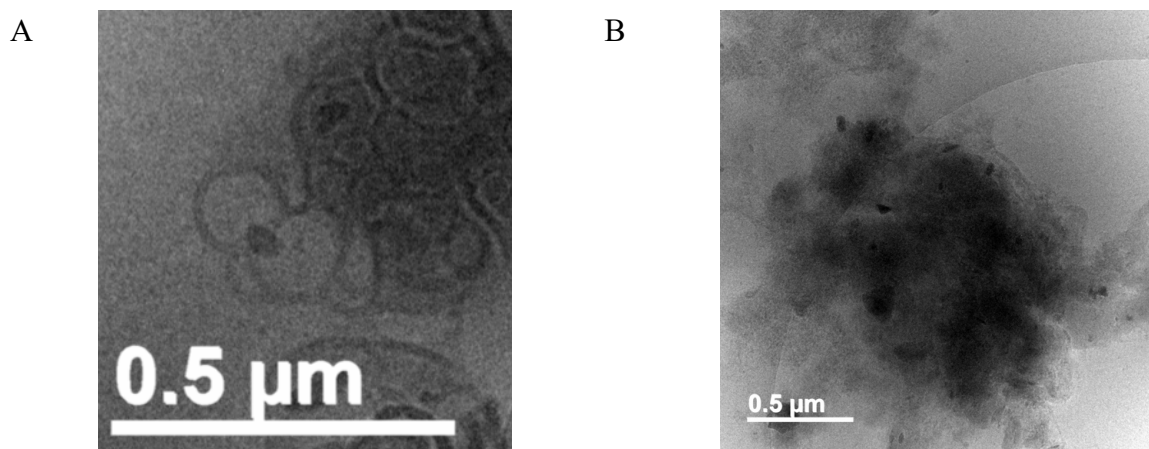


Figure 4 : Images cryo-TEM de polymersomes de PEG₄₃-coumarine-*b*-PTMC₈₁ A) avant et B) après irradiation

Une deuxième voie a été explorée pour contrôler la libération d'espèces par irradiation : le changement de pression osmotique dans les polymersomes induisant leur déstabilisation. L'augmentation rapide de la pression osmotique dans le milieu interne des polymersomes n'a pas pu être équilibré assez rapidement avec l'eau, ce qui a entraîné la rupture des polymersomes et la libération des espèces. L'augmentation de la pression osmotique a été contrôlée par des molécules clivables sensibles à la lumière.

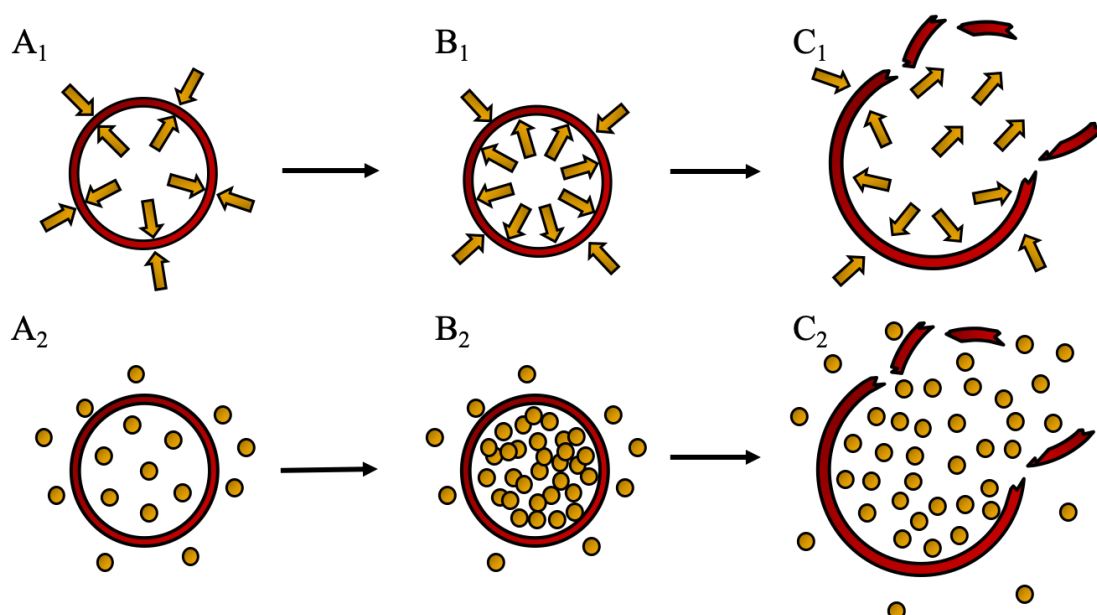


Figure 5: Stratégie utilisée pour induire l'éclatement des polymersomes. Les polymersomes sont stables lorsque la pression osmotique est la même dans le milieu interne et externe (A1). L'augmentation de pression osmotique (B1) a été utilisée pour induire la rupture du polymère (C1). Le contrôle de la concentration moléculaire permet de contrôler la pression osmotique. L'augmentation de la concentration des espèces présentes dans le polymersomes (A2, B2) entraîne une augmentation de la pression osmotique et une rupture des polymersomes (C2).

Deux molécules ayant deux mécanismes de clivage différents ont été étudiées : le clivage hétérolytique de la coumarine et le transfert d'électrons à médiation basée sur le N-alkyl-4-picolinium-thioxanthone (NAP-th).

Le NAP-th a été facilement synthétisé en 2 étapes, sa solubilité dans l'eau était le paramètre limitant et la concentration maximale de solubilité trouvée était de 1 mM. Plusieurs méthodes ont été testées pour augmenter sa solubilité dans l'eau, comme le changement du contre ion ou l'ajout d'un groupe hydrophile, mais sans permettre d'augmenter significativement la solubilité dans l'eau. Le rendement quantique mesuré en présence du médiateur triéthanolamine était de 0,16. Cette valeur a montré que le clivage était très efficace.

La coumarine modifiée a également été synthétisée avec succès en 6 étapes, deux groupes hydrophiles ont été ajoutés pour augmenter la solubilité de la molécule qui a pu être facilement mise en solution dans l'eau à des concentrations de l'ordre de 10 mM. Le rendement quantique mesuré était de 0,016 pour une illumination à 365 nm et de 0,029 pour 405 nm. Le clivage était moins efficace que le NAP-th, mais sa solubilité était meilleure. Une irradiation d'une heure à 365 nm a induit un clivage de la molécule de 87 %. Ce clivage a libéré une base : de la diéthylamine qui a pu être utilisée pour augmenter le pH de la solution. En effet, après seulement 10 minutes d'irradiation, le pH est passé de 4,5 à 6,5.

La deuxième étape a consisté à encapsuler les deux molécules à l'intérieur du polymersomes de PEO_{1,3}-b-PBut_{2,5} par la technique de émulsion-centrifugation. La coumarine modifiée a été encapsulée dans un polymersome avec une concentration de 10 mM et NAP-th a été encapsulé avec une concentration de 1 mM. L'irradiation à 405 nm sous microscope confocal a provoqué l'éclatement rapide des polymersomes contenant les deux molécules. Ces systèmes induisant une libération rapide et efficace pourraient être utilisés pour initier une réaction dans les microréacteurs et ainsi avoir un contrôle précis dans l'espace et le temps de systèmes cellulaires artificiels.

Afin de suivre la production de NO directement à l'intérieur du microréacteur, deux sondes à NO ont été étudiées. Ces sondes sont basées sur la formation d'une liaison azoïque induisant une fluorescence de la molécule, résultant en un signal stable et une sélectivité élevée par rapport aux autres composés nitro. Les deux sondes ont été conçues pour avoir des propriétés de solubilité différentes (l'une hydrophobe, l'autre hydrophile) afin de détecter le NO dans la membrane et dans le milieu aqueux interne du microréacteur. Les sondes ont été synthétisées en 5 et 6 étapes (Figure 80 A,B).

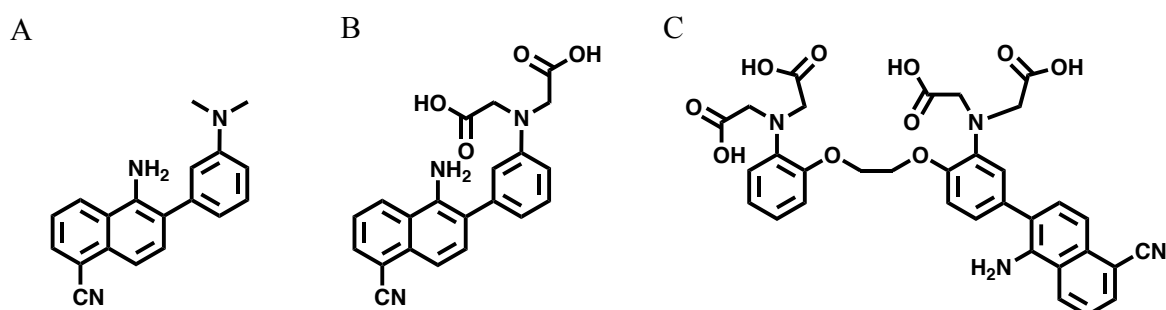


Figure 6: A) Sonde de NO fluorescente hydrophobe B) sonde fluorescente hydrophile de NO C) BAPTA-NOp

Des étapes critiques ont été rencontrées pour la protection et la déprotection de l'acide carboxylique de la sonde hydrophile. Le tert-butyle s'est avéré être un groupe protecteur efficace dans les conditions utilisées et le TES a permis d'éviter la dégradation de la sonde hydrophile pendant l'étape de déprotection. Afin de tester les propriétés des sondes, plusieurs sources de NO ont été testées comme le GSNO, le NO provenant NaNO₂ ou le NO gazeux provenant d'une bouteille. La concentration de NO obtenue a été mesurée grâce à l'absorption de l'hémoglobine. La libération de NO par le GSNO grâce à l'acide ascorbique et sa cinétique de libération a été étudiée. Cependant, l'acide ascorbique empêche la formation de la molécule fluorescente et le GSNO n'a pu être utilisé. Le NO de NaNO₂ a donné des solutions de faible concentration, c'est pourquoi a finalement été utilisée, la solution de NO provenant d'une bouteille de gaz. La détection du NO par les sondes a été testée. Les sondes ont montré une augmentation de l'intensité de fluorescence ($\lambda_{em\ max} = 530\ nm$, $\lambda_{ex\ max} = 440\ nm$ pour la sonde hydrophile, ($\lambda_{em\ max} = 530\ nm$, $\lambda_{ex\ max} = 440\ nm$ pour la sonde hydrophile) après addition de NO. L'intensité de fluorescence obtenue a une excellente corrélation linéaire ($R^2 = 0,99$) en fonction de la quantité de NO ajoutée permettant une mesure précise et quantitative de la concentration de NO (Figure 72). Les sondes sont actuellement testées in vitro au laboratoire CITHEFOR (Université de Lorraine EA 3452).

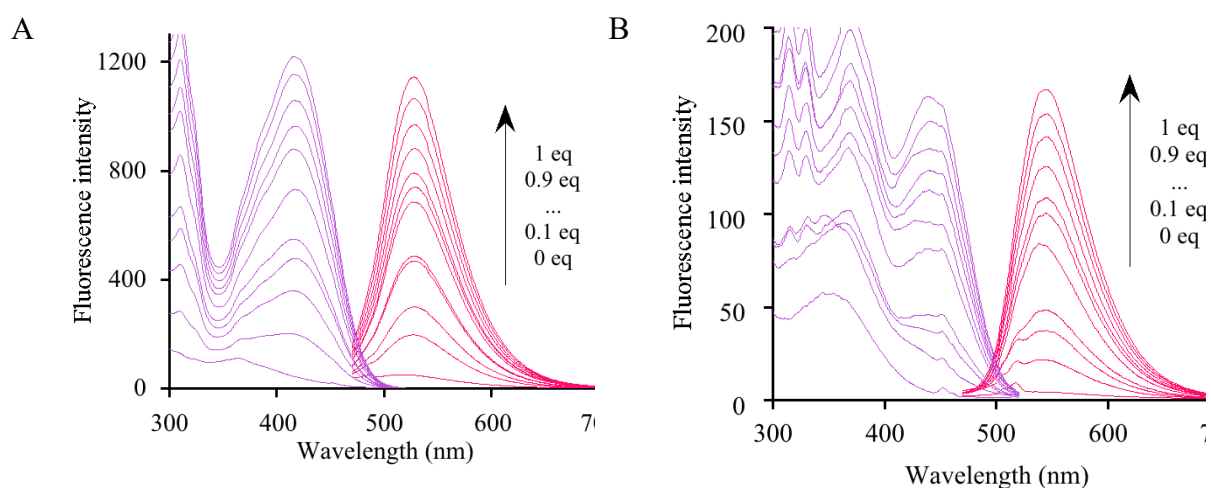


Figure 7: Spectre d'excitation (violet) et d'émission (rouge) de la sonde (A) hydrophile et (B) hydrophobe après addition d'une solution de NO. La sonde hydrophile a été solubilisée dans du tampon phosphate (50mM, pH 7.4) et la sonde hydrophobe a été solubilisée dans 80% tampon phosphate (50mM, pH 7.4) et 20% de DMSO. Les longueurs d'onde d'émission utilisées pour les spectres d'excitation étaient de 530 nm pour la sonde hydrophile et de 550 nm pour la sonde hydrophobe. La longueur d'onde d'excitation utilisée pour les spectres d'émission était de 416 nm pour la sonde hydrophile et de 440 nm pour la sonde hydrophobe.

Dans une deuxième partie, un autre outil moléculaire a été synthétisé afin d'étudier la NO synthase. L'introduction contrôlée de réactifs directement dans le microréacteur pourrait aider à suivre l'activité enzymatique et des informations sur le mécanisme de l'enzyme pourrait être obtenues. À cette fin, un outil moléculaire a été conçu pour contrôler avec précision le taux de production de NO par un processus de rétroaction. Nous avons émis l'hypothèse que la combinaison de la sonde BAPTA et de la sonde NO (BAPTA-NOp) pourrait induire une auto-activation de l'enzyme et pourrait contrôler la production d'oxyde nitrique. NO serait produit par l'enzyme et réagirait avec BAPTA-NOp pour donner BAPTA-AZO. En raison de la conjugaison plus élevée, le groupe cyano attracteur d'électrons attirerait les électrons de l'amine tertiaire du BAPTA, ce qui entraînerait une complexation plus faible du calcium et sa libération. Pour vérifier cette hypothèse, BAPTA-NOp et BAPTA-AZO ont été synthétisés en 10 étapes et leurs constantes de dissociation K_d ont été mesurées. Le K_d de BAPTA-NOp et de BAPTA-AZO étaient respectivement de $0,42 \mu\text{M}$ et $0,52 \mu\text{M}$. Les valeurs des K_d étaient en accord avec les valeurs des K_d des BAPTA. Cependant, le K_d de BAPTA-NOp et BAPTA-AZO sont relativement proches et le K_d de BAPTA-AZO est relativement faible, ce qui signifie que la forme AZO ne libère pas de calcium et que la molécule ne peut être utilisée pour le processus de rétroaction.

Finalement, afin d'assurer le contrôle de l'étape d'initiation et de déclencher une réaction enzymatique à un endroit et à un moment précis, la libération contrôlée de réactifs dans des microréacteurs a été étudiée. Les nanopolymersomes PEG₄₃-coumarine-*b*-PTMC₈₁ ont été encapsulés avec succès dans des microréacteurs composé d'émulsion d'eau stabilisés par des copolymères PEO_{1,3}-*b*-PBut_{2,5} et observés sous microscope confocal. L'irradiation à 405 nm a induit une déstabilisation efficace des nanopolymersomes à l'intérieur du microréacteur. Une irradiation de 2 min a induit une diminution de 83% du nombre de nanoparticules (Figure 80).

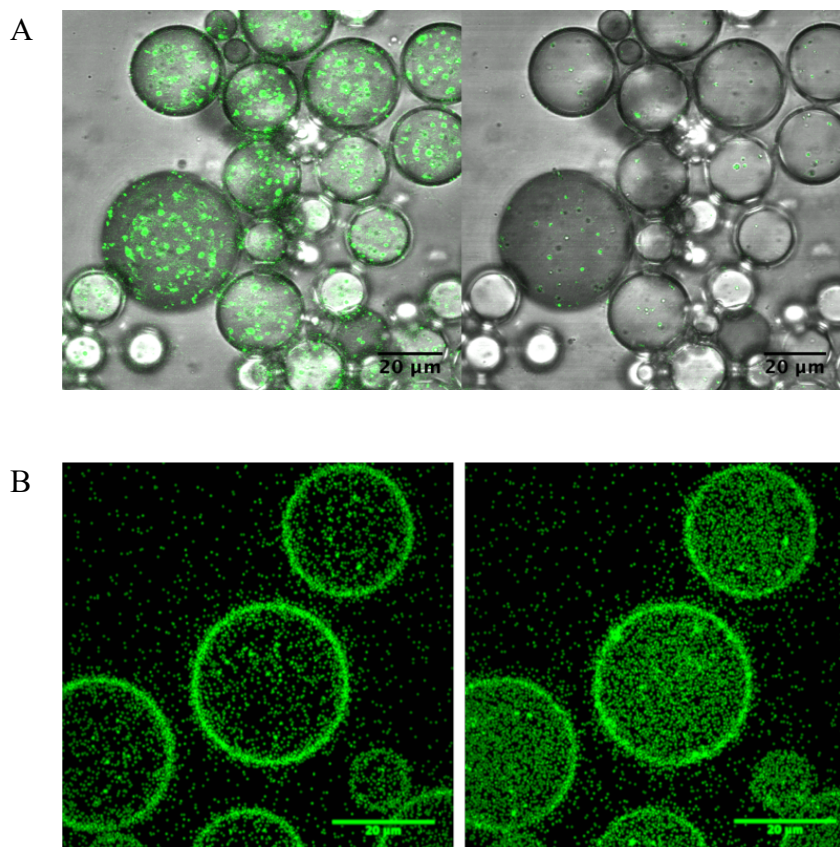


Figure 8: A) Observation en microscopie confocale d'une émulsion aqueuse stabilisée par $PEO_{1.3}\text{-}b\text{-}PBut_{2.5}$ contenant des nanopolymersomes $PEG_{43}\text{-coumarin-}b\text{-}PTMC_{81}$ photosensibles irradiés 2 min à 405 nm (80%, 50 mW) (canal vert, $\lambda_{ex} = 405$ nm, 50 mW, 3% observation dans la gamme d'émission de la coumarine, 485 nm). B) Observation confocale d'une émulsion aqueuse stabilisée par $PEO_{1.3}\text{-}b\text{-}PBut_{2.5}$ contenant des polymersomes $PEG_{43}\text{-coumarin-}b\text{-}PTMC_{81}$ avant et après une irradiation de 10 s à 405 nm (80%, 50 mW). La fluorescéine a été encapsulée dans les polymersomes (barre d'échelle 20 μm , canal vert $\lambda_{ex} = 488$ nm, 40 mW, 10%, observation dans la gamme d'émission de la fluorescéine, 520 nm).

Afin d'étudier la libération des nanopolymersomes $PEG_{43}\text{-coumarin-}b\text{-}PTMC_{81}$, de la fluorescéine a été encapsulé dans les nanopolymersomes (F-Nano). Afin de mesurer la quantité de fluorescéine encapsulée dans les nanopolymersomes, 80% en volume de DMSO a été ajouté à une solution de particules pour déstabiliser complètement les nanopolymersomes et libérer la fluorescéine. La concentration maximale théorique de fluorescéine que les nanopolymersomes pouvaient libérer était de 5,1 μM . Les F-Nano ont ensuite été encapsulés dans des gouttes d'émulsion stabilisées par du $PEO_{1.3}\text{-}b\text{-}PBut_{2.5}$ formant ainsi un microréacteur. Les microréacteurs obtenus ont été irradiés pendant 10 s, entraînant la libération de la fluorescéine des F-Nano dans le microréacteur.

La construction de microréacteurs capables d'imiter certaines fonctions cellulaires de base et de développer une cellule synthétique opérationnelle représente l'un des projets les plus difficiles de ce siècle. Il reste encore un long chemin à parcourir pour obtenir une cellule artificielle polyvalente permettant de reproduire certaines fonctions biologiques ou d'étudier le fonctionnement d'enzymes complexes. Cependant, les outils développés dans le cadre de ce travail de thèse visaient à aider à se rapprocher un peu plus d'une cellule artificielle fonctionnelle. La NO synthase est une enzyme complexe qui nécessite plusieurs substrats et des conditions particulières. Dans un premier temps, les outils développés ici pourraient être utilisés pour construire des microréacteurs contrôlables contenant des enzymes bien connues telles que HRP ou GOX grâce à la microfluidique.

Les éléments fondamentaux à la base de la vie sont bien connus, mais nous sommes loin de comprendre comment ces éléments interagissent, s'auto-organisent, et échangent des informations. Les questions fondamentales concernant l'apparition de la vie pourront ainsi être posées par les échecs et les succès de la construction d'une cellule artificielle.

List of abbreviations

λ_{em} : Emission wavelength
 λ_{ex} : Excitation wavelength
AcOH: Acetic acid
AR: Amplex[®] red
D: Dispersity
DBTL Dibutyltin dilaurate
DBU: 1,8-Diazabicyclo[5.4.0]undec-7-ene
DCC: Dicyclohexylcarbodiimide
DCM: Dichloromethane
DLS: Dynamic Light Scattering
DMAP: 4-Dimethylaminopyridine
DMF: N,N-Dimethylformamide
DMSO: Dimethyl Sulfoxide
DP: Degree of polymerization
E. coli: *Escherichia coli*
EDCI: 1-Ethyl-3-(3-diméthylaminopropyl)carbodiimide
EtOAc: Ethyl acetate
GOX: Glucose oxidase
HRP: Horseradish peroxidase
IR: Infra-Red
kD: kilo Dalton.
MeCN: Acetonitrile
MeOH: Methanol
NBS: N-bromosuccinimide
NMR: Nuclear Magnetic Resonance
NOS: NO synthase enzyme
ONB: *o*-Nitrobenzyl
PEG Polyethylene glycol
PEG: Poly(ethylene glycol)
PTMC: Poly(trimethylene carbonate)
RI: Refractive index
ROP: Ring Opening Polymerization
Rpm: Revolutions per minute
RT: Room temperature
SCE: Saturated Calomel Electrode
SEC: Size Exclusion Chromatography
TBAB: Tetra-n-butylammonium bromide
TBD: 1,5,7-Triazabicyclo-[4.4.0]dec-5-ene
TEM: Transmission Electron Microscopy
TES: Triethylsilane
TFA: Trifluoroacetic acid
THF: Tetrahydrofuran
TLC: Thin Layer Chromatography
TMC: Trimethylcarbonate
U/mL: Enzyme unit/mL
UV: Ultra-violet

Chapter 1: **State of the art**

1. Introduction

1.1. Project presentation

1.1.1. Nitric Oxide function in living organisms

Nitric oxide (NO) is a major chemical messenger in living organisms [1]. The Nobel prize was awarded to L. J Ignarro, R. I. Furchgott and F. Murad in 1998 due to their work on the major physiological importance of NO in mammals [2]. Due to its hydrophobic nature, NO can easily diffuse through cellular membrane and have antagonist effects. NO is involved in a wide range of positive effect in immune defense or signaling mechanisms such as neural communication, antitumor activity, blood pressure regulation and non-specific immune defense [3]. Negative effects involve large amount of NO that induce oxidative stress [4], cytotoxic activity [5] leading to neurodegenerative diseases [4] [6] or cancer [4] [7]. Additionally some negative effects are not directly linked to NO but NO by-products. Due to its high reactivity nitric oxide can form reactive nitrogen and oxygen species (RNOS) such as peroxynitrite anion (ONOO⁻) [8]. Peroxynitrite, for example, can damage tissues or deactivate proteins due to nitrosation or nitration [8]. The balance between the beneficial and deleterious activities of NO would depend on the localization and nature of RNOS production.

Therefore understanding the mechanism involved in NO production has been crucial to find new drugs and treat the previously cited diseases. Indeed, NO is produced by NO synthase which has different and even opposite biological functions [9] [10] [11]. A better understanding of the biological mechanism of NO synthase represents a highly relevant challenge.

1.1.2. NO synthase and its partially known mechanism

NO synthase (NOS) is a widespread enzyme discovered in numerous living organisms such as mushrooms [12] bacteria [13] invertebrates [14], vertebrates [15] and mammals [16]. NOS has three isoforms: inducible, endothelial, and neuronal (*e, n and i*). The three isoforms have different function and locations. All NOSs are homodimeric enzymes containing a catalytic heme group (Fe^{III}-protoporphyrin IX). NOSs catalyze two successive steps of oxidation of a single substrate: L-Arginine, consuming three exogenous electrons and two molecules of oxygen. Briefly, the first step consists in the hydroxylation of the N ω -nitrogen of L-Arg resulting in the formation of N ω -hydroxy-arginine (NOHA). The second step corresponds to the oxidation of the

hydroxyl-guanidinium group of NOHA into the corresponding urea, L-citrulline with release of NO [17] (Fig. 1).

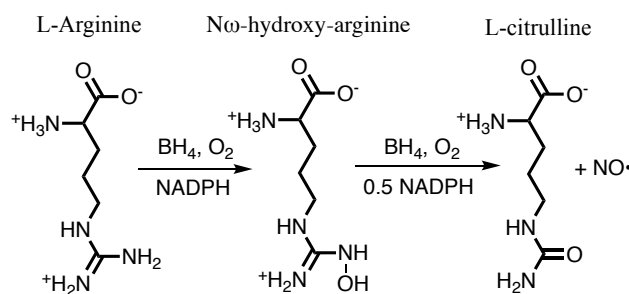


Fig. 1: Proposed mechanism of arginine oxidation by NO Synthase producing NO [17] BH₄ is a cofactor.

The exact mechanism of NO catalytic production is still debated especially with regard to electron and proton transfer and sources [17]. Moreover, mechanisms underlying the RNOS production are poorly understood and are dependent on physiological environments such as NO, O₂ concentration [17]. Understanding the parameters controlling NO/RNOS balance could help to favour beneficial effects against deleterious effects.

Controlling precisely the enzyme environment, substrate release and monitor the enzyme response could help to disentangle the NOS reaction pathway. By mimicking cellular encapsulation, the design of a synthetic cell-like microreactor could confer the desired environment for the enzyme study, in terms of local concentration, diffusion length and interfaces.

1.1.3. Microreactor

Cells are extraordinary bio-machines [18] that can process complex synthesis with a high level of control. As an example, synthesis of complex molecules, intricate processes or cascade biochemical reactions can be performed in cells. In addition, toxic species can be synthesized without damaging cells and incompatible species can coexist in the same medium due to compartmentalization [19]. All these reactions can be performed with a high level of control in space and time. Mimicking some cellular functions would afford access to these complex processes. To do so, scientists have been interested in designing microreactors in order to mimic the simplest cellular functions such as enzyme synthesis of molecules in a confined space [20]. As an example, monodispersed polymersome microreactors were prepared by formation of a double emulsion *via* microfluidic techniques [21]. Polymersome membranes were composed of poly(ethylene glycol)-*b*-poly(lactic acid) (PEG-*b*-PLA MW 5000 and 10 000 g/mol,

respectively). The inner aqueous medium contained biological machinery necessary for protein expression that was a mixture of the *Escherichia coli* ribosomal extract. The polymersome microreactor incubation at 32 °C induced DNA transcription into messenger RNA and this messenger RNA translation into polypeptides: MreB-RFP. The resulting polypeptide was fluorescent and observable under a confocal microscope (Fig. 2).

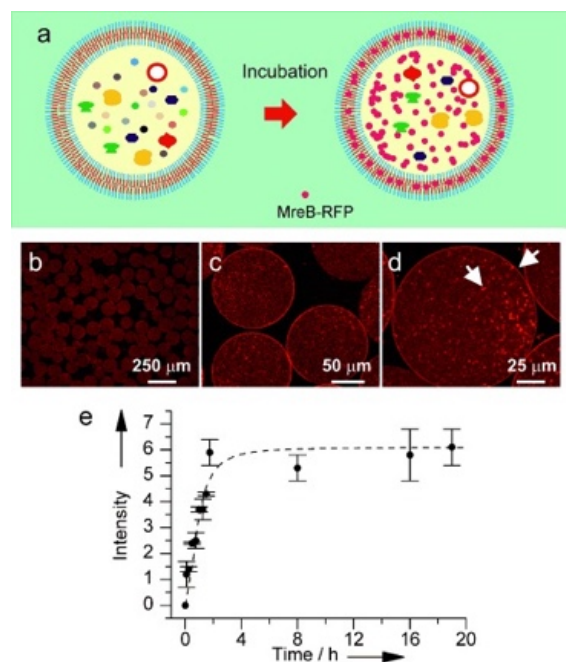


*Fig. 2: Protein expression in polymersomes formed by a microfluidic technique. a) schematic representation of a polymersome containing the *E. coli* ribosomal extract and the gene expression inducing protein synthesis. b-c-d) Confocal images of the polymersomes after MreB-RFP production. The protein is situated in the inner aqueous medium and in the membrane e) Fluorescence depending on the incubation time that allows to monitor protein production.*

This example showed that artificial cells afford access to complex biological processes. Another interesting example used multicompartmentalization or synthetic organelles to induce a three step processes in a synthetic cell. Three enzymes, phenylacetone monooxygenase (PAMO), *Candida antarctica* lipase B (CalB), and alcohol dehydrogenase (ADH), were separately encapsulated in nanopolymersomes made of polystyrene-*b*-poly(3-(isocyanato-L-alanyl-aminoethyl)thiophene (PS-*b*-PIAT). The nanopolymersomes were then encapsulated in giant unilamellar polymersomes(GUV) made of poly(ethylene oxide)-*b*-polybutadiene (PEO-*b*-PBut) (Fig. 3). The final enzymatic microreactor performed a three step cascade enzymatic reaction resulting in fluorescent resorufin. This example presents the first multicompartmentalization synthetic system that present active synthetic organelles.

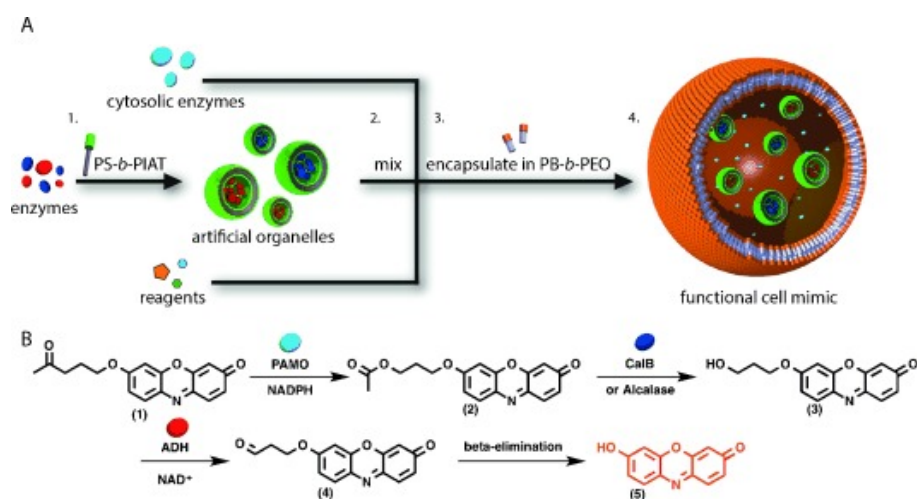


Fig. 3: A) Schematic representation of a multicompartmentalization microreactor. PAMO, CalB, and ADH, were encapsulated in nanopolymersomes of PS-b-PIAT. These nanopolymersomes were encapsulated in GUVs made of PEO-b-PBut. B) General reaction scheme of the three step catalytic process resulting in resorufin synthesis.

These examples showed that such a microreactor could mimic a cellular environment and would be adapted for NO synthase study. However, in these examples of microreactors and most of the others that can be found in the literature, the biochemical reactions are occurring based on mixing the different components or depend on diffusion properties through different membranes. As such, the study of reaction kinetics is very challenging, if not impossible. To this end, the design of stimuli responsive systems that could release reactive species directly in the microreactor and trigger the enzymatic reaction would represent very significant progress. Light was chosen as an exogenous stimulus, because its application is instantaneous, easy to control spatially and temporally, cheap to produce and non-invasive. In addition, the variety of light sensitive molecules is tremendous [22] and such activation can be used *in situ* under confocal microscopy.

Overall, we decided to develop a compartmentalized and light responsive microreactors to study the complex behavior of NOS, as schematically depicted in Fig. 4. To this end, the wide variety of available light sensitive delivery systems and approaches are reviewed in the next sections.

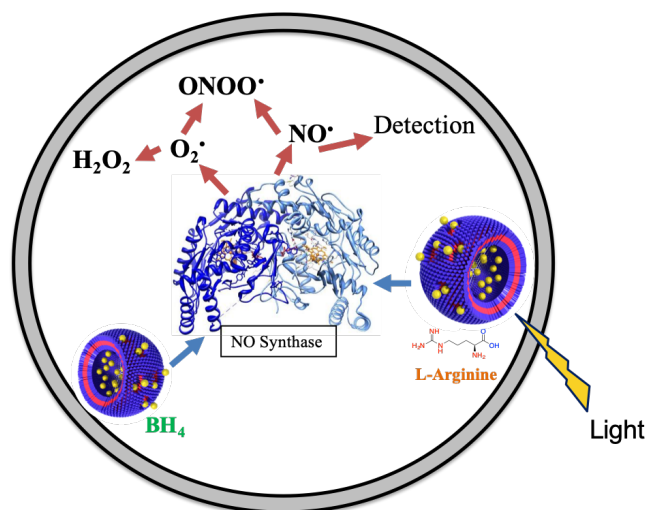


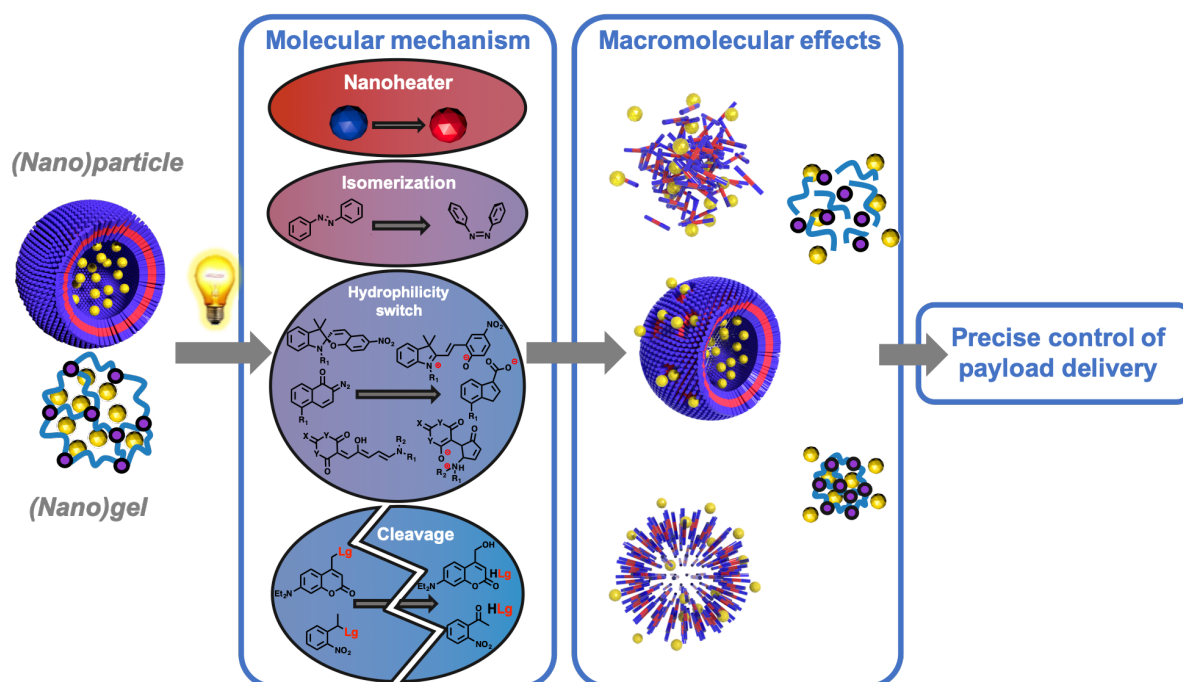
Fig. 4: Schematic representation of the NO-synthetic cell, which is based on compartmentalized polymersome-in-polymersome self-assembly and designed for the study of enzymatic activities of NOS. Modulation of the enzyme substrates and co-factors (L-Arg, BH₄) can be controlled by photo-activation.

1.2. Light-activated delivery system

The use of light as a trigger for species release presents many advantages compared to delivery systems based on a response to pH, temperature, or enzymes [23]. Indeed, such delivery triggers are often poorly controlled as they depend on physiological parameters and are subject to local variations.

Additionally, light is an attractive trigger, which can be applied with a high degree of temporal and spatial accuracy, and whose intensity can be easily controlled. The light spectrum is wide and potentially allows triggering different systems at the same time. The variety of light sensitive molecules is tremendous and light excitation can target a precise location during a specific time. For species delivery applications, light is non-invasive, easy to produce and not expensive.

In the first part, the effect of light at the molecular level will be discussed, together with the major mechanisms of action and their limitations. Secondly, the effect of light activation when photoactive substances are incorporated into delivery systems will be considered. Scheme 1 summarized the light-driven processes considered herein, extending from the molecular level to the macroscopic level, resulting in payload release.



Scheme 1: Light-driven molecular processes responsible for species release from nanocarriers.

1.2.1. Molecular mechanisms of light-activated delivery system

1.2.1.1. Physical effects

Light can induce two major physical effects: (1) increasing the system temperature and (2) converting radiation to other wavelengths. In both cases light energy can be used to promote species release.

1.2.1.1.1. General mechanism for conversion of light energy to heat

It is well known that light can produce heat, especially when interacting with some nanomaterials. In this part, materials able to convert light energy to heat energy, deemed “nanoheaters”, will be described.

In order to convert light energy into heat energy, several photothermal agents or nanoheaters can be used such as noble metals, transition metal dichalcogenides, carbon nanotubes (CNT), graphene oxide (GO) dye molecules and semiconductors (organic or inorganic). These photothermal agents absorb light and consequently their electrons become excited. The energy can be dissipated via non-radiative decay channels and heat the immediate environment. Dye molecules such as indocyanine green or naphthalocyanine have strong absorption nevertheless

they undergo photobleaching, thereby reducing their efficacy. Noble metals do not undergo photobleaching and can have absorption cross sections four to five orders of magnitude larger than dye molecules [24]. Electromagnetic waves interact with electrons on noble metal surface [25]. Indeed, these materials have free electrons on their surface that can oscillate with electromagnetic field. This phenomenon is called Surface Plasmon Resonance (SPR) [26]. Materials with SPR properties are, for instance, noble metals, transition metal dichalcogenides, carbon nanotubes (CNT), graphene oxide (GO) and semiconductors (organic or inorganic). At the appropriate electromagnetic resonance, the energy transfer is maximum [27]. The photon excites the electron and the energy is absorbed. The electron is then thermalized, the energy is transferred to the particles, creating heat that is then transferred to the surrounding medium. For metallic particles, their size and shape can be easily tuned to modulate and control the resonant wavelengths [28].

1.2.1.1.2. Design of nanoheaters for efficient light to heat energy transformation

There are a wide variety of materials that can transform light energy to heat energy and that have been developed over the past years.

The most popular nanoheaters are probably the noble metals like gold, silver, platinum or palladium. They have varying optical properties, they are easy to tune and to functionalize [29]. These properties make them very interesting for delivery systems. In addition, some organic molecules can also convert light into heat, such as porphyrin [30] or trisodium salt copper chlorophyllin (488 nm) [31].

Moreover, 2D materials have attracted a great interest recently for delivery applications because: they have a very large specific surface area so they absorb efficiently NIR and can adsorb molecules with aromatic character, such as doxorubicin [32] or chlorin e6 [33] due to π - π stacking. As an example graphene oxide and transition metal dichalcogenide are 2D materials which have been used as delivery systems [32] [33]. A recent review on stimuli responsive graphene oxide emphasized the interest of this kind of delivery system [34]. 2D transition metal dichalcogenides have also been recently reviewed [35]. One of them, MoS₂ possesses lower cytotoxicity than graphene oxide, which is better suited for biomedical applications.

Carbon nanotubes (CNT) have other advantages compared to 2D materials. Unlike nanosheets, CNT possess an intra-tube empty space where they can encapsulate a wider variety of species

(Fig. 5) [36]. Their absorption wavelengths are constant and do not depend on their lengths or size, contrary to gold nanoclusters [28]. Nevertheless, several problems should be overcome for delivery application, such as residual impurities: metal traces, small fullerenes amorphous carbon or their low solubility in aqueous solvent [37]. Also even if several species have been encapsulated inside CNTs [37], the only example, from our knowledge of releasing drug from their intra-tube empty space thanks to light is described in this review.

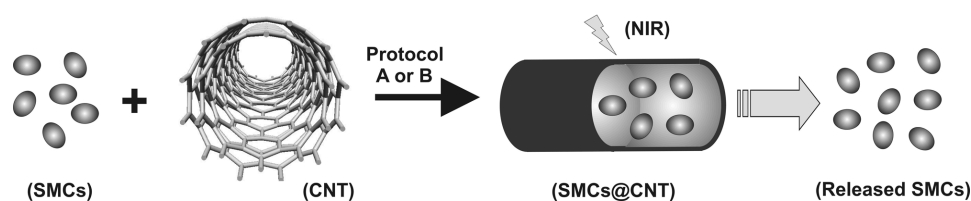


Fig. 5: Indole release from carbon nanotube after IR irradiation [36]

Another type of nanoheater is based on inorganic and organic semiconductors, which are attracting attention for payload delivery [38]. Indeed, they show a broad absorption in the NIR region and good photothermal conversion. They also are stable *in vivo*, easy to synthesize, low cost and insensitive to photobleaching. Huang et al. reported a system with $\text{Cu}_{1.75}\text{S}$ coated with a thermosensitive polymer, which was able to efficiently release doxorubicin under NIR light (808 nm) [39].

Organic semiconductor polymers were also proposed as a recent class of nanoheater. These polymers are better known for their application in organic electronics but some of them can also absorb in the NIR region. They are easy to synthesize, flexible, tunable, have a better biocompatibility [40]. A polymeric semiconductor poly(diketopyrrolopyrrole-alt-3,4-ethylenedioxythiophene) and pluronic 127 formed nanoparticles with a hydrodynamic diameter of 10 nm, that were successfully integrated in a poly(N-isopropylacrylamide) (pNIPAAm) gel. This nanoparticle / hydrogel system was demonstrated to release doxorubicin on demand under NIR light (808 nm) to cells *in vitro* [41]. Another study uses the second NIR window to penetrate the skin [42]. A polymeric semiconductor poly(bis(5-oxothieno[3,2-b]pyrrole-6-ylidene)benzodifurandione)-*co*-poly(bithiophene) which absorbs NIR light between 1000 and 1350 nm and converts it to heat was synthesized [43]. This organic semiconductor was self-assembled with an amphiphilic copolymer into micelles (diameter of 45 nm). These NIR sensitive micelles were then used to kill cancer cells due to the heat generated by the 1064 nm irradiation.

All the aforementioned particles are potentially promising for species delivery, but alone they are often insoluble or not biocompatible. The association of nanoheater with functional and biocompatible polymers is symbiotic as it allows combination of advantages of both systems: light sensitivity and thermosensitivity (Fig. 6).

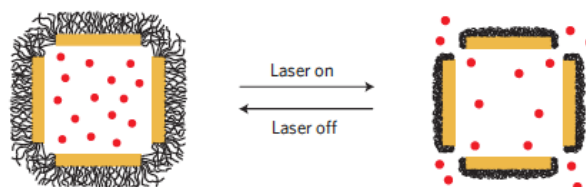


Fig. 6: Representation of gold nanocages coated with thermosensitive polymer chains (pNIPAAm-co-pAAM) which release doxorubicin under NIR radiation [44]

A wealth of polymers can be tuned to be thermoresponsive, biocompatible and biodegradable [45] making them suitable as thermosensitive systems for species delivery [46]. Grafting polymers can confer thermosensitivity, biocompatibility, and water solubility to the nanoheater. Polymers combined with nanoheaters can be used as a medium to encapsulate species. The wide variety of polymer and nanoheater offer tremendous possibilities to develop innovative new species delivery system.

As an elegant example of combining IR-sensitive systems that generate heat with temperature-sensitive systems, N-isopropylacrylamide (NIPAAm) and gold nanoparticles were combined [47] In this article nanoshell gold nanoparticles of around 20 nm were incorporated in temperature sensitive co-polymers hydrogel nanoparticles: NIPAAm and acryl-amide (AAm). Irradiation by NIR light (1064 nm) of the particles could enhance the release of methylene blue or model protein (bovine serum albumin).

1.2.1.1.3. Converting radiation: upconverting nanoparticles

Upconversion is a phenomenon that converts low energy radiation into high energy radiation (e.g. NIR photons into visible and UV photons). In biological applications these particles offer access to use of a wide variety of UV-activated molecules [48]. The upconversion mechanism involve two ions: one that absorbs the incident light called sensitizer ion, and another that emits the energy absorbed called activator ion. Several mechanisms with one or several sensitizers ions and one activator ion can result in the conversion of NIR into visible and UV light [49].

Here we describe the case where the sensitizer ion and the activator ion are the same. In this case ions that can upconvert radiation can absorb two or more low energy photons (Fig. 7, $h\nu_1$ and $h\nu_2$) and subsequently emit one high energy photon (or transfer the culminated excitation energy $h\nu_3$). To do so, these ions need to have excited states, which are optically active and have a long-excited state lifetime (E_l). The energy is accumulated and released in the form of one high energy photon. Upconverting nanoparticles (UCNPs) are composed of a crystalline host and a dopant, usually trivalent lanthanide ions, such as Lu, La, Pr, Nd, Sm, Eu, Gd, Tb, Dy, Ho, Er, Tm. The most common lanthanides used are Er^{3+} , Tm^{3+} , and Ho^{3+} . These inorganic ions have a lot of advantages such as very low background fluorescence, narrow emission band width, high resistance to photobleaching, and their absorbance wavelengths allow deep penetration into the tissues [50].

To illustrate the use of upconverting nanoparticles, a study used poly(ethylene oxide)-block-poly(4,5-dimethoxy-2-nitrobenzyl methacrylate) as a UV sensitive copolymer [51]. The copolymer formed 100 nm micelles and UCNPs were incorporated inside the self-assemblies during their formation. Under NIR irradiation (980 nm) the upconverting nanoparticles converted the wavelengths into visible and UV light directly inside the micelles. As a consequence o-nitrobenzyl groups were cleaved and the particles were destabilized. The disruption of the micelles induced Nile red release.

As another example, UCNPs composed of NaYF_4 , Y:25% and Tm:0.5% were synthesized with diameter of 20-30 nm [52]. A copolymer of hydrophilic pNIPAAm and hydrophobic poly(acrylate) containing spiropyran, was self-assembled on the surface of UCNPs (115 nm in diameter). Spiropyran becomes hydrophilic under UV light. These hybrid nanoparticles were irradiated with NIR (980 nm), UCNPs converted this radiation into UV and visible light (360 nm and 470 nm), spiropyran absorbed UV radiation and became hydrophilic, resulting in particle destabilization and coumarin 102 release.

Another elegant study used UCNPs and UV sensitive ortho-nitrobenzene (ONB) as the photocleavable moiety. Jalani et al. used lanthanide-doped UCNPs that were coated with hydrogel [53]. The inorganic nanoparticles used have a rhombus plate shape, an average length, width and thickness of 78 nm, 52 nm and 7 nm, respectively. These UCNPs can convert NIR into UV radiations (347 and 362nm). To form the hydrogel layer, chitosan was grafted on the UCNPs surface and then crosslinked thanks to a photocleavable ONB-PEG-ONB functional oligomers. A fluorescent protein FITC-BSA was loaded in the hydrogel layer. Then the nanoparticles were irradiated with NIR, that was converted into UV radiation.

Consequently, the UV radiation cleaved the ONB moiety, the nanogel disintegrated and released FITC-BSA protein.

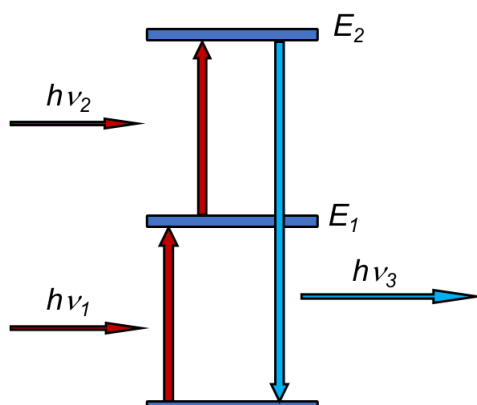


Fig. 7: Schematic representation of an upconverting energy diagram. Energy state E1 is optically active and has a long-excited state lifetime. E2 is the energy state from which the energy transfer can occur.

1.2.1.2. Chemical effects

1.2.1.2.1. Photoinduced chemical cleavage

Two main families of cleavable molecules based on coumarin (Fig. 8 A) and ONB (Fig. 8 B) have been developed.

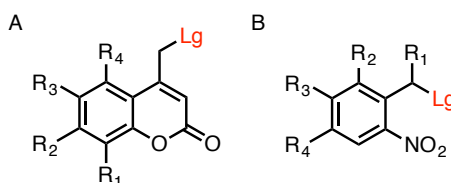


Fig. 8: The two main cleavable molecules used for delivery application, Lg is the leaving group A) Coumarin and possible substitutions, B) ortho-nitrobenzene and possible substitutions.

The design of efficient cleavable molecules requires the presence of good leaving groups in their structure. In addition, the product formed after irradiation should be stable in order to avoid any recombination and increase the cleavage efficiency. Therefore leaving groups often used are carboxylic acid, carbamate or carbonate [54].

The ortho-nitrobenzene family is probably the most popular cleavable group used in the past years. In particular o-nitrobenzyl (ONB) derivatives have been widely developed for delivery applications despite some major drawbacks. Indeed, their release rates are slower than those of

coumarin derivatives [55]. In addition, after irradiation, nitrosoaldehyde is formed and can react with amines to form an imine bound, which can especially be a problem for the surrounding proteins. Also nitrosoaldehyde can degrade to form brown compounds which act as an internal filter, thus decreasing the ONB cleavage efficiency [56] and can be potentially toxic [57].

A lot of ONB analogues have been synthesized in order to improve the cleavage efficiency, side product formation, solubility, or to tune irradiation wavelength [54]. Nevertheless, the substitution nature and position cannot predict the trend on photoreaction efficiency. Surprisingly, these analogues have been rarely used for payload delivery applications and most of these systems use the classic ONB without substitutions [58] [59] [60] [61] [62] [63].

To improve the ONB properties two main chemical substitutions were developed on the benzylic carbon and the aromatic ring. The benzylic position substitution corrects one drawback: the formation of the aldehyde, which leads to imine formation with an amine. Several moieties have been tested, especially electron withdrawing moieties. Trifluoromethyl on the benzylic position increases the quantum yield from 0.13 to 0.7 [64]. The methyl group also avoids aldehyde formation and increases the quantum yield to 0.64 (in MeCN) [65] and this derivative has been used in delivery applications [53] [66] [67].

Substitution on the aromatic ring has also been studied. It has been evidenced that the presence of one nitro group on the second ortho position increases the quantum yield significantly. One interesting feature of this kind of substitution is to change the absorption wavelengths. As such, the substitution with O-nitro-dibenzofuran increases the absorption wavelength maxima [67] and the introduction of two methoxy groups allows release of leaving groups at 405 nm (Fig. 9 A) [68].

Another class of o-nitrobenzene is o-nitrophenethyl group (Fig. 9 B). These compounds with a methyl on the benzylic position present a relatively high quantum yield: 0.35. A new class of o-nitrophenethyl group has been synthesized which increases the absorptivity and the release rate (Fig. 9 C and D) [69].

Coumarins constitute another important class of photochemically-active molecules, which can be used both as a crosslinker and as a cleavable group. It has numerous advantages and it is a good substitute to ONB, especially because of its faster release rate compared to ONB [55], its efficient release of a wide variety of leaving groups, and because it has important molar absorption coefficient with a larger absorption than ONB (λ_{max} from 310 nm to 490 nm). Depending on their substituent, coumarin derivatives that are released as a byproduct, can be toxic [70] or can have beneficial effects [71]. Coumarin derivatives can be easily tuned to adapt their toxicity. A lot of analogues have been synthesized to improve solubility or increase its

absorption wavelengths and easy structure modifications shift the absorption to the red [54]. As an example, 7-aminocoumarin has a λ_{\max} between 350-400 nm with a relatively good quantum yield: 0.21-0.28. Its relative efficient release made this coumarin derivative an interesting candidate for delivery application and it has been used many times for this purpose [72] [73] [74] [75]. Feringa and his group covalently attached an antibiotic to the coumarin derivatives and after UV irradiation (380 nm) the antibiotic was released in order to control the bacterial population.

Another example used coumarin as the light sensitive moiety in conjunction with well-defined hollow mesoporous silica particles (HMS) [74]. The particles (250 nm in diameter) were loaded with doxorubicin. In order to obstruct pores and avoid undesired doxorubicin release, a copolymer containing coumarin groups was self-assembled and loaded with HMS to form a layer that enveloped the particles. This copolymer was synthesized from 2-hydroxyethylacrylate (HEA), methacrylamide hydrochloride (APMA) and 7-(didodecylamino coumarin-4-yl)methyl methacrylate (DDACMM). A folate group was grafted on APMA, for selective cancer targeting and poly(DDACMM) is a poly(methacrylate) bearing hydrophobic coumarin derivatives. This polymer is both hydrophobic and light sensitive. The coumarin cleavage with UV or NIR light (365 nm or 800 nm with two photon absorption) made the copolymer layer hydrophilic, resulting in its solubilization in the medium. The pores were then open and as a consequence doxorubicin trapped in the hollow sphere was released. In order to red shift the absorption wavelength and improve the compatibility of radiation with cells, new coumarin molecules have been described. Three molecules with interesting photochemical properties have been identified: red shifted absorption with maximum absorption (λ_{\max}) up to 487 nm and significant release rate with blue-cyan light [76]. Electron-withdrawing groups were introduced at the coumarin 2- and 3- positions such as sulfur or cyano groups. In Fig. 9, coumarin derivative E has $\lambda_{\max}=472$ nm, F has $\lambda_{\max}=443$ nm and G has $\lambda_{\max}=487$ nm.

One side-reaction was reported as a drawback for the release of a thiol where the molecule underwent an isomerization instead of a cleavage [67]. The goal of the study was to protect cysteine on a peptide with a coumarin photo-removable group. Instead of thiol cleavage after irradiation, the coumarin isomerized and the thiol group was grafted on position 2. The final product is not photocleavable and consequently, the protecting group cannot be removed.

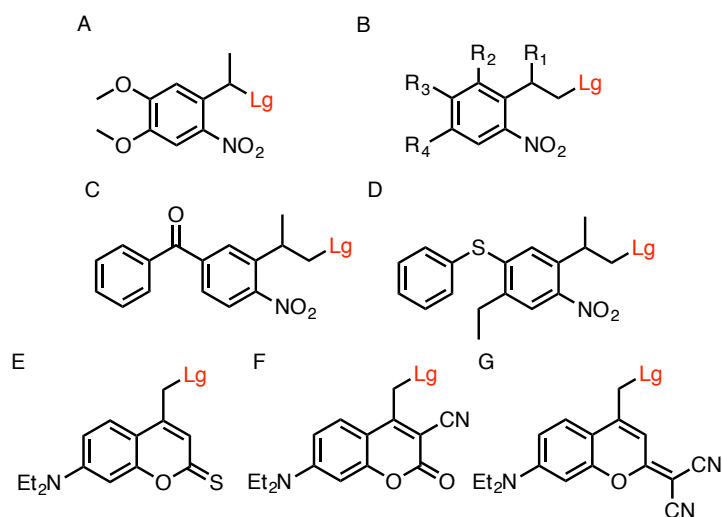
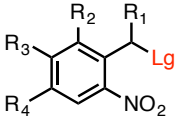
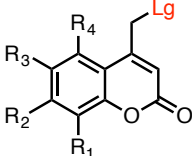
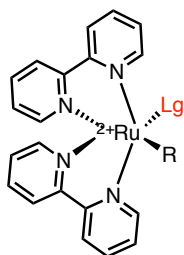


Fig. 9: Light-sensitive compounds that undergo cleavage under irradiation. These molecules have been designed in order to red shift their absorption. A) ONB with two methoxy groups B) o-nitrophenethyl and possible substitutions C) and D) o-nitrophenethyl derivatives with better release rate and absorptivity E) F) and G) Coumarin derivatives with significant release with blue-cyan light.

In this part, we mainly reported two main families of photocleavable molecules based on O-nitrobenzyl and coumarin. They have been widely studied and their properties were greatly improved to optimize their development for biological applications. In addition to these important derivatives, other cleavable molecules have been reported. A summary of these different classes of photocleavable molecular building blocks is presented in table 1.

Molecules	λ_{irra} (nm)	Quantum yield	Examples
O-nitrobenzyl			
	254-365 [54]	0.0013-0.7 [54]	[53] [58] [59] [60] [61] [62] [63] [66] [67]
Coumarin			
	310-490 [54]	0.005-0.28 [54]	[72] [73] [74] [75] [76] [77]

**Ruthenium
polypyridine**

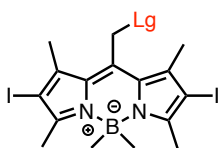


473 or 532

0.23

[78] [79] [80]

BODIPY



450 to 575 [81]

0.15 in methanol

[81][82]

Pyrene



300-375 [83]

0.22 for phosphate
release in MeOH [84]

[83]

Perylene

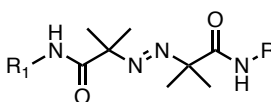


300-450 [85]

0.072-0.093 in
H₂O/MeCN for alcohol [62]
and carboxylic acid [86]

[62]

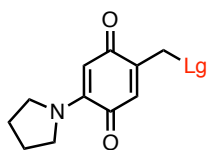
Azo linker



365 [87]

[87]

**amino-1,4-
benzoquinone**



590 [88]

0.003-0.007 in 30% aq.
CH₃CN [88]

[88]

Table 1: List of the main important classes of photocleavable molecules that have been developed for biomedical applications in recent years.

1.2.1.2.2. Isomerization and rearrangement

Azobenzene

Azobenzene is a popular molecular switch that has been used in delivery systems because it can be efficiently and reversibly isomerized between trans- and cis- forms. Indeed, upon UV irradiation (365 nm) the thermodynamically stable trans- form isomerizes into the cis- form. This isomer is metastable and has a substituent-dependent half-life of up to two days [89]. If irradiated with visible light (450 nm), azobenzene quickly returns to the trans- isomer [90] (Fig. 10 A).

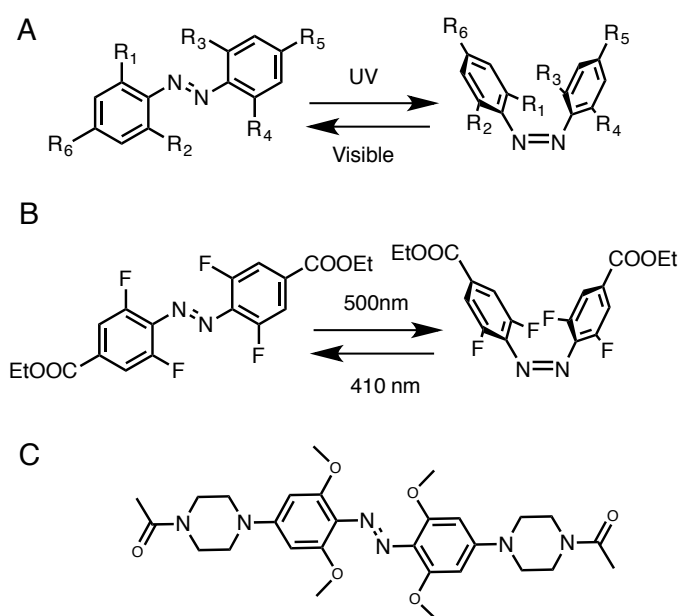


Fig. 10: A) Reversible azobenzene trans-cis isomerization under UV and visible light B) *o*-Fluoro-azobenzene showing a red shift in absorption and a stable cis isomer ($\tau_{1/2}=2$ years) [91] C) Azobenzene derivative showing particularly large red shifting [92].

This molecular switch is reversible over multiple cycles without deterioration. In delivery application this transformation is useful in inducing polymer or peptide property changes [93]. To improve the release, a range of derivatives has been developed to tune two major photochemical properties of azobenzene: the absorption wavelengths required to switch between the cis- and trans- forms and the isomer's thermal stability. For *in vivo* applications, light absorption should be in the near infrared in order to go deeply through the skin. In addition, thermal stability, characterized by the half-life of the less thermodynamically stable form, can be tuned depending on the system needs. A short half-life provides a fast back isomerization in the dark and an efficient on/off switch. A long half-life assures longterm system modifications.

Substitutions on the para- and ortho- positions have also been widely explored [94]. The para-position is often used to attach molecules of interest such as peptides or polymers [95]. The ortho- position red-shifts the absorption and tunes the thermal stability of the two isomers. A wide variety of groups have been tested including the amino [96] and chloro group [97]. Substitutions with four fluorines at the ortho- positions showed a significant red-shifting and an improvement in the thermal stability [91]. The irradiation of the trans- form with green light (>500nm) showed 90% Z isomerization and a half-life of circa 2 years (Fig. 10 B).

Substitution with 4 *o*-methyl groups showed significant red-shifting, with absorption up to 680 nm [92] (Fig. 10 C). Unfortunately these molecules are sensitive to reduction by glutathione which can be a problem for delivery applications [93]. The tetra-ortho-methoxy-substituted azobenzene has been used to release doxorubicin with red light [98]. These azobenzene derivatives show a great potential for payload delivery due to their long absorption wavelengths and excellent fatigue resistance.

Hydrophobicity / Hydrophilicity switch molecules

Certain molecules undergo hydrophobicity / hydrophilicity switching upon irradiation, which can be either reversible or irreversible. Three molecular derivatives were identified for delivery applications: spiropyran [99], 2-diazo-1,2-naphthoquinone (DNQ) [100] [101] and more recently donor-acceptor Stenhouse adducts (DASAs) [102]. These molecules can be incorporated into polymers, for example on the polymer backbone. After switching they can induce a significant change in the polymer property such as polymer hydrophobicity. This property is a key factor for some nanoparticle or gel stability. Changing the property at the molecular level can change the property at the macromolecular level and thus destabilize gels or nanoparticles [103] [104] [105] [106].

Under UV light, the closed ring form of spiropyran undergoes a C-O bond cleavage, resulting in the zwitterionic merocyanine form. The merocyanine can reversibly lead to the hydrophobic ring-closed form under blue light (420 nm) (Fig. 11 A). Spiropyran is biocompatible and can be easily grafted onto any matrix. Even if the response is fast, this molecular switch presents one major drawback, as after several switch cycles the molecule undergoes photodegradation [107].

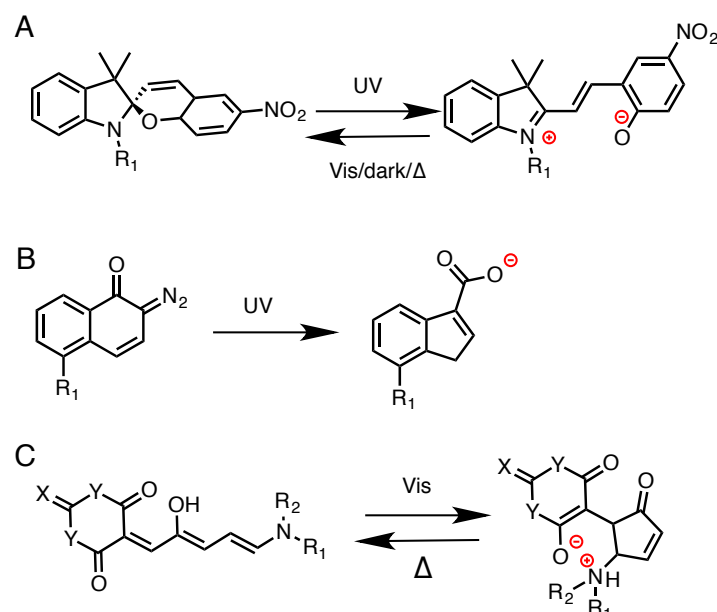


Fig. 11: Switch between hydrophobic isomer and hydrophilic isomer A) Spiropyran and merocyanine forms, B) Irreversible DNQ rearrangement induces hydrophilicity C) DASA molecular switch inducing hydrophilicity, $Y=O, NCH_3$; $X=O, (CH_3)_2$.

DNQ has attracted a lot of attention because of its ability to act as a hydrophilicity switch that can be activated by UV or by NIR light in a two photon process [100] [101] [104] [106] [108]. Under these radiations DNQ undergoes an irreversible Wolff rearrangement [109] leading to a carboxylic acid with a pKa of 4.5 [110] (Fig. 11 B) that is charged and thus hydrophilic in physiological conditions (pH=7.4). DNQ has been tested on cells and was interestingly shown to be cytocompatible [104] [106].

DASA is a relatively new class of molecules that have been developed for hydrophilicity switch. DASA photoswitches under visible light (Fig. 11 C), the reaction being reversible and displaying excellent fatigue resistance [102]. The two forms have important property differences. Without illumination, the molecule is hydrophobic and compact, and becomes zwitterionic and extended after irradiation. These differences lead to efficient particle destabilization for cargo release [103]. One example of controlled release reported the incorporation of DASA in the backbone of an amphiphilic copolymer [111]. To this end PEG was used as an initiator for the copolymerization of pentafluorophenyl methacrylate and hexyl methacrylate. Then DASA was grafted on the hydrophobic blocks. The resulting amphiphilic copolymer was self-assembled into polymersomes (30–100 nm). HRP was loaded in the polymersomes to form photoresponsive nanoreactors. Thanks to DASA switching, permeability of polymersome membranes were controlled under visible light irradiation (630 nm and 525 nm) thus enabling the control of the nanoreactors.

Dimerization and dimer cleavage

In a context of delivery application, dimerization processes have been proposed to form gels or stabilize particles before release [61] [112]. To induce the release of a loaded specie, the gel or particles are irradiated, uncrosslinked and, as a consequence, lose their stiffness or structural integrity [113] [114] [115] [116]. Three molecules are used as dimers for such application: coumarin [113] [114], cinnamate [115], and anthracene [116]. However, such release mechanisms by dimer cleavage is not really adapted for applications involving enzymes. Indeed, UV exposure typically leading to hydrogel scission is too long for enzyme viability, reactions are not complete with side reactions and the process is not resistant to fatigue.

1.2.2. Release mechanisms

In the previous part, the effect of light at the molecular level was discussed, together with the major mechanisms of action and their limitations. We now shift our focus to the effect of light activation when photoactive substances are incorporated into payload delivery systems. One can highlight two major mechanisms to induce and control specie release profiles: (1) a complete destabilization of the carrier / particle leading to a complete payload release, or (2) an acceleration of the species diffusion through the carrier (membrane permeation or gel shrinkage).

1.2.2.1. Light-induced structural changes inducing species carrier destabilization

A relevant question at this stage is: how can payload release be induced through carrier disruption? To answer this question, the underlying mechanisms responsible for the stabilization of the carrier structure have to be understood. With this in mind, two different classes of delivery system can be proposed: (1) particles which are stabilized thanks to hydrophilic / hydrophilic interactions (such as micelles or vesicles) and (2) gels that have a 3-dimensional structure that is maintained due to physical [117] [118] or chemical crosslinking [119] [120].

1.2.2.1.1. *Self-assembled nanoparticles*

Polymer nanoparticles such as micelles, worm-like micelles or polymersomes are thermodynamically or dynamically stable self-assemblies as a result of copolymer amphiphilic properties. Indeed, in order to minimize the interaction of the hydrophobic blocks with water, block copolymers assemble into well-defined structures. Micelles and worm-like micelles are nanoparticles that are composed of a hydrophobic core surrounded by a hydrophilic shell. The difference between these two structures is the shape: micelles are spherical nanoparticles and worm-like micelles are cylindrical and elongated nanoparticles. Polymersomes are small artificial vesicles enclosing an aqueous solution separated by a bilayer membrane made of amphiphilic block copolymers. A key property to obtain and stabilize these structures is the hydrophobic to hydrophilic ratio of the two blocks [121]. Depending on this ratio, different structures or no specific structure can be obtained.

As an interesting example, a hydrophilic block poly(glycerol monomethacrylate) (PGMA) was used as a chain transfer agent to polymerize in water 2-hydroxypropylmethacrylate (HPMA), a hydrophilic monomer [122], resulting in the formation of a well-defined amphiphilic diblock copolymer. During the HPMA polymerization, the hydrophobic ratio of the diblock increased leading the formation of different structures over time. The amphiphilic block starts to form micelles then worms and finally vesicles over time, depending on the ratio. This example shows how important the hydrophobic to hydrophilic ratio is in defining the structures formed. As a consequence, inducing a change in this equilibrium can destabilize the structure.

There are two ways to change the balance between the two chains of the amphiphilic polymer, either by modifying the hydrophobic to hydrophilic ratio [100] [103] or by separating the two blocks [123]. As far as we know, only one example of block separation has been reported for cargo delivery [123]. In this study poly(γ -methyl- ϵ -caprolactone) is used as the hydrophobic block and poly(acrylic acid) (PAA) as the hydrophilic block with a photo-cleavable *o*-nitrobenzyl (ONB) inserted between the two blocks. The amphiphilic block can self-assemble into polymersomes and micelles with a hydrodynamic radius of 83 nm and 31 nm, respectively. After UV irradiation (365 nm), the two structures were disrupted and aggregates were formed. The second way to disrupt particles is to play with the change in the hydrophobic balance. The conversion of the hydrophobic blocks into hydrophilic blocks is the most popular mechanism found in the literature. This change is induced at the molecular level by cleavage, switching hydrophilic / hydrophobic properties, or azobenzene isomerization.

As an example for cleavage-inducing destabilization, Jiang et al. synthesized amphiphilic copolymers of poly(ethylene oxide) and poly(methacrylate) bearing a hydrophobic pyrene moiety in the side group (PEO-*b*-PPy) [83]. These diblocks were able to self-assemble into micelles with an average diameter of 15 nm. Under UV irradiation, the pyrene ester moiety is cleaved, and the hydrophobic PPy is converted into hydrophilic poly(methacrylic acid). Thus, after irradiation of the micelle solution for 15 min with UV (365 nm), the micelles were destabilized and the Nile red previously loaded was released (Fig. 12).

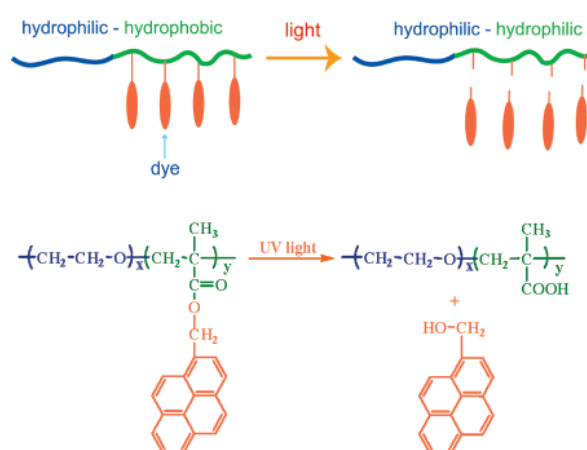


Fig. 12: Release of a hydrophobic group induced particle by destabilization [83].

Equally, an amphiphilic block of poly(benzyl carbamate) for the hydrophobic part and poly(N,N-dimethylacrylamide) as the hydrophilic part (PBC-*b*-PDMA) was employed. PBC exhibits, after chain-end cleavage, head to tail cascade depolymerization, which is also called self-immolation [62]. The hydrophobic block depolymerization induces a huge change in the hydrophilic to hydrophobic ratio of the copolymer. In this example the end chains are photocleavable thanks to perylen-3-yl (visible-light sensitive: 420 nm) and 2-nitrobenzylbenzyl (UV sensitive: 365 nm) groups. The PBC-*b*-PDMA can also self-assemble into vesicles with hydrodynamic diameters of around 250 nm. The combination of all these properties results in light-sensitive self-immolative polymersomes. As a consequence, after irradiation at the appropriate wavelength (depending on the light-sensitive moiety) the chain end is cleaved inducing depolymerization, polymersome destabilization and Doxorubicin release, which was previously encapsulated.

The two previous examples illustrate how photo-cleavage can destabilized self-assembled particles.

Switching molecular hydrophobicity is a popular way to destabilize nanostructures by changing the hydrophilic to hydrophobic ratio. To this end, molecules presented in Fig. 11 have been widely used such as spiropyran [52] [105] [124] [125], DNQ [100] [101] [104] [108] and DASA (Fig. 14) [102][103].

As an example with spiropyran, this hydrophobic light-sensitive molecule was grafted with a hydrophilic, hyperbranched polyglycerol (SP-*hb*-PG) resulting in an amphiphilic polymer (Fig. 13) [105]. Moreover, this polymer can self-assemble into well-defined micelles with an average hydrodynamic diameter of 30 nm. When these nanoparticles were irradiated with UV light (365 nm), the neutral hydrophobic spiropyran was isomerized into the hydrophilic zwitterionic merocyanine changing the hydrophilic ratio. As a consequence, micelles were destabilized and released pyrene, a hydrophobic test molecule.

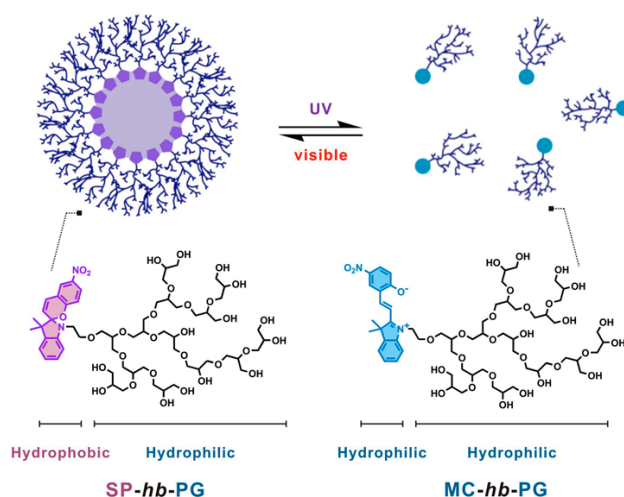


Fig. 13: Spiropyran hydrophilicity switch inducing particles destabilization [105].

Wang et al. used DNQ as light sensitive moiety to disrupted particles [101]. In this study a diblock of poly(ethylene glycol)-*block*-poly(dimethylaminoethyl methacrylate). (PEG-*b*-PDMAEMA) was synthesized by ATRP. In addition, DNQ was grafted on the PDMAEMA block making it hydrophobic. As a result, an amphiphilic diblock (PEG-*b*-PDMAEMA@DNQ) was obtained. This diblock can self-assemble into micelles with an average diameter of 150 nm. Irradiation by UV or NIR (365 nm or 808 nm) leads DNQ to undergo a Wolff rearrangement and conversion of the hydrophobic block into a hydrophilic block. As a consequence of the hydrophilic ratio change, micelles are disrupted and 60% of coumarin 102, chosen as a hydrophobic model drug, was released at pH=7.

As an example that uses DASA, two hydrophobic n-heptane groups were grafted on DASA and a PEG at the other molecular extremity resulting in amphiphilic blocks that can self-assemble into micelles [103]. Irradiation with visible light (530 nm to 570 nm) leads to the DASA conversion into its zwitterionic form, changes the copolymer hydrophilic ratio and releases Nile red or Paclitaxel.

These examples showed three light sensitive hydrophobicity switch molecules, which change the hydrophobic ratio of amphiphilic copolymers and disrupted self-assembled structures.

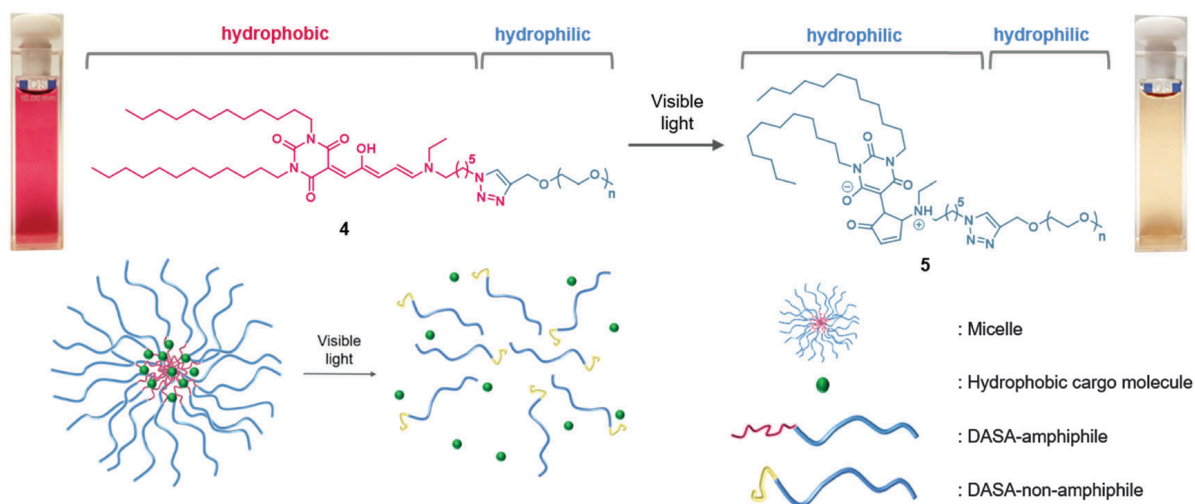


Fig. 14: DASA hydrophilicity switch inducing particles destabilization [103].

The azobenzene isomerization can also induce particle disruption. Azobenzene isomers (*Z* and *E*) have different dipole moments and as a consequence the *cis*- isomer is more hydrophilic than *trans*-isomer [126]. When azobenzene is integrated in polymer chains this hydrophobicity difference is enough to disrupt micelles or vesicles. As an example, amphiphilic block copolymers of poly(methacrylate) containing-azobenzene as the hydrophobic block and as the hydrophilic block a statistical copolymer of poly(acrylic acid) and poly(*tert*-butyl acrylate) (PAzoMA-*b*-PAA-*Pt*BA)), were synthesized [127]. Depending on the block sizes, copolymers self-assembled into micelles (15 nm with PAzoMA₃₁-*b*-PAA₃₃-*Pt*BA₁₉) or vesicles (100-300 nm with PAzoMA₇₄-*b*-PAA₂₂-*Pt*BA₄₆). Under UV light (360 nm, 10 min) azobenzene grafted on the hydrophobic polymer chain isomerized into its *cis*- form leading to micelle or vesicle disruption. Azobenzene isomerization is reversible and the copolymer solution previously irradiated self-assembled again into micelle or vesicles under visible light (440 nm, 3 min). Having been reset, this process can be repeated several times.

1.2.2.1.2. Giant polymersomes

Mechanisms involved in the release of species from giant polymersomes (whose size is $>1 \mu\text{m}$) are somewhat different than nano-polymersomes. Three examples, that may be considered particularly relevant and original, are presented here. Mabrouk et al. produced light sensitive asymmetric polymersomes that burst under a light stimulus [95]. The property differences between the inner and outer leaflet under UV irradiation induces membrane frustration and destabilization. To produce these micrometric asymmetric polymersomes, the emulsion-centrifugation [128] technique was used. This method consists in stabilizing water emulsion droplets in an organic solvent (in this case toluene) thanks to an amphiphilic block copolymer. After centrifugation, emulsion droplets crossed the interface of a water / organic phase, also stabilized by an amphiphilic block copolymer. With this technique, two different copolymers can be used for the emulsion and the interface in order to generate an asymmetric membrane. While the emulsion droplets cross the interface from the organic phase to the water phase, a second leaflet of copolymer is added around the droplets, thus forming polymersomes. In this study the two copolymers used were poly(ethylene glycol)-*b*-polybutadiene (PEG-*b*-PBD) and a liquid crystalline copolymer PEG-*b*-poly(4-butyloxy-2'-(4-(methacryloyloxy)butoxy)-4'-(4-butoxybenzoyloxy)azobenzene) (PEG-*b*-PMAazo444). The hydrophobic part consisted in a poly(methacrylate) bearing a modified azobenzene group. Without UV irradiation, azobenzene is in its thermodynamically stable *trans*- form and acts as a well-ordered liquid crystalline. Under UV irradiation azobenzene isomerizes into its *cis*- form. The leaflet containing PEG-*b*-PMAazo444 has a disordered state, its projected area increases and swells compared to the other leaflet. This induces a membrane tension increase and, consequently, in order to relax this tension, the membrane collapses and the polymersome bursts releasing its content.

In another study a ferritin protein, that stores and releases iron in cells, was encapsulated in PEG-*b*-PBD polymersomes (around $10 \mu\text{m}$) and adsorbed in the inner leaflet of the membrane [30]. In addition, bis[(porphinato)zinc] (PZn_2) was embedded in the polymersome membrane. This chromophore absorbs in the near UV, visible, and NIR light. The system was irradiated at 488 nm, 543 nm or 633 nm where the PZn_2 absorbs strongly. As a consequence, morphological changes in vesicles such as budding of smaller vesicles and vesicle rupture was induced. Indeed, the synergy of the ferritin and the PZn_2 converted light energy into heat energy that generated differential rigidification in the membrane, stressed the membrane and ruptured or budded vesicles. To demonstrate photorelease, biocytin was encapsulated and 25 - 50% was released after irradiation.

Recently, Peyret et al. loaded three photocleavable molecules in giant polymersomes, namely calcein, methylene blue and a coumarin derivative using an emulsion-centrifugation method [129]. These molecules served to rapidly increase the osmotic pressure inside the polymersome lumen by increasing the number of species after photocleavage under irradiation. Calcein polymersomes, methylene blue polymersomes and coumarin derivative polymersomes were, respectively, irradiated at 488 nm, 633 nm and 405 nm in a confocal microscope, which induced fast polymersome bursting, in the range of milliseconds to seconds. Indeed, as polymersomes are impermeable to water, rapid osmotic pressure change cannot be compensated, which results in membrane stress and consequently polymersome rupture. Polymersomes encapsulating the different aforementioned dyes, rendering them sensitive to different irradiation wavelengths, were burst independently with high specificity and temporal precision in the same medium. These light-sensitive polymersomes were further able to release nano-polymersomes and nano-liposomes. This approach can obviously be used to release any kind of loaded cargoes in a very precise manner.

1.2.2.1.3. Gels

Gels are effective delivery systems, having high loading capacity, stability and often good biocompatibility when inert hydrophilic segments are used. Gels are generally robust, especially in the case of chemically crosslinked 3D gels, can be formulated into large pieces (macro gels) that can be implanted or small nanoparticles (nanogels) that can circulate in the blood stream [130]. Nanogels can also be combined with inorganic nanoparticles to form a shell [53]. Gels are either chemically [119] [120] or physically crosslinked [117] [118]. Physical gels are reversible gels that are crosslinked *via* molecular interactions or secondary forces such as van der Waals, ionic or hydrophobic interactions. As an example of a physical gel, a triblock ABA was prepared with hydrophilic PEG as the B block and hydrophobic photolabile poly([6-bromo-7-hydroxycoumarin-4-yl]methyl methacrylate) (PBHCMM) as the A block resulting in PBHCMM-*b*-PEG-*b*-PBHCMM [117]. The ABA triblock was used to prepare a macro hydrogel. As shown in Fig. 15, the hydrophobic interactions of the A blocks are responsible for the formation of a 3D network. In another example, a polysaccharide, the polymaltotriose (or pullulan), bearing a hydrophobic cholesteryl group was used to form nanogel particles with a hydrodynamic diameter of 18 nm [118]. The hydrophobic moiety acts as the physical link to create the polymer network and the gel. Chemical gels or permanent gels are held with covalent

bonds. An example of chemical gel is presented in Fig. 17: a 4-armed PEG tetra coumarin bearing an azido group and a 4-armed PEG tetra-alkyne were synthesized [119]. The two 4-armed polymers in water undergo a Huisgen click reaction using the azido group, the alkyne and copper as a catalyst, creating covalent junctions resulting in a macro hydrogel. To induce release of the drug previously loaded in the hydrogel, the method widely used is to dissolve and disintegrate hydrogels by rupture of the chemical or physical junctions responsible for the network.

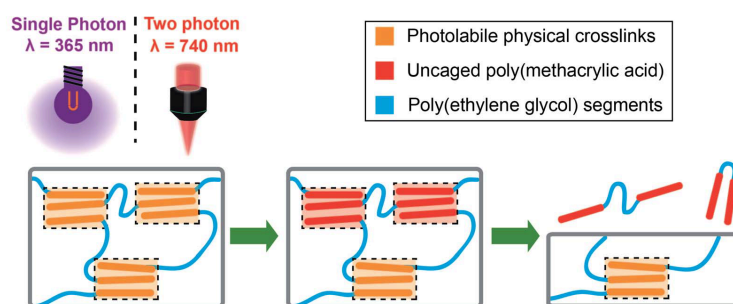


Fig. 15: Example of a light sensitive physical gel [117].

For physical gels, destabilization can be induced by cleavage of the hydrophobic moiety responsible for the physical junctions. As an example, we cited above the case of the triblock PBHCMM-*b*-PEG-*b*-PBHCMM [117]. Each end-chain of the triblock bears one cleavable hydrophobic coumarin. Under UV or NIR irradiation (365 nm or 740 nm) the coumarin is uncaged and the hydrophobic PBHCMM transforms into hydrophilic poly(methacrylic acid) (PMMA), thus destabilizing the hydrogel (Fig. 16). In another interesting example cited above, the hydrophobic cholesteryl group was covalently-linked to the hydrophilic polysaccharide by a photocleavable ONB [118]. FITC-insulin was encapsulated in the nanogel. A film was formed with the FITC-insulin nanogel particles and under UV irradiation (365 nm, 50 min) the cholesteryl group was cleaved. Consequently, the physical bonds are ruptured, the nanogel film is disrupted and FITC-insulin is released.

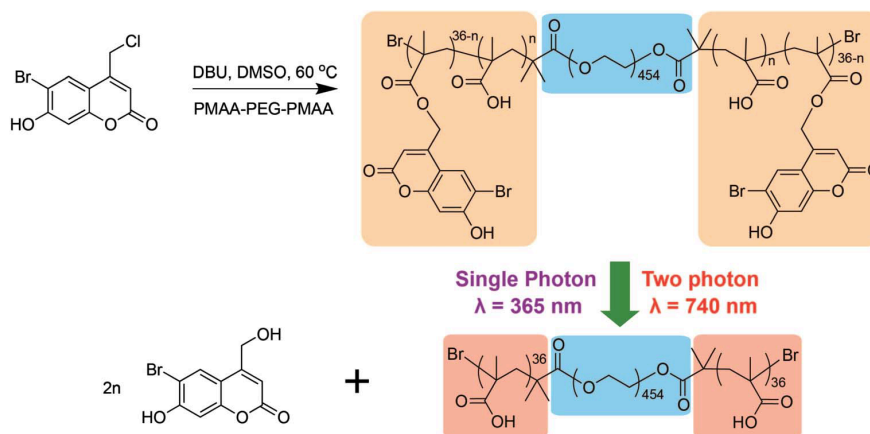


Fig. 16: Photocleavage of PBHCMM-b-PEG-b-PBHCMM inducing destabilization of the physical hydrogel [117].

In the case of chemical gels, destabilization occurs via covalent bond rupture (Fig. 17). These bonds can be cleaved using of coumarin [119] [131], ONB [53] [120] or a diazo linker [87]. In an aforementioned study, 4-armed PEG bearing photo-cleavable coumarin moieties were crosslinked [119]. The macro hydrogel was irradiated with UV light (365 nm or 405 nm), inducing coumarin cleavage and chemical junction rupture, resulting in the hydrogel destabilization (Fig. 17). Coumarin was further used as a crosslinker to form a polystyrene microgel by emulsion polymerization [131]. The final microgel particles were between 100 nm and 200 nm and under UV light (365 nm) the coumarin was cleaved, the hydrogel was degraded and Nile red was released.

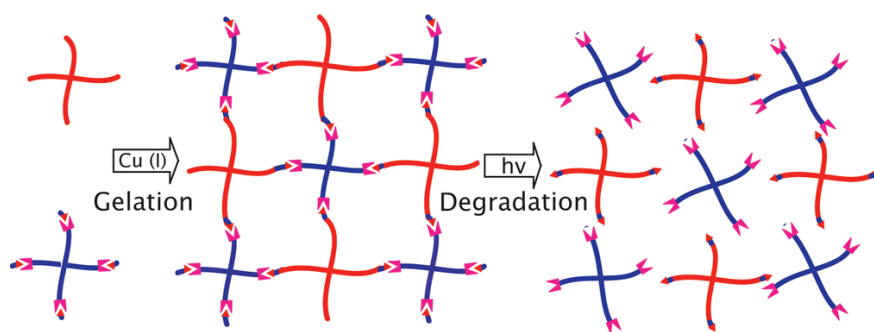


Fig. 17: Example of the destabilization of a chemically crosslinked gel [119].

In a last recent and very elegant example concerning light-sensitive degradable hydrogels, Badeau et al. reported gel junctions that behave according to Boolean logic. Three cleavable molecules which respond to different stimuli were chosen: one sensitive to light (ONB), one sensitive to reduction (disulfur bond) and one sensitive to an enzyme (metalloproteinase). By

connecting cleavable groups in series or in parallel (Fig. 18), they managed to tune the junctions sensitivity with AND/OR connectors, then crosslinked with the junction 4-armed PEG and formed a hydrogel with the same sensitivity. For example (Fig. 18), they synthesized a hydrogel that undergoes degradation after light irradiation (A) AND (reduction OR presence of the enzyme) [132].

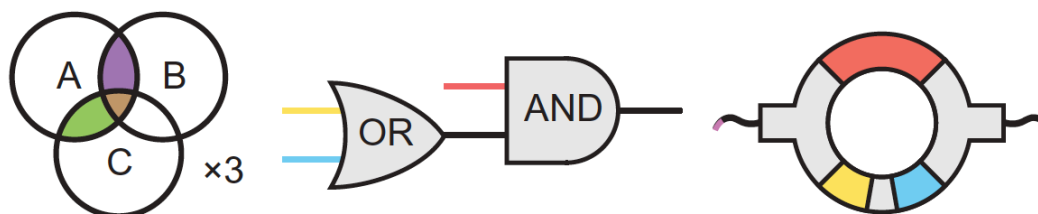


Fig. 18: Logic connector which can destabilize gel with AND and OR stimuli [132].

1.2.2.2. Light-induced increase of diffusion speed (Heat generation / permeability modification)

In contrast to the previous section, the systems described here can release their content while maintaining their structure. Release is induced by changing the diffusion properties from the carrier.

A simple way to increase the diffusion rate is based on temperature. As seen in part 1, nanoheaters increase system temperature due to light radiation. To have a light sensitive delivery system, nanoheaters can be combined with thermosensitive carriers. There are a wide variety of nanoheaters and a wide variety of thermosensitive polymers [133] [134] and consequently there are tremendous possibilities to combine them both to design of light sensitive delivery systems with appropriate properties.

In this review, we will focus on a few demonstrative examples that we consider the most relevant. Two different approaches are presented here, based on (1) polymers with a lower critical solution temperature (LCST) and (2) hydrophobic polymers that undergo phase transition.

1.2.2.2.1. Polymer / Gel shrinkage (solubility change)

The LCST is the temperature above which the component becomes insoluble in a given solvent. In water, when the temperature is increased above this critical temperature, the polymer chains

pass from a hydrophilic swollen state to hydrophobic shrunken state [133]. For payload delivery applications, species are trapped in the carrier swollen state. When light is activated the nanoheater increases the temperature above the LCST and the carrier shrinks. As a result of the resulting volume reduction, the payload is released [46]. To have an efficient delivery system the polymer LCST should be a slightly larger than the body temperature (37°C). The LCST can depend on the molar mass, component concentration or pH [133]. The most important polymers used for thermally sensitive delivery systems are poly(N-isopropylacrylamide) (pNIPAAm), copolymers of poly(ethylene oxide), poly(propylene oxide) (often referred as pluronics or jeffamine [135]) and elastin-like polypeptides (ELP [136]). However, mainly pNIPAAm combined with nanoheaters has been used for light sensitive delivery systems. pNIPAAm has interesting properties: its LCST only slightly depends on its molar mass, pH or concentration [137]. Its LCST that is around the body temperature (30°C to 35°C) has to be tuned to be higher. With this in mind, interesting gels based on the copolymerization of NIPAAm with methacrylic acid (MAA) and N,N'-methylene-bis-acrylamide (MBA) (crosslinker), were obtained with an appropriate LCST. These gels were polymerized directly around nanoheaters (Cu_{1.75}S nanocrystals) and when the system was irradiated with NIR (808 nm) it efficiently released doxorubicin that was previously trapped in the polymer blend (Fig. 19) [39].

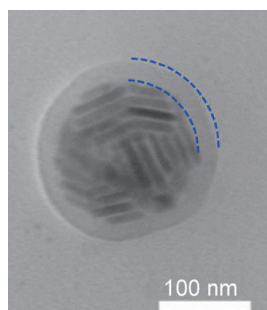


Fig. 19: Cu_{1.75}S nanocrystals encapsulated in a temperature-responsive polymer [39].

In another study, NIPAAm and acrylamide (AAM) were copolymerized to tune the LCST. The obtained copolymers were covalently anchored on gold nanocages (Fig. 6). These cages have pores that are obstructed when the polymer is in its swollen state (below LCST). After irradiation in the NIR, the gold nanocages locally heated the polymer chains that collapsed and shrank. The pores were no longer obstructed leading to doxorubicin release [44].

Temperature change is not the only way to induce polymers or gels shrinkage. Hydrophobic transition thanks to cleavage or the introduction of hydrophobicity switched molecules can also provoke a volume transition in materials. In this context, a hydrophobic coumarin moiety was

grafted on a hyaluronic acid (HA) hydrogel (Fig. 20). This gel formed well-defined nanoparticles that could efficiently load doxorubicin due to the hydrophobic interactions with coumarin. After UV irradiation (315-400 nm) the hydrophobic coumarin derivatives were cleaved, making the HA nanogels more hydrophilic, thus allowing its swelling and the release of doxorubicin [75].

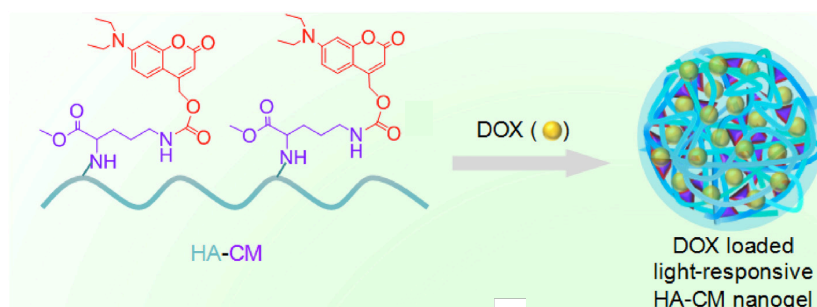


Fig. 20: Coumarin release induces gel swelling [75].

In another study the transition from the hydrophobic spiropyran form to the hydrophilic zwitterionic merocyanine form was also shown to shrink micelle particles (Fig. 21). This shrinkage allows a faster release of drugs and a deeper tissue penetration [99]. Spiropyran (SP) linked to a lipidic chain (thus fully hydrophobic) (SP-C9) and 1,2-distearoyl-sn-glycero-3-phosphoethanolamine-poly(ethylene glycol) (DSPE- PEG) were nanoprecipitated together resulting in hybrid micelle formation. These nanoparticles had a very low dispersity (PDI = 0.03) with a hydrodynamic diameter of 150 nm. Moreover, they were irradiated under UV light (365 nm) and the hydrophobic chain of SP-C9 became amphiphilic. Consequently, the micelles shrunk to a size of 47 nm (PDI = 0.05). Different species were successfully loaded in these micelles: rhodamine B, coumarin 6, cyanine 5 (Cy5), paclitaxel, docetaxel, proparacaine, and doxorubicin, up to 10 wt%. Particle shrinkage induced release of encapsulated species. Another major advantage of such particle shrinkage was demonstrated in this study: after UV irradiation, diffusion of the nanoparticles into collagen tissues increased due to their reduced sizes. Finally, the authors used the micelles to successfully deliver Cy5 into porcine cornea thanks to their reduced sizes after irradiation.

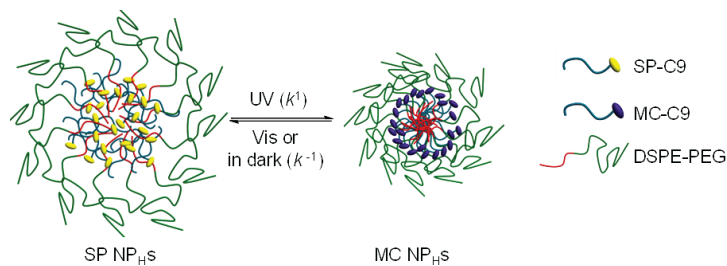


Fig. 21: Spiropyran hydrophilicity switch induces nanoparticle shrinkage [99].

1.2.2.2.2. Glass transition and melting induced release

Two intrinsic polymer properties are mainly controlling the species diffusion rate in a self-assembled polymer system: their glass transition (T_g) and melting (T_m) temperatures. The glass transition temperature is the temperature at which the polymer goes from an amorphous state (hard and brittle) to a rubbery or liquid viscous one. Melting temperature is the temperature at which the crystalline part of a polymer becomes liquid. These polymers can be associated with nanoheaters and the heat generated during the irradiation can increase the diffusion rate.

Poly(lactic-co-glycolic acid) (PLGA) is an amorphous polymer with a T_g above 37°C [138]. Above its T_g the polymer is softened and more permeable to species. An interesting example took advantage of the low T_g of PLGA. PLGA nanoparticles containing doxorubicin were formed thanks to nanoemulsion technique [139]. Gold nanospheres were fixed around the PLGA nanoparticles, an additional gold layer was added, resulting in PLGA loaded particles surrounded by a gold nanoshell with diameter of 80 nm (Fig. 22). Anti-EGFR (epithelial growth factor receptor) antibody (Cetuximab) was grafted on the gold nanoshell in order to target epithelial cancer cells. Irradiation with NIR laser (820 nm) increased the gold nanoshell temperature. The heat produced was transferred to the polymer matrix and rose its temperature above its T_g . As a consequence, the polymer matrix was softened and doxorubicin diffusion was accelerated compared to non-irradiated nanoparticles. These PLGA loaded doxorubicin nanoparticles with a gold nanoshell and antibody were then tested on cells. Nanoparticles showed a significantly greater affinity with cells expressing a high level of EGFR. In addition, irradiated cells with nanoparticles presented a 69.8% lower cell viability compared to non-irradiated cells with nanoparticles, showing the system efficacy. Another study used the same principle using PLGA loaded doxorubicin nanoparticles with a gold nanoshell and antibody [140]. In addition, these nanoparticles were tested on mice showing an active targeting of the

tumor. As a result, the tumor was completely destroyed thanks to both heat and delivered doxorubicin.

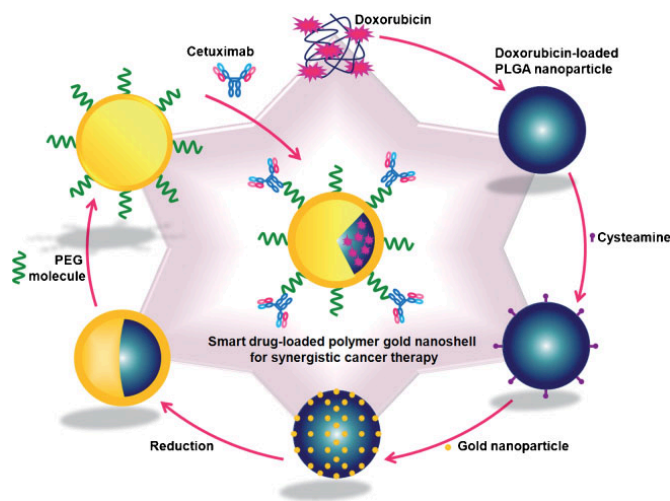


Fig. 22: PLGA surrounded with gold nanocarriers and NIR induced doxorubicin release [139].

Agarose gel was also used to release protein with visible light due to heating from gold nanospheres incorporated inside the gel (Fig. 23) [141]. In this example, gold nanospheres, with a diameter of 70 nm, were incorporated in a macroscopic agarose hydrogel loaded with bevacizumab, a protein used for its anti-angiogenic properties. Under visible light (400–500 nm) the gold nanospheres convert light energy into heat energy and transfer it to the hydrogel. The temperature increase induced a softening effect of the agarose gel and as a consequence increased the diffusion rate of the therapeutic protein. The softening effect is reversible, thus the system can be turned on and off for several cycles. This system was injected in bovine eyes and after visible light irradiation protein release was detected.

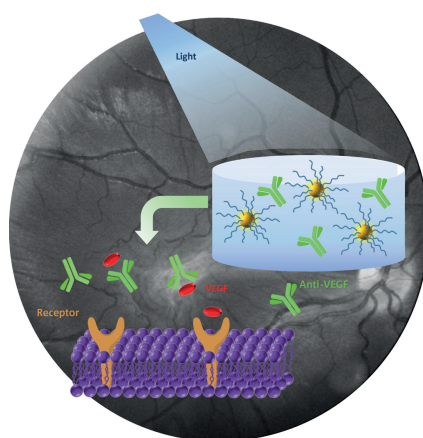


Fig. 23: Agarose gel releases protein under light stimulus [141].

Melting temperature is the second intrinsic parameter that can be used to increase the diffusion rate. In this case, two polymers are particularly well-adapted due to their low melting temperature and biocompatibility: PTMC and PCL, with melting temperatures of 37°C and 52°C, respectively [133]. To the best of our knowledge these polymers have not been used for light sensitive systems, even if a similar concept consisting in a local heating induced by magnetic hyperthermia has shown selective release of doxorubicin from PTMC based polymersomes [142].

1.2.3. Pore blocking / unblocking

One way to trigger release from nano-carriers is through pores, which offers a way for cells to release species [143]. This can be highly selective [144] and triggered with different stimuli, like light [97]. Forming or unblocking pores can be achieved via cleavage, isomerization, hydrophobicity switched molecules or nanoheaters.

In an example using isomerization for pore unblocking, azobenzene was used to open pore proteins in a cell membrane (Fig. 24). In this case the final study purpose was to control cellular chemistry. This example is detailed being an interesting proof-of-concept. An amino acid-sensitive membrane channel that opens in the presence of glutamate was used. The goal of this study is to be able to open the channel on demand thanks to light and to have a precise control of cellular chemistry in space and time. To do so, tetra-*ortho* substituted azobenzene was used because of its stability, red-light switching and its *cis*- to *trans*- thermal relaxation presented a relative long half-life at 37°C: 3.5 h. This azobenzene derivative was modified to bear one glutamate molecule on one extremity. The other extremity was used to graft the azobenzene derivative on the protein channel and two azobenzene derivatives were grafted on the protein channel. Without light, the azobenzene is in its *trans*- isomer form, glutamate is too far from the receptor to be activated and the channel remains closed. After UV or red-light irradiation the *trans*- isomer switched to the *cis*- isomer the glutamate gets closer to the receptor and activates it, resulting in its opening. Several wavelengths have been tested from 340 nm to 640 nm, and the systems shows responses up to 640 nm. The switching was reversible with blue light (440 nm) [97].

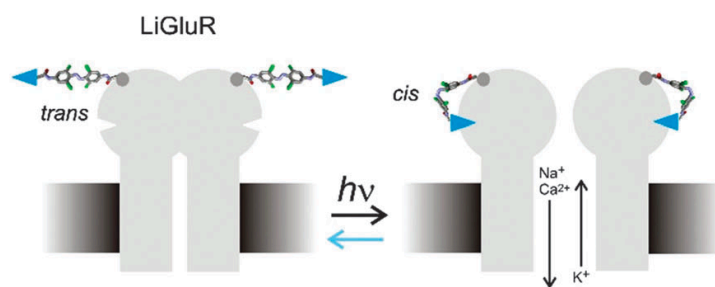


Fig. 24: Light induced azobenzene isomerization and pore opening [97].

In another example using azobenzene isomerization, mesoporous silica nanoparticles (MSNs) with length and width of 200 nm and 150 nm, whose pores were blocked with azobenzene and cyclodextrin, were used. The azobenzene has 4-methoxy substitutions to shift the isomerization wavelength to the red. Due to the azobenzene trans-form geometry, β -cyclodextrin can envelop this isomer and form a complex. The azobenzene was linked to pores, as a consequence, due to the presence of β -cyclodextrin and the resulting complex, pores were obstructed. An interesting property of this complex is that the cis- isomer of azobenzene can no longer form a complex with β -cyclodextrin, therefore under visible light (625 nm) the β -cyclodextrin is released from azobenzene cis- form and pores were unblocked. This mechanism allowed to release doxorubicin stuck inside the pores [98].

Besides isomerization, cleavage have been used to unblock pores for delivery applications. Ruthenium complexes ($[\text{Ru}(\text{bpy})_2(\text{PPh}_3)\text{Cl}]\text{Cl}$) were covalently linked to the MSN walls and obstructed the pores [79]. In this study, MSNs had diameters of 100-200 nm and their pores sizes were 2.2 nm. In addition, the ruthenium complex measured about 1.5 nm and was able to obstruct the MSNs pores. Under visible light (455 nm) the ruthenium complex was cleaved, released, the pores were opened and sulforhodamine 101 dye was released.

Additionally, polymer LCST have been used to unblock pores. As an example, stimuli-responsive pNIPAAm-co-pAAM was used to obstruct pores of gold nanocage [44] (Fig. 6). Gold nanocage sizes were around 50 nm and their pores on the edges measured between 5 nm and 10 nm. The pores were closed due to swollen pNIPAAm-co-pAAM covalently linked to the cage and the layer of copolymer at its swollen state had a thickness of 5 nm that was sufficient to obstruct the pores. As mentioned previously, pNIPAAm has a LCST around the body temperature. A Ti:sapphire laser was used to irradiate NIR on the gold nanocage-copolymer system. As a result, the gold nanocage increased the copolymer temperature, which consequently shrunk. The copolymer thickness was reduced, the pores were no longer obstructed and previously loaded doxorubicin was released.

An alternative to pore unblocking is to directly create pores in the carrier. To this end isomerization hydrophobicity / hydrophilicity switch molecules and nanoheaters have been used. As an example, azobenzene isomerization was used to induce pore formation. A cationic azobenzene derivative: 4-cholesterocarbonyl- 4'-(N,N,N-triethylamine butyloxyl bromide) azobenzene and surfactant sodium dodecyl sulfate were self-assembled into unilamellar and multilamellar vesicles with an average hydrodynamic diameter of 250 nm. The UV irradiation (365 nm) triggered azobenzene isomerization and increased the inter-lamellar spacing. This nano-structural changes in the membrane induced pores formation and doxorubicin release [145]. This system was tested on rat retinas and could efficiently release drug and maintain high level of drug concentration for 8 hours.

Equally spiropyran was used to create pores in the delivery system. For self-assembled particles such as polymersomes, hydrophobic blocks prevent the specie from leaving the payload carriers. A slight change in the hydrophilic balance of the block can induce a permeability increase without disturbing the payload carriers. This permeability change can be induced by a molecular hydrophobicity switch like spiropyran. In one article, spiropyran was grafted on an amphiphilic block copolymer PEG-*b*-PMMA using carbamate linkage: PEG-*b*-PSPA (Fig. 25). This copolymer was self-assembled into well-defined vesicles (70 nm or 450 nm depending on the block lengths and PDI<0.1). Irradiation with UV light (365 nm) induces switching of spiropyran incorporated in the vesicle membranes and conversion of the spiropyran into the hydrophilic merocyanine. This switch increased the membrane permeability without destabilizing it. The carbamate hydrogen bonding helped to maintain the structure, which was destabilized by a significant hydrophilicity change in the membrane. After irradiation, the vesicles released small hydrophilic molecules 2'-deoxy-5-fluorouridine an anticancer drugs [146]. Permeability change of the vesicle membrane was reversible under visible light (530 nm).

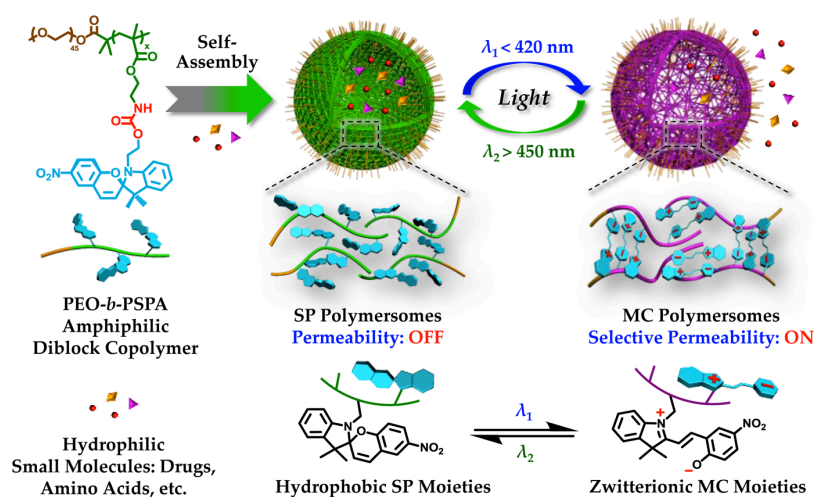


Fig. 25: PEG-b-PSPA self-assembled into light-sensitive polymersomes, whose permeability can be modulated under light irradiation using a spiropyran group [146].

Another group of particles made of gold sphere crosslinked together were used as a delivery systems [147]. Gold nanospheres (10 nm) were self-assembled and formed hollow spheres with an average hydrodynamic diameter of 65 nm. Then the gold nanospheres were crosslinked with a dithiol-PEG in order to increase the stability in water. Visible or NIR light (532 nm and 790 nm) irradiation induces a temperature increase of the gold nanospheres. As a consequence, the size of the nanogaps between the gold nanosphere increased from 2.5 nm to 4 nm while maintaining the hollow sphere structure thanks to the crosslinking. The difference of sizes with or without irradiation is enough to induce cargo leakage. The Rhodamine B dye and doxorubicin were loaded in the hollow spheres and under visible or NIR light, were released. Besides spiropyran, DASA was used as a hydrophobicity switch molecule to increase permeability in polymersome membranes under visible light irradiation. In a very recent example PEG was used as a macro chain transfer with RAFT radical polymerization to extend the chain with the hydrophobic monomers pentafluorophenyl methacrylate (PFPMA) and hexyl methacrylate (HMA) both randomly distributed [111]. The backbone was then modified to graft on the PFPMA two different DASA moiety: Meldrum's acid based furan adduct (MELD) and a novel five-membered ring pyrazolone-based furan adduct. As a result two different amphiphilic block copolymer were synthesized and can self-assemble into vesicles between 30 nm and 200 nm depending on the copolymer used. MELD and PYRA polymersomes showed fast hydrophilic switching kinetics, membrane permeability increase and dye release under irradiation with respectively green light ($\lambda_{em} = 525 \text{ nm}$) and red light ($\lambda_{em} = 630 \text{ nm}$). GOx and HRP enzymes were encapsulated separately in these polymersomes which are sensitive to two

different wavelengths.. On mixing together the nanoreactors cascade reactions activated by red and green light at the same time could be performed.

1.3. Conclusion

The development of innovative delivery systems, able to control the appropriate dose both spatially and temporally, is still very challenging. Long lasting delivery of molecular species and even macromolecules is rather well controlled, especially using biocompatible and biodegradable polymers. Indeed, many polymers and biopolymers have been designed over the past decades and are now widely used as biomaterials. Exogenous triggers are of particular interest as they can be activated on demand. Many different external stimuli have been developed, the most popular being temperature, magnetic/electric fields, hyperthermia, or ultrasound. In addition, light is attracting increasing attention and presents many advantages as a trigger for delivery systems. Its application is instantaneous, easy to control spatially and temporally, cheap to produce and non-invasive. The different molecular and physical mechanisms induced by light irradiation have been reviewed, that is, which molecules and systems are involved in light-sensitive delivery system and what is the effect of light on them. Thus, the different physical mechanisms are light energy converted into heat thanks to nanoheaters, upconversion, and the different molecular mechanisms involved are cleavage, isomerization and hydrophobicity / hydrophilicity switch. The property changes at the molecular level induced macromolecular effects on delivery system structure such as destabilization, shrinkage, permeabilization and pore opening. Several delivery applications have been successfully developed. Equally, nanoheaters such as gold nanoparticles combined with temperature responsive polymers such as pNIPAAm are an interesting and advanced approach. Light sensitive delivery systems have to face several challenges, such as reduced unwanted species leakage and control the encapsulation quantity, the most important being the design of efficient systems. This implies finding functional molecules with enhanced light absorption and quantum yield/efficiency of photoconversion and/or seeking different and less energy-demanding mechanisms to effect switching and consequently perturb the carrier.

References

- [1] L.J. Ignarro, Nitric oxide: biology and pathobiology, Academic press, 2000.
- [2] F. Murad, Discovery of some of the biological effects of nitric oxide and its role in cell signaling, *Biosci. Rep.* 24 (2004) 452–474. doi:10.1007/s10540-005-2741-8.
- [3] J. Lincoln, C.H.V. Hoyle, G. Burnstock, Nitric Oxide in Health and Disease, Cambridge University Press, Cambridge, 1997. <http://discovery.ucl.ac.uk/186320/> (accessed March 20, 2019).
- [4] A.L. Bianchi, M. Denavit-Saubie, J. Champagnat, Central control of breathing in mammals: neuronal circuitry, membrane properties, and neurotransmitters, *Physiol. Rev.* 75 (1995) 1–45. doi:10.1152/physrev.1995.75.1.1.
- [5] E. Clementi, The Contribution of Salvador Moncada to Our Understanding of the Biology of Nitric Oxide, *IUBMB Life.* 55 (2003) 563–565. doi:10.1080/15216540310001628664.
- [6] K.S. Christopherson, D.S. Bredt, Nitric oxide in excitable tissues: physiological roles and disease., *J. Clin. Invest.* 100 (1997) 2424–2429.
- [7] S.K. Choudhari, M. Chaudhary, S. Bagde, A.R. Gadbail, V. Joshi, Nitric oxide and cancer: a review, *World J. Surg. Oncol.* 11 (2013) 118. doi:10.1186/1477-7819-11-118.
- [8] C. Szabó, Multiple pathways of peroxynitrite cytotoxicity, *Toxicol. Lett.* 140–141 (2003) 105–112.
- [9] W.C. Sessa, eNOS at a glance, *J. Cell Sci.* 117 (2004) 2427–2429. doi:10.1242/jcs.01165.
- [10] I.N. Mungrue, D.S. Bredt, nNOS at a glance: implications for brain and brawn, *J. Cell Sci.* 117 (2004) 2627–2629. doi:10.1242/jcs.01187.
- [11] C.J. Lowenstein, E. Padalko, iNOS (NOS2) at a glance, *J. Cell Sci.* 117 (2004) 2865–2867. doi:10.1242/jcs.01166.
- [12] G. Werner-Felmayer, G. Golderer, E.R. Werner, P. Gröbner, H. Wachter, Pteridine biosynthesis and nitric oxide synthase in *Physarum polycephalum*, *Biochem. J.* 304 (Pt 1) (1994) 105–111.
- [13] B.R. Crane, J. Sudhamsu, B.A. Patel, Bacterial nitric oxide synthases, *Annu. Rev. Biochem.* 79 (2010) 445–470. doi:10.1146/annurev-biochem-062608-103436.
- [14] A. Martínez, Nitric oxide synthase in invertebrates, *Histochem. J.* 27 (1995) 770–776. doi:10.1007/BF02388302.
- [15] G.E. Nilsson, V. Söderström, Comparative aspects on nitric oxide in brain and its role as a cerebral vasodilator, *Comp. Biochem. Physiol. A Physiol.* 118 (1997) 949–958.
- [16] Q.W. Xie, H.J. Cho, J. Calaycay, R.A. Mumford, K.M. Swiderek, T.D. Lee, A. Ding, T. Troso, C. Nathan, Cloning and characterization of inducible nitric oxide synthase from mouse macrophages, *Science.* 256 (1992) 225–228.
- [17] J. Santolini, The molecular mechanism of mammalian NO-synthases: A story of electrons and protons, *J. Inorg. Biochem.* 105 (2011) 127–141. doi:10.1016/j.jinorgbio.2010.10.011.
- [18] B. Alberts, A. Johnson, J. Lewis, M. Raff, K. Roberts, P. Walter, *Molecular Biology of the Cell*, 4th ed., Garland Science, 2002.
- [19] S.M. Adl, A.G.B. Simpson, C.E. Lane, J. Lukeš, D. Bass, S.S. Bowser, M.W. Brown, F. Burki, M. Dunthorn, V. Hampl, A. Heiss, M. Hoppenrath, E. Lara, L. Le Gall, D.H. Lynn, H. McManus, E.A.D. Mitchell, S.E. Mozley-Stanridge, L.W. Parfrey, J. Pawlowski, S. Rueckert, L. Shadwick, L. Shadwick, C.L. Schoch, A. Smirnov, F.W. Spiegel, The revised classification of eukaryotes, *J. Eukaryot. Microbiol.* 59 (2012) 429–493. doi:10.1111/j.1550-7408.2012.00644.x.
- [20] Y. Tu, F. Peng, A. Adawy, Y. Men, L.K.E.A. Abdelmohsen, D.A. Wilson, Mimicking the Cell: Bio-Inspired Functions of Supramolecular Assemblies, *Chem. Rev.* 116 (2016) 2023–2078. doi:10.1021/acs.chemrev.5b00344.
- [21] C. Martino, S.-H. Kim, L. Horsfall, A. Abbaspourrad, S.J. Rosser, J. Cooper, D.A. Weitz, Protein Expression, Aggregation, and Triggered Release from Polymersomes as Artificial Cell-like Structures, *Angew. Chem.* 124 (2012) 6522–6526. doi:10.1002/ange.201201443.
- [22] L. Beauté, N. McClenaghan, S. Lecommandoux, Photo-triggered polymer nanomedicines: From molecular mechanisms to therapeutic applications, *Adv. Drug Deliv. Rev.* (2018).

-
- doi:10.1016/j.addr.2018.12.010.
- [23] S. Mura, J. Nicolas, P. Couvreur, Stimuli-responsive nanocarriers for drug delivery, *Nat. Mater.* 12 (2013) 991–1003. doi:10.1038/nmat3776.
- [24] X. Huang, P.K. Jain, I.H. El-Sayed, M.A. El-Sayed, Plasmonic photothermal therapy (PPTT) using gold nanoparticles, *Lasers Med. Sci.* 23 (2007) 217. doi:10.1007/s10103-007-0470-x.
- [25] H.H. Richardson, M.T. Carlson, P.J. Tandler, P. Hernandez, A.O. Govorov, Experimental and Theoretical Studies of Light-to-Heat Conversion and Collective Heating Effects in Metal Nanoparticle Solutions, *Nano Lett.* 9 (2009) 1139–1146. doi:10.1021/nl8036905.
- [26] S. Linic, U. Aslam, C. Boerigter, M. Morabito, Photochemical transformations on plasmonic metal nanoparticles, *Nat. Mater.* 14 (2015) 567–576. doi:10.1038/nmat4281.
- [27] C. Voisin, N. Del Fatti, D. Christofilos, F. Vallée, Ultrafast Electron Dynamics and Optical Nonlinearities in Metal Nanoparticles, *J. Phys. Chem. B.* 105 (2001) 2264–2280. doi:10.1021/jp0038153.
- [28] Y. Xia, Y. Xiong, B. Lim, S.E. Skrabalak, Shape-controlled synthesis of metal nanocrystals: simple chemistry meets complex physics?, *Angew. Chem. Int. Ed Engl.* 48 (2009) 60–103. doi:10.1002/anie.200802248.
- [29] J. Conde, G. Doria, P. Baptista, Noble Metal Nanoparticles Applications in Cancer, *J. Drug Deliv.* (2012). doi:10.1155/2012/751075.
- [30] G.P. Robbins, M. Jimbo, J. Swift, M.J. Therien, D.A. Hammer, I.J. Dmochowski, Photoinitiated Destruction of Composite Porphyrin–Protein Polymersomes, *J. Am. Chem. Soc.* 131 (2009) 3872–3874. doi:10.1021/ja808586q.
- [31] A. Suzuki, T. Tanaka, Phase transition in polymer gels induced by visible light, *Nature.* 346 (1990) 345–347. doi:10.1038/346345a0.
- [32] W. Yin, L. Yan, J. Yu, G. Tian, L. Zhou, X. Zheng, X. Zhang, Y. Yong, J. Li, Z. Gu, Y. Zhao, High-Throughput Synthesis of Single-Layer MoS₂ Nanosheets as a Near-Infrared Photothermal-Triggered Drug Delivery for Effective Cancer Therapy, *ACS Nano.* 8 (2014) 6922–6933. doi:10.1021/nn501647j.
- [33] B. Tian, C. Wang, S. Zhang, L. Feng, Z. Liu, Photothermally Enhanced Photodynamic Therapy Delivered by Nano-Graphene Oxide, *ACS Nano.* 5 (2011) 7000–7009. doi:10.1021/nn201560b.
- [34] K. Yang, L. Feng, Z. Liu, Stimuli responsive drug delivery systems based on nano-graphene for cancer therapy, *Adv. Drug Deliv. Rev.* 105 (2016) 228–241. doi:10.1016/j.addr.2016.05.015.
- [35] L. Gong, L. Yan, R. Zhou, J. Xie, W. Wu, Z. Gu, Two-dimensional transition metal dichalcogenide nanomaterials for combination cancer therapy, *J. Mater. Chem. B.* 5 (2017) 1873–1895. doi:10.1039/C7TB00195A.
- [36] Z. Su, S. Zhu, A.D. Donkor, C. Tzoganakis, J.F. Honek, Controllable Delivery of Small-Molecule Compounds to Targeted Cells Utilizing Carbon Nanotubes, *J. Am. Chem. Soc.* 133 (2011) 6874–6877. doi:10.1021/ja1084282.
- [37] M. Martincic, G. Tobias, Filled carbon nanotubes in biomedical imaging and drug delivery, *Expert Opin. Drug Deliv.* 12 (2015) 563–581. doi:10.1517/17425247.2015.971751.
- [38] X. Huang, W. Zhang, G. Guan, G. Song, R. Zou, J. Hu, Design and Functionalization of the NIR-Responsive Photothermal Semiconductor Nanomaterials for Cancer Theranostics, *Acc. Chem. Res.* 50 (2017) 2529–2538. doi:10.1021/acs.accounts.7b00294.
- [39] S. Huang, J. Liu, Q. He, H. Chen, J. Cui, S. Xu, Y. Zhao, C. Chen, L. Wang, Smart Cu 1.75S nanocapsules with high and stable photothermal efficiency for NIR photo-triggered drug release, *Nano Res.* 8 (2015) 4038–4047. doi:10.1007/s12274-015-0905-9.
- [40] N. Kamaly, Z. Xiao, P.M. Valencia, A.F. Radovic-Moreno, O.C. Farokhzad, Targeted polymeric therapeutic nanoparticles: design, development and clinical translation, *Chem. Soc. Rev.* 41 (2012) 2971–3010. doi:10.1039/c2cs15344k.
- [41] Y. Wu, K. Wang, S. Huang, C. Yang, M. Wang, Near-Infrared Light-Responsive Semiconductor Polymer Composite Hydrogels: Spatial/Temporal-Controlled Release via a Photothermal “Sponge” Effect, *ACS Appl. Mater. Interfaces.* 9 (2017) 13602–13610. doi:10.1021/acsami.7b01016.
- [42] A.M. Smith, M.C. Mancini, S. Nie, Bioimaging: Second window for *in vivo* imaging, *Nat. Nanotechnol.* 4 (2009) 710–711. doi:10.1038/nnano.2009.326.
- [43] Z. Cao, L. Feng, G. Zhang, J. Wang, S. Shen, D. Li, X. Yang, Semiconducting polymer-based
-

-
- nanoparticles with strong absorbance in NIR-II window for in vivo photothermal therapy and photoacoustic imaging, *Biomaterials*. 155 (2018) 103–111. doi:10.1016/j.biomaterials.2017.11.016.
- [44] M.S. Yavuz, Y. Cheng, J. Chen, C.M. Cobley, Q. Zhang, M. Rycenga, J. Xie, C. Kim, A.G. Schwartz, L.V. Wang, Y. Xia, Gold nanocages covered by smart polymers for controlled release with near-infrared light, *Nat. Mater.* 8 (2009) 935–939. doi:10.1038/nmat2564.
- [45] M.A. Ward, T.K. Georgiou, Thermoresponsive polymers for biomedical applications, *Polymers*. 3 (2011) 1215–1242.
- [46] M. Karimi, P. Sahandi Zangabad, A. Ghasemi, M. Amiri, M. Bahrami, H. Malekzad, H. Ghahramanzadeh Asl, Z. Mahdieh, M. Bozorgomid, A. Ghasemi, M.R. Rahmani Taji Boyuk, M.R. Hamblin, Temperature-Responsive Smart Nanocarriers for Delivery Of Therapeutic Agents: Applications and Recent Advances, *ACS Appl. Mater. Interfaces*. 8 (2016) 21107–21133. doi:10.1021/acsami.6b00371.
- [47] S.R. Sershen, S.L. Westcott, N.J. Halas, J.L. West, Temperature-sensitive polymer–nanoshell composites for photothermally modulated drug delivery, *J. Biomed. Mater. Res.* 51 (2000) 293–298. doi:10.1002/1097-4636(20000905)51:3<293::AID-JBM1>3.0.CO;2-T.
- [48] F. Wang, D. Banerjee, Y. Liu, X. Chen, X. Liu, Upconversion nanoparticles in biological labeling, imaging, and therapy, *Analyst*. 135 (2010) 1839–1854. doi:10.1039/C0AN00144A.
- [49] G. Chen, H. Qiu, P.N. Prasad, X. Chen, Upconversion Nanoparticles: Design, Nanochemistry, and Applications in Theranostics, *Chem. Rev.* 114 (2014) 5161–5214. doi:10.1021/cr400425h.
- [50] X. Li, F. Zhang, D. Zhao, Lab on upconversion nanoparticles: optical properties and applications engineering via designed nanostructure, *Chem. Soc. Rev.* 44 (2015) 1346–1378. doi:10.1039/C4CS00163J.
- [51] B. Yan, J.-C. Boyer, N.R. Branda, Y. Zhao, Near-Infrared Light-Triggered Dissociation of Block Copolymer Micelles Using Upconverting Nanoparticles, *J. Am. Chem. Soc.* 133 (2011) 19714–19717. doi:10.1021/ja209793b.
- [52] S. Chen, Y. Gao, Z. Cao, B. Wu, L. Wang, H. Wang, Z. Dang, G. Wang, Nanocomposites of Spiropyran-Functionalized Polymers and Upconversion Nanoparticles for Controlled Release Stimulated by Near-Infrared Light and pH, *Macromolecules*. 49 (2016) 7490–7496. doi:10.1021/acs.macromol.6b01760.
- [53] G. Jalani, R. Naccache, D.H. Rosenzweig, L. Haglund, F. Vetrone, M. Cerruti, Photocleavable hydrogel coated upconverting nanoparticles: a multifunctional theranostic platform for NIR imaging and on-demand macromolecular delivery, *J. Am. Chem. Soc.* (2015). doi:10.1021/jacs.5b12357.
- [54] P. Klán, T. Šolomek, C.G. Bochet, A. Blanc, R. Givens, M. Rubina, V. Popik, A. Kostikov, J. Wirz, Photoremovable Protecting Groups in Chemistry and Biology: Reaction Mechanisms and Efficacy, *Chem. Rev.* 113 (2013) 119–191. doi:10.1021/cr300177k.
- [55] B. Schade, V. Hagen, R. Schmidt, R. Herbrich, E. Krause, T. Eckardt, J. Bendig, Deactivation Behavior and Excited-State Properties of (Coumarin-4-yl)methyl Derivatives. 1. Photocleavage of (7-Methoxycoumarin-4-yl)methyl-Caged Acids with Fluorescence Enhancement, *J. Org. Chem.* 64 (1999) 9109–9117. doi:10.1021/jo9910233.
- [56] P. Pitter, Determination of biological degradability of organic substances, *Water Res.* 10 (1976) 231–235. doi:10.1016/0043-1354(76)90132-9.
- [57] S. des experts-chimistes de France, *Annales des falsifications, de l'expertise chimique et toxicologique*, La Société, 1983.
- [58] X. Hu, J. Tian, T. Liu, G. Zhang, S. Liu, Photo-Triggered Release of Caged Camptothecin Prodrugs from Dually Responsive Shell Cross-Linked Micelles, *Macromolecules*. 46 (2013) 6243–6256. doi:10.1021/ma400691j.
- [59] Z. Zhang, H. Hatta, T. Ito, S. Nishimoto, Synthesis and photochemical properties of photoactivated antitumor prodrugs releasing 5-fluorouracil, *Org. Biomol. Chem.* 3 (2005) 592–596. doi:10.1039/B417734G.
- [60] C. Wang, G. Zhang, G. Liu, J. Hu, S. Liu, Photo- and thermo-responsive multicompartement hydrogels for synergistic delivery of gemcitabine and doxorubicin, *J. Controlled Release*. 259 (2017) 149–159. doi:10.1016/j.jconrel.2016.11.007.
- [61] W.-J. Zhang, C.-Y. Hong, C.-Y. Pan, Efficient Fabrication of Photosensitive Polymeric Nano-
-

-
- objects via an Ingenious Formulation of RAFT Dispersion Polymerization and Their Application for Drug Delivery, *Biomacromolecules*. 18 (2017) 1210–1217. doi:10.1021/acs.biomac.6b01887.
- [62] G. Liu, X. Wang, J. Hu, G. Zhang, S. Liu, Self-Immolative Polymersomes for High-Efficiency Triggered Release and Programmed Enzymatic Reactions, *J. Am. Chem. Soc.* 136 (2014) 7492–7497. doi:10.1021/ja5030832.
- [63] M. Álvarez, J.M. Alonso, O. Filevich, M. Bhagawati, R. Etchenique, J. Piehler, A. del Campo, Modulating Surface Density of Proteins via Caged Surfaces and Controlled Light Exposure, *Langmuir*. 27 (2011) 2789–2795. doi:10.1021/la104511x.
- [64] A. Specht, M. Goeldner, 1-(o-Nitrophenyl)-2,2,2-trifluoroethyl Ether Derivatives as Stable and Efficient Photoremovable Alcohol-Protecting Groups, *Angew. Chem. Int. Ed.* 43 (2004) 2008–2012. doi:10.1002/anie.200353247.
- [65] E. Reichmanis, B.C. Smith, R. Gooden, O-nitrobenzyl photochemistry: Solution vs. solid-state behavior, *J. Polym. Sci. Polym. Chem. Ed.* 23 (1985) 1–8. doi:10.1002/pol.1985.170230101.
- [66] R.E. Kohman, S.S. Cha, H.-Y. Man, X. Han, Light-Triggered Release of Bioactive Molecules from DNA Nanostructures, *Nano Lett.* 16 (2016) 2781–2785. doi:10.1021/acs.nanolett.6b00530.
- [67] M.M. Mahmoodi, D. Abate-Pella, T.J. Pundsack, C.C. Palsuledesai, P.C. Goff, D.A. Blank, M.D. Distefano, Nitrodibenzofuran: A One- and Two-Photon Sensitive Protecting Group That Is Superior to Brominated Hydroxycoumarin for Thiol Caging in Peptides, *J. Am. Chem. Soc.* 138 (2016) 5848–5859. doi:10.1021/jacs.5b11759.
- [68] K.A. Mosiewicz, L. Kolb, A.J. van der Vlies, M.M. Martino, P.S. Lienemann, J.A. Hubbell, M. Ehrbar, M.P. Lutolf, In situ cell manipulation through enzymatic hydrogel photopatterning, *Nat. Mater.* 12 (2013) 1072–1078. doi:10.1038/nmat3766.
- [69] N. Kretschy, A.-K. Holik, V. Somoza, K.-P. Stengele, M.M. Somoza, Next-Generation o-Nitrobenzyl Photolabile Groups for Light-Directed Chemistry and Microarray Synthesis, *Angew. Chem. Int. Ed.* 54 (2015) 8555–8559. doi:10.1002/anie.201502125.
- [70] G.J. Finn, B. Creaven, D.A. Egan, Study of the in vitro cytotoxic potential of natural and synthetic coumarin derivatives using human normal and neoplastic skin cell lines, *Melanoma Res.* 11 (2001) 461.
- [71] K.C. Fylaktakidou, D.J. Hadjipavlou-Litina, K.E. Litinas, D.N. Nicolaides, Natural and Synthetic Coumarin Derivatives with Anti-Inflammatory / Antioxidant Activities, (2004). doi:info:doi/10.2174/1381612043382710.
- [72] W.A. Velema, J.P. van der Berg, W. Szymanski, A.J.M. Driessen, B.L. Feringa, Orthogonal Control of Antibacterial Activity with Light, *ACS Chem. Biol.* 9 (2014) 1969–1974. doi:10.1021/cb500313f.
- [73] Q. Huang, C. Bao, W. Ji, Q. Wang, L. Zhu, Photocleavable coumarin crosslinkers based polystyrene microgels: phototriggered swelling and release, *J. Mater. Chem.* 22 (2012) 18275–18282. doi:10.1039/C2JM33789D.
- [74] W. Ji, N. Li, D. Chen, X. Qi, W. Sha, Y. Jiao, Q. Xu, J. Lu, Coumarin-containing photo-responsive nanocomposites for NIR light-triggered controlled drug release via a two-photon process, *J. Mater. Chem. B.* 1 (2013) 5942–5949. doi:10.1039/C3TB21206H.
- [75] C. Hang, Y. Zou, Y. Zhong, Z. Zhong, F. Meng, NIR and UV-responsive degradable hyaluronic acid nanogels for CD44-targeted and remotely triggered intracellular doxorubicin delivery, *Colloids Surf. B Biointerfaces.* 158 (2017) 547–555. doi:10.1016/j.colsurfb.2017.07.041.
- [76] L. Fournier, I. Aujard, T. Le Saux, S. Maurin, S. Beaupierre, J.-B. Baudin, L. Jullien, Coumarinylmethyl Caging Groups with Redshifted Absorption, *Chem. – Eur. J.* 19 (2013) 17494–17507. doi:10.1002/chem.201302630.
- [77] S. Karthik, A. Jana, M. Selvakumar, Y. Venkatesh, A. Paul, S.S. Shah, N.D.P. Singh, Coumarin polycaprolactone polymeric nanoparticles: light and tumor microenvironment activated cocktail drug delivery, *J. Mater. Chem. B.* 5 (2017) 1734–1741. doi:10.1039/C6TB02944B.
- [78] L. Zayat, M.G. Noval, J. Campi, C.I. Calero, D.J. Calvo, R. Etchenique, A New Inorganic Photolabile Protecting Group for Highly Efficient Visible Light GABA Uncaging, *ChemBioChem.* 8 (2007) 2035–2038. doi:10.1002/cbic.200700354.
- [79] N.Z. Knezevic, B.G. Trewyn, V.S.-Y. Lin, Functionalized mesoporous silica nanoparticle-based
-

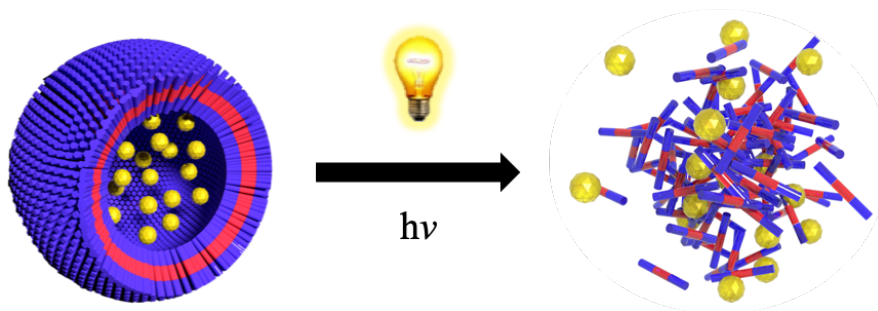
-
- visible light responsive controlled release delivery system, *Chem. Commun.* 47 (2011) 2817–2819. doi:10.1039/C0CC04424E.
- [80] W. Sun, M. Parowatkin, W. Steffen, H.-J. Butt, V. Mailänder, S. Wu, Ruthenium-Containing Block Copolymer Assemblies: Red-Light-Responsive Metallopolymers with Tunable Nanostructures for Enhanced Cellular Uptake and Anticancer Phototherapy, *Adv. Healthc. Mater.* 5 (2016) 467–473. doi:10.1002/adhm.201500827.
- [81] T. Slanina, P. Shrestha, E. Palao, D. Kand, J.A. Peterson, A.S. Dutton, N. Rubinstein, R. Weinstain, A.H. Winter, P. Klán, In Search of the Perfect Photocage: Structure–Reactivity Relationships in meso-Methyl BODIPY Photoremovable Protecting Groups, *J. Am. Chem. Soc.* 139 (2017) 15168–15175. doi:10.1021/jacs.7b08532.
- [82] P.P. Goswami, A. Syed, C.L. Beck, T.R. Albright, K.M. Mahoney, R. Unash, E.A. Smith, A.H. Winter, BODIPY-Derived Photoremovable Protecting Groups Unmasked with Green Light, *J. Am. Chem. Soc.* 137 (2015) 3783–3786. doi:10.1021/jacs.5b01297.
- [83] J. Jiang, X. Tong, Y. Zhao, A New Design for Light-Breakable Polymer Micelles, *J. Am. Chem. Soc.* 127 (2005) 8290–8291. doi:10.1021/ja0521019.
- [84] T. Furuta, H. Torigai, T. Osawa, M. Iwamura, New photochemically labile protecting group for phosphates, *Chem. Lett.* 22 (1993) 1179–1182.
- [85] H. Du, R.-C.A. Fuh, J. Li, L.A. Corkan, J.S. Lindsey, PhotochemCAD: A Computer-Aided Design and Research Tool in Photochemistry, *Photochem. Photobiol.* 68 (1998) 141–142. doi:10.1111/j.1751-1097.1998.tb02480.x.
- [86] A. Jana, M. Iqbal, N.D.P. Singh, Perylen-3-ylmethyl: fluorescent photoremovable protecting group (FPRPG) for carboxylic acids and alcohols, *Tetrahedron.* 68 (2012) 1128–1136. doi:10.1016/j.tet.2011.11.074.
- [87] M.A. Ayer, S. Schrettl, S. Balog, Y.C. Simon, C. Weder, Light-responsive azo-containing organogels, *Soft Matter.* 13 (2017) 4017–4023. doi:10.1039/C7SM00601B.
- [88] C.-J. Carling, J. Olejniczak, A. Foucault-Collet, G. Collet, M.L. Viger, V.A.N. Huu, B.M. Duggan, A. Almutairi, Efficient red light photo-uncaging of active molecules in water upon assembly into nanoparticles, *Chem. Sci.* 7 (2016) 2392–2398. doi:10.1039/C5SC03717D.
- [89] J. Broichhagen, J.A. Frank, D. Trauner, A Roadmap to Success in Photopharmacology, *Acc. Chem. Res.* 48 (2015) 1947–1960. doi:10.1021/acs.accounts.5b00129.
- [90] G.S. Hartley, The Cis-form of Azobenzene, *Nature.* 140 (1937) 281. doi:10.1038/140281a0.
- [91] D. Bléger, J. Schwarz, A.M. Brouwer, S. Hecht, o-Fluoroazobenzenes as Readily Synthesized Photoswitches Offering Nearly Quantitative Two-Way Isomerization with Visible Light, *J. Am. Chem. Soc.* 134 (2012) 20597–20600. doi:10.1021/ja310323y.
- [92] S. Subhas, B. Amirhossein, D. Ming-xin, W.G. Andrew, Photoswitching of ortho-Substituted Azonium Ions by Red Light in Whole Blood, *Angew. Chem. Int. Ed.* 52 (2013) 14127–14130.
- [93] S. Samanta, A.A. Beharry, O. Sadvovskii, T.M. McCormick, A. Babalhavaeji, V. Tropepe, G.A. Woolley, Photoswitching Azo Compounds in Vivo with Red Light, *J. Am. Chem. Soc.* 135 (2013) 9777–9784. doi:10.1021/ja402220t.
- [94] M. Dong, A. Babalhavaeji, S. Samanta, A.A. Beharry, G.A. Woolley, Red-Shifting Azobenzene Photoswitches for in Vivo Use, *Acc. Chem. Res.* 48 (2015) 2662–2670. doi:10.1021/acs.accounts.5b00270.
- [95] E. Mabrouk, D. Cuvelier, F. Brochard-Wyart, P. Nassoy, M.-H. Li, Bursting of sensitive polymersomes induced by curling, *Proc. Natl. Acad. Sci.* 106 (2009) 7294–7298. doi:10.1073/pnas.0813157106.
- [96] O. Sadvovskii, A.A. Beharry, F. Zhang, G.A. Woolley, Spectral Tuning of Azobenzene Photoswitches for Biological Applications, *Angew. Chem. Int. Ed.* 48 (2009) 1484–1486. doi:10.1002/anie.200805013.
- [97] A. Rullo, A. Reiner, A. Reiter, D. Trauner, E.Y. Isacoff, G.A. Woolley, Long wavelength optical control of glutamate receptor ion channels using a tetra-ortho-substituted azobenzene derivative, *Chem. Commun.* 50 (2014) 14613–14615. doi:10.1039/C4CC06612J.
- [98] D. Wang, S. Wu, Red-Light-Responsive Supramolecular Valves for Photocontrolled Drug Release from Mesoporous Nanoparticles, *Langmuir.* 32 (2016) 632–636. doi:10.1021/acs.langmuir.5b04399.
- [99] R. Tong, H.D. Hemmati, R. Langer, D.S. Kohane, Photoswitchable Nanoparticles for Triggered
-

-
- Tissue Penetration and Drug Delivery, *J. Am. Chem. Soc.* 134 (2012) 8848–8855. doi:10.1021/ja211888a.
- [100] A.P. Goodwin, J.L. Mynar, Y. Ma, G.R. Fleming, J.M.J. Fréchet, Synthetic Micelle Sensitive to IR Light via a Two-Photon Process, *J. Am. Chem. Soc.* 127 (2005) 9952–9953. doi:10.1021/ja0523035.
- [101] Q. Li, Z. Cao, G. Wang, Diazonaphthoquinone-based amphiphilic polymer assemblies for NIR/UV light- and pH-responsive controlled release, *Polym. Chem.* 9 (2018) 463–471. doi:10.1039/C7PY01822C.
- [102] S. Helmy, F.A. Leibfarth, S. Oh, J.E. Poelma, C.J. Hawker, J. Read de Alaniz, Photoswitching Using Visible Light: A New Class of Organic Photochromic Molecules, *J. Am. Chem. Soc.* 136 (2014) 8169–8172. doi:10.1021/ja503016b.
- [103] S.O. Poelma, S.S. Oh, S. Helmy, A.S. Knight, G.L. Burnett, H.T. Soh, C.J. Hawker, J.R. de Alaniz, Controlled drug release to cancer cells from modular one-photon visible light-responsive micellar system, *Chem. Commun.* 52 (2016) 10525–10528. doi:10.1039/C6CC04127B.
- [104] G.-Y. Liu, C.-J. Chen, D.-D. Li, S.-S. Wang, J. Ji, Near-infrared light-sensitive micelles for enhanced intracellular drug delivery, *J. Mater. Chem.* 22 (2012) 16865–16871. doi:10.1039/C2JM00045H.
- [105] S. Son, E. Shin, B.-S. Kim, Light-Responsive Micelles of Spiropyran Initiated Hyperbranched Polyglycerol for Smart Drug Delivery, *Biomacromolecules.* 15 (2014) 628–634. doi:10.1021/bm401670t.
- [106] C. Chen, G. Liu, X. Liu, S. Pang, C. Zhu, L. Lv, J. Ji, Photo-responsive, biocompatible polymeric micelles self-assembled from hyperbranched polyphosphate-based polymers, *Polym. Chem.* 2 (2011) 1389–1397. doi:10.1039/C1PY00094B.
- [107] R. Klajn, Spiropyran-based dynamic materials, *Chem. Soc. Rev.* 43 (2013) 148–184. doi:10.1039/C3CS60181A.
- [108] L. Sun, B. Zhu, Y. Su, C.-M. Dong, Light-responsive linear-dendritic amphiphiles and their nanomedicines for NIR-triggered drug release, *Polym. Chem.* 5 (2014) 1605–1613. doi:10.1039/C3PY00533J.
- [109] W. Kirmse, 100 Years of the Wolff Rearrangement, *Eur. J. Org. Chem.* 2002 (2002) 2193–2256. doi:10.1002/1099-0690(200207)2002:14<2193::AID-EJOC2193>3.0.CO;2-D.
- [110] J.I.K. Almstead, B. Urwyler, J. Wirz, Flash Photolysis of .alpha.-Diazonaphthoquinones in Aqueous Solution: Determination of Rates and Equilibria for Keto-Enol Tautomerization of 1-Indene-3-carboxylic Acid, *J. Am. Chem. Soc.* 116 (1994) 954–960. doi:10.1021/ja00082a016.
- [111] O. Rifaie-Graham, S. Ulrich, N.F.B. Galensowske, S. Balog, M. Chami, D. Rentsch, J.R. Hemmer, J.R. de Alaniz, L.F. Boesel, N. Bruns, Wavelength-Selective Light-Responsive DASA-Functionalized Polymersome Nanoreactors, *J. Am. Chem. Soc.* (2018). doi:10.1021/jacs.8b04511.
- [112] J. Jiang, B. Qi, M. Lepage, Y. Zhao, Polymer Micelles Stabilization on Demand through Reversible Photo-Cross-Linking, *Macromolecules.* 40 (2007) 790–792. doi:10.1021/ma062493j.
- [113] S.R. Trenor, A.R. Shultz, B.J. Love, T.E. Long, Coumarins in Polymers: From Light Harvesting to Photo-Cross-Linkable Tissue Scaffolds, *Chem. Rev.* 104 (2004) 3059–3078. doi:10.1021/cr030037c.
- [114] M.V.S.N. Maddipatla, D. Wehrung, C. Tang, W. Fan, M.O. Oyewumi, T. Miyoshi, A. Joy, Photoresponsive Coumarin Polyesters That Exhibit Cross-Linking and Chain Scission Properties, *Macromolecules.* 46 (2013) 5133–5140. doi:10.1021/ma400584y.
- [115] Y. Zheng, F.M. Andreopoulos, M. Micic, Q. Huo, S.M. Pham, R.M. Leblanc, A Novel Photoscissile Poly(ethylene glycol)-Based Hydrogel, *Adv. Funct. Mater.* 11 (2001) 37–40. doi:10.1002/1616-3028(200102)11:1<37::AID-ADFM37>3.0.CO;2-V.
- [116] Y. Sako, Y. Takaguchi, A photo-responsive hydrogelator having gluconamides at its peripheral branches, *Org. Biomol. Chem.* 6 (2008) 3843–3847. doi:10.1039/B810900A.
- [117] C. Zhu, C.J. Bettinger, Light-induced remodeling of physically crosslinked hydrogels using near-IR wavelengths, *J. Mater. Chem. B.* 2 (2014) 1613–1618. doi:10.1039/C3TB21689F.
- [118] T. Nishimura, M. Takara, S. Mukai, S. Sawada, Y. Sasaki, K. Akiyoshi, A light sensitive self-assembled nanogel as a tecton for protein patterning materials, *Chem. Commun.* 52 (2016)
-

-
- 1222–1225. doi:10.1039/C5CC08416D.
- [119] M.A. Azagarsamy, D.D. McKinnon, D.L. Alge, K.S. Anseth, Coumarin-Based Photodegradable Hydrogel: Design, Synthesis, Gelation, and Degradation Kinetics, *ACS Macro Lett.* 3 (2014) 515–519. doi:10.1021/mz500230p.
- [120] D. Klinger, K. Landfester, Dual Stimuli-Responsive Poly(2-hydroxyethyl methacrylate-co-methacrylic acid) Microgels Based on Photo-Cleavable Cross-Linkers: pH-Dependent Swelling and Light-Induced Degradation, *Macromolecules.* 44 (2011) 9758–9772. doi:10.1021/ma201706r.
- [121] B.M. Discher, Y.Y. Won, D.S. Ege, J.C. Lee, F.S. Bates, D.E. Discher, D.A. Hammer, Polymersomes: tough vesicles made from diblock copolymers, *Science.* 284 (1999) 1143–1146.
- [122] A. Blanazs, J. Madsen, G. Battaglia, A.J. Ryan, S.P. Armes, Mechanistic Insights for Block Copolymer Morphologies: How Do Worms Form Vesicles?, *J. Am. Chem. Soc.* 133 (2011) 16581–16587. doi:10.1021/ja206301a.
- [123] E. Cabane, V. Malinova, W. Meier, Synthesis of Photocleavable Amphiphilic Block Copolymers: Toward the Design of Photosensitive Nanocarriers, *Macromol. Chem. Phys.* 211 (2010) 1847–1856. doi:10.1002/macp.201000151.
- [124] S. Chen, F. Jiang, Z. Cao, G. Wang, Z.-M. Dang, Photo, pH, and thermo triple-responsive spiropyran-based copolymer nanoparticles for controlled release, *Chem. Commun.* 51 (2015) 12633–12636. doi:10.1039/C5CC04087F.
- [125] Y. Xue, J. Tian, W. Tian, P. Gong, J. Dai, X. Wang, Significant Fluorescence Enhancement of Spiropyran in Colloidal Dispersion and Its Light-Induced Size Tunability for Release Control, *J. Phys. Chem. C.* 119 (2015) 20762–20772. doi:10.1021/acs.jpcc.5b06905.
- [126] Y. Zhao, Photocontrollable block copolymer micelles: what can we control?, *J. Mater. Chem.* 19 (2009) 4887–4895. doi:10.1039/B819968J.
- [127] G. Wang, X. Tong, Y. Zhao, Preparation of Azobenzene-Containing Amphiphilic Diblock Copolymers for Light-Responsive Micellar Aggregates, *Macromolecules.* 37 (2004) 8911–8917. doi:10.1021/ma048416a.
- [128] S. Pautot, B.J. Frisken, D.A. Weitz, Engineering asymmetric vesicles, *Proc. Natl. Acad. Sci.* 100 (2003) 10718–10721. doi:10.1073/pnas.1931005100.
- [129] Peyret Ariane, Ibarboure Emmanuel, Tron Arnaud, Beauté Louis, Rust Ruben, Sandre Olivier, McClenaghan Nathan D., Lecommandoux Sebastien, Polymersome Popping by Light-Induced Osmotic Shock under Temporal, Spatial, and Spectral Control, *Angew. Chem. Int. Ed.* 56 (2017) 1566–1570. doi:10.1002/anie.201609231.
- [130] R.T. Chacko, J. Ventura, J. Zhuang, S. Thayumanavan, Polymer nanogels: A versatile nanoscopic drug delivery platform, *Adv. Drug Deliv. Rev.* 64 (2012) 836–851. doi:10.1016/j.addr.2012.02.002.
- [131] Q. Huang, C. Bao, W. Ji, Q. Wang, L. Zhu, Photocleavable coumarin crosslinkers based polystyrene microgels: phototriggered swelling and release, *J. Mater. Chem.* 22 (2012) 18275–18282. doi:10.1039/C2JM33789D.
- [132] B.A. Badeau, M.P. Comerford, C.K. Arakawa, J.A. Shadish, C.A. DeForest, Engineered modular biomaterial logic gates for environmentally triggered therapeutic delivery, *Nat. Chem.* 10 (2018) 251–258. doi:10.1038/nchem.2917.
- [133] S. Hocine, M.-H. Li, Thermoresponsive self-assembled polymer colloids in water, *Soft Matter.* 9 (2013) 5839–5861. doi:10.1039/C3SM50428J.
- [134] D. Roy, W.L.A. Brooks, B.S. Sumerlin, New directions in thermoresponsive polymers, *Chem. Soc. Rev.* 42 (2013) 7214–7243. doi:10.1039/C3CS35499G.
- [135] W. Agut, A. Brûlet, D. Taton, S. Lecommandoux, Thermoresponsive Micelles from Jeffamine-b-poly(l-glutamic acid) Double Hydrophilic Block Copolymers, *Langmuir.* 23 (2007) 11526–11533. doi:10.1021/la701482w.
- [136] Garanger Elisabeth, Lecommandoux Sébastien, Towards Bioactive Nanovehicles Based on Protein Polymers, *Angew. Chem. Int. Ed.* 51 (2012) 3060–3062. doi:10.1002/anie.201107734.
- [137] M. Beijs, J.-D. Marty, M. Destarac, Thermoresponsive poly(N-vinyl caprolactam)-coated gold nanoparticles: sharp reversible response and easy tunability, *Chem. Commun.* 47 (2011) 2826–2828. doi:10.1039/C0CC05184E.
- [138] H.K. Makadia, S.J. Siegel, Poly Lactic-co-Glycolic Acid (PLGA) as Biodegradable Controlled
-

-
- Drug Delivery Carrier, *Polymers*. 3 (2011) 1377–1397. doi:10.3390/polym3031377.
- [139] J. Yang, J. Lee, J. Kang, S.J. Oh, H.-J. Ko, J.-H. Son, K. Lee, J.-S. Suh, Y.-M. Huh, S. Haam, Smart Drug-Loaded Polymer Gold Nanoshells for Systemic and Localized Therapy of Human Epithelial Cancer, *Adv. Mater.* 21 (2009) 4339–4342. doi:10.1002/adma.200900334.
- [140] S.-M. Lee, H. Park, J.-W. Choi, Y.N. Park, C.-O. Yun, K.-H. Yoo, Multifunctional Nanoparticles for Targeted Chemophotothermal Treatment of Cancer Cells, *Angew. Chem. Int. Ed.* 50 (2011) 7581–7586. doi:10.1002/anie.201101783.
- [141] Basuki Johan S., Qie Fengxiang, Mulet Xavier, Suryadinata Randy, Vashi Aditya V., Peng Yong Y., Li Lingli, Hao Xiaojuan, Tan Tianwei, Hughes Timothy C., Photo-Modulated Therapeutic Protein Release from a Hydrogel Depot Using Visible Light, *Angew. Chem.* 129 (2016) 986–991. doi:10.1002/ange.201610618.
- [142] C. Sanson, O. Diou, J. Thevenot, E. Ibarboure, A. Soum, A. Brûlet, S. Miraux, E. Thiaudière, S. Tan, A. Brisson, V. Dupuis, O. Sandre, S. Lecommandoux, Doxorubicin Loaded Magnetic Polymersomes: Theranostic Nanocarriers for MR Imaging and Magneto-Chemotherapy, *LLB Highlights* 2011. (2012) 48–49.
- [143] T. Trantidou, M. Friddin, Y. Elani, N.J. Brooks, R.V. Law, J.M. Seddon, O. Ces, Engineering Compartmentalized Biomimetic Micro- and Nanocontainers, *ACS Nano*. 11 (2017) 6549–6565. doi:10.1021/acsnano.7b03245.
- [144] P. Shrager, S.Y. Chiu, J.M. Ritchie, Voltage-dependent sodium and potassium channels in mammalian cultured Schwann cells, *Proc. Natl. Acad. Sci.* 82 (1985) 948–952.
- [145] S. Geng, Y. Wang, L. Wang, T. Kouyama, T. Gotoh, S. Wada, J.-Y. Wang, A Light-Responsive Self-Assembly Formed by a Cationic Azobenzene Derivative and SDS as a Drug Delivery System, *Sci. Rep.* 7 (2017) 39202. doi:10.1038/srep39202.
- [146] X. Wang, J. Hu, G. Liu, J. Tian, H. Wang, M. Gong, S. Liu, Reversibly Switching Bilayer Permeability and Release Modules of Photochromic Polymersomes Stabilized by Cooperative Noncovalent Interactions, *J. Am. Chem. Soc.* 137 (2015) 15262–15275. doi:10.1021/jacs.5b10127.
- [147] K. Niikura, N. Iyo, Y. Matsuo, H. Mitomo, K. Ijio, Sub-100 nm gold nanoparticle vesicles as a drug delivery carrier enabling rapid drug release upon light irradiation, *ACS Appl. Mater. Interfaces*. 5 (2013) 3900–3907. doi:10.1021/am400590m.

Chapter 2: **Light-sensitive Nano- polymersomes**



2. Light-sensitive Nano-polymerosomes

2.1. Introduction

Cells are extraordinary bio-machines [1] that can process complex synthesis with a high level of control. As an example, synthesis of complex molecules, intricate processes or cascade biochemical reactions can be performed in cells [2]. All these reactions can be performed with a high level of control in space and time. Mimicking some cellular functions would afford access to these complex processes. To do so, scientists have been interested in designing microreactors in order to mimic the simplest cellular functions such as enzyme synthesis of molecules in a confined space [3]. This work aims to lay the foundation for temporal and spatial control of enzyme function by controlling substrate release. Polymerosomes are ideal candidates to tackle this challenge. Indeed, they have a thick membrane which reduces uncontrolled release, they are relatively more stable than liposomes, and a wide variety of copolymers can be used and tuned to form polymerosomes with appropriate properties [4]. Light was chosen as an exogenous stimulus, because its application is instantaneous, it is easy to control spatially and temporally, cheap to produce, non-invasive and the variety of light sensitive molecules is tremendous [5]. The different physical mechanisms induced by light irradiation, are light energy converted into heat via nanoheaters, upconversion, and the different molecular mechanisms involved are cleavage, isomerization and hydrophobicity / hydrophilicity switch. Property changes at the molecular level induced macromolecular effects on polymerosome structure, such as destabilization, shrinkage, permeabilization and pore opening [5]. The strategy presented in this chapter to effect controlled release is to destabilize polymerosomes by block separation, induced by copolymer photocleavage (Figure 9).

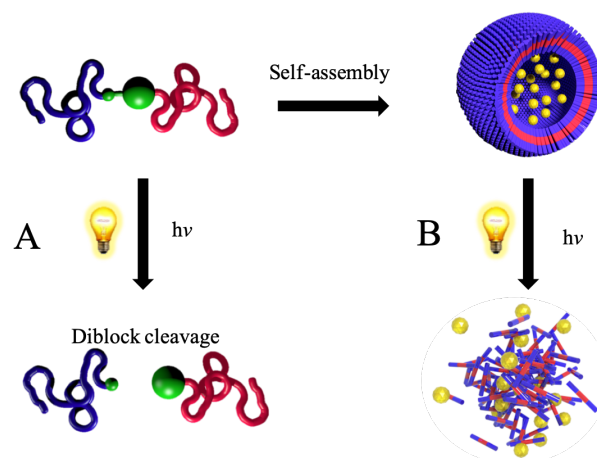


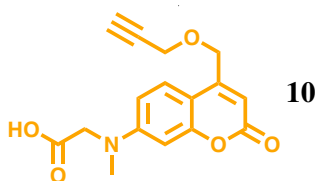
Figure 9: Strategy used to control reactant release temporally and spatially via light-sensitive polymerosomes (B), comprising photodegradable diblock copolymers (A).

A light cleavable molecule is inserted between the two blocks of an amphiphilic copolymer, such that under photoirradiation at the appropriate wavelength the blocks would be separated (Figure 9 A). Due to its amphiphilic property, the diblock can self-assemble into polymersomes and, under irradiation, the copolymers which compose the polymersome are also cleaved, resulting in polymersome destabilization (Figure 9 B). This strategy was chosen because it should induce fast destabilization and thus release [5]. Moreover light sensitive molecule and polymer choices are not restricted: any polymer chains can be grafted onto the light sensitive molecule. This strategy was previously used, resulting in an efficient light-sensitive system [6]. An *o*-nitrobenzyl linker was used as a junction between poly(γ -methyl- ϵ -caprolactone) and poly(acrylic acid). The resulting amphiphilic copolymer could self-assemble into polymersomes that was destabilized under UV irradiation. However we decided to use a more efficient photocleavable molecule based on a coumarin derivative [7] and to modify it in order to be cleaved under typical excitation wavelength of commercial confocal microscopes. This chapter presents the synthesis, and the self-assembly study of the light sensitive copolymer as well as the irradiation effects on the copolymer and the resulting polymersomes.

2.2. Coumarin synthesis (a light-sensitive cleavable molecular synthon)

2.2.1. Light-sensitive amphiphilic block copolymer design.

Several photocleavable species exist as presented in chapter 1. Coumarin was chosen because it has fast and efficient cleavage and is amenable to a double functionalization. On introduction of an amino substituent, it can absorb light at 405 nm [7], which represents a typical excitation wavelength on commercial confocal microscopes. The target coumarin derivative **10** (Scheme 2) was designed in order to be able to accommodate the grafting of two different copolymer blocks.



Scheme 2: Photocleavable linker of the light-sensitive block copolymer.

The orthogonal grafting reactions were chosen in order to provide high yield and no side reactions. The first coupling reaction of choice was the copper-catalyzed Huisgen (“click”) 1,3-

cycloaddition between an azide and a terminal alkyne [8], the second type of coupling being amide formation between an amine and an acid chloride (derived from a carboxylic acid) [9]. Thus, coumarin was modified to have both carboxylic acid and alkyne groups.

The polymers chosen were first poly(trimethylene carbonate) (PTMC), as the hydrophobic block. This polymer is biocompatible, biodegradable, has low toxicity and is well-defined [10]. The hydrophilic block chosen was the poly(ethylene glycol), (PEG), due to its known biocompatibility, availability and facile functionalization [11]. Polymer lengths have been chosen to have the appropriate hydrophilic:hydrophobic ratio to allow self-assembly into polymersomes in aqueous media [12]. These sizes were selected based on a study presented in part 2.5.

2.2.2. Synthesis

The synthetic route to the ditopic target coumarin synthon is shown in Scheme 3. The synthesis started with the commercially-available 3-aminophenol (**1**), which was reacted with ethyl chloroformate. This reaction introduced a carbamate link in order to protect the amine moiety[13]. The protected 3-aminophenol (**2**) was obtained in almost quantitative yield (98%). This amine protection allows grafting of a single methyl group on the amine later on in the synthetic pathway. **2** was reacted with 1-ethoxybutane-1,3-dione under acidic conditions forming the coumarin skeleton [14]. Transesterification of the dione with the phenol followed by cyclization yielded the protected 7-amino-4-methylcoumarin (**3**) in 70% yield. The protected amine bearing the aromatic ring does not react during coumarin formation. The introduction of a methyl on the protected amine of **3** was achieved by adding sodium hydride (a strong base) and methyl iodide. The deprotonated amine reacted with the methyl iodide. Methylation gave the modified coumarin **4** in 54% yield after crystallization in ethanol. The methylation at this point allows selective introduction of only one carboxylic acid bearing group on the coumarin later on. The tertiary amine group of **4** was deprotected under acidic conditions and high temperature (125°C) leading to the 4-methyl-7-(methylamino)coumarin (**5**) in 91% yield. The newly formed secondary amine was used to introduce the carboxylic acid grafting group. To that end, **5** was reacted with tert-butyl 2-bromoacetate to alkylate the amine under basic conditions. The carboxylic acid-protected coumarin derivative (**6**) was obtained in 34% yield. The tert-butyl protects the carboxylic acid during subsequent oxidation and reduction steps. The first grafting group was introduced, then the alkyne (the second grafting group) was added onto the coumarin. To that end, the methyl in the 4-position was used to introduce a hydroxyl group

in two steps described in previous studies [15]. First the methyl was oxidized with selenium dioxide to obtain an aldehyde (**7**) in almost quantitative yield (98%) and used without further purification other than removing metal waste. The aldehyde was then reduced into an alcohol with sodium borohydride to obtain the modified 4-hydroxy-methylcoumarin (**8**) in 52% yield. The newly formed alcohol was used to introduce the alkyne group. To that end, **8** was reacted with propargyl bromide to give the desired coumarin, linked to the alkyne (**9**). Several sets of parameters have been tested to perform this nucleophilic addition. Due to the highly water-sensitivity of NaH, solvent and reactant were dried before use. DMSO was not used as a solvent here because explosions have been reported when combined with NaH [16]. The first set of parameters

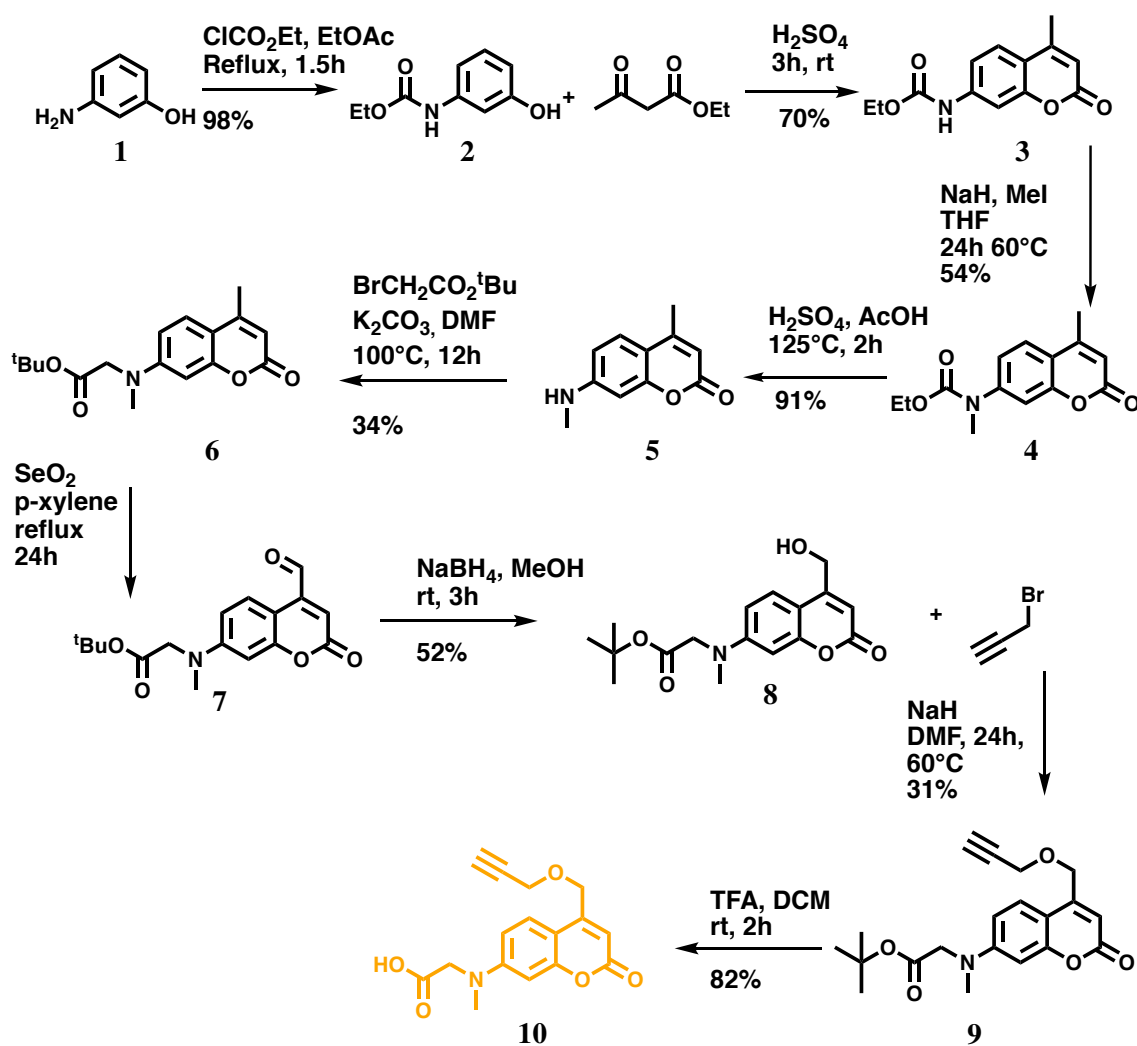
Table 2 n°1) used was: DMF as the solvent, an excess of NaH and an excess of alkyne at room temperature. Also the reaction mixture was not heated to avoid NaH reacting with DMF [16]. The resulting reaction was not complete. In order to be able to heat and increase the reaction rate, the DMF solvent was replaced by THF. Several sets of parameters with THF as the solvent (Table 2 n°2, 3 and 4) were tested but none gave the desired product. As DMF is known to promote nucleophilic substitution reactions [17], DMF was used with moderate heating (Table 2 n°5-6). Several side products were obtained because of the 72 hour reaction time. Under optimized conditions, **9** could be obtained in 31% yield on heating at a temperature of 60°C in DMF with an excess of NaH, propargyl bromide and a 24 hour reaction time (Table 2 n°6).

N°	Temperature	Solvent	Reaction time	NaH equivalent	Propargyl bromide equivalent	Results
1	RT	DMF	24h	3	1.25	Substrate
2	RT	THF	72h	3	1.25	Substrate
3	65°C	THF	72h	3	3	Substrate
4	65°C	THF	72h	5	5	Substrate
5	60°C	DMF	72h	3	3	No more substrate but several side products
6	60°C	DMF	24h	2	3	Product

Table 2: Sets of parameters used for the alkyne addition on the coumarin to obtain 9.

The last step to obtain the target modified coumarin as photosensitive linker of the two polymers blocks was to deprotect the carboxylic acid. The desired carboxylic acid allows grafting of an

amine-terminated polymer onto the coumarin by formation of an amide bond. To that end, **9** was deprotected in acidic conditions using TFA. Nevertheless the desired product turned out to be sensitive to acidic conditions. Two TFA:DCM ratios (1:1 and 1:2) were tested without diminishing the observed degradation. Reaction time was the key parameter, long enough to deprotect the carboxylic acid yet not too long to avoid degradation. A reaction time of 6 hours degraded the product and 2 hours was found to be a good compromise. Finally, coumarin **10**, bearing a carboxylic acid and an alkyne, was obtained in 82% yield in the final step.



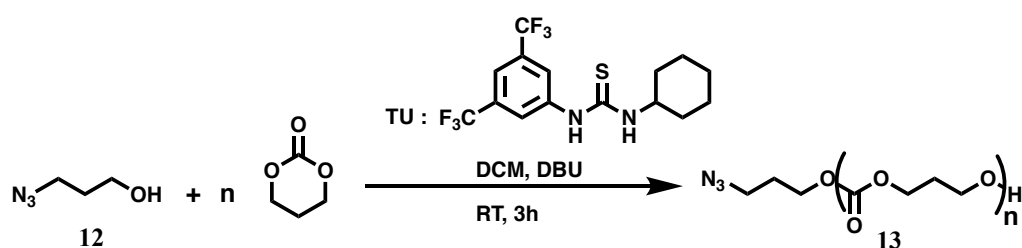
Scheme 3: Synthetic route for the coumarin photo-cleavable group, the linker between the two amphiphilic polymers.

2.3. Polymer synthesis and chain-end modifications

2.3.1. TMC polymerization to obtain well-defined PTMC

2.3.1.1. Introduction to Ring Opening Polymerization

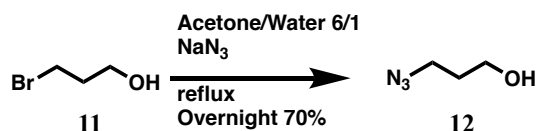
In order to use light-sensitive particles in the presence of enzymes, and more generally speaking in a biological context, the hydrophobic block has to be biocompatible and non-toxic, thus PTMC was chosen. PTMC is also biodegradable, easy to synthesize and well-defined [10]. The synthesis of PTMC from a ring opening polymerization (ROP) mechanism depicted on Scheme 4 allows to directly obtain the right end group on the chain.



Scheme 4: General scheme for the trimethylene carbonate (TMC) ring opening polymerization catalyzed with DBU and cocatalyzed with TU.

This polymerization method is widely used to synthesize a wide variety of polymers such as polycaprolactone, polylactides or PEG [18]. This is a controlled and living polymerization that affords low dispersity polymers. The chain-end functionality can be controlled thanks to the initiator (here an initiator containing an azido group was used). This initiator is activated to polymerize the TMC.

2.3.1.2. Initiator synthesis

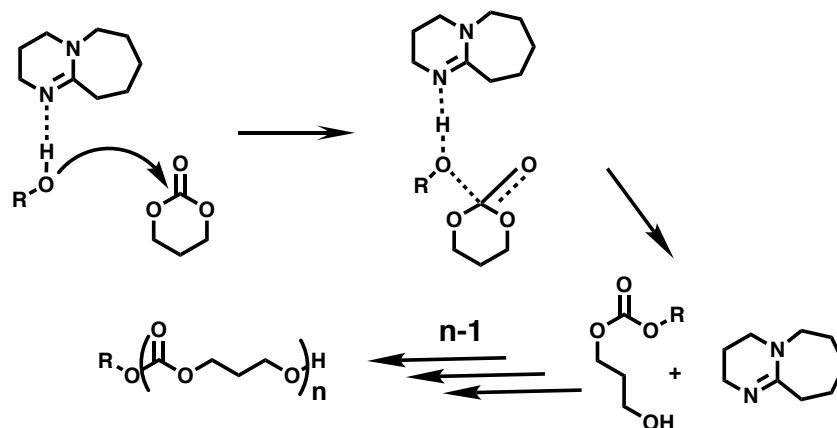


Scheme 5: General scheme for the functional initiator synthesis.

The first step was to synthesize the initiator that bears an azide group, the commercially-available 3-bromo-1-propanol (**11**) was reacted with sodium azide to replace the bromine with an azide and thus obtain 3-azido-1-propanol (**12**). The hydroxyl function of **12** allows initiation of the TMC ring opening polymerization and to lead to a PTMC bearing an azido group at one chain end. DMF was initially used [19], however DMF traces remained and a low yield was obtained. One key parameter to control the polymerization was the reactant purity, thus a mixture of acetone / water was used [8] and was fully removed. The polymerization is also very sensitive to water [20]. In order to have a living polymerization, all water traces were removed by drying **12** with CaH₂ overnight and double cryo-distillation to purify it. Three carbons were necessary between the azido group and the alcohol because it renders the initiator less explosive [21].

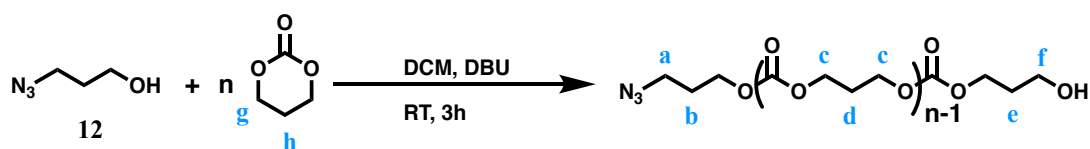
2.3.1.3. Polymerization mechanism

In order to obtain well-defined PTMC, and avoid metal-containing reagents, organocatalysts were used to polymerize TMC. The final goal is to use PTMC in the presence of enzyme, thus metal traces could reduce its biocompatibility [22]. Also organocatalysts yield narrow dispersity, predictable end chain groups and polymer lengths [10]. The polymerization mechanism is a three step process: initiation, propagation and termination (Scheme 6). The first step starts with the initiator (**12**), via deprotonation by a catalyst. A wide range of catalysts have been tested in previous studies [10], such as N-heterocyclic carbenes; 1,5,7-triazabicyclo[4.4.0]dec-5-ene (TBD). The best dispersity (\bar{D}) obtained was with 1,8-diazabicyclo[5.4.0]undec-7-ene (DBU): 1.04 [10]. DBU has a pK_a of 24.3 [23], allowing it to deprotonate the alcohol of **12** to obtain the corresponding alkoxide. In the second propagation step, the TMC monomer undergoes a nucleophilic attack by the alkoxide. This attack opens the ring to form a new alcohol. Then the catalyst deprotonated the newly formed alcohol and the same process is repeated. The last step is the termination. Acetic acid or methanol were used as terminating agent. The ROP active center is nucleophilic (that permits the polymerization) and also acts as a base. Acetic acid or methanol protonate the active center and terminate the polymerization [24].



Scheme 6: Ring opening polymerization mechanism of TMC.

The resulting polymer was analyzed by ^1H NMR. The resonances associated with TMC monomer protons in CDCl_3 shifted from 4.44 ppm (g) to 4.22 ppm (c) and 2.13 ppm (h) to 2.04 ppm (d) after polymerization (Scheme 7 and Figure 10).

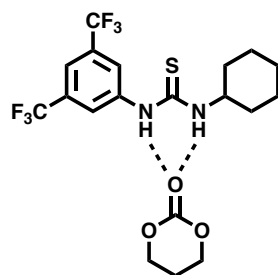


Scheme 7: General scheme for the trimethylene carbonate (TMC) ring opening polymerization with an azido chain end.

In order to remove the unreacted monomers, PTMC was purified by precipitation in cold methanol (0°C) three times. To confirm that no monomers remained, ^1H NMR in CDCl_3 was used, and resonances associated with TMC monomer protons (4.44 ppm and 2.13 ppm) disappeared after precipitation.

2.3.1.4. Polymerization Kinetic and DP measurement

Considering a PEG molar mass of 2000 g/mol and a hydrophilic:hydrophobic ratio of 19 wt% a DP of 81 for the PTMC block was targeted in order to form vesicles (this ratio was determined from the part 2.5.1). 80% conversion was targeted and 48 hours were required to obtain the desired DP with only DBU. In order to increase the polymerization kinetics, a cocatalyst was used: *N*'-[3,5-bis(trifluoromethyl)phenyl]-*N*-cyclohexylthiourea (TU) [25]. This cocatalyst activates the monomer electrophilic carbonyl by hydrogen bonding, as shown in Scheme 8.



Scheme 8: TU activation of the monomer carbonyl via hydrogen bonding.

The polymerization is thus activated twice: DBU activates the initiator and the resulting alcohol and TU activates the monomer. Consequently, to obtain a PTMC with a DP 81, 48 hours were necessary without the cocatalyst whereas only 3 hours were necessary with TU. To measure the DP by ^1H NMR, protons a and b were used as references (Figure 10). Owing to their proximity with the alcohol and the azido groups, a and f protons signals are shifted compared to the main resonance c.

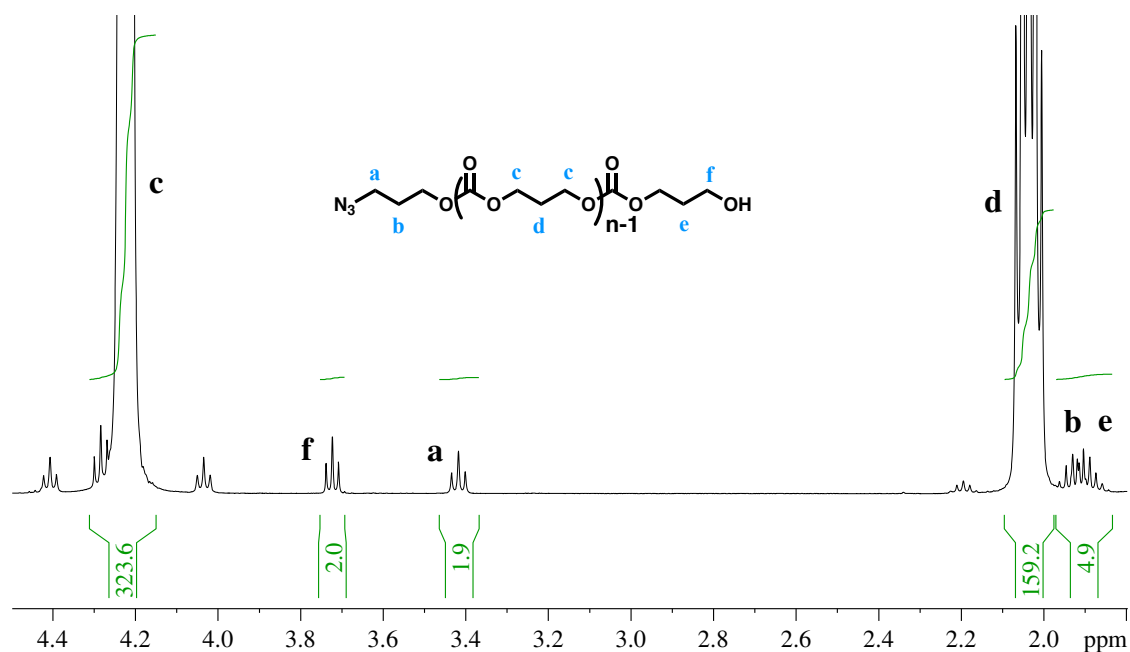


Figure 10: ^1H NMR in CDCl_3 of PTMC with a DP of 81 and an azide group as chain end group.

Polymerization kinetics were studied by collecting several samples during the polymerization process. These samples were quenched directly after being collected and analyzed by ^1H NMR and Size Exclusion Chromatography (SEC) in THF. In order to verify the living nature of the polymerization, the logarithm of $[\text{M}_0]/[\text{M}]$ (ratio of the initial monomer concentration over the monomer concentration) depending on the reaction time was plotted (Figure 11 A). The linear fit proved the first order living nature of the polymerization ([26]). The controlled nature of the

polymerization was verified by plotting the PTMC molar mass depending on the conversion (Figure 11 B). The linear fit proved the controlled nature of the polymerization ([26]). The optimized reaction time, as judged by the kinetic study, to obtain the desired DP (81) was 3 h. The proton resonance of c in ^1H NMR, integrated for 324 (DP of 81) compared to the chain-end signals (Figure 10).

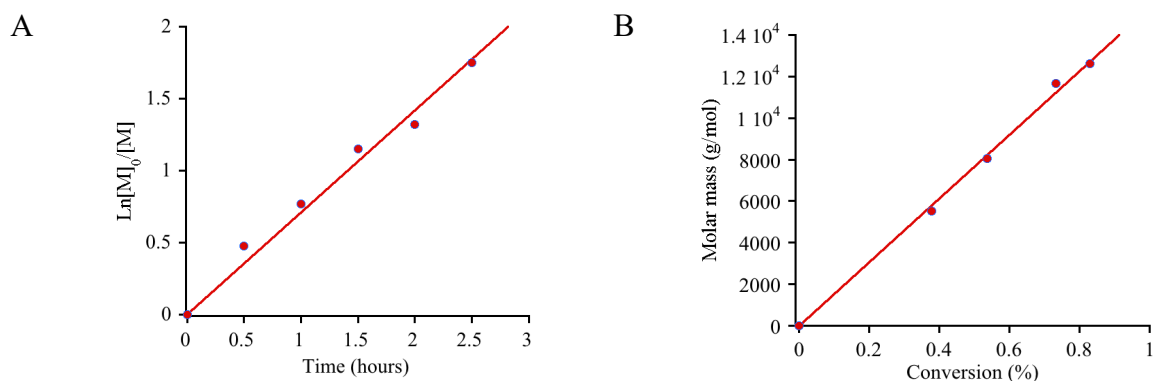


Figure 11: Kinetic study of TMC polymerization. The molar mass was determined by NMR: A) logarithm of $[M]_0/[M]$: (ratio of the initial monomer concentration over the monomer concentration) depending on the reaction time showing the living nature of the polymerization; B) PTMC molar mass depending on the TMC conversion. showing the controlled nature of the polymerization.

2.3.1.5. Unwanted diblock: possible mechanism of formation

The PTMC obtained by ROP was analyzed by Size Exclusion Chromatography (SEC) in THF. The SEC traces (Figure 12) showed that the polymer obtained had a bimodal distribution.

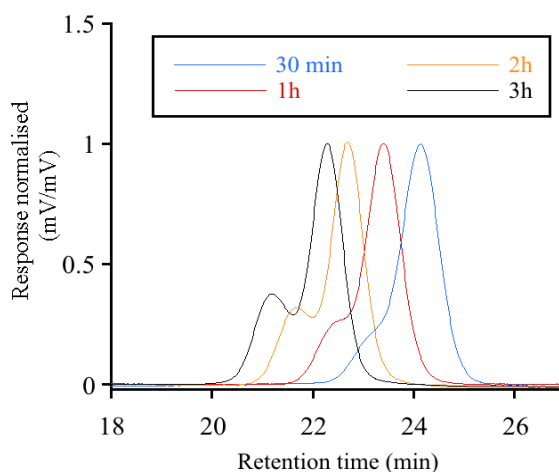


Figure 12: SEC in THF analysis of TMC polymerization at different reaction times.

An uncontrolled bimodal distribution could compromise the end chain fidelity and furthermore the copolymer formation. The unwanted shoulder had a mass twice larger than the main peak, showing that a diblock was formed. In previous studies of TMC polymerization with such an organocatalyst, no bimodal distribution were mentioned. [10] [20]. Thus several hypotheses were tested. In order to avoid any contaminant, TMC was recrystallized twice, the initiator was distilled twice, solvents were dried and distilled and all the glassware was flame dried under vacuum three times. Also the reactants were mixed in a glovebox.

2.3.1.5.1. Side reactions

Side reactions during polymerization have been considered. Several side reactions have been reported for polycarbonate and polyester [27][28]. The first one is polymer degradation. As explained, PTMC is biodegradable [28]. During polymerization the backbone chain could undergo hydrolysis and create new reactive sites. A small polymer fraction could have two reactive sites and polymer growth could be bidirectional. The polymer grows twice as fast, resulting in a higher molar mass and bimodal distribution. The hydrolysis reaction is sensitive to temperature [28]. In order to test this hypothesis, the reaction was performed at 17°C instead of room temperature (Table 3 n°2 and 6). However, the polymer molar mass was not affected and the bimodal distribution was still observed.

Another hypothesis was the transcarbonation. The reactive site attacks the polymer backbone chain instead of TMC. This side reaction exists for polyester also referred to as transesterification in that case [29]. Two polymer chains could be combined and give molar masses higher than expected. To avoid this side reaction, monomer concentration was increased, and to obtain a DP of 81 the conversion was lowered (Table 3 n°3 to 6). The reaction mixture was also diluted (Table 3 n°7). However, polymer molar mass was not affected and the peak with higher mass was still observed by SEC.

REACTION N°	CONDITIONS	RESULTS
1	Conversion 80% RT	Multimodal
2	Conversion 80% 17°C	Multimodal
3	Conversion 60% RT	Multimodal
4	Conversion 30% RT	Multimodal
5	Conversion 30% RT	Multimodal
6	Conversion 30% 17°C	Multimodal
7	Diluted twice 25°C	Multimodal
8	Deoxygenated acetic acid	Multimodal
9	Deoxygenated Methanol	Multimodal
10	Use of bromopropanol as initiator	Multimodal

Table 3: Summary of conditions tested to avoid side reactions during the ROP of TMC.

2.3.1.5.2. O₂ coupling

The other hypothesis explored was O₂ coupling. In a previous study, the authors found that secondary reactions could happen during the deactivation reaction, especially for anionic processes and polymers with OH functional groups [30]. The side reaction pathway is described in Scheme 9.



Scheme 9: O₂ coupling reaction that could induce the bimodal distribution of PTMC.

Thus O₂ presence in acid acetic and methanol, during the deactivation reaction could generate PTMC diblocks. To test this hypothesis, before deactivation, acetic acid or methanol were deoxygenated to prevent block coupling (Table 3 n°8 and 9). After SEC analysis, a bimodal distribution was still observed.

2.3.1.5.3. Post-functionalization

Post-functionalization has been used in previous studies ([31]) to introduce an azide group. 3-Bromo-1-propanol (**11**) was used as initiator to polymerize TMC and then modified to obtain the azide group with the same reaction described in Scheme 5. The resulting polymer was analyzed by SEC in THF. The PTMC obtained also had a similar bimodal distribution.

2.3.1.5.4. Reactant purity

During the polymerization, traces of water or impurities could affect the polymer dispersity. In order to obtain a monomodal polymer distribution, reactants and solvent were highly purified for all the previous described polymerizations: TMC was recrystallized in toluene twice under inert conditions to remove water and trace impurities. Toluene removed water due to azeotrope formation. Solvents such as toluene or DCM, were dried over CaH₂ overnight and then distilled. The initiator as described above was also dried over CaH₂ overnight and distilled twice. Further investigations revealed an almost undetectable impurity in the initiator mixture after distillation. The impurity was first detected in bromopropanol (**11**) mixture by thin Layer Chromatography (TLC) as shown in Figure 13 A.

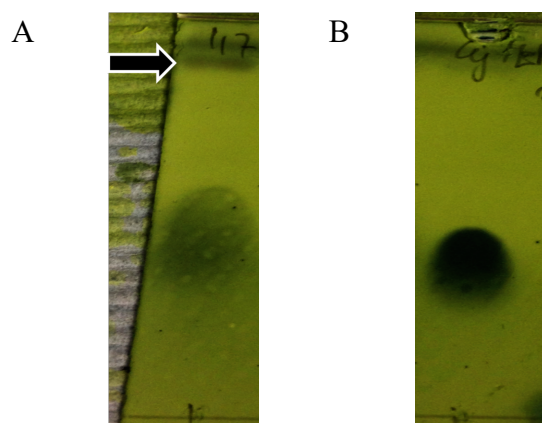


Figure 13: Bromopropanol silica TLC (A) before and (B) after silica column purification (B). The spots were revealed with phosphomolybdic acid.

The spots were revealed with phosphomolybdic acid. A closer look on ¹H NMR spectra of the azido propanol (**12**) also showed non-attributed signals hidden by the main peak (arrow in Figure 14 A). In order to remove this impurity from the 3-azido-1-propanol (**12**), 3-bromo-1-propanol was purified before initiator synthesis by column chromatography on a silica stationary phase (Figure 13 B). The resulting oil was then distilled. **12** was then synthesized using pure **11**, dried with CaH₂ overnight and distilled twice. The impurity was successfully removed from **12** as shown on the ¹H NMR spectra in Figure 14 B.

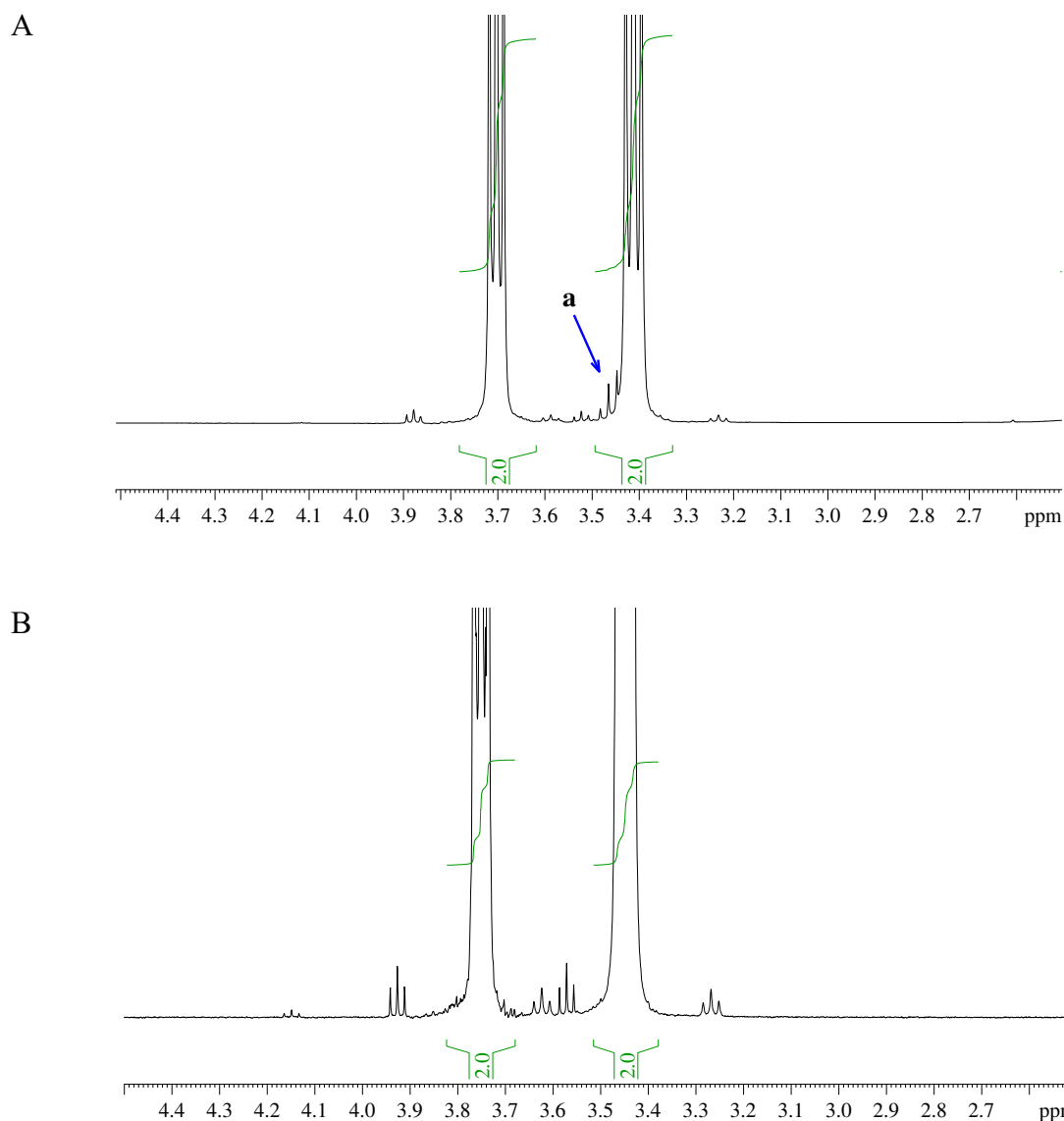


Figure 14: ^1H NMR in CDCl_3 of 3-azido-1-propanol (A) before and (B) after silica column purification. The arrow indicates an undefined impurity (a) that was removed via chromatographic purification.

The pure initiator was then used to polymerize TMC, the dispersity of the PTMC obtained was greatly improved (PTMC n°2). The diblock proportion decreased from 27% before initiator purification (PTMC n°1) to 5% after initiator purification (PTMC n°2) (Figure 15).

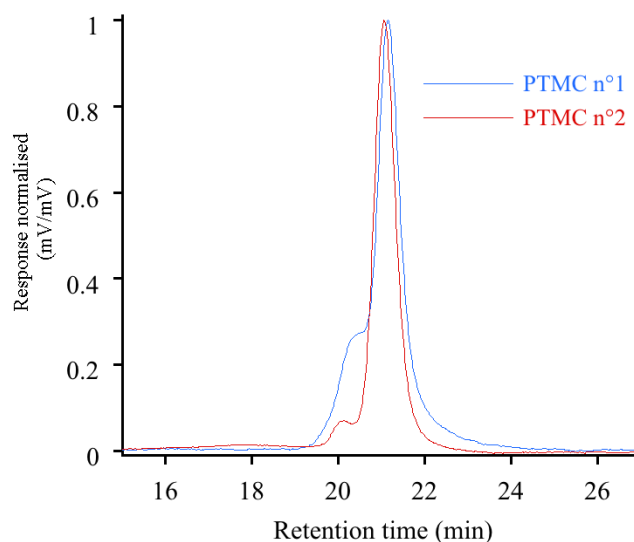
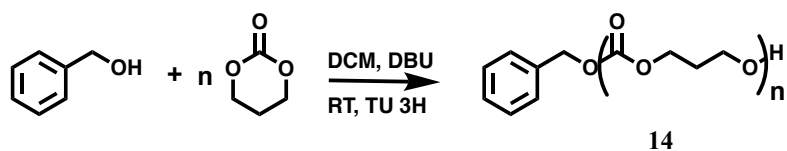


Figure 15: SEC in THF traces of PTMC₈₁-N₃ with unpurified initiator 3-azido-1-propanol (PTMC n°1) and purified initiator (PTMC n°2).

Thanks to the previous kinetic study, the resulting polymer had a DP of 81, a molar mass of 8200g/mol and a narrow dispersity of 1.05.

2.3.1.6. PTMC end chain analysis, alcohol benzylic PTMC formation and IR spectra comparison

The next step of the copolymer synthesis, which is the PTMC grafting on the coumarin, requires control over the PTMC end chain. The PTMC azide group will click with the alkyne group of the coumarin. High end chain-functionalization rate and end chain fidelity had to be verified. To that end, PTMC was analyzed by infrared spectroscopy. The typical signal of the azido group appeared at 2100 cm⁻¹ [32] as shown by the black arrow in Figure 16 A. The high molar mass of the PTMC (8200 g/mol) compared to the chain end molar mass explains the signal strength difference. To ensure that the weak signal not an artefact, the same polymer was synthesized with a different end chain. TMC was polymerized with benzyl alcohol as the initiator as shown in Scheme 10.



Scheme 10: General scheme for the trimethylene carbonate (TMC) ring opening polymerization with a benzyl chain-end.

The two IR spectra were compared in Figure 16 B, and these spectra clearly showed the difference at 2100 cm^{-1} due to the azido group end chain on the synthesized PTMC₈₁ 13.

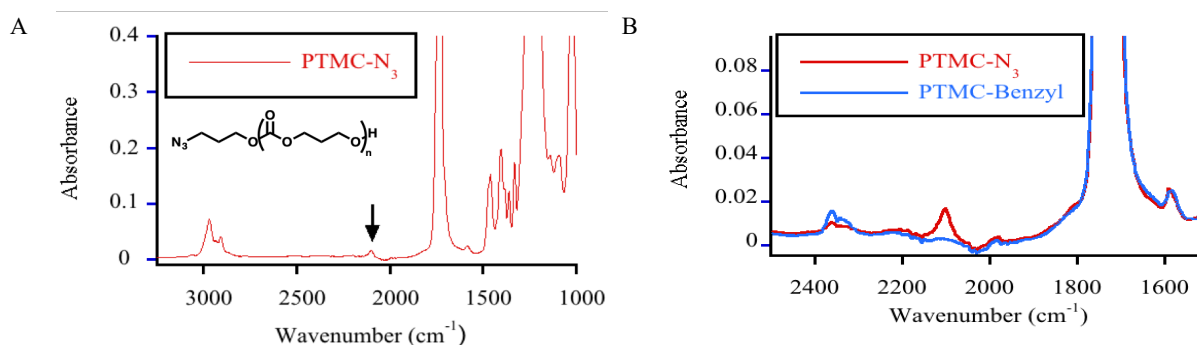


Figure 16: A) Azide terminated PTMC₈₁ IR spectra. The arrow indicated the typical azide signal (2100 cm^{-1}) B) IR spectra comparison between benzyl-terminated and azido-terminated PTMC.

A high degree of functionalization was verified by ¹H NMR spectroscopy. The resonance of the alpha proton (a) of the azido group in Figure 10 proved that 95% of the end chain groups were functionalized.

MALDI-TOF mass spectra were difficult to obtain and not sufficiently precise to be able to unambiguously identify the end chain group molar mass (Figure 17).

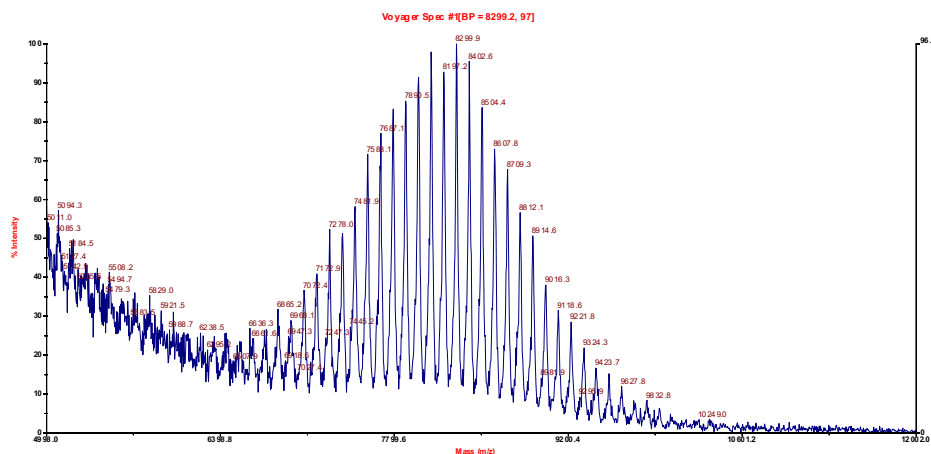
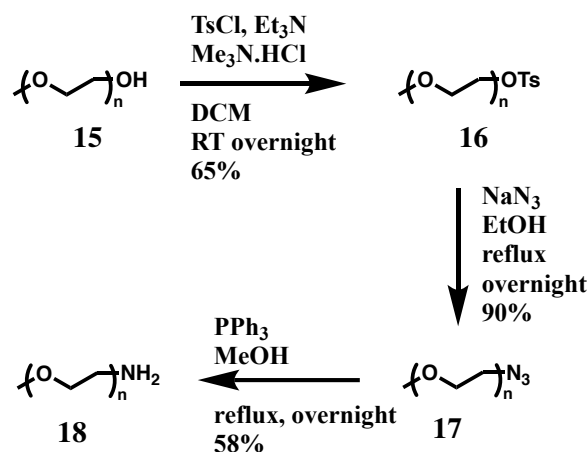


Figure 17: Characteristic MALDI-TOF spectrum of PTMC₈₁-azide.

However, the molar mass measured of the main peak was 8200 g/mol and the difference between the peaks was 102.0 g/mol, which corresponds to one TMC monomer added.

2.3.1. PEG₄₅-OH end chain modification

The hydrophilic block (PEG) end chain group was then modified in order to graft this block onto the photocleavable coumarin molecule (Scheme 11).



Scheme 11: General scheme for PEG₄₅-OH end chain modification to obtain PEG₄₅-NH₂.

An amine-terminated PEG₄₅ was necessary to be able to form an amide bond by reacting with the coumarin carboxylic acid later in the synthesis. Commercially-available bifunctional methoxy-PEG₄₅-OH (**15**) was used. The two different end groups allow modification of only one PEG chain end.

2.3.1.1. Tosylation

Alcohols are poor leaving groups, the methoxy-PEG₄₅-OH was thus converted into a more reactive tosylate [33] (Scheme 11). This moiety is a good leaving group and favours the S_N2 reaction later on in the synthesis. To that end, methoxy-PEG₄₅-OH was reacted with tosyl chloride under basic conditions. The reaction achievement was easy to follow by ¹H NMR spectroscopy. The aromatic protons of the tosylate shift compare the aromatic proton of the unreacted tosyl chloride from 7.47 ppm and 7.11 ppm to 7.79 and 7.48 ppm. After reaction overnight, the reaction was not complete, prompting us to use Me₃N.HCl as a catalyst [34]. These new reaction conditions were tested, giving full conversion after one night to give

methoxy-PEG₄₅-tosylate (**14**) in 65% yield. This relatively low yield was caused by the precipitation in diethyl ether that can be improved.

2.3.1.2. Azide formation

Methoxy-PEG₄₅-tosylate was reacted with sodium azide in order to replace the tosylate group with an azido group [33] (Scheme 11). The tosylate undergoes a nucleophilic attack by the azide anion to give methoxy-PEG₄₅-N₃ (**15**) in 90% yield. The progression of the reaction was verified by disappearance of the aromatic tosylate proton resonance in NMR experiments.

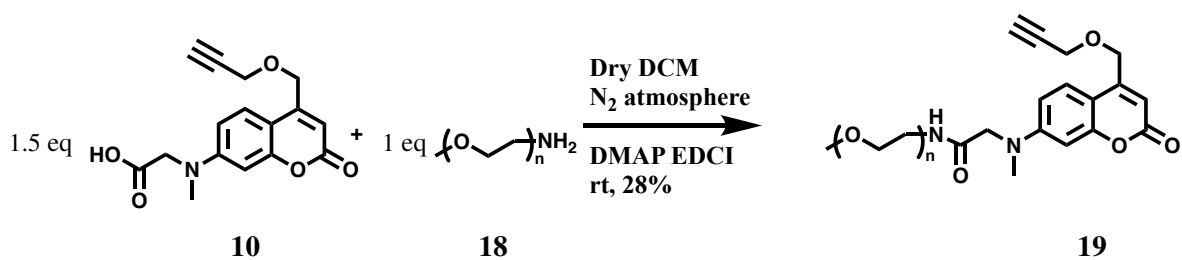
2.3.1.3. Amination

In the next step, the azido group was hydrogenated to give an amine group [33] (Scheme 11). Macromolecule **15** was reacted with triphenylphosphine to give the methoxy-PEG₄₅-NH₂ (**16**) in 58% yield. In order to verify that the previous reactions did not modify PEG molar mass distribution, SEC in THF analysis was performed on the PEG₄₅-NH₂ showing the distribution was still monomodal.

2.4. Polymer grafting on the light-sensitive coumarin linker

2.4.1. Amidation reaction

The light sensitive linker was synthesized with two grafting groups. OH-PTMC₈₁-N₃ could not be grafted first because during the next step (amide formation to graft PEG₄₅), EDCI would activate the carboxylic acid on the coumarin of HO-PTMC-coumarin and the hydroxyl group of PTMC₈₁ would react with the activated carboxylic acid [35]. Therefore the PEG₄₅-NH₂ was firstly coupled onto the coumarin. To this end, PEG₄₅-NH₂ (**15**) was reacted with the modified coumarin (**10**) using coupling agents DMAP and EDCI to give PEG₄₅-coumarin (**17**) in 28% yield (Scheme 12).



Scheme 12: General scheme for PEG₄₅-NH₂ coupling on the coumarin by amide bond formation.

EDCI was used to activate the carboxylic acid and the resulting urea is water soluble [9], so can be removed easily with solution phase chemistry.

¹H NMR spectroscopy showed that the reaction was not complete. 50% of the PEG₄₅-NH₂ remained unfunctionalized with the coumarin. After silica column purification, the percentage of functionalized PEG₄₅-NH₂ was slightly better: 80%. Separation of the coumarin unfunctionalized PEG from the functional PEG is difficult because of a similar molar mass. However, after PTMC₈₁-N₃ grafting on the PEG₄₅-coumarin, the remaining unreacted PEG could be easily removed by dialysis due to the molar mass difference (10 000 g/mol for the copolymer again 2000 g/mol for the unreacted PEG) as it will be evidenced later.

In order to verify that the coumarin was grafted on the PEG₄₅-NH₂, SEC analysis was performed on the newly-formed polymer. Due to the coumarin group the PEG signal absorbed in the UV [36], contrary to the PEG before reaction, as shown in Figure 18 A. Also the signal in UV and RI in SEC analysis overlap perfectly, as shown in Figure 18 B. These SEC analyses confirmed that coumarin was grafted on the PEG₄₅-NH₂ chain-end.

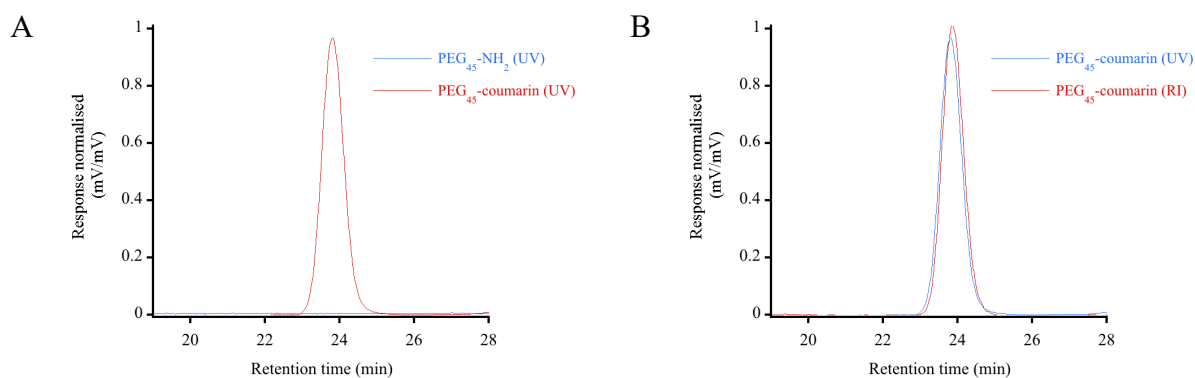
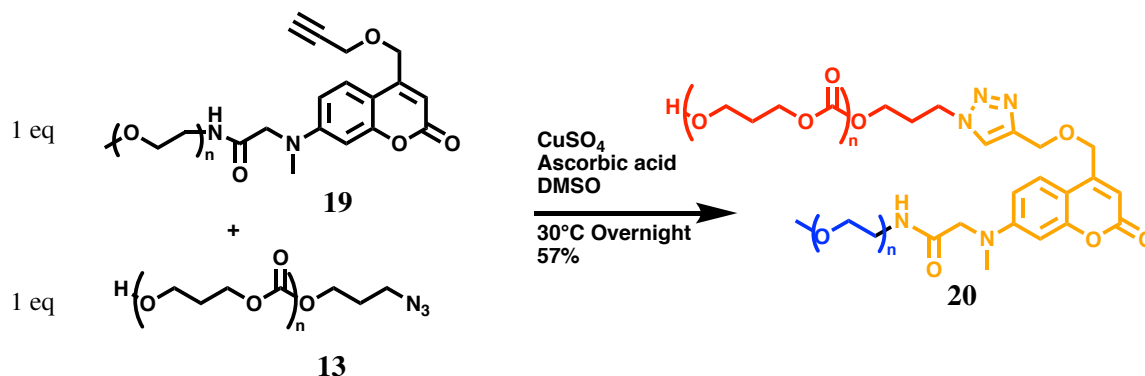


Figure 18: A) SEC in THF traces of PEG₄₅-coumarin before (no signal) and after (signal) coumarin coupling. B) SEC in THF traces of PEG₄₅-coumarin, monitoring changes in RI and UV absorption. The two traces overlaid perfectly.

2.4.2. Copper-catalyzed Huisgen (“click”) 1,3-cycloaddition

PTMC₈₁-N₃ (**13**) was then grafted on the PEG₄₅-coumarin (**19**) to give the copolymer PEG₄₅-coumarin-*b*-PTMC₈₁ (**20**) in 57% yield. To that end, the PTMC₈₁ azide chain end group was reacted with the coumarin alkyne in presence of a copper catalyst (Scheme 13).



Scheme 13: General scheme for PTMC₈₁-N₃ grafting on PEG₄₃-coumarin via a copper-catalysed CuAAC / “click” reaction.

This copper-catalysed CuAAC reaction is commonly called a “click reaction”. The copper was then easily removed by several days of dialysis in water. ¹H NMR in CDCl₃ in Figure 19 proved that the click reaction had occurred. Resonances associated with PTMC₈₁ protons (4.24 and 2.05 ppm) and PEG₄₅ (3.64 ppm) appeared, the triazole proton signal was clearly visible at 7.75 ppm and the alkyne triplet from PEG₄₅-coumarin observed at 2.63 ppm in CDCl₃ disappeared. The integrals of signals associated with PTMC and PEG protons were slightly higher than expected, which was probably due to a small fraction of unreacted PTMC₈₁-N₃ and PEG₄₅.

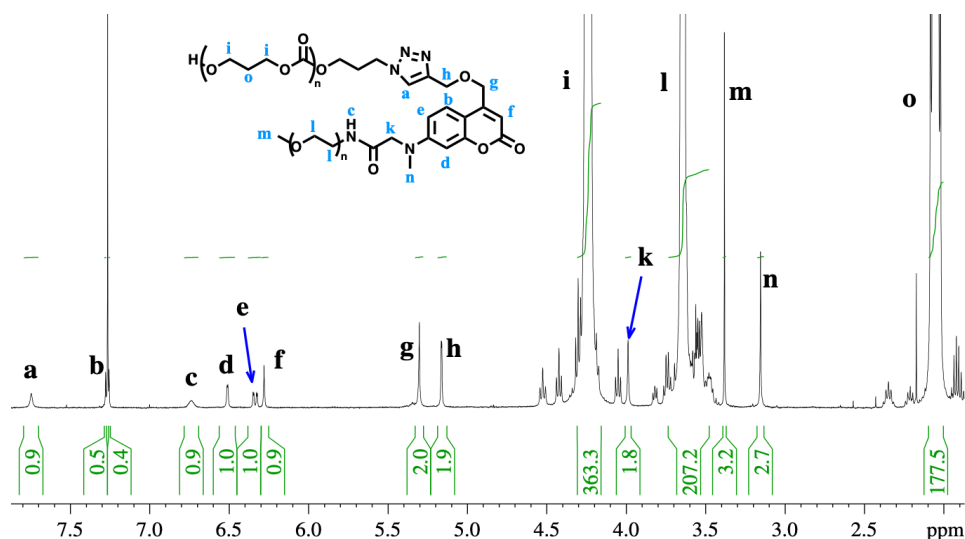


*Figure 19: ¹H NMR in CDCl₃ of the light sensitive copolymer PEG₄₅-coumarin-*b*-PTMC₈₁.*

In order to verify the progress of the reaction, the resulting copolymer was then analyzed by SEC in THF. The copolymer molar mass matched the sum of PEG₄₅-coumarin and PTMC₈₁-N₃ molar mass, as shown in Figure 20 A. Also PTMC₈₁-N₃ alone does not absorb in the UV spectral region contrary to the resulting polymer. The absorption spectrum of the copolymer corresponded with that of the coumarin group, as shown in Figure 20 B. These results clearly confirmed that the light-sensitive PEG₄₅-coumarin-*b*-PTMC₈₁ was successfully obtained with a dispersity of 1.05.

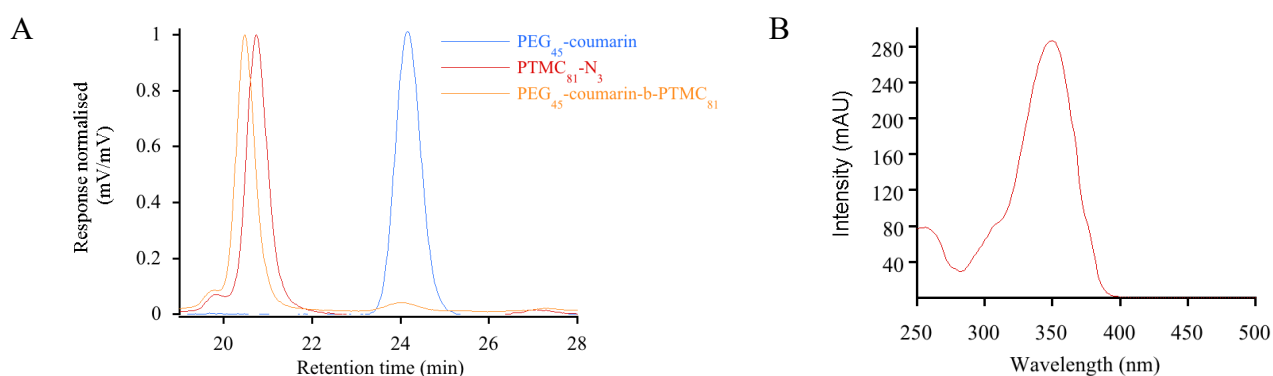


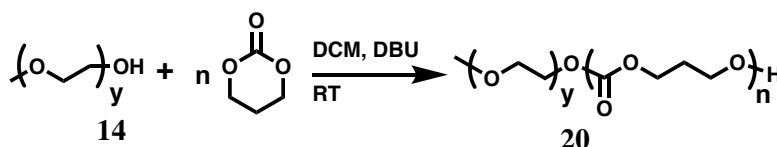
*Figure 20: SEC in THF traces of the PEG₄₅-OH, PTMC₈₁-N₃ and resulting PEG₄₅-coumarin-*b*-PTMC₈₁ B) PEG₄₅-coumarin-*b*-PTMC₈₁ absorption in THF obtained from SEC analysis (Diode-array UV detector).*

2.5. Self-assembly characterization

2.5.1. Study on PEG-*b*-PTMC Copolymer

2.5.1.1. Synthesis

Due to the complexity of the light-sensitive copolymer synthesis, PEG-*b*-PTMC without the coumarin molecule inserted between the blocks was first used to study its self-assembly properties. Several copolymer block lengths have been easily synthesized (Table 4 and Scheme 14). One key parameter to obtain polymersomes is the proportion of the hydrophilic and hydrophobic block [4]. To this end, the hydrophilic ratio was defined by the molar mass of the hydrophilic block over the molar mass of the hydrophobic block (Table 4).



Scheme 14: General scheme for the trimethylene carbonate (TMC) ring opening polymerization with PEG₄₅-OH as the initiator to form the block copolymer PEG₄₅-b-PTMC_x.

Samples	Hydrophilic ratio (%)	Molar mass (g/mol)	Mn PEG (g/mol)	Mn PTMC (g/mol)	\bar{D}
PEG ₄₅ -b-PTMC ₂₇₂	7	29700	2000	27700	1.17
PEG ₄₅ -b-PTMC ₈₁	19	10200	2000	8200	1.05
PEG ₄₅ -b-PTMC ₃₃	37	5300	2000	3300	1.05

Table 4: Several PEG₄₅-b-PTMC_x synthesized with different PTMC lengths and different hydrophilic ratios.

The aim of this study was to find the precise hydrophilic ratio that allows self-assembly into polymersomes. Methoxy-PEG₄₅-OH was used as an initiator and TMC was polymerized with DBU as catalyst in the same manner as described previously. In a first step, different methods to form reproducible and well-defined self-assembled structures were tested using these copolymers.

2.5.1.2. Nanoprecipitation

The nanoprecipitation (or solvent displacement) method was first used to self-assemble our block copolymers. This method consists in dissolving the copolymer in an organic solvent that dissolved the two blocks well. This organic solvent also has to be soluble in water. Water is then added to the copolymer solution. The hydrophobic block becomes progressively insoluble in the water/organic solvent mixture and stacks in order to minimize the unfavorable interactions with water. When the water ratio is high enough, the copolymer self-assembles into ordered structures such as micelles, worm-like micelles or polymersomes (Figure 21).

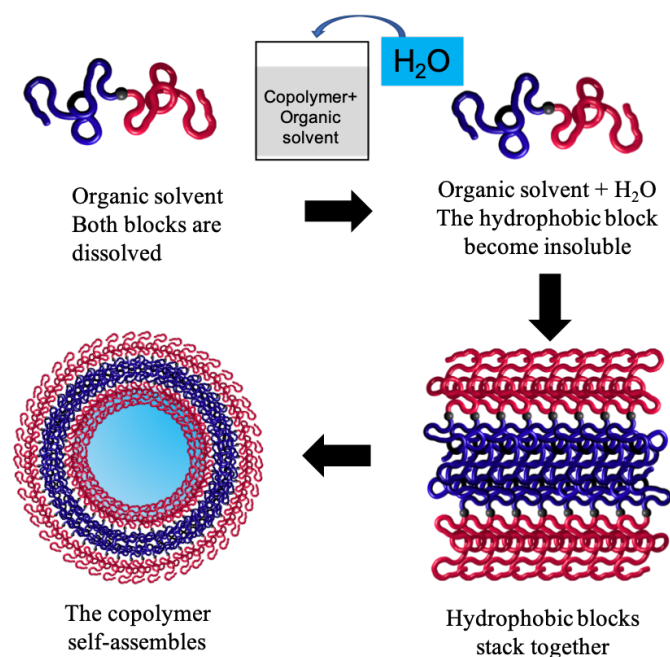


Figure 21: Schematic representation of the nanoprecipitation method.

Polymeric vesicles, also known as polymersomes, are small artificial bilayer vesicles enclosing an aqueous solution, resulting from the self-assembly of amphiphilic block copolymers. The aim of this study is to determine the appropriate hydrophilic fraction for PEG-*b*-PTMC copolymers that allows the formation of vesicles.

THF and DMSO have been tested as the organic solvent in the nanoprecipitation process. Several tests showed that DMSO was more efficient than THF to self-assemble the copolymers. The efficient initial copolymer concentration in the organic solution was 10 mg/mL and 90% in volume of water was rapidly (≈ 1 second) added into the organic polymer solution while stirring at 500 rpm with a magnetic stirring bar. In order to remove the organic solvent, the resulting particle solution was dialyzed against water using a 3.5 kDa dialysis bag. The dialysis bags were immersed in 5 L of water for 3 h, then the water was changed. This operation was repeated 3 times. Dynamic light scattering (DLS) at 90° (Malvern) was used to measure particle size and the polydispersity index (PDI) of the particle solution. Measurements by DLS at 90° were performed 3 times and the resulting average is presented.

2.5.1.3. Syringe pump to control particle sizes

Water was added manually in the previously reported nanoprecipitation tests, making this method largely irreproducible. In order to have more repeatable batches, a syringe pump was used to add water at a constant rate. The particle size could also be tuned depending on the speed of water injections while maintaining a low PDI (Table 5). Water injection by a syringe pump allows then to obtain sizes between 120 and 380 nm for PEG₄₅-*b*-PTMC₈₁. An almost linear increase of the size as function of the injection time could be observed (Figure 15).

Injection Time (Min)	Diameters (nm)	PDI
0	121	0.12
1	225	0.09
2	276	0.10
5	384	0.17

Table 5: Particle diameters and PDI depending on the injection speed of water for PEG₄₅-*b*-PTMC₈₁.

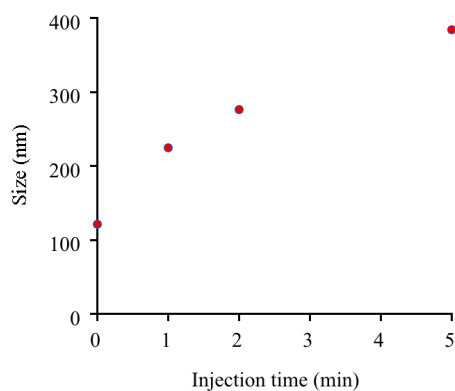


Figure 22: Particle diameters depending on the injection speed of water for PEG₄₅-*b*-PTMC₈₁.

2.5.1.4. Determination of the appropriate hydrophilic ratio to obtain polymersomes

The self-assembly properties of the 3 synthesized copolymers were first studied with a fast water addition (≈ 1 second), dialyzed then analyzed by DLS at 90°. Several copolymers showed a narrow distribution and low PDI by DLS such as PEG₄₅-*b*-PTMC₂₇₂ and PEG₄₅-*b*-PTMC₈₁ (Table 6), with respectively, hydrophilic ratios of 7 and 19%. These copolymers self-assemble

into particles with monomodal distribution, polydispersity around 0.1 and sizes around 150 nm contrary to PEG₄₅-*b*-PTMC₃₃ as shown in Figure 23. PEG₄₅-*b*-PTMC₈₁ with a hydrophilic ratio of 19% was chosen to go further in the investigation because the particles formed have a lower PDI.

Samples	Diameter (nm)	PDI
PEG ₄₅ - <i>b</i> -PTMC ₂₇₂	182	0.149
PEG ₄₅ - <i>b</i> -PTMC ₈₁	127	0.118
PEG ₄₅ - <i>b</i> -PTMC ₃₃	38	0.370

Table 6: Particle diameters and PDI for different PTMC lengths of PEG₄₅-*b*-PTMC.

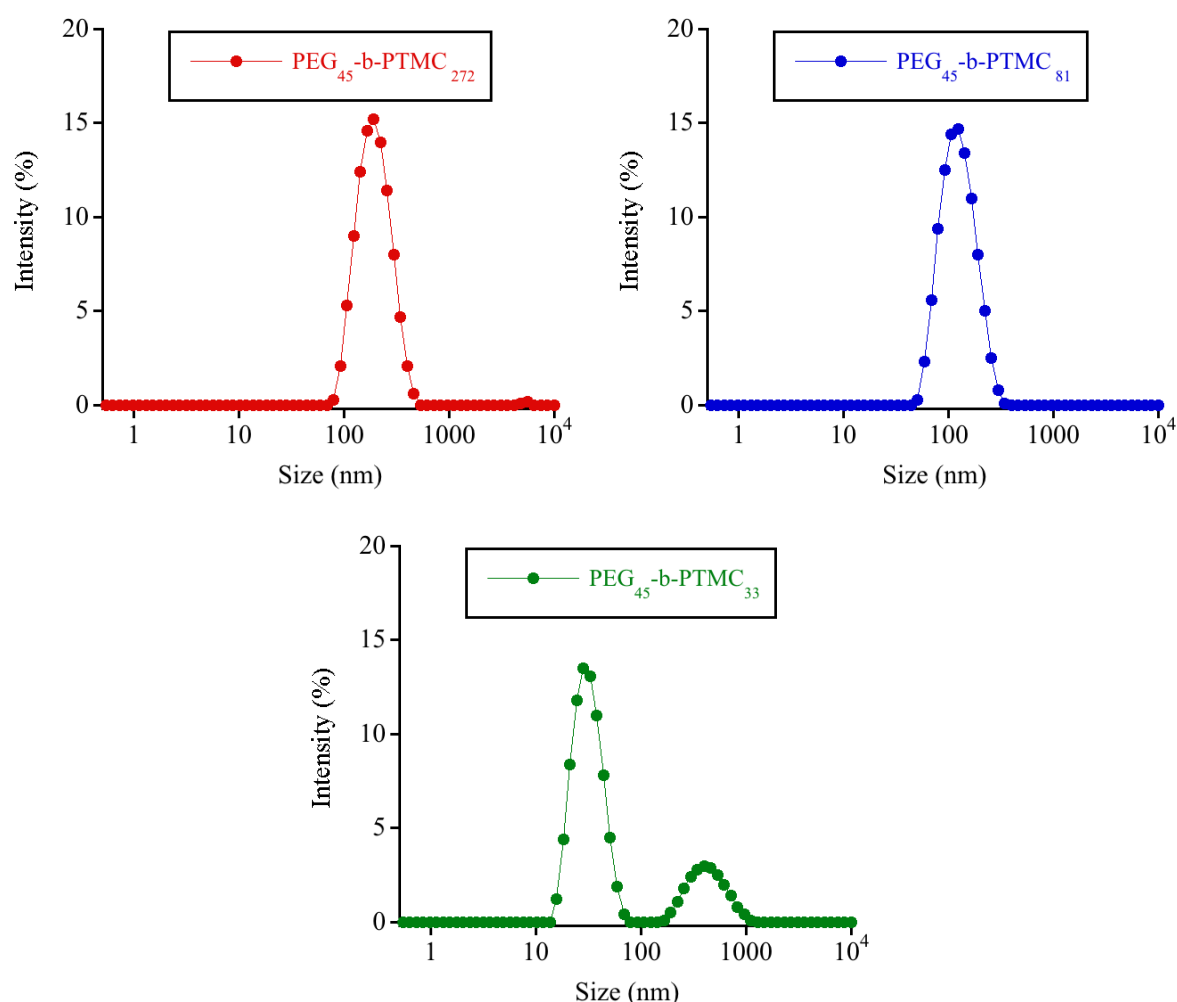
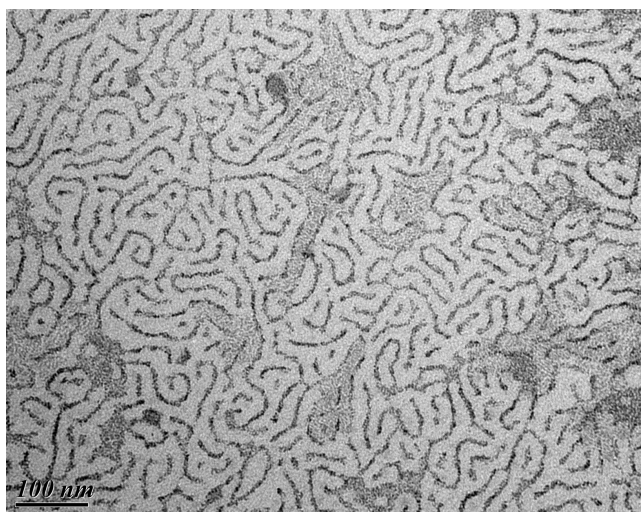


Figure 23: Intensity-averaged hydrodynamic diameter distributions, recorded by DLS at 90° (Malvern) in water of different PEG₄₅-*b*-PTMC.

2.5.1.5. TEM

In order to identify the structures formed by nanoprecipitation, TEM was first used to observe the particle solution. PEG₄₅-*b*-PTMC₈₁ copolymers have a weak contrast in electron microscopy, consequently, this copolymer was hardly detectable by TEM. In order to render the copolymer more visible, samples were stained with Uranyless (from Delta Microscopies). TEM grids (Formvar / carbon film on 200 mesh copper grid: S162) were prepared by deposition of a drop of solution of particles (0.1 mg/mL) onto the grids for 1 min. The grids were stained with one Uranyless drop during 1 min, the drop was removed with an absorbent tissue, then the grids were dried for at least one hour at room temperature. The resulting image of PEG₄₅-*b*-PTMC₈₁ particles solution is shown in Figure 24.



*Figure 24: TEM images of PEG₄₅-*b*-PTMC₈₁ stained with Uranyless.*

Due to preparation conditions, and especially the drying process, particles were probably destroyed. However, the hallmark of lamellar structures could be observed, indicating that copolymer may form bilayers that could result from vesicular structures in solution. This analysis is of course not sufficient to conclude about the copolymer structure in solution.

2.5.1.6. Cryo-TEM

Cryo-TEM was then used to observe the copolymer particle solution (Figure 25). One advantage of Cryo-TEM compared to TEM is that samples are not dried before observation. Since they are frozen, the structures observed are considered the same as the structures in the

solution. Samples from PEG₄₅-*b*-PTMC₈₁ were sent to Aalto University, applied physics nanomicroscopy center in Finland, in the framework of a collaboration with the LCPO.

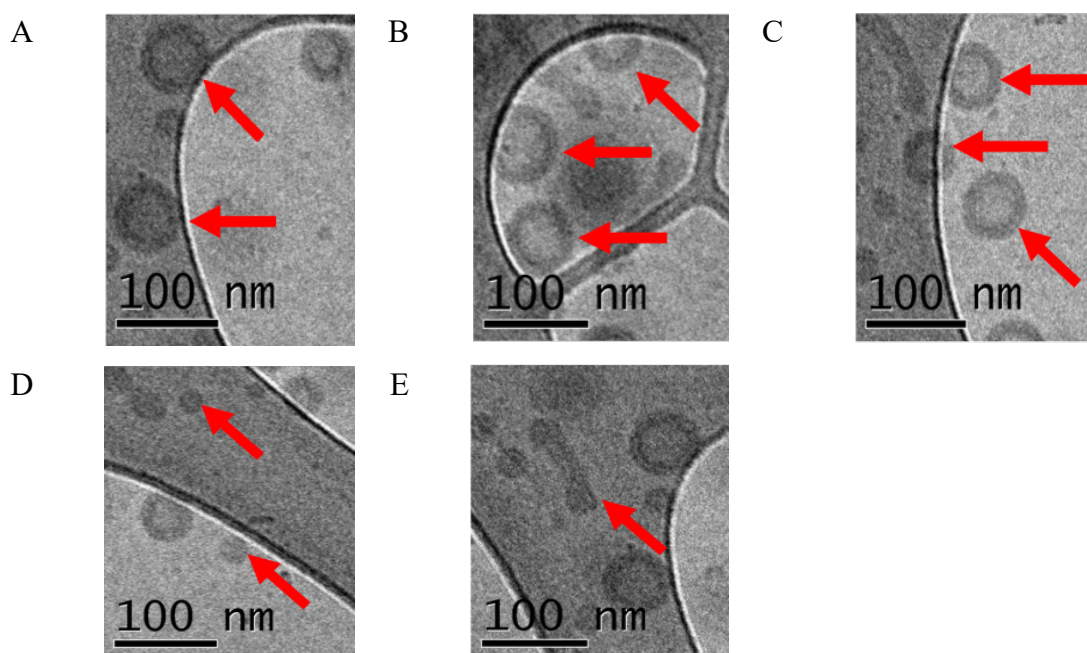


*Figure 25: Cryo-TEM images of PEG₄₅-*b*-PTMC₈₁ self-assembled in water.*

The obtained Cryo-TEM images showed closed membranes, clearly indicating that PEG₄₅-*b*-PTMC₈₁ can self-assemble into vesicular structures (Figure 25 A, B, and C). A few micelles (Figure 25 E) and worms (Figure 25 D) were also observed. Vesicle membranes had a homogeneous thickness of around 12 nm which was consistent with a polymersome bilayer membrane [4]. Observed polymersome size was around 50-100 nm, which was smaller than the size observed by DLS (\approx 120 nm). The observed particle size distribution was relatively polydisperse with several morphologies and several sizes, which was not consistent with DLS at 90°. Indeed, one can expect that the sample could be destabilized during transportation, which could explain the difference between the observation by DLS and the Cryo-TEM. However, we can definitely conclude that the hydrophilic ratio for PEG₄₅-*b*-PTMC₈₁ was appropriate with self-assembly into polymersomes. Therefore the hydrophilic ratio chosen for the light-sensitive copolymer synthesis was 19% with PTMC block of 8200 g/mol and PEG block of 2000 g/mol.

2.5.2. Self-assembly characterization of light-sensitive PEG₄₅-coumarin-*b*-PTMC₈₁

In the previous section PEG₄₅-coumarin-*b*-PTMC₈₁ was synthesized. The previous study on non-light sensitive PEG₄₅-*b*-PTMC (part 2.5.1) showed that a copolymer with a hydrophilic ratio of 19% (2000 g/mol for PEG and 8200 g/mol for the PTMC) self-assembled into polymersomes. Therefore the PEG and the PTMC used for the synthesis of the light-sensitive copolymer PEG-coumarin-*b*-PTMC (part 2.4) had the same lengths to give PEG₄₅-coumarin-*b*-PTMC₈₁. This copolymer was expected to self-assemble into polymersomes as well. This copolymer was self-assembled by nanoprecipitation. The initial copolymer concentration of the organic solution was 10 mg/mL and 90% in volume of water was added into the organic polymer solution while stirring at 500 rpm with a magnetic stirring bar. In order to remove the organic solvent, the resulting particle solution was dialyzed against water using a 3.5 kDa dialysis bag. The dialysis bags were immersed in 5 L of water for 3 h then the water was changed. This operation was repeated 3 times.

2.5.2.1. Dynamic light scattering at 90°

Depending on the quantity needed, 900 μL of water was injected into 100 μL of copolymer solution or 2.7 mL of water was injected into 0.3 mL of copolymer solution. Injection was performed in 5 mL brown glassware to protect against ambient light. The resulting particles showed a narrow PDI (0.12), monomodal distribution and sizes (120 nm) that can correspond to vesicles as shown in Figure 26.

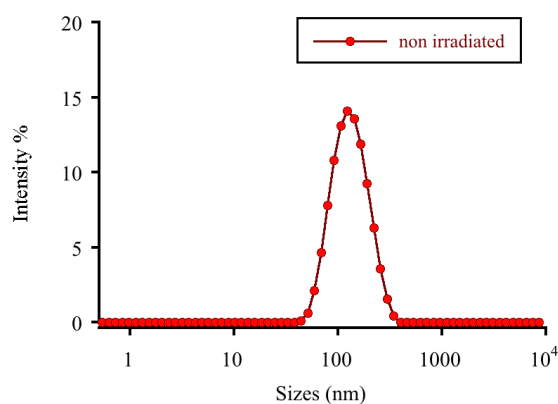


Figure 26: Intensity-averaged hydrodynamic diameter distributions, recorded by DLS at 90° (Malvern) in water of PEG₄₅-coumarin-*b*-PTMC₈₁.

2.5.2.2. Multi-angle light scattering (static and dynamic)

Multi-angle light scattering (static and dynamic) was additionally performed in order to calculate the radius of gyration (R_g) and the hydrodynamic radius (R_h). The radius of gyration is the root mean square distance of the object's parts from its center of mass. This radius is related to where the mass is distributed in the particles. R_h is the radius of the object size corresponding to their Brownian motion, which is independent of mass distribution of the particles. Depending on the particle morphology the ratio of R_g/R_h is different as schematically shown in Figure 27. Theoretically $R_g/R_h \approx 0.7$ for micellar structures and $R_g/R_h \approx 1$ for vesicular structures [37]. Indeed, considering that the radius of vesicle is significantly larger than the membrane thickness, the two radii (R_g and R_h) would be similar.

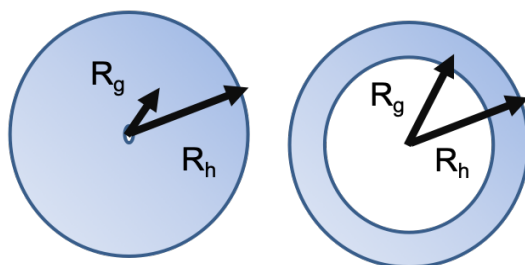


Figure 27: Schematic representation of the position of R_g and R_h for micellar and vesicular structures.

From these measurements, we obtained a R_g around 65 nm and a R_h around 71 nm. The average ratio R_g/R_h obtained was 0.93. This analysis seemed to indicate that particles had a vesicular structure, but does not allow us to fully conclude about the copolymer structure in solution.

	R_g (nm)	R_h (nm)	R_g/R_h
Batch 1	63	63	1
Batch 2	67	79	0.85
Average	65	71	0.93

Table 7: R_g and R_h measured by multi-angle light scattering of two PEG₄₅-coumarin-b-PTMC₈₁ particle batches in water.

2.5.2.3. TEM

TEM analysis was then used to identify particle structures following the sample preparation protocol described in part 2.5.1.5. Round shape and essentially monodispersed structures were observed. Particle sizes were around 150 nm, which is consistent with DLS at 90° measurements. However, these TEM images were insufficient to conclude that self-assembled PEG₄₅-coumarin-*b*-PTMC₈₁ particles were polymersomes, as the formation of hollow structures could not be determined.

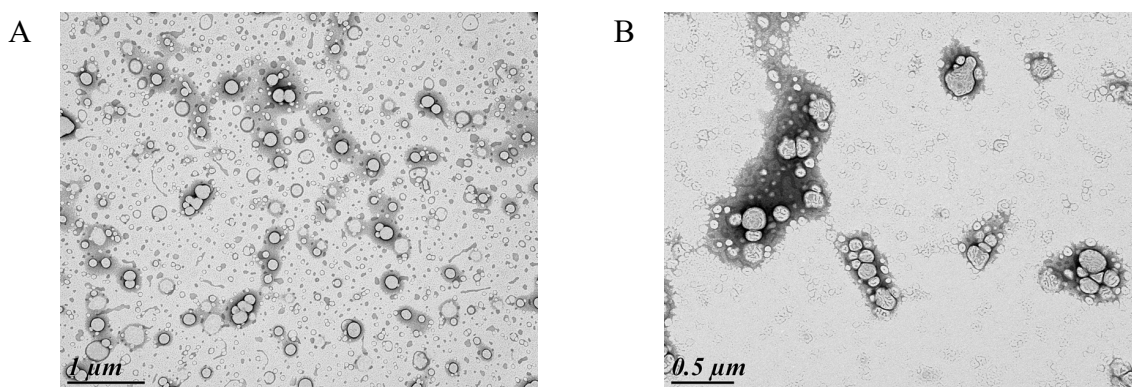
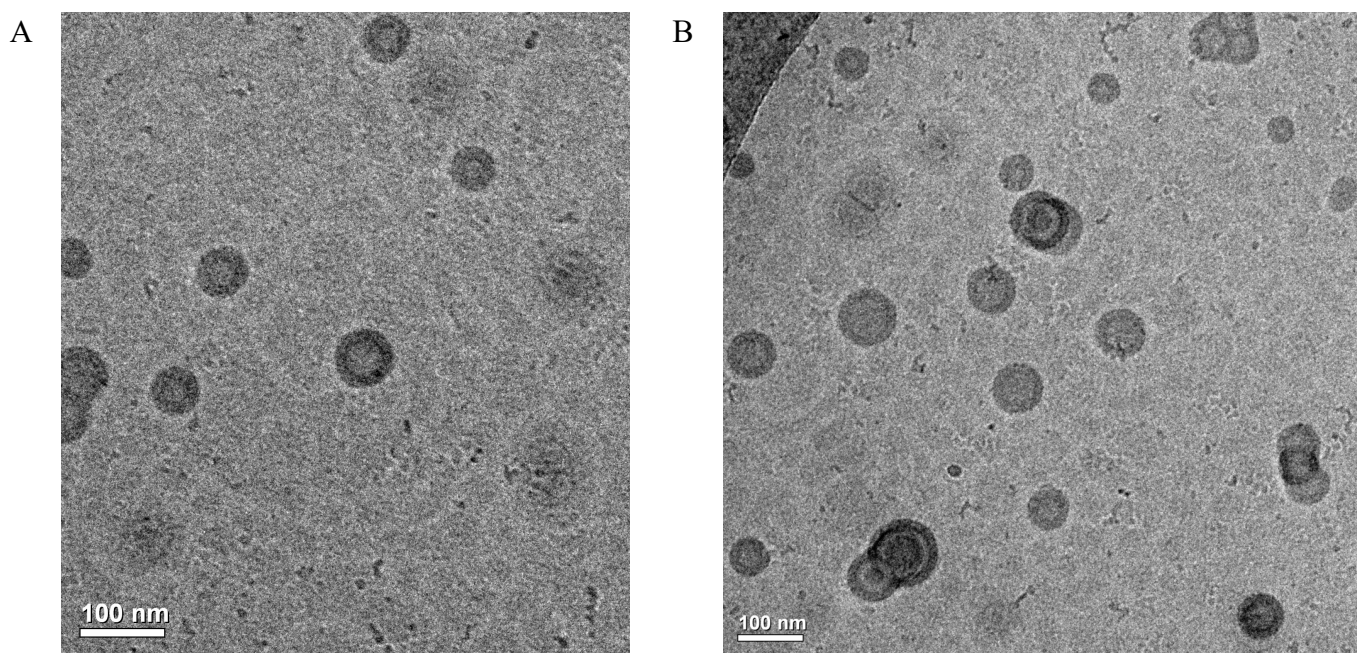


Figure 28: TEM images of self-assembled PEG₄₅-coumarin-*b*-PTMC₈₁.

2.5.2.4. Cryo-TEM

Figure 29 shows Cryo-TEM images of freshly prepared samples recorded at the Institut de minéralogie, de physique des matériaux et de cosmochimie (IMPMC, Sorbonne université J-M. Guigner). The images showed closed membranes, clearly indicating that PEG₄₅-coumarin-*b*-PTMC₈₁ self-assemble into polymersomes. Vesicle membranes had a homogeneous thickness of 12 nm which was consistent with a polymersome bilayer membrane [4]. The observed polymersome size was around 100 nm, which was the same order of magnitude as the size observed by DLS (\approx 120 nm). The observed polymersome distribution was relatively narrow which was also consistent with DLS at 90° and multi-angle light scattering. A few polymersomes contained in their lumen polymersomes or micelles (Figure 29 B) also called nested vesicles [38]. These nested vesicles resulted from invagination, probably induced by an osmotic pressure difference between the inner and the outer medium. The structures obtained were more homogeneous compared to the non-light sensitive PEG₄₅-*b*-PTMC₈₁ in part 2.5.1.6, without the presence of worm-like micelles.



*Figure 29: Cryo-TEM images of self-assembled PEG₄₅-coumarin-*b*-PTMC₈₁ in water showing the presence of well-defined polymersomes.*

These images allow to definitely conclude on the PEG₄₅-coumarin-*b*-PTMC₈₁ polymersome structure. Samples showed a narrow distribution and size of around 100 nm that was consistent with previous measurements (DLS).

2.6. Irradiation effects

2.6.1. Introduction

Particle morphology was studied in the previous part and PEG₄₅-coumarin-*b*-PTMC₈₁ self-assembly into well-defined polymersomes was confirmed. In order to confer light-sensitivity to the copolymer, a photosensitive coumarin was inserted between the two blocks. This part consists in studying the photosensitivity of the copolymer at the molecular and macromolecular level, together with the resulting effect on self-assembled particles and their release properties. Irradiation experiments were carried out with a 200 W Mercury-Xenon lamp. A filter was used centering the light emission at 365 nm (output emission spectrum is shown in the experimental part). Samples were placed at 1 cm from the light guide output and irradiated for a defined time (Figure 30).

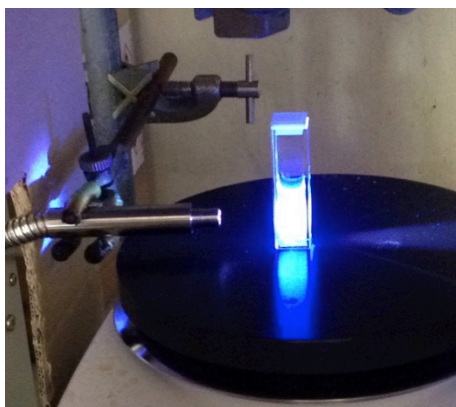
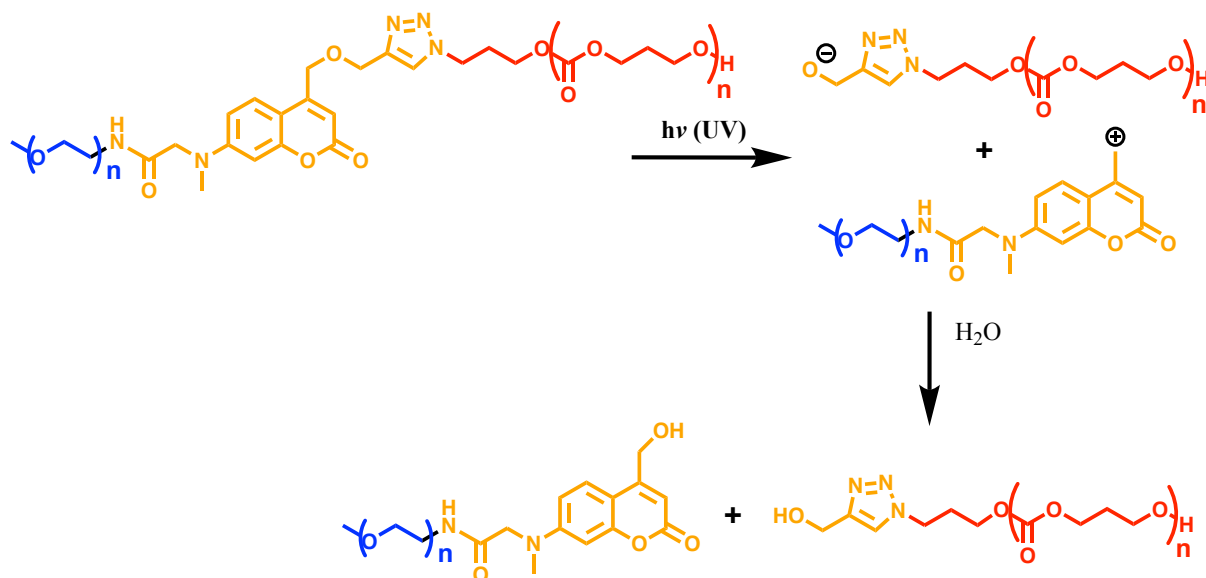


Figure 30: UV (365 nm) sample irradiation.

Irradiation was carried out on the self-assembled particles in water. The coumarin undergoes heterolytic cleavage between the carbon and the oxygen to form a carbocation and an alkoxide (Scheme 15). Then the two ions react with water to form two alcohols and avoid recombination.



Scheme 15: General scheme for the molecular mechanism of PEG₄₅-coumarin-*b*-PTMC₈₁ photocleavage under UV irradiation.

2.6.2. Irradiation effect at the molecular level

Quantum yields were measured on the self-assembled particles at 365 nm and 405 nm, wavelengths relevant for experiments in spectrometer and confocal microscope, respectively. Samples were irradiated using a monochromator to obtain precise wavelengths. The UV lamp output was calibrated using potassium ferrioxalate-phenanthroline as a chemical actinometer. The absorption spectra were measured for every 10 min irradiation (Figure 31).

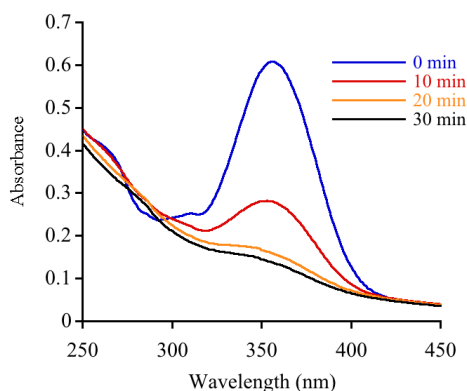


Figure 31: Electronic absorption spectra of PEG₄₅-coumarin-*b*-PTMC₈₁ polymersomes upon irradiation at 365 nm at different times.

Because particles themselves absorb light, the baseline was not at 0. However, coumarin absorption was clearly visible. The irradiation induced a decrease in the coumarin absorption that traduced a photoreaction of the coumarin. This absorption decrease allowed calculation of the quantum yield (quantum yield calculation in the experimental part). The quantum yield for cleavage of the copolymer was 0.0034 upon 365 nm irradiation and 0.0012 at 405 nm. This value is conform with the values found in the literature [7].

2.6.3. Effect of irradiation at the macromolecular level

Polymersomes made from PEG₄₅-coumarin-*b*-PTMC₈₁ copolymer were irradiated in aqueous solvent. In order to understand the photochemical mechanism at the macromolecular level, samples were irradiated for 1, 2 and 3 min. The water was then evaporated and samples were analyzed by SEC. The SEC traces are shown in Figure 32.

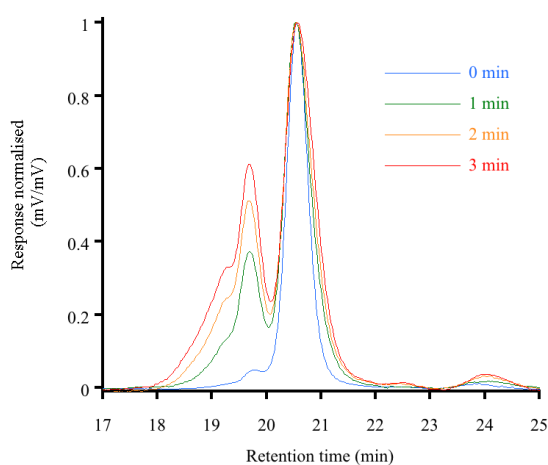
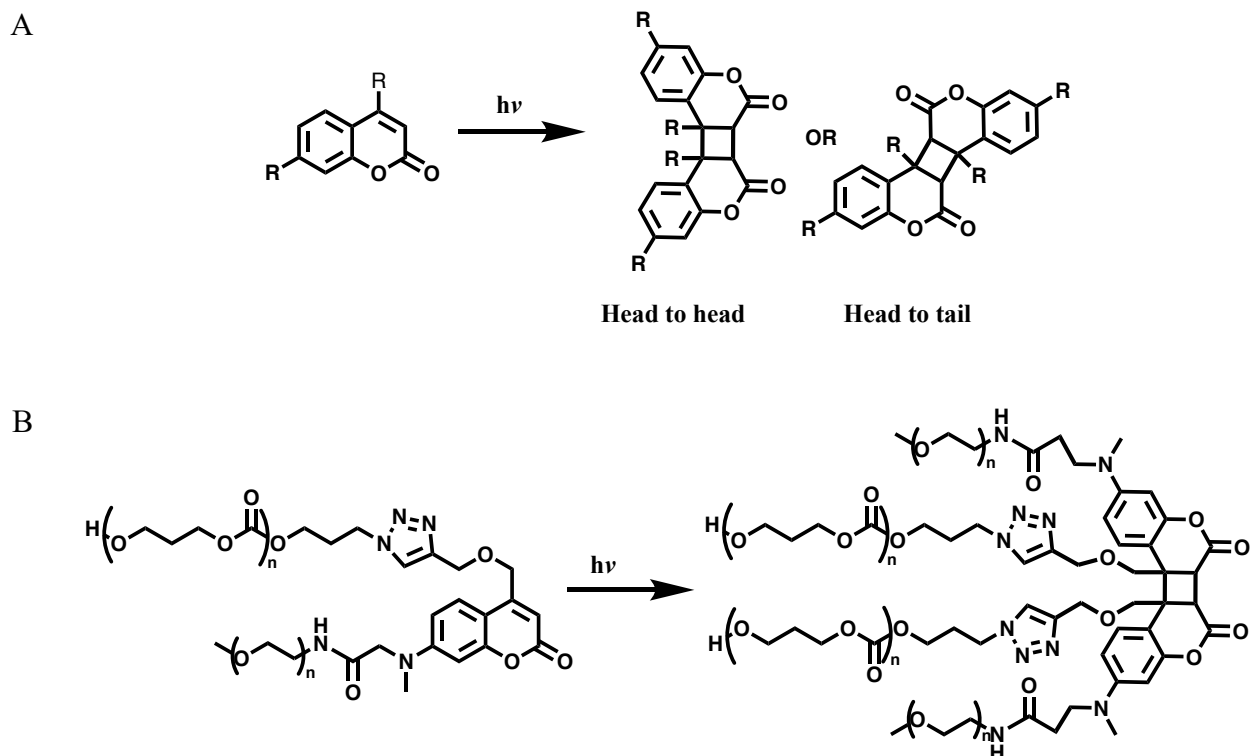


Figure 32: SEC analysis in THF of the irradiated PEG₄₅-coumarin-*b*-PTMC₈₁ polymersomes. The water was removed and the resulting copolymer was analyzed after redispersion in THF.

The traces clearly showed dimer formation (19.5 min). In previous studies coumarin dimerization (Scheme 16 A) has been elucidated [39]. From SEC analysis the copolymer dimerization mechanism can be deduced as shown in Scheme 16 B.



Scheme 16: A) Coumarins can dimerize under UV irradiation in two different ways: head to head and head to tail. B) Diblock formation of the copolymer due to coumarin dimerization.

Coumarin dimerized and forms copolymer diblocks that are no longer photosensitive. Small copolymer fractions were also cleaved (main peak molar mass decreased). However, the cleavage mechanism was expected to be more efficient, faster and dimerization negligible. SEC analysis showed, surprisingly, that dimerization was favored upon cleavage. Self-assembly induced a well-ordered copolymer at the interface due to bilayer formation. As a consequence, the local coumarin concentration is much higher than the average solution concentration. In order to test the hypothesis that self-assembly promotes dimerization, the block copolymers were dissolved in chloroform, a common solvent for the two blocks, resulting in a complete dissolution of copolymer chains with coumarin segments that were not locally concentrated. The copolymer solution was irradiated for 5 min and the resulting irradiated copolymer was analyzed by SEC (Figure 33).

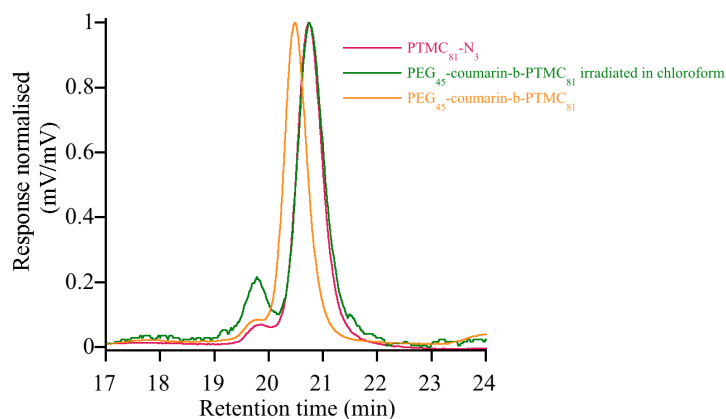


Figure 33: SEC in THF traces of PTMC₈₁-N₃ and PEG₄₅-coumarin-b-PTMC₈₁ copolymer before and after irradiation in chloroform.

The results showed that after irradiation copolymer SEC trace (green) overlap PTMC₈₁-N₃ SEC trace (red), indicating that the irradiated copolymer molar mass was reduced to PTMC₈₁ molar mass. As a conclusion, this clearly indicated that the PEG₄₅-coumarin-b-PTMC₈₁ copolymers can be efficiently cleaved if dissolved. Conversely, when self-assembled into vesicles, the dimerization process was favored, confirming our hypothesis.

Nevertheless, cleavage was still induced by longer irradiation periods. The copolymer was self-assembled and irradiated in water during one hour. After water evaporation, SEC analysis clearly showed that copolymer SEC trace (green) overlapped with the PTMC₈₁-N₃ SEC trace (red). After irradiation the copolymer molar mass was reduced to PTMC₈₁ and PEG₄₅-coumarin molar mass (Figure 34). Dimer formation was also observed. Thus irradiation simultaneously induced cleavage and dimerization.

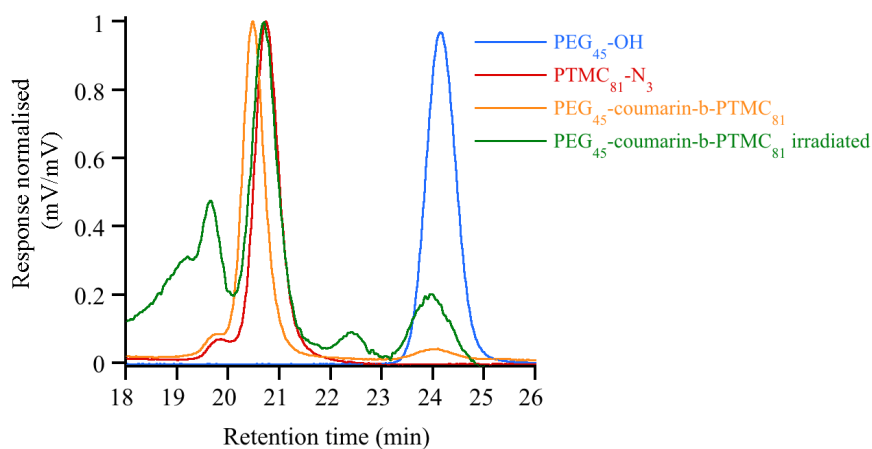


Figure 34: SEC in THF traces of PEG₄₅-coumarin-b-PTMC₈₁ copolymer irradiated 1 hour in water. The irradiated copolymer trace overlap with PTMC₈₁-N₃ trace and PEG₄₅-OH trace.

Another signal also appeared at 22.5 min in Figure 34. This signal has twice the molar mass of the PEG₄₅-coumarin. After PEG₄₅-coumarin cleavage and release, the coumarin is still photoactive and can still be photodimerized. Released PEG₄₅-coumarin dimerized resulting in PEG₄₅-coumarin diblocks (Figure 35).

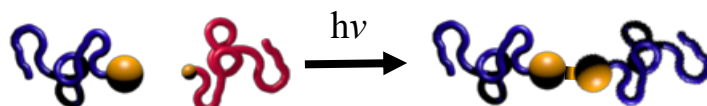


Figure 35: Photocleaved diblock and subsequent PEG₄₅-coumarin dimerization.

To summarize, there are two mechanisms occurring during irradiation: cleavage and dimerization as shown in Figure 36. These two mechanisms have opposite consequences on the self-assembled structures: dimerization induces stabilization, while cleavage induces destabilization.

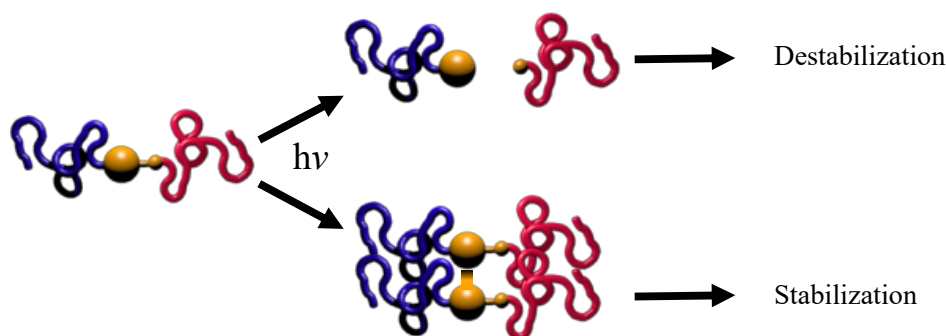


Figure 36: Two mechanisms induced by irradiation: cleavage and dimerization.

2.6.4. Effect of the irradiation on the particles morphology

2.6.4.1. Multi-angle light scattering

Multi-angle light scattering (static and dynamic) analysis before and after irradiation was used in order to assess the influence of irradiation on particle morphology. R_g and R_h were measured on the same batch of particles before and after 2.5 hours irradiation in phosphate buffer 50 mM pH 7.4. The results are presented in Table 8.

	Rg	Rh	Rg/Rh
Before irradiation	67	79	0.85
2.5 hours irradiation	67	79	0.85

*Table 8: Rg and Rh measured by multi-angle light scattering of PEG₄₅-coumarin-*b*-PTMC₈₁ particle before and after irradiation.*

A solution of PEG₄₅-coumarin-*b*-PTMC₈₁ particles was irradiated for 1 hour and then analyzed by Cryo-TEM. Freshly prepared samples were studied at the IMPMC. Images are presented in Figure 37. Particles were more difficult to observe due to a smaller particle number that could be observed in the sample. This was probably partly due to particle destabilization during irradiation. Some of the observed particles showed closed membranes, clearly indicating a vesicular structure (Figure 37 A and B) while morphology was difficult to identify on other particles (Figure 37 A, B, C). The remaining observed particles had the same size as before irradiation (≈ 100 nm). Drawing conclusions about the dispersity was more difficult due to the low number of particles observed, however rather similar sizes were observed. Additionally, some changes were detected on the particle membrane. Polymersomes had a thicker membrane (20 nm) and no membrane or a thinner membrane on undefined particles was noted. To summarize, the observed particle size dispersity was not modified (consistent with multi-angle light scattering measurements), however a modification of the particle membrane was observed.

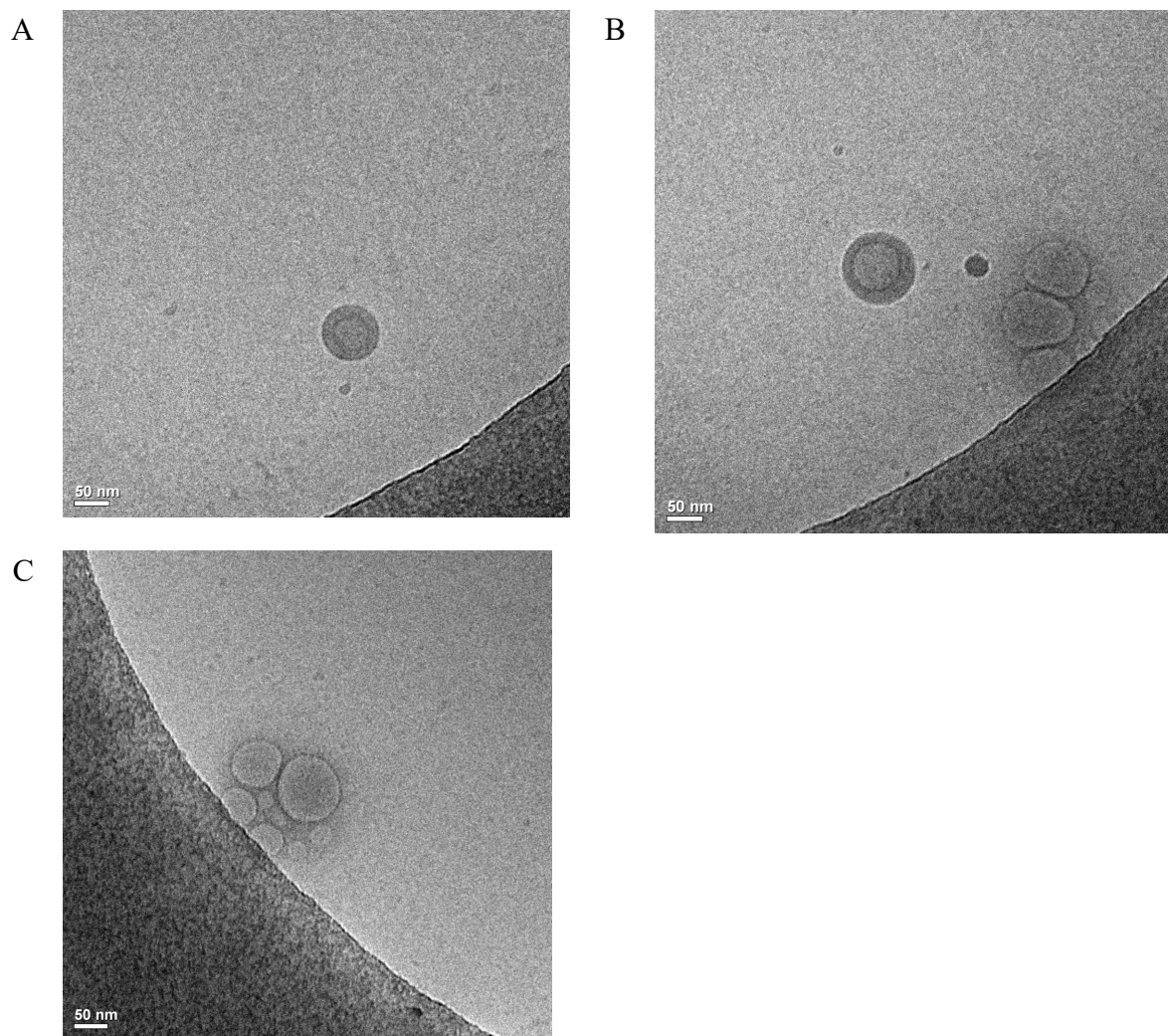


Figure 37: Cryo-TEM images of particles after irradiation (A, B, C).

2.6.4.2. Dynamic light scattering analysis at 90°

In order to measure irradiation effects on polymersome stability on the whole sample, contrary to cryo-TEM, the average intensity of light scattered by particles was measured by DLS at 90° (Malvern) at different irradiation times. Scattered light intensity is directly related to the concentration of particles in the medium and their molar mass. If the irradiation destabilized particles the signal should decrease. The scattered light was measured by DLS at 90° after 30 min, 1.5 hours and 2.5 hours of irradiation. The results are shown in Figure 38.

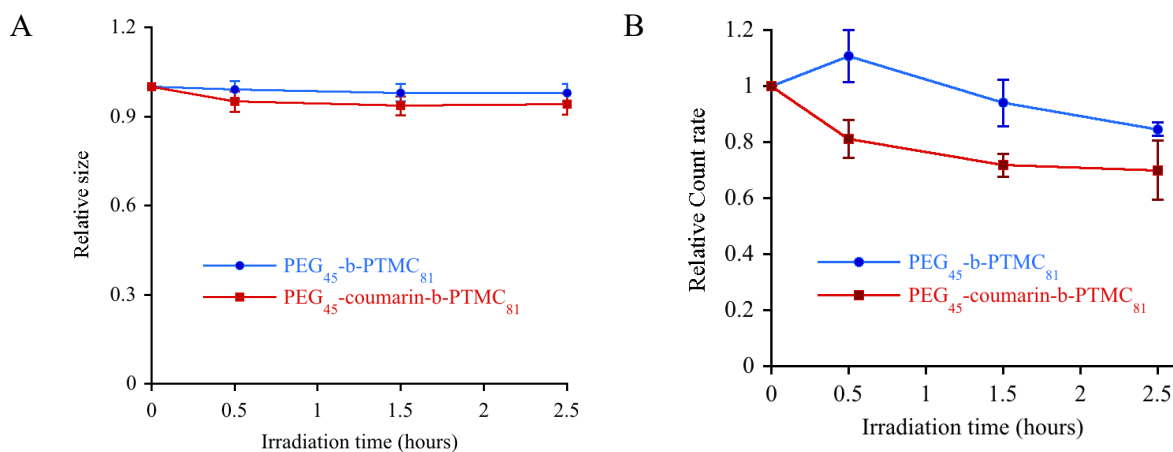


Figure 38: Relative sizes and scattered light intensity measured by DLS at 90° with light sensitive and non-light sensitive PEG₄₅-b-PTMC₈₁ depending on the irradiation time.

The results were compared with non-light sensitive polymersomes from PEG₄₅-b-PTMC₈₁ with the same molar mass. Particles were irradiated in phosphate buffer (50 mM, pH 7.4). Measurements were repeated 3 times with several particle batches. The result shows that the irradiation decreased the particle size by 5%. The intensity of light scattered by the nanoparticles decreases by 30% after 2.5 hours. The control shows that the scattered light intensity of non-photosensitive particles decreased by 16% after 2.5 hours irradiation. These results indicated that particles either were destabilized or lost their mass after irradiation. However, a significant proportion (70%) of the scattered light intensity and thus particles still remained, probably due to dimerization. These results showed that the light sensitive polymersomes were not fully destabilized by UV irradiation. Dimerization observed by SEC analysis (part 2.6.3) was suspected to improve particle stability. Indeed, dimerization prevents PEG release and thus improves particle stability.

2.7. Conclusion

Light-sensitive copolymer PEG₄₅-coumarin-b-PTMC₈₁ was synthesized. To this end, the coumarin light-sensitive linker was first synthesized with two grafting groups (carboxylic acid and alkyne group), in order to be able to graft one hydrophilic and one hydrophobic polymer. The PEG₄₅ chain-end was modified into an amine in order to be grafted on the carboxylic acid of the coumarin. TMC was polymerized to form PTMC with an azide chain-end. The key parameter to obtain a low dispersity (1.05) was the initiator purification. Several PEG₄₅-b-PTMC with different PTMC length were synthesized in order to find the appropriate hydrophilic ratio to form polymersomes. PEG₄₅-b-PTMC₈₁, with a hydrophilic ratio of 19%,

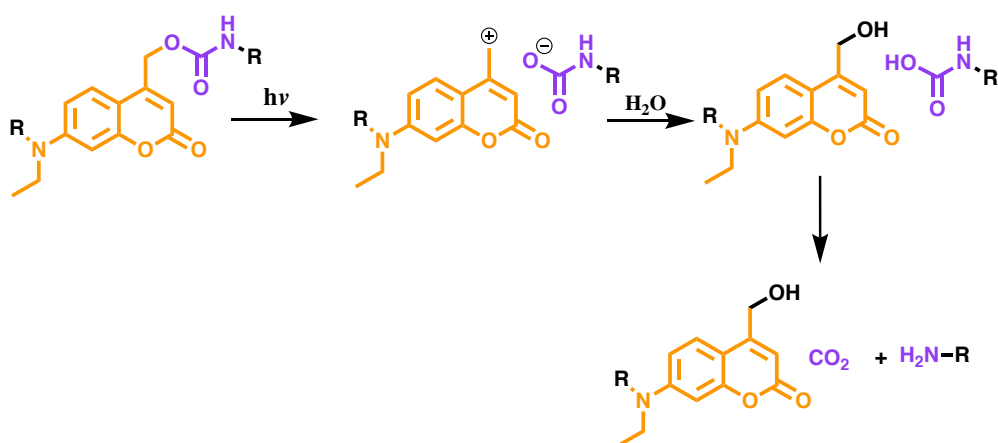
self-assembled into well-defined polymersomes. PEG₄₅-NH₂ and PTMC₈₁-N₃ were successively grafted onto the coumarin linker to give the light sensitive amphiphilic block copolymer PEG₄₅-coumarin-*b*-PTMC₈₁. The copolymer had a narrow dispersity of 1.05. This copolymer self-assembled into well-defined polymersomes with a hydrodynamic diameter of 120 nm and a narrow dispersity (PDI \approx 0.1). UV irradiation of polymersomes induced no change in the morphology or the particle sizes. DLS at 90° showed particles were either partly destabilized or lost partly their mass after irradiation (30% signal loss after 2.5 hours irradiation). However, most nanoparticles (70%) were not destabilized by irradiation. The stability of the polymersomes could be explained by coumarin dimerization, favoured by self-assembly, that prevents PEG release. In order to improve the destabilization efficiency a new copolymer design was synthesized and analyzed in the next part.

2.8. 2nd generation design of the light sensitive copolymer

2.8.1. New copolymer Strategy

Most of 1st generation particles were stable under irradiation. This part aimed to improve the efficiency of particle destabilization under irradiation. In the previous part, dimerization was suspected to improve particle stability. Indeed, dimerization prevents PEG release and thus improves particle stability. Coumarin dimerization would be difficult to prevent due to coumarin confinement as shown part (2.6.3). However, we hypothesized that increasing PEG release from particles could improve particle destabilization. To this end, two means were explored to increase PEG release from particles. Firstly, a better cleavage efficiency in order to release PEG before it could dimerize. Secondly, coumarin cleavage position: releasing only PEG instead of PEG-coumarin could favoured PEG release as explained in more detail in the following paragraphs.

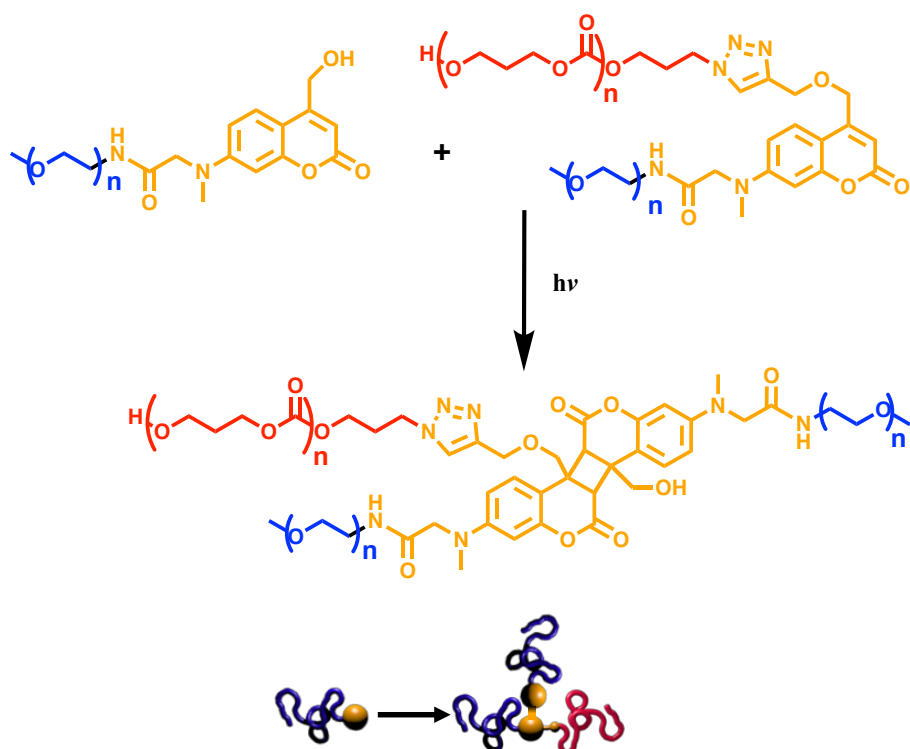
Firstly cleavage efficiency was improved and a new coumarin linker was designed as shown in Scheme 17.



Scheme 17: Photoinduced degradation of carbamate linkage liberating carbon dioxide and amine.

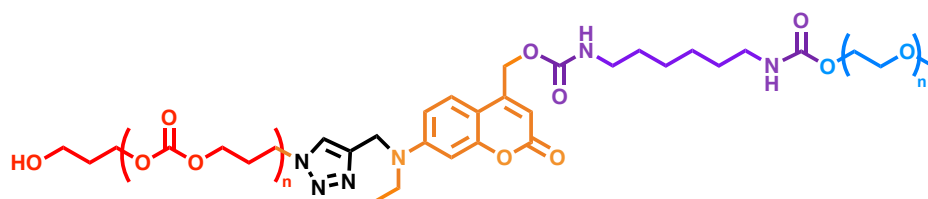
The coumarin was changed in order to generate a better leaving group after irradiation. To that end, a carbamate linkage replaced the ether linkage. Thus irradiation induces the release of a carbamate anion that is more stable than an alkoxide, so it is a better leaving group. Furthermore, carbamate anions undergo spontaneous decarboxylation inducing irreversible cleavage contrary to the previous design. This new coumarin was chosen to link PTMC and PEG to form a more efficient light-sensitive copolymer.

The second feature changed was the polymer position on the linker. The first design induced PEG₄₅-coumarin release after irradiation. Two problems arose from this design. Coumarin is a hydrophobic molecule of 260 g/mol and PEG is a hydrophilic polymer of 2000 g/mol. The hydrophobic ratio of the releasing PEG₄₅-coumarin is 12%, which means that an amphiphilic molecule is released. PEG₄₅-coumarin release from PTMC₈₁ is not favored due to hydrophobic interactions and particles are less likely to be destabilized. The second problem is that the released PEG₄₅-Coumarin is still photoactive. The coumarin can still dimerize as shown in Scheme 18 and in part 2.6.3.



Scheme 18: Proposed photodimerization of PEG₄₅-coumarin with the intact triad which would lead to particle stabilization.

This hydrophilic block can be grafted onto the copolymer and stabilize the nanoparticles and therefore not induce particle destabilization. In order to solve this issue, the PEG and PTMC positions were exchanged. Finally, the new design chosen for the photocleavable triad is shown in Scheme 19. The purple hexamethylene dicarbamate was introduced for synthesis reasons that are explained later part 2.8.2.2.

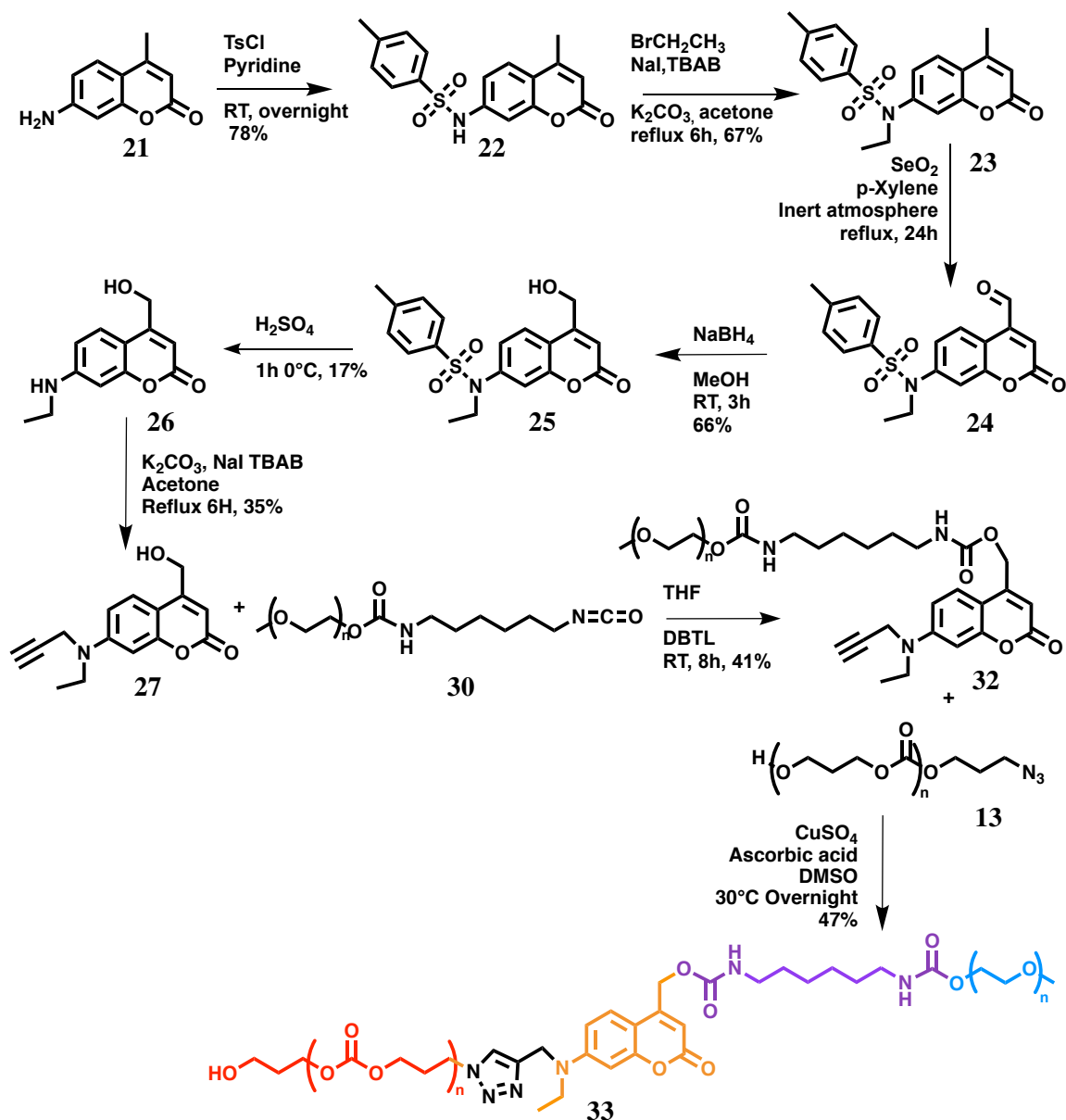


Scheme 19: 2nd generation design of photosensitive PEG-coumarin-b-PTMC₈₁ on modular rearrangement.

2.8.2. Synthesis

2.8.2.1. Light-sensitive linker

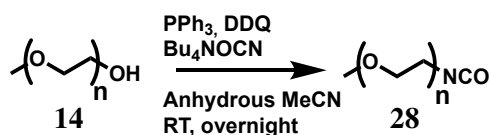
Synthesis of the new light sensitive copolymer was inspired from [40]. The synthesis started with the commercially-available 7-amino-4-methylcoumarin (**21**) that was reacted with tosyl chloride to yield 7-p-toluenesulfonamide-4-methylcoumarin (**22**) in 78% yield. The tosyl was used as a protecting group. This protection permitted monoalkylation of the amine later on in the synthesis. **22** was then alkylated with bromoethane under basic conditions. First this reaction was performed with only K_2CO_3 and the reaction rate was too slow. In order to increase the reaction rate, tetra-n-butylammonium bromide (TBAB) was used as a phase transfer catalyst. **23** was obtained in 67% yield. In order to be able to form the carbamate linkage the methyl was reacted to obtain an alcohol in two steps. The methyl of **23** was oxidized into an aldehyde with selenium dioxide to obtain **24**. The corresponding aldehyde **24** was then directly reduced into an alcohol with sodium borohydride to give tosylated 4-hydroxy-methylcoumarin (**25**) in 66% yield. **25** was then deprotected under acidic conditions. The corresponding coumarin with a secondary amine (**26**) was obtained in 17% yield. The yield could be improved by tuning the reaction time and temperature. The amine was then alkylated with the same conditions as described previously to obtain **23**. This alkylation allows introduction of an alkyne group in order to graft the $PTMC_{81-N_3}$ via a click reaction. The final linker **27** was obtained in 35% yield. This linker **27** has an alcohol group in order to graft the PEG_{43} and the alkyne to graft the $PTMC_{81-N_3}$.



Scheme 20: Synthetic route for a second generation light sensitive PEG₄₃-coumarin-b-PTMC₈₁.

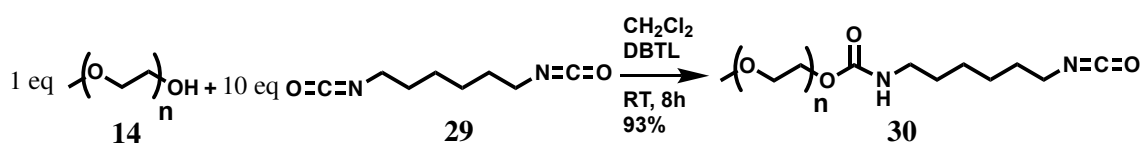
2.8.2.2. PEG₄₃ end chain modifications

The first strategy used to graft PEG₄₃ on the coumarin group with a carbamate link was to react an isocyanate with an alcohol in the presence of a tin catalyst. The alcohol was added on the coumarin linker, thus the isocyanate group had to be added on the PEG₄₃-OH. In a previous study [41], an alcohol was converted into an isocyanate on several molecules. The same method was used to modify the hydroxyl chain end of the PEG₄₃ (Scheme 21).



Scheme 21: General scheme for PEG₄₃-OH end chain modification from an alcohol to an isocyanate.

However, purification was complicated because isocyanates are sensitive to water and alcohol. Several purification methods were tested. Precipitation in dry diethyl ether did not purify the PEG₄₃ isocyanate, nor did dialysis in dry THF for several days allow separation of the PEG₄₃ isocyanate from the impurity. Usually the best eluent to purify PEG with a silica column is methanol:DCM, however the methanol would react with the isocyanate. The purification was not possible so another method was used [42]. PEG₄₃-OH (1900 g/mol) was thus reacted with a diisocyanate. One isocyanate was reacted with PEG₄₃-OH to give a carbamate link. The other isocyanate was available for further reaction (Scheme 22).



Scheme 22: General scheme for PEG₄₃-OH end chain modification with HMDI to obtain an isocyanate as the end chain group.

In order to avoid the addition of two PEGs on the same diisocyanate, an excess of diisocyanate was used, and PEG₄₃-OH was added over a two hour period. PEG₄₃-OH was reacted with hexamethylene diisocyanate (HMDI: **29**) to give PEG₄₃-HMDI (**30**) in 93% yield

¹H NMR showed that 96% of the PEG₄₃-OH was converted into PEG₄₃-HMDI. Infrared spectroscopy clearly showed new signals compared to the initial PEG₄₃-OH that correspond to isocyanate (2271 cm⁻¹) and carbamate groups (1718cm⁻¹) in Figure 39.

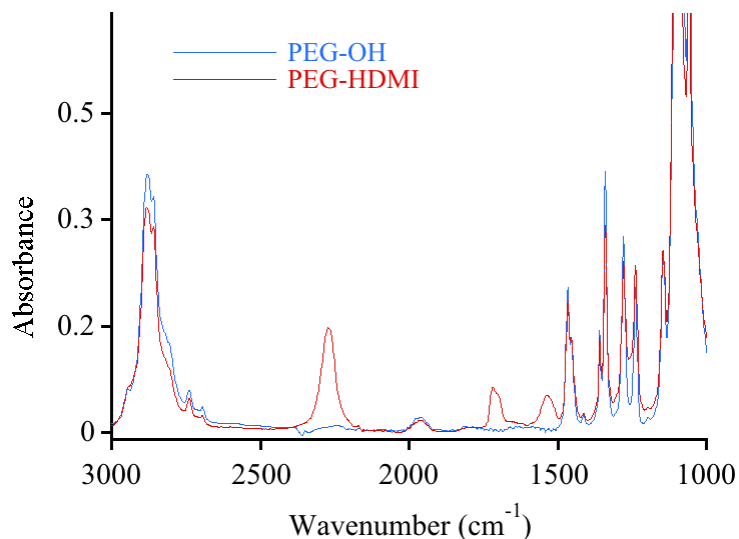


Figure 39: Comparison of infrared spectroscopy signals of PEG₄₃-OH and PEG₄₃-HMDI. Signals corresponding to carbamate (2271 cm⁻¹) and isocyanate (1718 cm⁻¹) groups appeared.

SEC analysis was performed in THF (Figure 40). The PEG₄₃-HMDI SEC trace showed a slight difference in retention time (23.60 min) compared to the PEG₄₃-OH (23.86 min) due to the higher PEG₄₃-HMDI molar mass. As expected, a small fraction of PEG₄₃ dimer was observed. The dimer was formed by two PEG₄₃-OH that reacted on the same HMDI (PEG₄₃-HMDI-PEG₄₃). It was removed further on in the synthesis by column chromatography on a silica stationary phase.

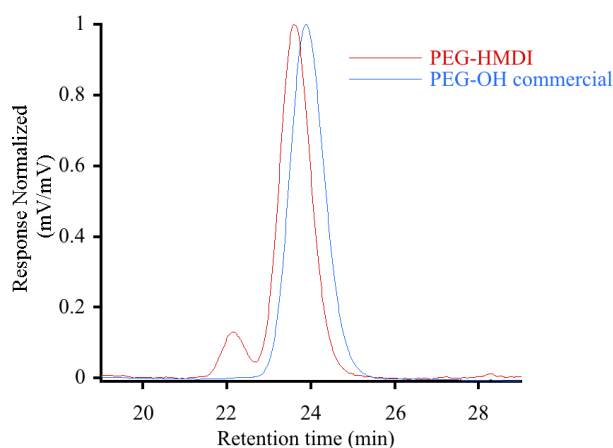
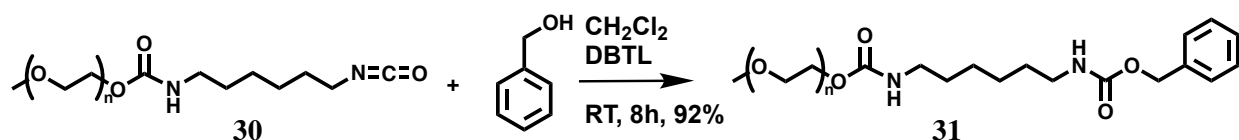


Figure 40: SEC in THF traces mPEG₄₃-HMDI and PEG₄₃-OH.

2.8.2.3. PEG grafting on coumarin via amide bond formation

2.8.2.3.1. Test Reaction

A test reaction was performed to assess the grafting reaction catalyzed by dibutyltin dilaurate (DBTL). Benzyl alcohol (BA) was used as a surrogate for the coumarin to be grafted on PEG₄₃-HMDI (Scheme 23).



Scheme 23: General scheme for the grafting reaction of benzyl alcohol on PEG₄₃-HMDI.

Precipitation in diethyl ether was used to remove excess benzyl alcohol. ¹H NMR showed that PEG₄₃-HMDI-BA (31) was obtained in 92% yield. Also infrared spectroscopy of PEG₄₃-HMDI-BA compared to that of PEG₄₃-HMDI clearly showed disappearance of the isocyanate signal (2271 cm⁻¹) and increase of carbamate group signals (1718 cm⁻¹) (Figure 41).

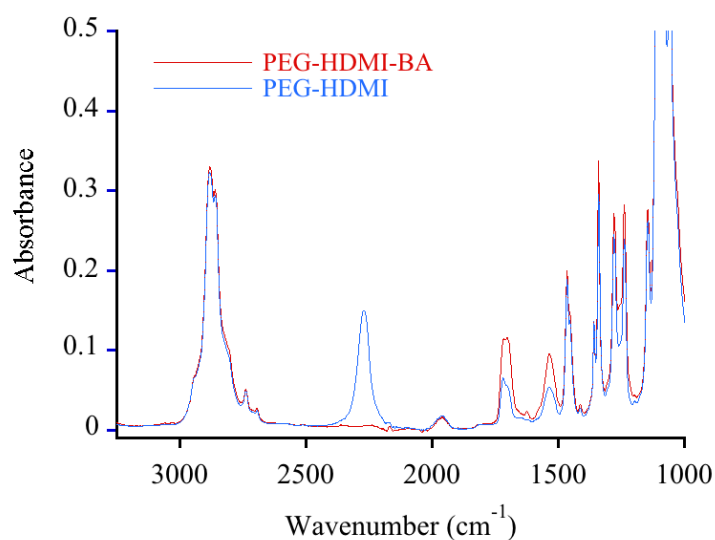
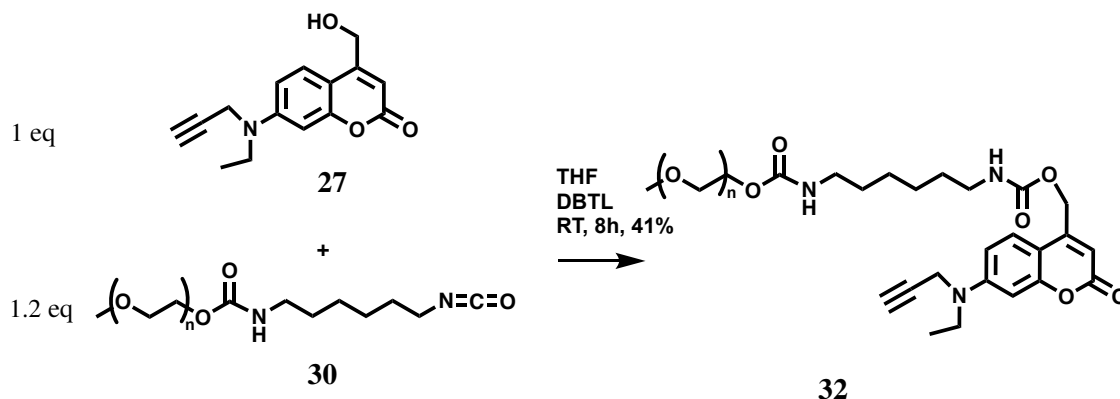


Figure 41: Comparison of infrared spectroscopy signals of PEG₄₃-HMDI-BA and PEG₄₃-HMDI. Isocyanate (2271 cm⁻¹) signal disappearance and carbamate (1718 cm⁻¹) signals increase.

2.8.2.3.2. PEG₄₃-HMDI grafting reaction on Coumarin

Thus PEG₄₃-HMDI was reacted with a coumarin linker to form a carbamate bond thanks to a DBTL catalyst to give PEG₄₃-HMDI-Coumarin (**32**) in 41% yield.



Scheme 24: General scheme for PEG₄₃-HMDI grafting on coumarin with carbamate link.

The resulting copolymer was analyzed by SEC and the comparison between the UV signal and the RI signal (Figure 42) shows that only the monoblock absorbs in the UV.

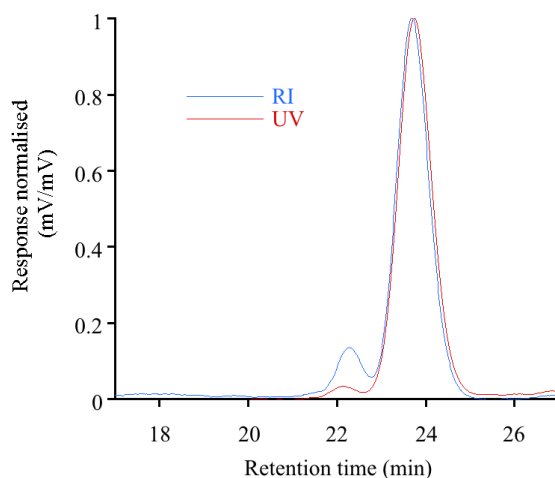


Figure 42: SEC in THF traces in RI and UV of PEG₄₃-HMDI-coumarin.

The dimer did not have an isocyanate group, thus coumarin was not grafted on it and the dimer did not absorb. Also the absorption band attributed to the monoblock was centered at 360 nm (Diode-array UV detector of the SEC) that was typical of coumarin. These results show that coumarin was linked to the monoblock PEG₄₃-HMDI.

SEC analysis revealed an impurity (retention time 27 min) even after several precipitation steps in diethyl ether (Figure 43 A). The absorption spectrum of this impurity showed the typical coumarin signal as shown in Figure 43 B. This impurity was unreacted coumarin.

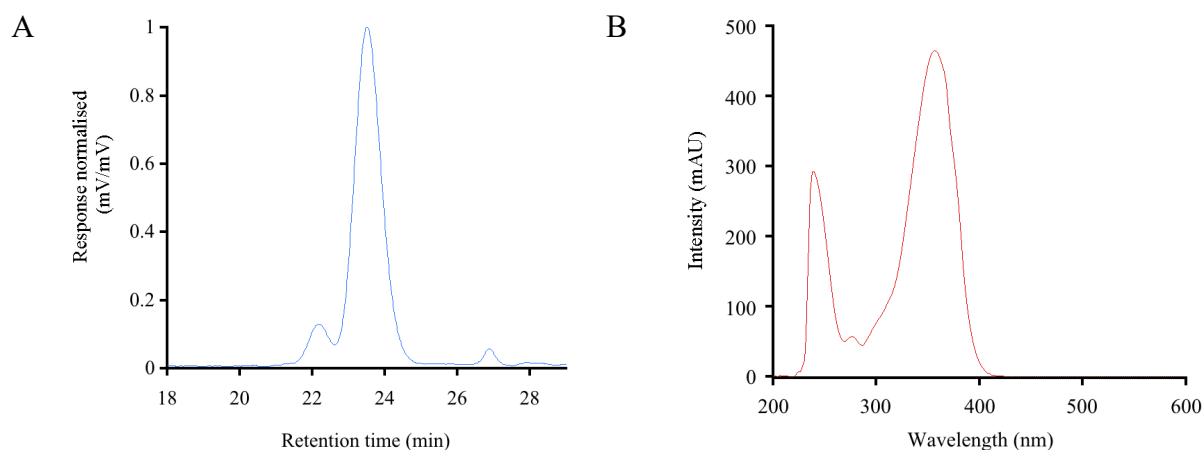


Figure 43: A) SEC in THF trace of PEG₄₃-HMDI-coumarin. B) Absorption spectra of the impurity detected in SEC THF (Diode-array UV detector) with a retention time of 27 min.

The free coumarin could react with PTMC₈₁-N₃ in the last step of the copolymer formation, and PTMC₈₁-coumarin could be difficult to remove. In order to remove the free coumarin several methods have been tested and the resulting SEC traces are shown in Figure 44.

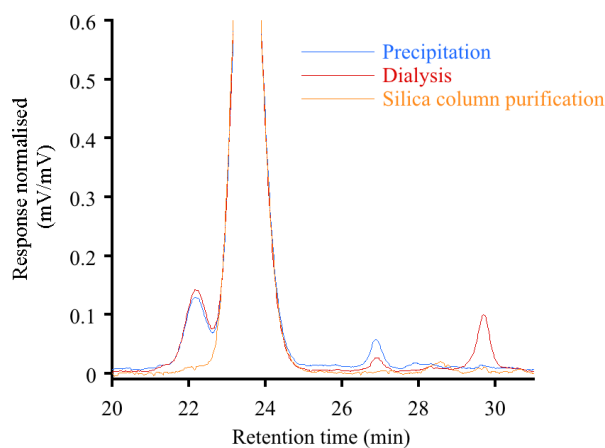


Figure 44: SEC in THF traces of PEG₄₃-HMDI-coumarin after different purification method (precipitation, dialysis, and silica column purification).

Coumarin was rather soluble in THF, the PEG₄₃-HMDI-coumarin was first dialyzed in THF with a 1 kDa dialysis bag for several days. Some free coumarin was removed as the SEC trace showed. However, some remained. Moreover a large proportion of material was lost during the dialysis and a new impurity appeared at 29 min (butylated hydroxytoluene, a THF stabilizer). The second purification process tested was silica column with methanol:DCM as the eluent. This method removed the free coumarin, the butylated hydroxytoluene and surprisingly even

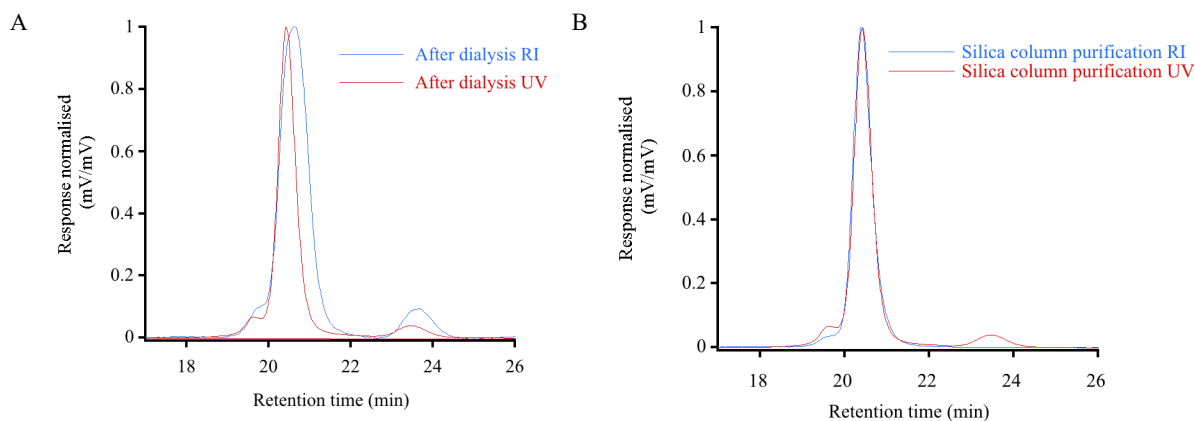


Figure 45: A) SEC traces in UV and RI of PEG₄₃-coumarin-*b*-PTMC₈₁ in THF after dialysis. B) SEC traces in UV and of PEG₄₃-coumarin-*b*-PTMC₈₁ in THF after silica column purification.

A large majority of the PEG₄₃-HMDI-coumarin was removed because no more signal was detected in RI. The resulting copolymer had a mass that corresponds to the mass of the PTMC₈₁-N₃ and PEG₄₃-HMDI-coumarin, also the absorption signal at 20.5 min is typical of the coumarin (same absorption bands as Figure 43 B). ¹H NMR showed the appearance the triazole proton resonance at 8.0 ppm. All these analyses proved that the PEG₄₃-coumarin-*b*-PTMC₈₁ copolymer was successfully synthesized. The dispersity of the final copolymer was satisfactorily very low (1.04).

2.8.3. Self-assembly

PTMC and PEG lengths were chosen in order to have the right hydrophilic ratio to obtain a vesicular structure. These lengths were studied in part 2.5.1. The meth-PEG₄₃-OH molar mass was 1900 g/mol. Considering the coumarin and HMDI as hydrophobic molecules of respectively 257 g/mol and 168 g/mol, the hydrophilic ratio of the newly synthesized copolymer PEG₄₃-coumarin-*b*-PTMC₈₁ was 18%. This hydrophilic ratio is close to the one studied previously with PEG₄₅-*b*-PTMC₈₁. Thus, this new light-sensitive copolymer was expected to self-assemble into polymersomes. The method used to self-assemble this new copolymer was nanoprecipitation with the injection speed being controlled by a syringe pump as explained in part 2.5.1.3.

Nanoprecipitation was performed with a syringe pump in order to be able to have a precise control on the particle size. 2.7 mL of water was added during 15 s in 300 μL of DMSO containing the copolymer at 10 mg/mL. During the water addition the mixture was stirred at

500 tr/min in a 5 mL brown glass vial. To remove DMSO the particle suspension was dialyzed 3 times again 5 L of deionized water with a 3.5 kDa membrane during 3 hours. The resulting nanoparticle suspension had a concentration of 1mg/mL. 3 samples were prepared in order to study the nanoprecipitation repeatability. Particles sizes, PDI and count rate were measured by DLS at 90° after dialysis. Results are presented in Table 9 and Figure 46. Sizes, signal intensity and PDI were close as the low value of coefficient of variation indicated. These 3 samples showed that the method used was repeatable. This technique allows us to have monomodal particles with a low PDI around 0.1 and sizes around 300 nm.

Samples	Count rate (kcps)	Sizes (nm)	PDI
N°1	5424	324	0.113
N°2	5400	326	0.128
N°3	5766	317	0.148
Average	5530	322	0.130
Standard deviation	204	4.7	0.018
Coefficient of variation	3.7%	1.5%	13.5%

Table 9: Parameters measured by DLS at 90° (Malvern) of PEG₄₃-coumarin-b-PTMC₈₁ nanoparticle batches prepared under the same conditions.

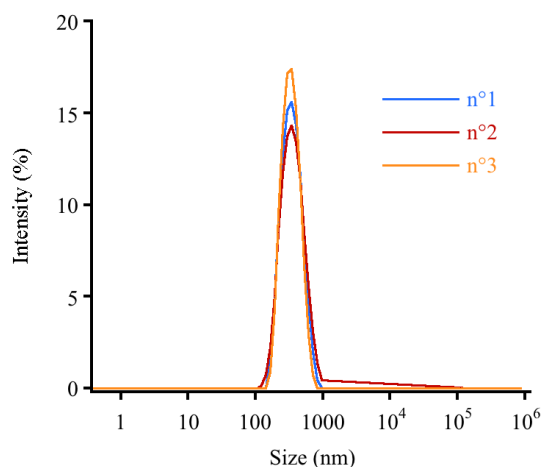


Figure 46: Intensity-averaged hydrodynamic diameter distributions of 3 batches of PEG₄₃-coumarin-b-PTMC₈₁ nanoparticles in water, recorded by DLS at 90°.

In order to have a stable medium during irradiation, and the right conditions for enzyme use, nanoparticles have to be dispersed in a buffered medium. To that end, the nanoparticle medium was changed from pure water to phosphate buffer (PB: 50mM, pH 7.4). The medium was

changed after nanoparticle formation and dialysis. However, the change in osmotic pressure or the presence of additional ions could destabilize particles. Thus the particle stability after buffer addition was verified. To do so, 900 μL of phosphate buffer at 56 mM pH 7.4 was added in 100 μL of particle solution. The solution obtained was stable particles with similar sizes and similar PDI in 50 mM phosphate buffer, as shown in Figure 47 and Table 10. Particles were very stable, no modifications of the sizes, PDI or scattered light intensity were observed over at least one week.

Sample	Count rate (kcps)	Sizes (nm)	PDI
In water n°1	5549	271	0.097
After Buffer addition n°1	1123	266	0.068
In water n°2	4493	349	0.113
After buffer addition n°2	1210	326	0.157

Table 10: Comparison of diffused intensity, sizes and PDI of $\text{PEG}_{43}\text{-coumarin-b-PTMC}_{81}$ particles before and after phosphate buffer addition.

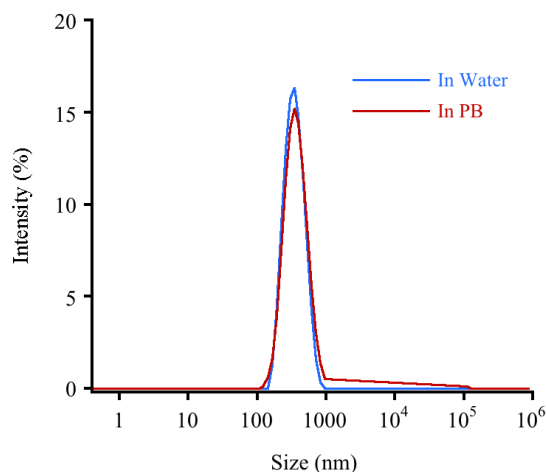


Figure 47: Intensity-average hydrodynamic diameter distributions of $\text{PEG}_{43}\text{-coumarin-b-PTMC}_{81}$ nanoparticles in water and PB, recorded by DLS at 90° .

2.8.4. Self-assembly characterization

2.8.4.1. Visual

Under UV lamp irradiation ($\lambda=365$ nm), nanoparticle solution showed homogeneous coumarin fluorescence (Figure 48).



Figure 48: Nanoparticles of PEG₄₃-coumarin-b-PTMC₈₁ under UV light (365 nm)

2.8.4.2. Multi-angle light scattering

Multi-angle light scattering (static and dynamic) was used to measure the Rg and Rh of the obtained particles. These particles were in a phosphate buffer (50 mM, pH 7.4). Two separate batches of nanoparticles were prepared. The low values of coefficient of variation showed that the two sets of nanoparticles had reproducible parameters (Table 11). Rg/Rh was close to 1, which is typical of vesicular structure.

	Rg (nm)	Rh (nm)	Rg/Rh
Batch 1	141.9	145.0	0.98
Batch 2	135	142	0.95
Average	138	144	0.97
Standard deviation	4.8	2.1	0.021
Coefficient of variation	3.5%	1.5%	2.2%

Table 11: Multi-angle light scattering measurements of Rg and Rh for two nanoparticle batches.

2.8.4.3. Cryo-TEM

Cryo-TEM required a concentration high enough in order to be able to observe enough nanoparticles. To that end, nanoparticle solutions were ultrafiltered to increase the concentration from 1 mg/mL to 5 mg/mL. Freshly prepared samples were then sent to Institut de minéralogie, de physique des matériaux et de cosmochimie for Cryo TEM analysis. Images are presented in Figure 49.

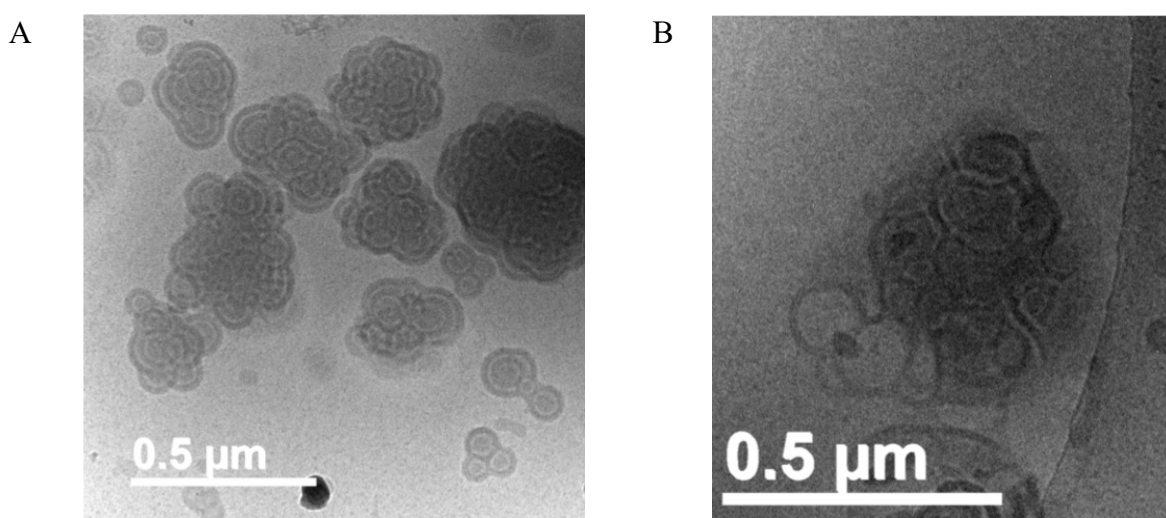


Figure 49: Cryo-TEM images of self-assembled particles of PEG₄₃-coumarin-b-PTMC₈₁ in water.

Cryo-TEM images showed aggregates of particle (Figure 49 A). Individual aggregates clearly have a vesicle shape. Membrane had an homogeneous size of 12 nm which was consistent with polymersome membrane [4] and previous observations. Vesicle size observed was around 300 nm that was the same order of magnitude than that observed by DLS (≈ 300 nm). We suggest that ultrafiltration destabilized the vesicles and made them aggregate. Figure 49 B showed vesicular structures stacked to form particle aggregates, which could suggest polymersome aggregation. In order to know if these structures are due to ultrafiltration, additional cryo-TEM analyses prepared from more dilute system are necessary.

2.8.5. Irradiation effects

PEG₄₃-coumarin-*b*-PTMC₈₁ particle morphologies were studied in the previous part. In order to confer light-sensitivity to the copolymer, a photosensitive coumarin was inserted between the two blocks. This part consists in studying the photosensitivity of the copolymer at the molecular level, macromolecular level, the effects on self-assembled particles and the release properties. Irradiation experiments were carried out with a 200 W Mercury-Xenon lamp. A filter was used, centering the light emission at 365 nm (emission spectra can be found in the experimental part). Samples were placed at 1 cm from the light guide output end and irradiated for a defined time. Irradiation was carried out on self-assembled particles in phosphate buffer (50 mM, pH 7.4).

2.8.5.1. Irradiation effect at the molecular level

The quantum yield of the self-assembled particles was measured in phosphate buffer (50 mM, pH 7.4) at 365 nm and 405 nm. Samples were irradiated across a monochromator to obtain precise wavelengths. The UV lamp was calibrated using potassium ferrioxalate-phenanthroline as a chemical actinometer. The absorption spectra were measured after every 1 min of irradiation (Figure 50).

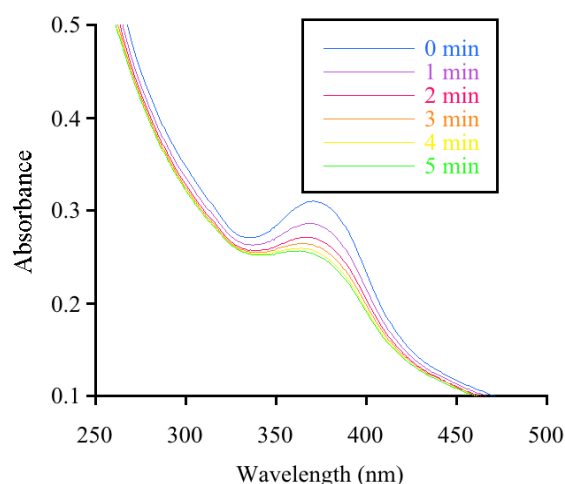


*Figure 50: Absorption of the polymersomes of PEG₄₃-coumarin-*b*-PTMC₈₁ in water at different irradiation times. The absorption decrease allowed measurement of the quantum yield.*

The particles scattered the light therefore the baseline was not at 0. However coumarin absorption was still clearly visible. The irradiation induced a decrease in the coumarin absorption, which means a photoreaction of the coumarin. This absorption decrease allows

calculation of the quantum yield. Copolymer cleavage quantum yield was found to be 0.012 upon irradiation at both 365 nm and 405 nm. These quantum yield values showed that the cleavage is much more efficient than the 1st generation copolymer.

2.8.5.2. Effect of Irradiation at the macromolecular level

The self-assembled copolymer was irradiated for 150 min in phosphate buffer solution. Water was removed from the resulting solution and the irradiated copolymer was analyzed by SEC in THF (Figure 51).

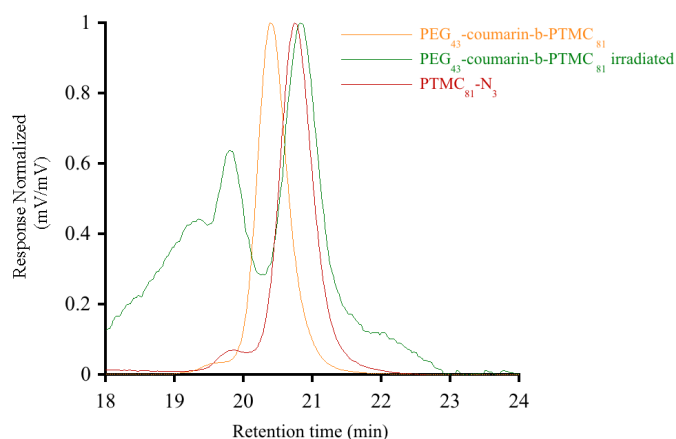


Figure 51: SEC in THF traces of PTMC₈₁-N₃ and the self-assembled PEG₄₃-coumarin-b-PTMC₈₁ before and after irradiation.

The trace clearly showed dimer formation (19.7 min) and that the irradiated PEG₄₃-coumarin-b-PTMC₈₁ SEC trace (green) overlapped the PTMC₈₁-N₃ SEC trace (red). After irradiation, the initially observed PEG₄₃-coumarin-b-PTMC₈₁ molar mass was reduced to that of PTMC₈₁. Thus irradiation induced both cleavage and dimerization. Surprisingly, the 2nd generation design thus did not prevent dimer formation as expected. One can argue that dimer formation was favoured by copolymer self-assembly and local confinement of the coumarin derivatives (as shown in part 2.6.3).

2.8.6. Irradiation Effect on the particle stability

2.8.6.1. Light scattering analysis

2.8.6.1.1. Comparison between 1st and 2nd generation of copolymer.

Object stability was measured by DLS at 90° (Malvern). In order to measure irradiation effects on polymersomes, light intensity scattered by particles was measured by DLS at 90° depending on irradiation time. Scattered light intensity is directly related to particle number and molar mass. The scattered light intensity was measured by DLS at 90° after 30 min, 1.5 hours and 2.5 hours irradiation. The results are shown in Figure 52. The results are compared to the 1st copolymer generation and non-light sensitive polymersomes from PEG₄₃-*b*-PTMC₈₁ with the same molar mass. All particles were irradiated in phosphate buffer (50 mM, pH 7.4) and with the UV lamp centered at 365 nm. Measurements were repeated 3 times with 3 particle batches. The light intensity scattered by the nanoparticles decreases by 66% after 2.5 hours and 44% the first half hour. The 1st generation particles scattered light intensity decreased by 30% and the scattered light intensity of non-photosensitive particles decreased only by 16% after 2.5 hours of irradiation. These results suggested that 2nd generation particles decreased their mass or were destabilized by irradiation. Loss of mass could be caused by PEG₄₃ release that could lead to particle destabilization. 2nd generation particles were more affected by irradiation than the 1st generation or non-photosensitive nanoparticles. Also an increase of 20% of the particle size was observed (Figure 52 B) suggesting particle aggregation. In order to know if the particles decreased in mass or were destabilized, cryo-TEM measurements were performed and results are shown in part 2.8.6.3.

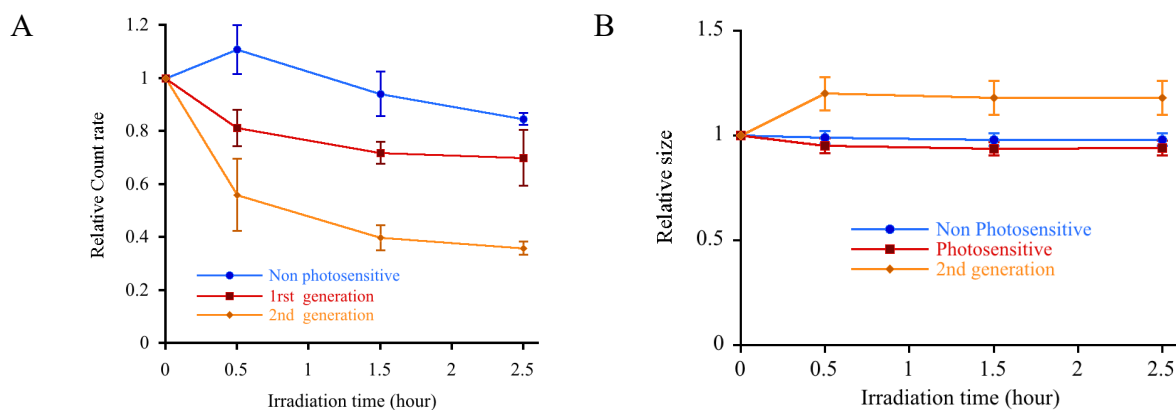
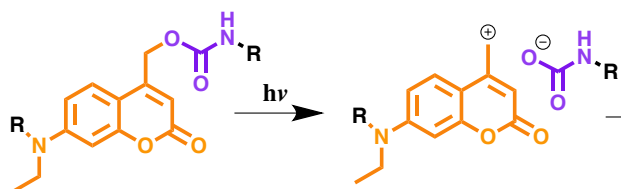


Figure 52: DLS at 90° (Malvern) measurements of A) relative scattered light intensity and B) sizes of the 1st and the 2nd generation of PEG₄₃-coumarin-*b*-PTMC₈₁ and PEG₄₃-*b*-PTMC₈₁ polymersomes in PB buffer depending on the irradiation time.

2.8.6.1.2. Buffer effect

A previous study showed that ion pair stabilization after the coumarin heterolytic cleavage plays a key role to avoid recombination. Thus stabilizing the newly formed ions greatly improves the cleavage efficiency [43]. We hypothesized that buffered medium could help screen ion pairing (Scheme 26) and thus improve the cleavage efficiency and the particle destabilization.



Scheme 26: After irradiation, carbocation and carbamate anions could be stabilized by buffer thereby avoiding recombination.

In order to test this hypothesis, particles were irradiated without buffer and with two different phosphate buffers. The scattered light intensity was measured depending on irradiation time and the results are presented in Figure 53.

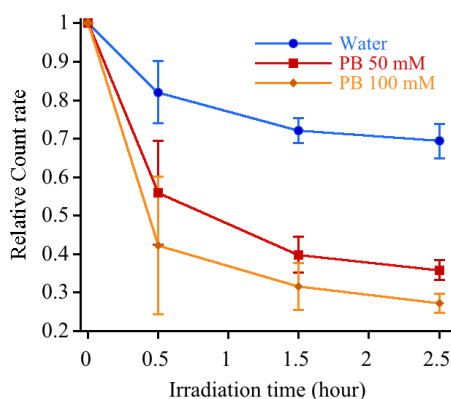


Figure 53: DLS at 90° (Malvern) measurements of relative scattered light intensity of the 2nd generation of PEG₄₃-coumarin-*b*-PTMC₈₁ polymersomes in different medium depending on the irradiation time.

Without buffer, irradiation did not destabilize particles efficiently: 70% of the initial signal remains after 150 min irradiation. However, nanoparticle irradiation in phosphate buffer (50 mM) was much more efficient: only 35% of the scattered light intensity remains after the same irradiation time. Phosphate buffer strength was increased to 100 mM and particles were irradiated, the scattered light intensity decreased even more: 29%. These results suggested that buffer increased particle destabilization. We tentatively suggest that the carbocation and carbamate anion generated after irradiation (Scheme 26) are stabilized by the buffer and limits unwanted recombination.

2.8.6.2. Multi-angle light scattering (static and dynamic)

To understand irradiation effect on the particle morphology, multi-angle light scattering (static and dynamic) was used to measure Rg and Rh before and after irradiation. To that end, the same particle batch was used before and after irradiation. The results (Table 12) clearly showed that Rg and Rh were modified as well as their ratio after irradiation. The Rg/Rh before irradiation was typical of vesicles (0.98) then this ratio after irradiation was typical of dense particles (0.64). This suggested densification of the particles core and change in the morphology.

	Before irradiation	After irradiation (2h30)
Rg (nm)	141.9	225.6
Rh (nm)	145	350
Rg/Rh	0.98	0.64

Table 12: Multi-angle light scattering measurements of Rg and Rh of PEG₄₃-coumarin-b-PTMC₈₁ particles in phosphate buffer before and after irradiation.

2.8.6.3. Cryo-TEM

Freshly prepared samples were sent to Institut de minéralogie, de physique des matériaux et de cosmochimie for Cryo TEM analysis. Images are presented in Figure 54. The same sample was observed after 150 min irradiation.

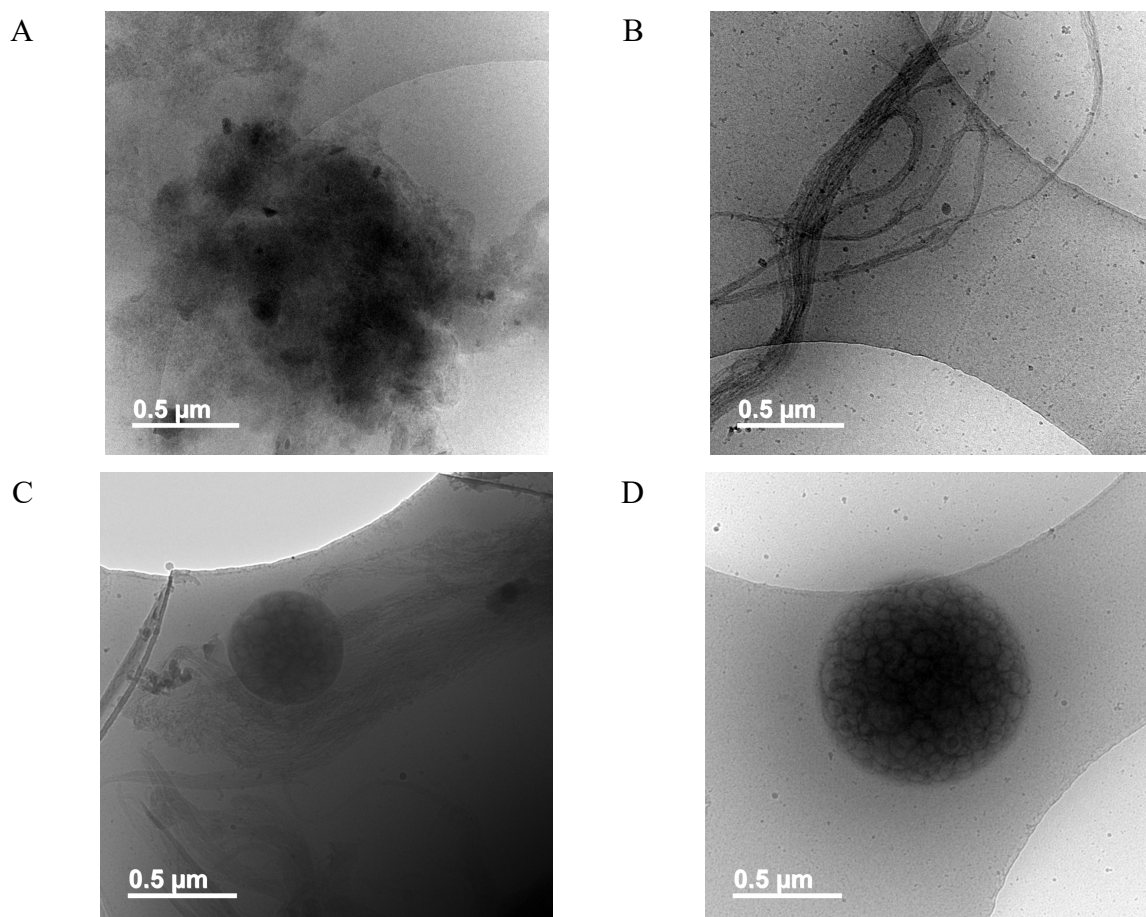


Figure 54: Cryo-TEM images of PEG₄₃-coumarin-b-PTMC₈₁ nanoparticles in water after UV irradiation (2h30) showing a large diversity of particles and aggregates.

Undefined aggregates (Figure 54 A), filaments (Figure 54 B, C) and well-defined round particles (Figure 54 C, D) were observed. The undefined aggregates observed showed that irradiation induced destabilization. The round particles suggest that the irradiated PEG₄₃-coumarin-*b*-PTMC₈₁ decreased water interactions by reducing the particle surface area to its minimum because of the increased hydrophobicity of the surface. The increase of the hydrophobic surface could be caused by PEG₄₃-HMDI release. The round particles seemed to contain aggregated particles in its core (Figure 54 C, D). These observations confirmed the DLS at 90° measurements: decrease of the scattered light intensity due to particle destabilization and that the remaining particle size increased by 20% due to the round particles. Multi-angle light scattering measurements were also performed: the densification of the remaining particles observed by the decrease of the ratio Rg/Rh could be due to the round shape particle aggregates observed in the cryo-TEM images. These results proved that particles aggregated and were destabilized after irradiation.

2.9. Conclusion

A 2nd design of a light sensitive copolymer based on a photocleavable coumarin linker was implemented. The first generation of light sensitive particles was not fully destabilized and dimerization was suspected to improve particle stability. Indeed, dimerization prevents PEG release and thus improves particle stability. In order to improve PEG release from particles and thus favour particle destabilization, copolymer design was modified in two different ways. The cleavage efficiency was improved by changing the leaving group. The quantum yield obtained by irradiation at 365 nm (0.012) was greater than the one of the 1st generation (0.0034). The PEG could be more efficiently cleaved before it could dimerize. The second modification was the polymer position on the coumarin. Therefore only PEG was released instead of PEG-coumarin that induces a more efficient escape of the PEG.

In order to synthesize the 2nd generation of PEG₄₃-coumarin-*b*-PTMC₈₁, the coumarin light sensitive linker was first synthesized with two grafting groups (hydroxyl and alkyne group), in order to be able to graft the hydrophilic and the hydrophobic polymer. PEG₄₃ chain-end was modified into isocyanate in order to be grafted on the hydroxyl group of the coumarin. PEG₄₃-NCO and PTMC₈₁-N₃ were successively grafted on the coumarin linker to give the 2nd generation light sensitive amphiphilic block copolymer PEG₄₃-coumarin-*b*-PTMC₈₁. The copolymer obtained had a narrow dispersity of 1.04. Light scattering measurements showed that the copolymer could self-assemble into well-defined particles with a hydrodynamic radius

of 150 nm and a narrow dispersity ($PDI \approx 0.1$). Cryo-TEM showed polymersomes and polymersome aggregates.

Polymersome irradiation induced change in the polymersome morphology. After irradiation the remaining particles had a ratio R_g/R_h that decreased suggesting particle densification. The polymersome solution was irradiated for 150 min and the scattered light intensity decreased up to 71%, suggesting particle destabilization and aggregation. The light scattering measurements were confirmed by cryo-TEM. The images obtained showed undefined aggregates and round particle aggregates.

These results showed that a light-sensitive copolymer was successfully synthesized that could self-assemble into polymersomes, which were destabilized upon UV irradiation.

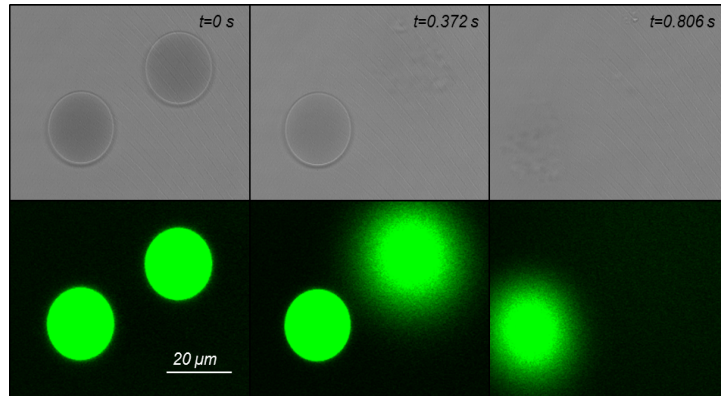
References

- [1] B. Alberts, A. Johnson, J. Lewis, M. Raff, K. Roberts, P. Walter, *Molecular Biology of the Cell*, 4th ed., Garland Science, 2002.
- [2] S.M. Adl, A.G.B. Simpson, C.E. Lane, J. Lukeš, D. Bass, S.S. Bowser, M.W. Brown, F. Burki, M. Dunthorn, V. Hampl, A. Heiss, M. Hoppenrath, E. Lara, L. Le Gall, D.H. Lynn, H. McManus, E.A.D. Mitchell, S.E. Mozley-Stanridge, L.W. Parfrey, J. Pawlowski, S. Rueckert, L. Shadwick, L. Shadwick, C.L. Schoch, A. Smirnov, F.W. Spiegel, The revised classification of eukaryotes, *J. Eukaryot. Microbiol.* 59 (2012) 429–493. doi:10.1111/j.1550-7408.2012.00644.x.
- [3] Y. Tu, F. Peng, A. Adawy, Y. Men, L.K.E.A. Abdelmohsen, D.A. Wilson, Mimicking the Cell: Bio-Inspired Functions of Supramolecular Assemblies, *Chem. Rev.* 116 (2016) 2023–2078. doi:10.1021/acs.chemrev.5b00344.
- [4] D.E. Discher, F. Ahmed, Polymersomes, *Annu. Rev. Biomed. Eng.* 8 (2006) 323–341. doi:10.1146/annurev.bioeng.8.061505.095838.
- [5] L. Beauté, N. McClenaghan, S. Lecommandoux, Photo-triggered polymer nanomedicines: From molecular mechanisms to therapeutic applications, *Adv. Drug Deliv. Rev.* (2018). doi:10.1016/j.addr.2018.12.010.
- [6] E. Cabane, V. Malinova, W. Meier, Synthesis of Photocleavable Amphiphilic Block Copolymers: Toward the Design of Photosensitive Nanocarriers, *Macromol. Chem. Phys.* 211 (2010) 1847–1856. doi:10.1002/macp.201000151.
- [7] P. Klán, T. Šolomek, C.G. Bochet, A. Blanc, R. Givens, M. Rubina, V. Popik, A. Kostikov, J. Wirz, Photoremovable Protecting Groups in Chemistry and Biology: Reaction Mechanisms and Efficacy, *Chem. Rev.* 113 (2013) 119–191. doi:10.1021/cr300177k.
- [8] D. Quémener, T.P. Davis, C. Barner-Kowollik, M.H. Stenzel, RAFT and click chemistry: A versatile approach to well-defined block copolymers, *Chem. Commun.* 0 (2006) 5051–5053. doi:10.1039/B611224B.
- [9] N. Nakajima, Y. Ikada, Mechanism of Amide Formation by Carbodiimide for Bioconjugation in Aqueous Media, *Bioconjug. Chem.* 6 (1995) 123–130. doi:10.1021/bc00031a015.
- [10] F. Nederberg, B.G.G. Lohmeijer, F. Leibfarth, R.C. Pratt, J. Choi, A.P. Dove, R.M. Waymouth, J.L. Hedrick, Organocatalytic Ring Opening Polymerization of Trimethylene Carbonate, *Biomacromolecules.* 8 (2007) 153–160. doi:10.1021/bm060795n.
- [11] J.M. Harris, Introduction to Biotechnical and Biomedical Applications of Poly(Ethylene Glycol), in: J.M. Harris (Ed.), *Polyethyl. Glycol Chem.*, Springer US, 1992: pp. 1–14. http://link.springer.com/chapter/10.1007/978-1-4899-0703-5_1 (accessed May 15, 2015).
- [12] M. Dionzou, A. Morère, C. Roux, B. Lonetti, J.-D. Marty, C. Mingotaud, P. Joseph, D. Goudouneche, B. Payre, M. Leonetti, A.F. Mingotaud, Comparison of methods for the fabrication and the characterization of polymer self-assemblies: what are the important parameters, *Soft Matter.* 12 (2016) 2166–2176. doi:10.1039/c5sm01863c.
- [13] P.G.M. Wuts, T.W. Greene, *Greene's Protective Groups in Organic Synthesis*, John Wiley & Sons, 2006.
- [14] S. Sethna, R. Phadke, The Pechmann Reaction, in: *Org. React.*, American Cancer Society, 2011: pp. 1–58. doi:10.1002/0471264180.or007.01.
- [15] W.A. Velema, J.P. van der Berg, W. Szymanski, A.J.M. Driessen, B.L. Feringa, Orthogonal Control of Antibacterial Activity with Light, *ACS Chem. Biol.* 9 (2014) 1969–1974. doi:10.1021/cb500313f.
- [16] D. Hesek, M. Lee, B.C. Noll, J.F. Fisher, S. Mobashery, Complications from Dual Roles of Sodium Hydride as a Base and as a Reducing Agent, *J. Org. Chem.* 74 (2009) 2567–2570. doi:10.1021/jo802706d.
- [17] J. March, *Advanced organic chemistry: reactions, mechanisms, and structure*, John Wiley & Sons, 1992.
- [18] P. Dubois, O. Coulembier, J.-M. Raquez, *Handbook of Ring-Opening Polymerization*, John Wiley & Sons, 2009.
- [19] J.G. Badiang, J. Aubé, One-Step Conversion of Aldehydes to Oxazolines and 5,6-Dihydro-4H-

-
- 1,3-oxazines Using 1,2- and 1,3-Azido Alcohols, *J. Org. Chem.* 61 (1996) 2484–2487. doi:10.1021/jo9521256.
- [20] S. Tempelaar, L. Mespouille, O. Coulembier, P. Dubois, A. P. Dove, Synthesis and post-polymerisation modifications of aliphatic poly(carbonate)s prepared by ring-opening polymerisation, *Chem. Soc. Rev.* 42 (2013) 1312–1336. doi:10.1039/C2CS35268K.
- [21] S. Bräse, C. Gil, K. Knepper, V. Zimmermann, Organic Azides: An Exploding Diversity of a Unique Class of Compounds, *Angew. Chem. Int. Ed.* 44 (2005) 5188–5240. doi:10.1002/anie.200400657.
- [22] J. Black, *Biological Performance of Materials: Fundamentals of Biocompatibility*, Fourth Edition, CRC Press, 2005.
- [23] I. Kaljurand, A. Kütt, L. Sooväli, T. Rodima, V. Mäemets, I. Leito, I.A. Koppel, Extension of the Self-Consistent Spectrophotometric Basicity Scale in Acetonitrile to a Full Span of 28 pKa Units: Unification of Different Basicity Scales, *J. Org. Chem.* 70 (2005) 1019–1028. doi:10.1021/jo048252w.
- [24] J.M.W. Chan, X. Zhang, M.K. Brennan, H. Sardon, A.C. Engler, C.H. Fox, C.W. Frank, R.M. Waymouth, J.L. Hedrick, Organocatalytic Ring-Opening Polymerization of Trimethylene Carbonate To Yield a Biodegradable Polycarbonate, *J. Chem. Educ.* 92 (2015) 708–713. doi:10.1021/ed500595k.
- [25] B. Lin, R.M. Waymouth, Urea Anions: Simple, Fast, and Selective Catalysts for Ring-Opening Polymerizations, *J. Am. Chem. Soc.* 139 (2017) 1645–1652. doi:10.1021/jacs.6b11864.
- [26] K. Matyjaszewski, A.H. Müller, *Controlled and living polymerizations: from mechanisms to applications*, John Wiley & Sons, 2009.
- [27] M. Hakkarainen, Aliphatic Polyesters: Abiotic and Biotic Degradation and Degradation Products, in: *Degradable Aliphatic Polyest.*, Springer Berlin Heidelberg, Berlin, Heidelberg, 2002: pp. 113–138. doi:10.1007/3-540-45734-8_4.
- [28] A.-C. Albertsson, M. Eklund, Influence of molecular structure on the degradation mechanism of degradable polymers: In vitro degradation of poly(trimethylene carbonate), poly(trimethylene carbonate-co-caprolactone), and poly(adipic anhydride), *J. Appl. Polym. Sci.* 57 (1995) 87–103. doi:10.1002/app.1995.070570109.
- [29] J. Otera, Transesterification, *Chem. Rev.* 93 (1993) 1449–1470. doi:10.1021/cr00020a004.
- [30] Coupling Reactions of Carbanionic Polymers by Elemental Compounds Such as Oxygen and Sulfur - ACS Symposium Series (ACS Publications), (n.d.). <https://pubs.acs.org/doi/abs/10.1021/bk-1981-0166.ch031> (accessed February 10, 2019).
- [31] R.J. Ono, S.Q. Liu, S. Venkataraman, W. Chin, Y.Y. Yang, J.L. Hedrick, Benzyl Chloride-Functionalized Polycarbonates: A Versatile Platform for the Synthesis of Functional Biodegradable Polycarbonates, *Macromolecules.* 47 (2014) 7725–7731. doi:10.1021/ma501734y.
- [32] B.H. Stuart, *Infrared Spectroscopy: Fundamentals and Applications*, John Wiley & Sons, 2004.
- [33] P.A. Ledin, N. Kolishetti, G.-J. Boons, Multifunctionalization of polymers by strain-promoted cycloadditions, *Macromolecules.* 46 (2013) 7759–7768.
- [34] Y. Yoshida, Y. Sakakura, N. Aso, S. Okada, Y. Tanabe, Practical and efficient methods for sulfonylation of alcohols using Ts (Ms) Cl/Et₃N and catalytic Me₃H· HCl as combined base: Promising alternative to traditional pyridine, *Tetrahedron.* 55 (1999) 2183–2192.
- [35] B. Neises, W. Steglich, Simple method for the esterification of carboxylic acids, *Angew. Chem. Int. Ed. Engl.* 17 (1978) 522–524.
- [36] B. Schade, V. Hagen, R. Schmidt, R. Herbrich, E. Krause, T. Eckardt, J. Bendig, Deactivation Behavior and Excited-State Properties of (Coumarin-4-yl)methyl Derivatives. 1. Photocleavage of (7-Methoxycoumarin-4-yl)methyl-Caged Acids with Fluorescence Enhancement, *J. Org. Chem.* 64 (1999) 9109–9117. doi:10.1021/jo9910233.
- [37] W. Burchard, Static and dynamic light scattering from branched polymers and biopolymers, in: *Light Scatt. Polym.*, Springer Berlin Heidelberg, 1983: pp. 1–124.
- [38] R. Salva, J.-F. Le Meins, O. Sandre, A. Brûlet, M. Schmutz, P. Guenoun, S. Lecommandoux, Polymersome Shape Transformation at the Nanoscale, *ACS Nano.* 7 (2013) 9298–9311. doi:10.1021/nn4039589.
- [39] S.R. Trenor, A.R. Shultz, B.J. Love, T.E. Long, Coumarins in Polymers: From Light Harvesting
-

-
- to Photo-Cross-Linkable Tissue Scaffolds, *Chem. Rev.* 104 (2004) 3059–3078. doi:10.1021/cr030037c.
- [40] Q. Lin, C. Bao, G. Fan, S. Cheng, H. Liu, Z. Liu, L. Zhu, 7-Amino coumarin based fluorescent phototriggers coupled with nano/bio-conjugated bonds: Synthesis, labeling and photorelease, *J. Mater. Chem.* 22 (2012) 6680–6688. doi:10.1039/C2JM30357D.
- [41] B. Akhlaghinia, A new and convenient method of generating alkyl isocyanates from alcohols, thiols and trimethylsilyl ethers using triphenylphosphine/2, 3-dichloro-5, 6-dicyanobenzoquinone/Bu₄NOCN, *Synthesis*. 2005 (2005) 1955–1958.
- [42] P. Li, Z. Fu, Z. Fan, Polyethylene-b-poly(ethylene glycol) diblock copolymers: New synthetic strategy and application, *J. Appl. Polym. Sci.* 132 (2015). doi:10.1002/app.42236.
- [43] R. Schmidt, D. Geissler, V. Hagen, J. Bendig, Mechanism of Photocleavage of (Coumarin-4-yl)methyl Esters, *J. Phys. Chem. A.* 111 (2007) 5768–5774. doi:10.1021/jp071521c.

Chapter 3: **GUV** rupture through light-driven osmotic pressure increase



3. GUV rupture through light-driven osmotic pressure increase

3.1. Introduction

In order to study some basic cellular functions such as enzymatic reactions, complex structures have been developed over the past decades to be able to host these reactions. Liposomes and polymersomes have been widely used as synthetic envelopes for microreactors to perform enzymatic reactions inside their lumens [1]. However, initiation of most microreactor reactions occurs by the passive diffusion of species through the membrane. Thus there is a lack of spatial and temporal control of the initiation of the reaction inside microreactor. To this end, release of species in a controlled manner using an exogenous stimulus is of particular interest. In the previous chapter, light-sensitive nanopolymersomes were studied to control the release by cleavage of the block copolymer. In this chapter, another way to destabilize polymersomes is investigated: induced intra-polymersome osmotic pressure change. In nature, cells undergo osmotic pressure stresses. Consequently, they developed mechanisms to control and balance osmotic pressure in order to avoid hypotonic or hypertonic shock that could result in their destabilization. It was shown that liposomes can resist osmotic pressure shock to a certain extent [2]. When an osmotic pressure gradient appears between the inner core and the outer medium, osmotic pressure forces water to flow in or out of the liposomes depending on the gradient direction. Due to high membrane water permeability the osmotic pressure is compensated quickly and liposomes do not burst, rather they swell. Polymersomes are stable when osmotic pressure is the same in the inner and outer medium (Figure 1 A1) however polymersomes generally have a lower water permeability [3]. When osmotic pressure increases in the inner medium, water flow is slower to balance the osmotic pressure difference (Figure 1 B1). We hypothesized that a fast osmotic pressure increase of the internal medium could not be compensated fast enough by water flow, resulting in polymersome rupture and internalized species release (Figure 1 C1). Osmotic pressure is directly linked to solute concentration. Control of the solute concentration leads to control of the osmotic pressure (Figure 1 A1, A2). Increase of the solute concentration in the GUV (Figure 1 B2) leads to osmotic pressure increase and polymersome rupture (Figure 1 C2).

Light was used as the versatile exogenous stimulus to induce release [4]. Our strategy was to quickly increase the solute concentration via light excitation, thus photocleavable molecules were used. Two molecules with two different cleavage mechanisms have been studied: coumarin cleavage and photoinduced electron transfer using a picolinium derivative.

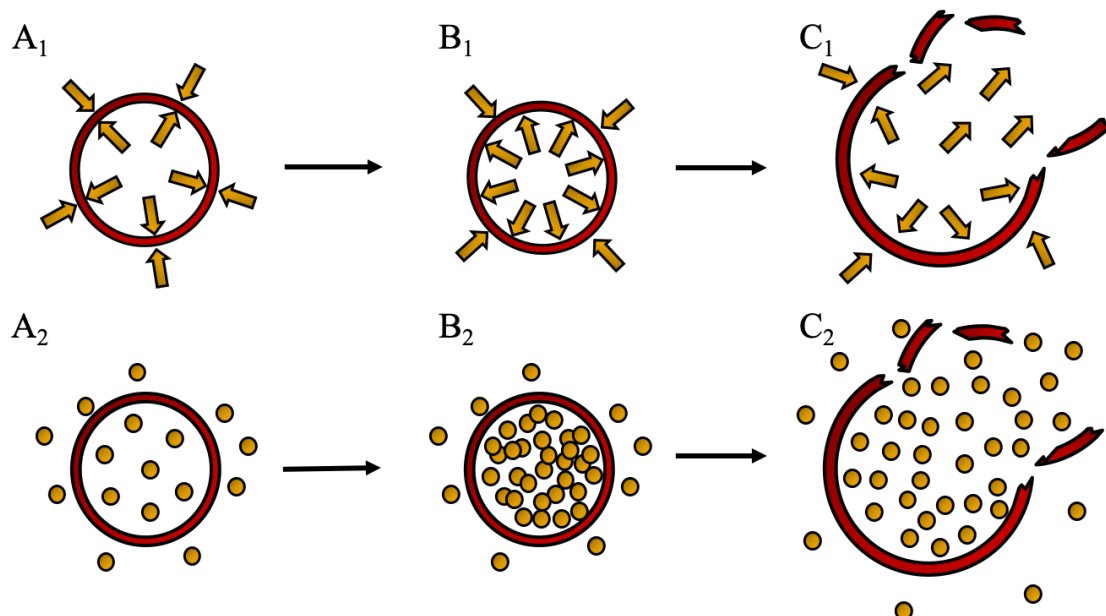
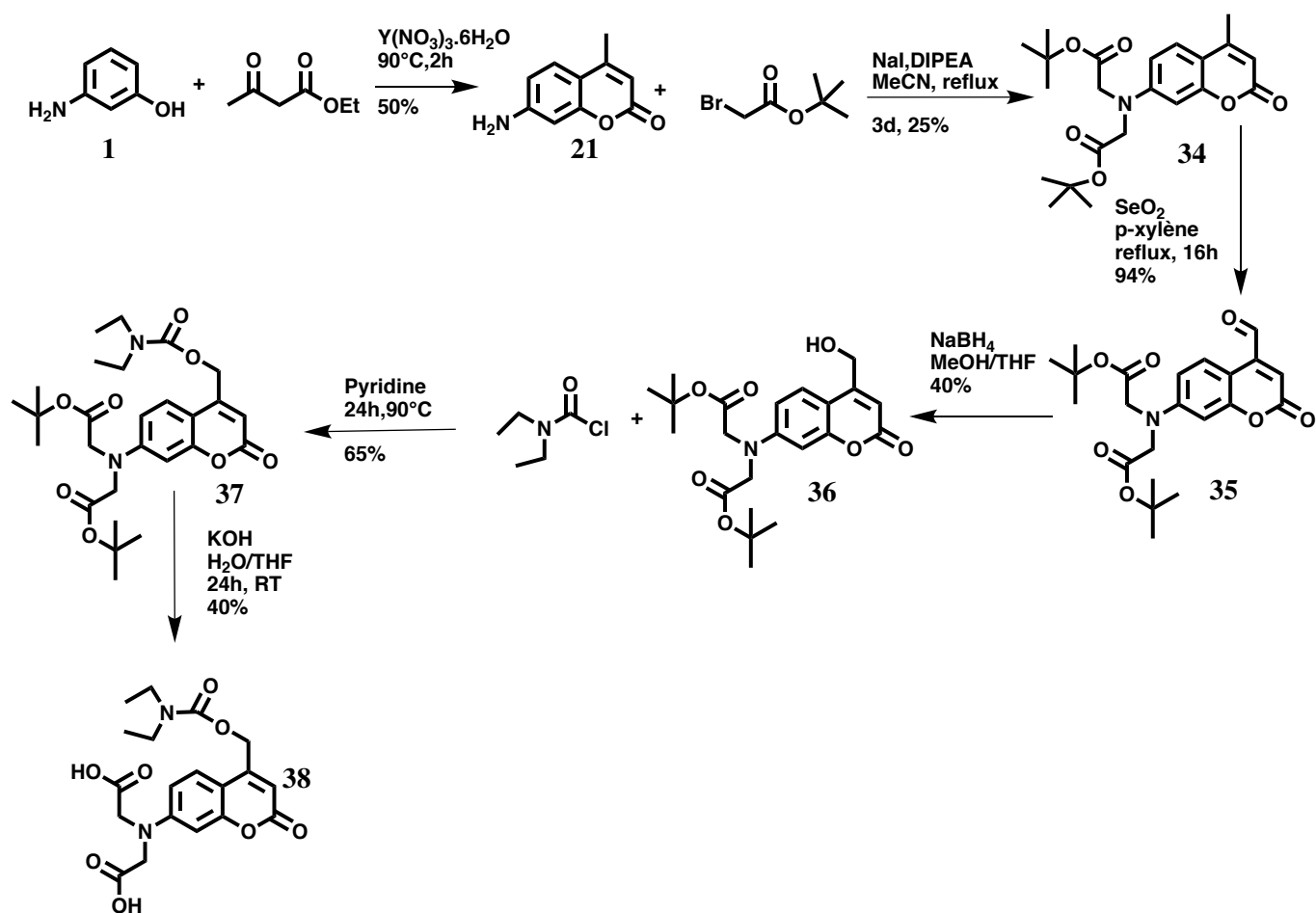


Figure 55: Strategy used to induce polymersome bursting. GUVs are stable while osmotic pressure is the same in the inner and outer medium (A1). Osmotic pressure increase (B1) was used to induce polymersome rupture (C1). Control of the molecular concentration leads to control of the osmotic pressure. Increase of the molecular concentration in the GUV (A1 to B2) leads to osmotic pressure increase and polymersome rupture (C2).

3.2. Coumarin cleavable molecule

3.2.1. Synthesis

The first molecule chosen in order to increase the osmotic pressure inside the polymersome inner medium was coumarin. Coumarin absorbs light at 405 nm, which is required to irradiate it under confocal microscopy. It has a large absorption coefficient and fast release rate [5]. However coumarin is a hydrophobic molecule, thus two carboxylic acid groups were added in order to render the molecule water soluble. The carbamate moiety was chosen as the leaving group due to the stable carbamate ion release after irradiation [6]. Recombination is less favored resulting in a more efficient cleavage and faster osmotic pressure increase. The carbamate ion also undergoes decarboxylation resulting in release of an amine and carbon dioxide. Photoirradiation results in formation of three molecules for each molecule cleaved and a faster of osmotic pressure increase. The final design chosen is presented Scheme 27 (molecule **38**).



Scheme 27: Synthetic route of the photocleavable coumarin.

The synthetic protocol was adapted from a structurally related molecule [7]. The synthesis started with the commercially available 3-aminophenol (**1**) that was reacted with 1-ethoxybutane-1,3-dione. Acidic conditions were not used to form the coumarin molecule, contrary to part 2.1. A new method was tested using yttrium catalyst [8] in order to compare the two reactions. 7-Amino-4-methylcoumarin (**21**) was obtained in 50 % yield. The obtained yield was lower than the acid catalyzed coumarin formation (70 %). **21** was reacted with *tert*-butyl 2-bromoacetate to alkylate the amine twice and obtain a tertiary amine. The modified coumarin (**34**) was obtained in 25 % yield. This reaction yield was not high because the monoalkylated amine was also obtained in significant quantity even after three days reaction. The methyl of **34** was then oxidized into an aldehyde with selenium dioxide without intermediate purification to obtain **35** in 94 % yield. The corresponding aldehyde **35** was reduced into an alcohol with sodium borohydride to obtain **36** in 40 % yield. The alcohol of **36** was then reacted with an acyl chloride in order to form a carbamate link and

obtained **37** in 40 % yield. The last step consists in deprotection of the two *tert*-butyl esters in order to obtain the corresponding carboxylic acid. To that end **37** was reacted with potassium hydroxide to deprotect the carboxylic acid under basic conditions. The final water soluble molecule **38** was obtained in 40 % yield.

Due to the two carboxylic acids, the modified coumarin **38** was highly water soluble (at least 10 mM at pH 7).

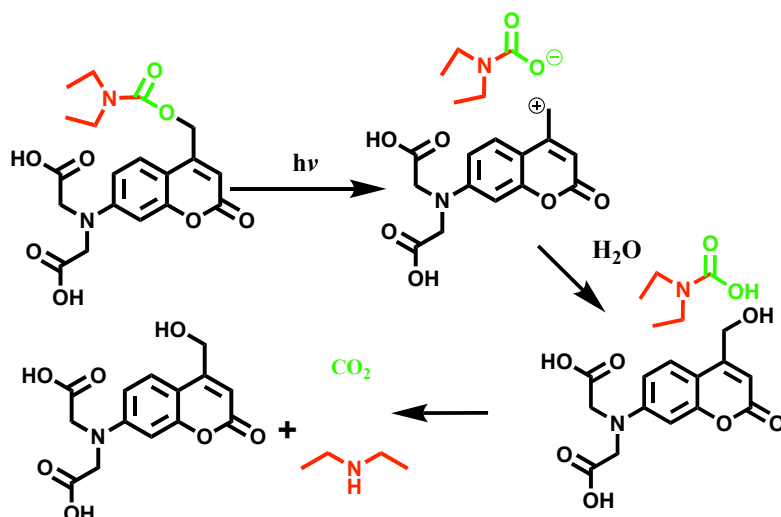
3.2.2. Irradiation study

Irradiation experiments were carried out with a 200 W Mercury-Xenon lamp (except for quantum yield measurements). A filter was used to center light emission at 365 nm (emission spectra in the experimental section). Samples were placed at 1 cm from the light guide output end and irradiated for a defined time.

3.2.2.1. Cleavage Mechanisms

Under photoirradiation the coumarin undergoes heterolytic cleavage [9]. UV light irradiation induces carbocation and carbamate anion formation. The carbamate anion is a good leaving group due to its stability. Consequently it decreases the recombination rate and improves cleavage efficiency. The last step consists in spontaneous decarboxylation of the carbamate inducing carbon dioxide and diethyl amine formation. Therefore recombination is no longer possible and the cleavage is irreversible [10]. The decarboxylation step is the rate limiting step and it can be catalyzed by acidic or basic conditions. The initial state before irradiation involved one molecule. After irradiation the final state involved three molecules inducing osmotic pressure increase. Coumarin cleavage is fast with release rate constant reaching $k=2 \times 10^{10} \text{ s}^{-1}$ (for phosphate ester [5]) inducing fast osmotic pressure increase. Consequently this cleavage mechanism is well suited to burst polymersomes.

Moreover, the released diethyl amine is a base with a pKa of 10.98 [11]. In addition to controlling the osmotic pressure, we expected to be able to control the solution pH using **38**.



Scheme 28: Cleavage mechanism of coumarin under irradiation. The carbamate link forms a stable intermediate molecule and the final decarboxylation make the cleavage irreversible.

3.2.2.2. Absorption and Fluorescence

The absorption spectrum of **38** in water (Figure 56) showed that the coumarin derivatives can absorb visible light up to 450 nm, a requirement to be able to irradiate **38** in a confocal microscope. There are two band maximum absorptions, λ_{max} at 247 and 378 nm. The molar extinction coefficient was measured at 13 000 L·mol⁻¹·cm⁻¹ considering the lowest energy absorption band.

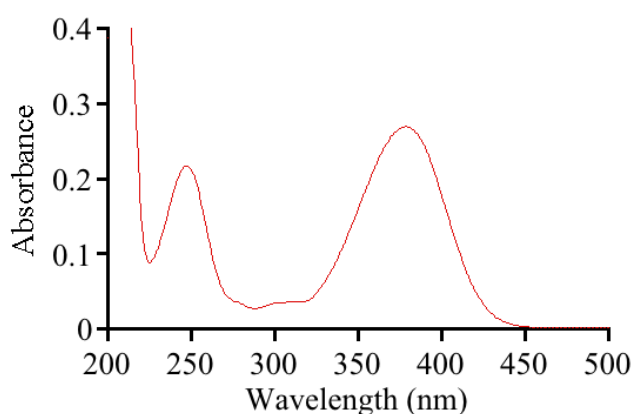


*Figure 56 Electronic absorption spectrum of coumarin derivative **38** in water. Coumarin derivative **38** was irradiated at 365 nm in water. The electronic absorption spectra were recorded after several different irradiation times.*

Figure 57 A). A modification of the absorption spectrum was observed after irradiation. The maximum absorption decreased from 0.27 at 0 min irradiation to 0.20 after 2 hours irradiation. The maximum absorption wavelength (λ_{\max}) also decreased from 378 nm to 369 nm after 2 hours irradiation. These results could indicate molecular modification after irradiation and the coumarin cleavage.

Fluorescence emission spectra were also recorded before and after 30 min of 365 nm irradiation ($\lambda_{\text{ex}}=365$ nm).

Figure 57 B). The emission spectra modification was observed after irradiation. The maximum emission wavelengths increased and were blue shifted (from 492 to 482 nm) which could indicate that the coumarin substitutions were modified in accordance with coumarin cleavage.

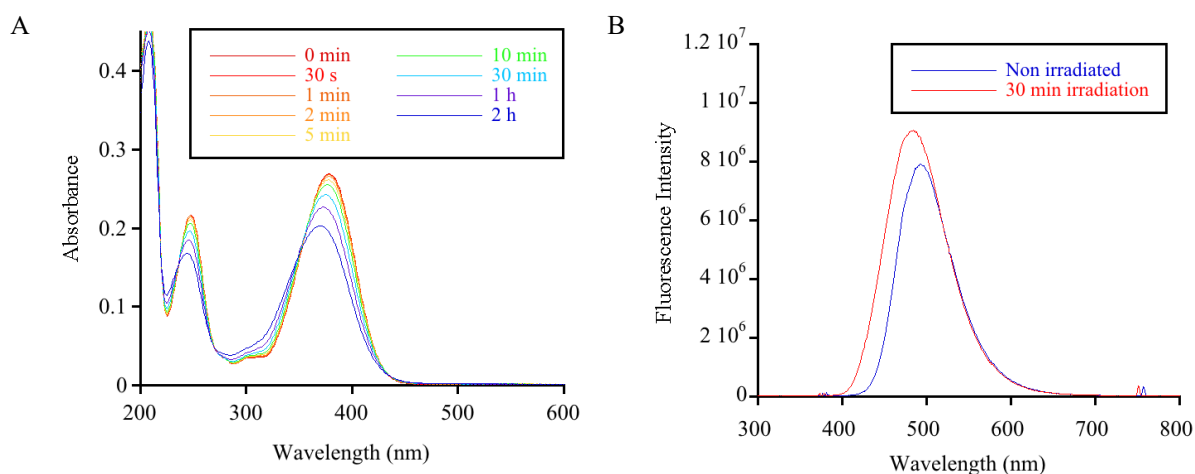


Figure 57: A) Electronic absorption spectra of the coumarin derivative at different irradiation times. The absorption spectra change as a function of irradiation time. B) Fluorescence emission spectra before and after 30 min irradiation. Excitation wavelength used was 365 nm. The maximum emission wavelengths increased and were blue shifted.

3.2.2.3. Monitoring cleavage via NMR

In order to study the effect of irradiation at the molecular scale, **38** was dissolved in D₂O and the ¹H NMR spectra were recorded before and after 1 hour of irradiation. The resulting spectra are shown in Figure 58. Diethyl amine signals of **38** (a and b) shifted from 3.45 and 1.15 ppm to 3.1 and 1.3 ppm. These new signals correspond to free diethyl amine in water. This result clearly indicates coumarin cleavage. Some residual signals of diethyl amine linked to coumarin

were spotted after irradiation showing that a small fraction was not cleaved. Peak integration showed that 13% of diethyl amine was not cleaved and 87% was cleaved.

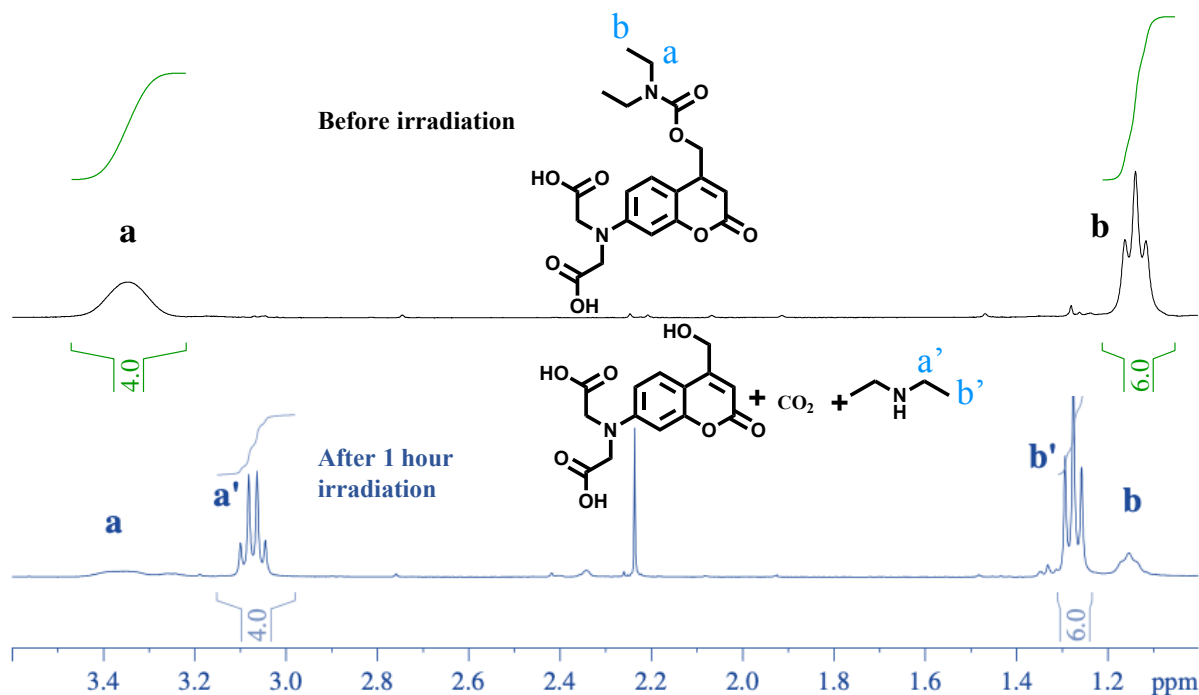


Figure 58: ¹H NMR spectra of **38** in D₂O before and after 1 hour irradiation (365 nm 200 W Mercury-Xenon lamp). These results indicate coumarin cleavage and release of diethyl amine. Peak integration indicates 87 % of **38** was cleaved.

3.2.2.4. Quantum yield

The photocleavage efficiency (quantum yield) of **38** was measured under 365 nm and 405 nm irradiation. Samples were irradiated across a monochromator to obtain precise wavelengths. The UV lamp was calibrated using potassium ferrioxalate-phenanthroline [12] as a chemical actinometer (experimental section). The values found are summarized in Table 13. These values were conform with the values found in literature [5]. Cleavage efficiency in methanol was 10 times lower than cleavage efficiency in water in accordance with the cleavage mechanism presented in 3.2.2.1. Water is necessary to stabilize the resulting ions after cleavage. The quantum yield at 405 nm and 365 nm are on the same order of magnitude. The quantum yield at 405 nm was significant enough to be able to irradiate and cleave the coumarin derivative under confocal microscopy.

Irradiation 365 nm

	Φ PH	Φ METHANOL
N°1	0.0017	X
N°2	0.0015	0.0002
AVERAGE	0.0016	0.0002

Irradiation 405 nm

	Φ PH 7	Φ METHANOL
N°1	0.0035	X
N°2	0.0023	0.0002
AVERAGE	0.0029	0.0002

Table 13: Cleavage quantum yield of the coumarin derivative **38** on irradiating at 365 nm and 405 nm.

3.2.2.5. pH control

Irradiation of coumarin derivative **38** released basic diethyl amine. The pKa of diethyl amine is 10.98. Theoretically the pH should increase due to base release. **38** was dissolved in water at a concentration of 270 μ M. The initial pH was low (4.5) due to the two carboxylic acid groups that acidified the medium. The medium was not buffered in order to maximize the base release effect. The resulting solution was irradiated as explained in the introduction. The pH was measured after irradiation until a stable value was obtained. The results are shown in Figure 59. A fast increase of pH was measured. The pH started from 4.6 and after only 4 min irradiation pH was raised to 6.2. These results clearly indicate diethyl amine release.

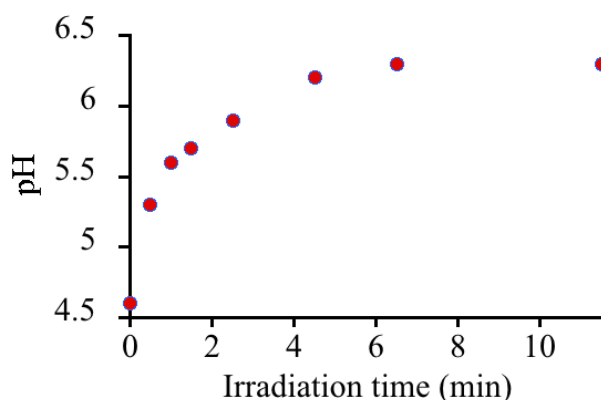
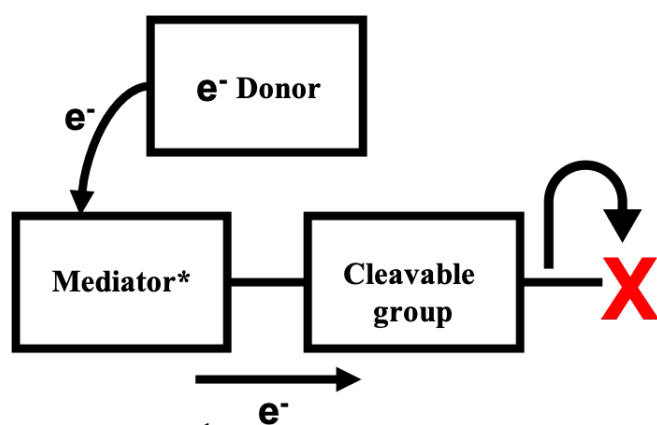


Figure 59: pH depending on irradiation time of a solution of molecule **38** at 270 μ M. The results clearly showed that irradiation increased pH due to diethyl amine release.

3.3. N-alkyl-4-picolinium

3.3.1. Introduction

In this section another cleavable molecule that invokes photoinduced electron transfer was studied. The high cleavage efficiency of this mechanism (quantum yield up to 0.72 [13]) attracted our interest. This mechanism could in principle induce fast cleavage and fast osmotic pressure increase suitable to burst polymersomes. Most cleavable molecules combine light absorption and a cleavable moiety, thus improving both absorption and cleavage efficiency is beneficial. Photoinduced electron transfer in a modular molecular design strategy allows separation of electron source, light absorption and photochemical reaction [14] (Figure 60). Due to the modular nature, light absorption, electron donor properties and cleavage efficiency can be improved separately. Light absorption wavelength can be tuned without impacting cleavage efficiency. To this end mediated electron transfer mechanism involved an electron donor, a photosensitizer (mediator) and a cleavable group. The mediator absorbs light and it is promoted to its excited state. This state has enough energy to be reduced by the electron donor. Finally an electron is transferred from the mediator to the cleavable group. The cleavable group is reduced which induces cleavage and release of the leaving group X.

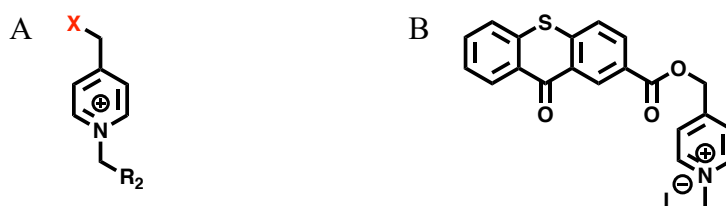


*Figure 60: Photorelease via mediated transfer. X is the leaving group. * represented the excited state of the mediator after irradiation.*

3.3.2. Synthesis

3.3.2.1. Design

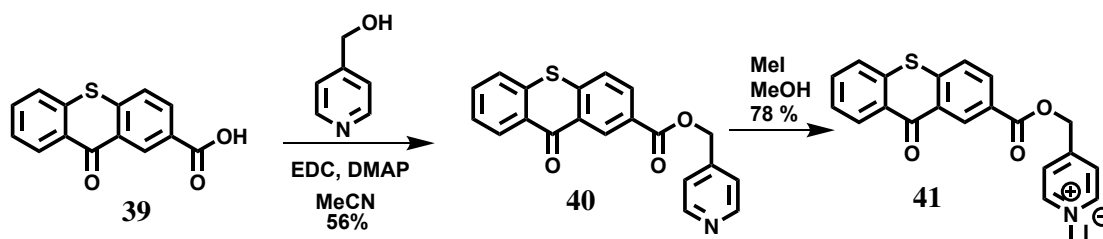
Many of electron donors have been studied, such as ascorbic acid, N,N-diethyl aniline or dithiothreitol [15]. Triethanol amine was used due to its water solubility and its low oxidation potential (0.57 V vs SCE [15]). The cleavable group use was N-alkyl-4-picolinium (NAP) group (Scheme 29 A). NAP has low reduction potential (-1.1 V vs SCE [14]) and can be easily reduced. Reduced NAP undergoes spontaneous cleavage. A range of photosensitizers have been used for mediated electron transfer such as xanthone, benzophenone, 9,10-diphenylanthracene [13], Ru(bpy)₃Cl₂ [16]. In this study thioxanthone, which has a large molar absorptivity (4000 M⁻¹cm⁻¹ [17]) was used as the photosensitizer. The molecule design is presented in Scheme 29 B.



Scheme 29: A) N-alkyl-4-picolinium. X is the leaving group B) Design of the light cleavable molecule base on mediated electron transfer.

3.3.2.2. 1st generation

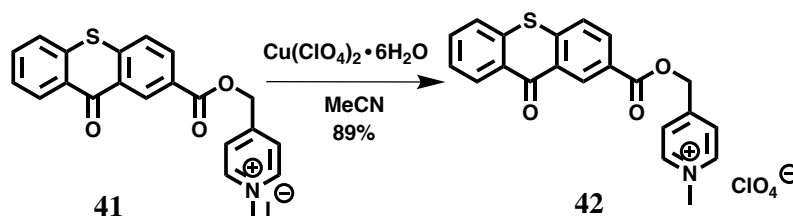
The target molecule was easily obtained in a two-step synthesis (Scheme 30). The commercially available 9-oxothioxanthene-2-carboxylic acid (**39**) was reacted with 4-pyridinemethanol. The hydroxyl group of the pyridine methanol reacted with the carboxylic acid group of **39** to form an ester linkage. To this end, coupling agent EDC along with DMAP were used to give **40** in 56 % yield. EDCI was used to activate the carboxylic acid. **40** was then reacted with iodomethane to convert the pyridine into the N-alkyl-4-picolinium group to obtain the final molecule **41** in 78 % yield [13]. The counter anion of the positively charged picolinium is the iodide. Water solubility of **41** was then tested.



Scheme 30: Synthetic route to obtain photocleavable NAP-thioxanthone.

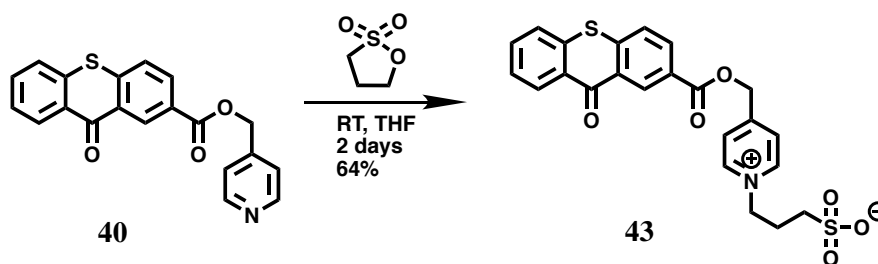
3.3.2.3. Solubility properties

In order to have a high induced osmolarity increase, concentration of the light-sensitive molecule has to be maximized. To this end several concentrations were tested to find the **41** saturation concentration. Saturation concentration found was 1 mM. This concentration is not as high as expected, probably due to the high proportion of hydrophobic groups in the molecule. In order to improve the water solubility, the iodide counter ion was changed to perchlorate ion in a one-step reaction [11]. **41** was reacted with copper (II) perchlorate [18]. The perchlorate salt (**42**) was obtained in 82 % yield. The solubility of the new compound was not improved.



Scheme 31: General scheme for the counter ion modification from iodide to perchlorate ion.

Another strategy was developed to improve the water solubility, consisting in adding a different solubilizing group in a one-step reaction. The methyl of the pyridine moiety was thus replaced by a sulfonate group. To this end **40** was reacted with 1,3-propanesultone. The propanesultone ring opened leading to the sulfonate group formation [19]. This new zwitterionic molecule was expected to be more hydrophilic.



Scheme 32: General scheme for the sulfonate grafting on the pyridine moiety.

Several tests have been performed in order to solubilize **41**. Several concentrations of **41** in water have been tested, however the molecule became totally insoluble. Surprisingly the sulfonate group did not improve the solubility properties. In order to maximize the solubilization of the molecule, it was sonicated and then stirred overnight. However, **43** was not solubilized. The molecule was also first dissolved in DMSO and then water was added. However a turbid mixture was obtained that destabilized under sonication. We hypothesized that the new molecule formed act as a surfactant as shown in Figure 61 and could not be totally solubilized or tight ion pairing would limit solubility. Finally, **41** was used for the polymersome bursting experiments.

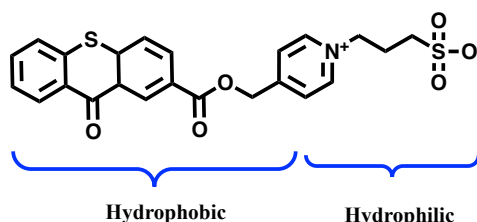
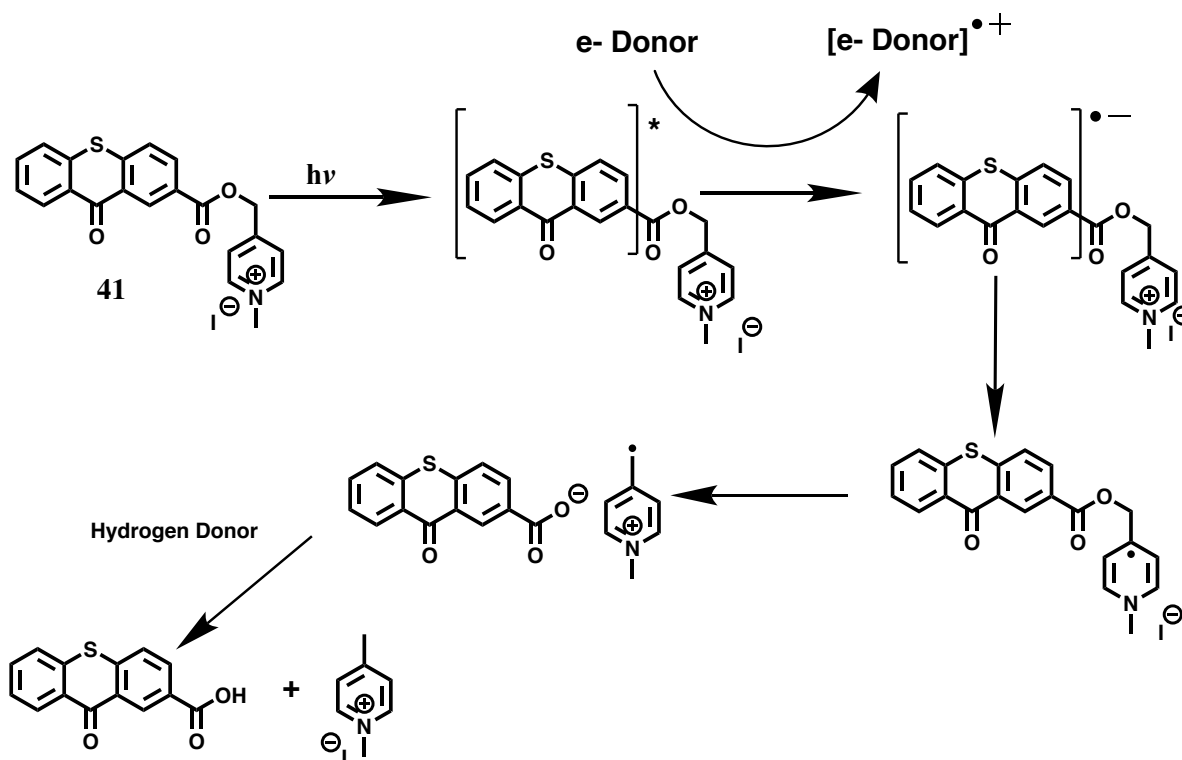


Figure 61: Sulfonate group was added with the aim to improve the solubility of 41.

3.3.3. Irradiation study

3.3.3.1. Mechanisms

The first step starts with thioxanthone irradiation. Irradiation excites thioxanthone to its excited state, rendering electron transfer from the electron donor (0.57 Vs SCE [15]) to thioxanthone energetically favourable. The resulting reduced thioxanthone has a lower reduction potential (-1.7 V vs SCE) than NAP (-1.1 V vs SCE). Consequently thioxanthone transfers an electron to NAP. The reduced NAP undergoes a spontaneous heterolytic cleavage.



Scheme 33: Photocleavable mechanism of mediated electron transfer of triethanol amine, thioxanthone and NAP.

3.3.3.2. Quantum yield

In order to assess the efficacy of the mediated electron transfer mechanism, the cleavage quantum yield was measured. Samples were irradiated across a monochromator centered at 365 nm. The UV lamp was calibrated using potassium ferrioxalate-phenanthroline [12] as a chemical actinometer (experimental section). The quantum yield was measured in water with and without the sacrificial reductant in order to assess the electron donor role. 0.0032 was found without triethanol amine and 0.16 was found with triethanol amine. Without triethanol amine the cleavage was not efficient. With the triethanol amine the quantum yield was 50 times higher. These results were in accordance with the cleavage mechanism. With triethanol amine, the cleavage quantum yield was high, showing that the cleavage is very efficient.

3.4. Encapsulation in polymersome

In order to assess the effect of the irradiation on osmotic pressure and the bursting consequences, the two molecules were encapsulated in giant unilamellar vesicles (GUV) thanks to the emulsion centrifugation technique [20] (Figure 62). This method consists in stabilizing water emulsion droplets in an organic solvent (in this case toluene) using an amphiphilic block copolymer (Figure 62 A). In this study the copolymer used was poly(ethylene glycol)-*b*-polybutadiene (PEO_{1.3}-*b*-PBut_{2.5}). Sucrose is dissolved in the water droplet in order to increase the density of the emulsions. A second vial is prepared consisting of a toluene phase on top of a water glucose phase (Figure 62 B). The interface of the two phases is separated by a leaflet of PEO_{1.3}-*b*-PBut_{2.5}. The glucose solution allows an osmotic pressure equilibrium to be reached between the inner and outer phase of the giant polymersome. The sucrose emulsion droplets were added on top of a toluene/ water interface (Figure 62 C) and then centrifuged. Due to the higher density of sucrose emulsion, the droplets crossed the interface of the water / toluene phase, and the copolymer leaflet (Figure 62 D). While the emulsion droplets cross the interface from the organic phase to the water phase, a second leaflet of copolymer is added around the droplets, thus forming polymersomes. Polymersomes with a precise control of the concentration and species encapsulated can be obtained *via* this technique.

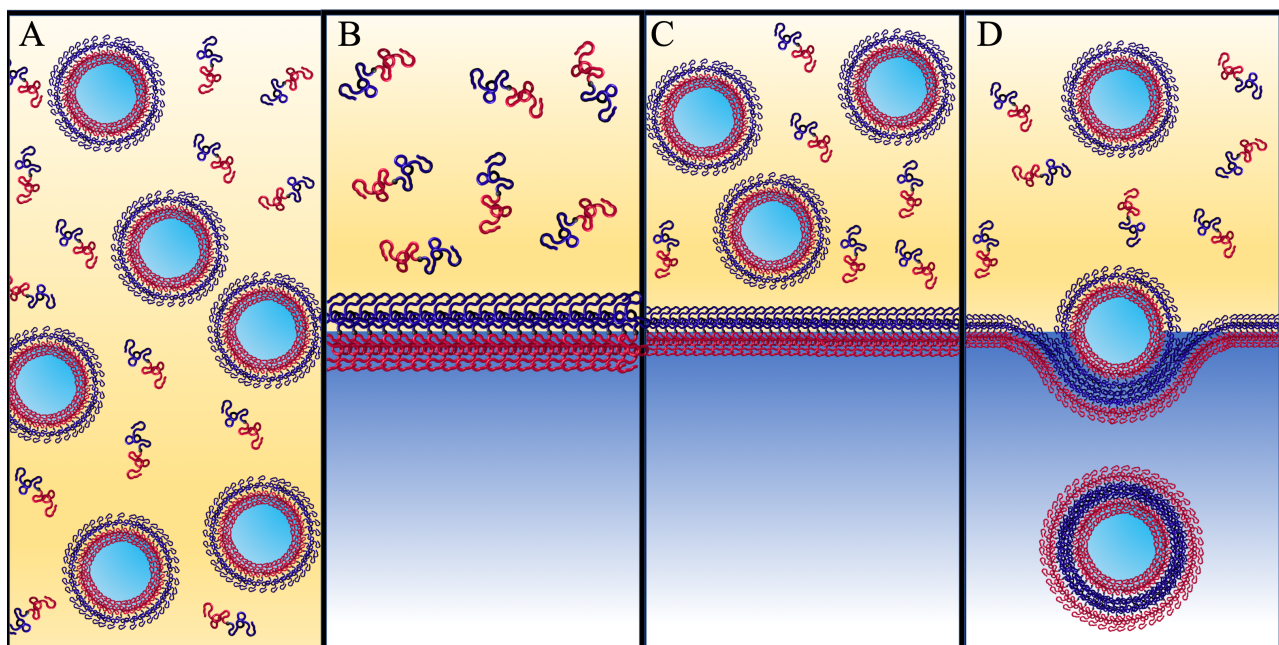


Figure 62: Schematic representation of the emulsion centrifugation technique.

3.4.1. Thioxanthone encapsulation method

30 μL of glucose 380 mM was added at the bottom of a 2 mL plastic eppendorf. 30 μL of a PBut_{2.5}-*b*-PEO_{1.3} (3 mg/mL) toluene solution was added gently on the glucose phase. The two phases solution was allowed to stabilize 30 min in order to form a stable copolymer leaflet at the interface. In a 380 mM sucrose solution, the light sensitive thioxanthone derivative **41** (1 mM) and an excess of triethanolamine (10 mM) was dissolved. 5 μL of the sucrose solution was poured in 500 μL of PEO_{1.3}-*b*-PBut_{2.5} (3 mg/mL) toluene solution. The solution was vigorously hand shaken for 25 seconds in order to form the sucrose emulsion in toluene that was stabilized by the copolymer. 75 μL of the emulsion was poured quickly and gently in the toluene phase of the first vial containing the glucose phase. Quickly the resulting emulsion in toluene was centrifuged (3 min, 500 g, room temperature) on top of the glucose solution. The toluene of the centrifuge solution was partly removed, 80 μL of glucose (380 mM) solution was gently added. The solution was again centrifuged (3 min at 500 g room temperature). All the toluene was removed. On the bottom of the vial, a pellet of polymersomes is visible. After toluene removal, the solution was left to rest for few hours until all the polymersomes were dispersed and the aggregates at the bottom disappeared.

The resulting solution was observed under confocal microscopy. Polymersomes were obtained containing the sucrose (380 mM) thioxanthone (1 mM) and triethanol amine solution (10 mM). Irradiation (405 nm; 50 mW, 50%) induced polymersomes bursting as shown in Figure 63. The observed coiling phenomenon has been previously observed and described by Li et al. [21]. As a control, thioxanthone free (sucrose-loaded) polymersomes were irradiated at 405 mW, 50%, and no rupture was observed, confirming that the explosion results from thioxanthone selective irradiation.

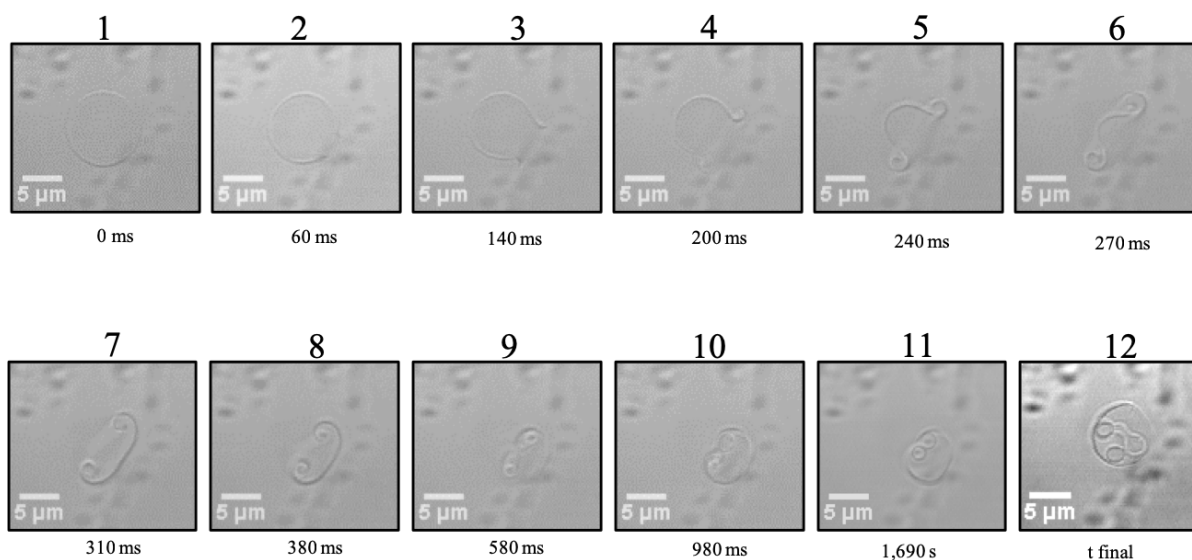


Figure 63: Confocal observation of a 1 mM Thioxanthone derivative loaded GUV. The vesicle undergoes rupture upon irradiation at 405 nm 50 mW, 50% (transmission 633 nm 10 mW 10 %).

3.4.2. Coumarin encapsulation method

The technique used to form giant polymersomes loaded with coumarin derivatives **38** was the same as the one described in 3.4.1. However, a solution of sucrose 380 mM and coumarin derivatives **38** at 10 mM was used for the polymersomes inner phase. Polymersomes were obtained in high yield. Due to coumarin fluorescence, loading efficiency and leakage in the glucose phase were easily detectable. The wavelength used to observe coumarin fluorescence and to cleave the molecule is the same, but the power used to observe the fluorescence of loaded polymersomes was very low (3 %). The coumarin derivative was first dissolved in the sucrose solution without adjusting the pH. The few vesicles obtained did not explode under UV irradiation, (405 nm; 50 mW, 100%). We supposed that the coumarin derivatives were not fully dissolved limiting the fast osmotic increase. Coumarin was then dissolved in the sucrose solution at pH 7. Figure 64 clearly showed the coumarin derivatives loading success (excitation: 405 nm, 50 mW, 3%).

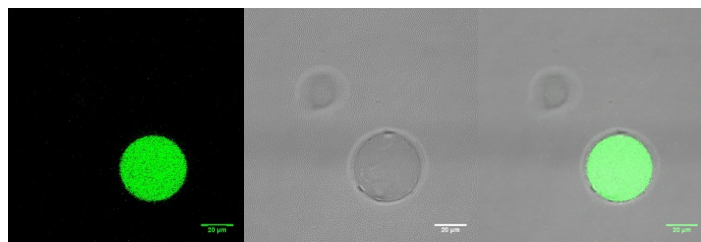


Figure 64: Confocal observation of a 10 mM coumarin-loaded GUV. Green channel, emission range of coumarin: 485 nm; excitation: 405 nm (50 mW, 3%); transmission: 633 nm (10 mW 10 %).

The resulting loaded GUVs were then irradiated with a higher power (405 nm, 50 mW, 25%). Polymersomes bursting was very fast, typically less than one second (Figure 65). As a control, coumarin free (sucrose-loaded) polymersomes were irradiated in the same conditions and no rupture could be observed, confirming that the explosion results from coumarin selective irradiation.

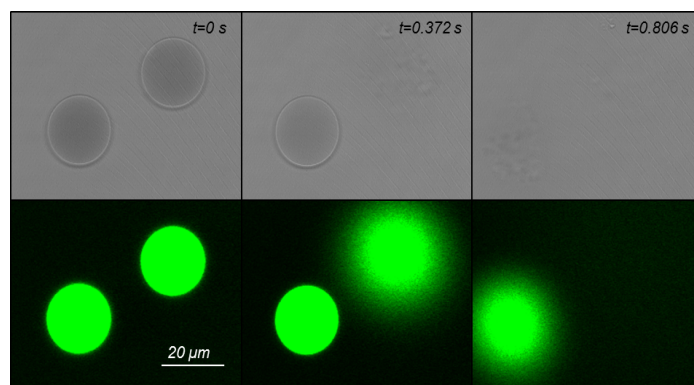


Figure 65: Confocal observation of a 10 mM coumarin-loaded GUV. Green channel, emission range of coumarin: 485 nm; excitation: 405 nm (50 mW, 25%); transmission: 633 nm (10 mW 10 %). The vesicles undergo fast (less than one second) rupture upon irradiation at 405 nm (50 mW, 25%).

3.5. Conclusion

Mimicking basic cell functions could help understanding complex cell molecular mechanism. One major chemical messenger in cells and living organism have drawn interest the past decades: Nitric oxide (NO) [22]. Several studies suggested that NO could play a key role in the apparition and the expansion of a broad range of disease [23] [24]. NO synthase mechanisms are not yet clearly understood and the design of a microreactor that could encapsulate the enzyme and provide a confined and controlled environment mimicking the cell may be used to better understand such a complex enzyme. Controlling species release and concentration inside the microreactor and measuring the enzyme response could help to disentangle the complex reaction pathway of the enzyme and develop kinetics models.

With such an ultimate goal in mind, an osmotic pressure shock was used to destabilize polymersomes and to release species. The fast osmotic pressure increase in the internal medium of polymersomes could not be compensated fast enough by water flow, resulting in polymersome rupture and species release. Osmotic pressure increase was controlled *via* a light sensitive cleavable molecule. Two molecules with two different cleavage mechanisms were studied: coumarin heterolytic cleavage and N-alkyl-4-picolinium-thioxanthone (NAP-th) based on mediated electron transfer.

NAP-th was easily synthesized in 2 steps, its water solubility was the limiting parameter and the maximal solubility concentration found was 1 mM. Several methods were tested to increase its water solubility, such as changing the counter ion or adding a hydrophilic group, without increasing the water solubility. The quantum yield measured in the presence of the mediator triethanol amine was 0.16. This value showed that the cleavage was very efficient. Modified coumarin was also successfully synthesized in 6 steps, two hydrophilic groups were added to increase the solubility of the molecule and 10 mM of the molecule was easily solubilized in water. The quantum yield measured was 0.016 for 365 nm and 0.029 for 405 nm. The cleavage was less efficient than NAP-th however its solubility was better. One hour of irradiation (365 nm 200 W Mercury-Xenon lamp) induced 87 % cleavage of the molecule. This cleavage released diethyl amine that can be used to increase the solution pH. Indeed, after only 10 min irradiation the pH increased from 4.5 to 6.5.

The second step consisted in encapsulating both molecules inside the polymersome made of PEO_{1,3}-*b*-PBut_{2,5} *via* an emulsion-centrifugation technique. Modified coumarin was encapsulated inside polymersome with a concentration of 10 mM and NAP-th of 1 mM.

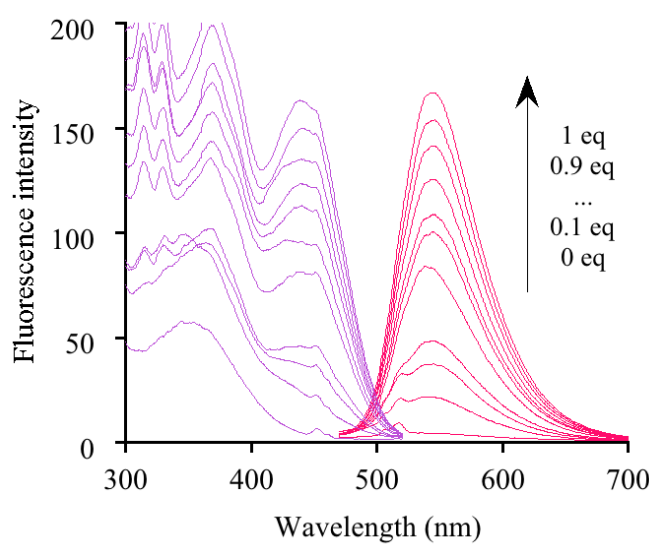
Irradiation at 405 nm induced fast polymersomes bursting for both molecules. These systems inducing fast and efficient release could be used to initiate reaction of microreactors and thus to have a precise control in space and time for the design of artificial cellular systems.

References

- [1] D.M. Vriezema, P.M.L. Garcia, N. Sancho Oltra, N.S. Hatzakis, S.M. Kuiper, R.J.M. Nolte, A.E. Rowan, J.C.M. van Hest, Positional Assembly of Enzymes in Polymersome Nanoreactors for Cascade Reactions, *Angew. Chem.* 119 (2007) 7522–7526. doi:10.1002/ange.200701125.
- [2] C. Taupin, M. Dvolaitzky, C. Sauterey, Osmotic pressure-induced pores in phospholipid vesicles, *Biochemistry*. 14 (1975) 4771–4775. doi:10.1021/bi00692a032.
- [3] J.-F. Le Meins, O. Sandre, S. Lecommandoux, Recent trends in the tuning of polymersomes' membrane properties., *Eur. Phys. J. E Soft Matter Biol. Phys.* 34 (2011) 34. doi:10.1140/epje/i2011-11014-y.
- [4] L. Beauté, N. McClenaghan, S. Lecommandoux, Photo-triggered polymer nanomedicines: From molecular mechanisms to therapeutic applications, *Adv. Drug Deliv. Rev.* (2018). doi:10.1016/j.addr.2018.12.010.
- [5] P. Klán, T. Šolomek, C.G. Bochet, A. Blanc, R. Givens, M. Rubina, V. Popik, A. Kostikov, J. Wirz, Photoremovable Protecting Groups in Chemistry and Biology: Reaction Mechanisms and Efficacy, *Chem. Rev.* 113 (2013) 119–191. doi:10.1021/cr300177k.
- [6] M. Skwarczynski, M. Noguchi, S. Hirota, Y. Sohma, T. Kimura, Y. Hayashi, Y. Kiso, Development of first photoresponsive prodrug of paclitaxel, *Bioorg. Med. Chem. Lett.* 16 (2006) 4492–4496. doi:10.1016/j.bmcl.2006.06.030.
- [7] W.A. Velema, J.P. van der Berg, W. Szymanski, A.J.M. Driessen, B.L. Feringa, Orthogonal Control of Antibacterial Activity with Light, *ACS Chem. Biol.* 9 (2014) 1969–1974. doi:10.1021/cb500313f.
- [8] B. Karami, M. Kiani, Synthesis of the Coumarins via Pechmann Method in the Presence of Environmentally Friendly $Y(NO_3)_3 \cdot 6H_2O$, *J. Chin. Chem. Soc.* 61 (2014) 213–216. doi:10.1002/jccs.201200610.
- [9] M.A. Azagarsamy, D.D. McKinnon, D.L. Alge, K.S. Anseth, Coumarin-Based Photodegradable Hydrogel: Design, Synthesis, Gelation, and Degradation Kinetics, *ACS Macro Lett.* 3 (2014) 515–519. doi:10.1021/mz500230p.
- [10] A.S.C. Fonseca, M.S.T. Gonçalves, S.P.G. Costa, Photocleavage studies of fluorescent amino acid conjugates bearing different types of linkages, *Tetrahedron*. 63 (2007) 1353–1359. doi:10.1016/j.tet.2006.11.082.
- [11] W.M. Haynes, *CRC Handbook of Chemistry and Physics*, 93rd Edition, CRC Press, 2012.
- [12] M. Montalti, A. Credi, L. Prodi, M.T. Gandolfi, *Handbook of photochemistry*, CRC press, 2006.
- [13] C. Sundararajan, D.E. Falvey, Photorelease of carboxylic and amino acids from N-methyl-4-picolinium esters by mediated electron transfer, *Photochem. Photobiol. Sci.* 5 (2006) 116–121. doi:10.1039/B511269A.
- [14] C. Sundararajan, D.E. Falvey, Photolytic Release of Carboxylic Acids Using Linked Donor–Acceptor Molecules: Direct versus Mediated Photoinduced Electron Transfer to N-Alkyl-4-picolinium Esters, *Org. Lett.* 7 (2005) 2631–2634. doi:10.1021/ol050744n.
- [15] Y. Pellegrin, F. Odobel, Sacrificial electron donor reagents for solar fuel production, *Comptes Rendus Chim.* 20 (2017) 283–295. doi:10.1016/j.crci.2015.11.026.
- [16] J.B. Borak, H.-Y. Lee, S.R. Raghavan, D.E. Falvey, Application of PET deprotection for orthogonal photocontrol of aqueous solution viscosity, *Chem. Commun.* 46 (2010) 8983–8985. doi:10.1039/C0CC02203A.
- [17] N. Karaca, N. Ocal, N. Arsu, S. Jockusch, Thioxanthone-benzothiophenes as photoinitiator for free radical polymerization, *J. Photochem. Photobiol. Chem.* 331 (2016) 22–28. doi:10.1016/j.jphotochem.2016.01.017.
- [18] R. Richarz, P. Krapf, F. Zarrad, E.A. Urusova, B. Neumaier, B.D. Zlatopolskiy, Neither azeotropic drying, nor base nor other additives: a minimalist approach to ^{18}F -labeling, *Org. Biomol. Chem.* 12 (2014) 8094–8099. doi:10.1039/C4OB01336K.
- [19] D. Dupont, S. Raiguel, K. Binnemans, Sulfonic acid functionalized ionic liquids for dissolution of metal oxides and solvent extraction of metal ions, *Chem. Commun. Camb. Engl.* 51 (2015)

-
- 9006–9009. doi:10.1039/c5cc02731d.
- [20] S. Pautot, B.J. Frisken, D.A. Weitz, Engineering asymmetric vesicles, *Proc. Natl. Acad. Sci.* 100 (2003) 10718–10721. doi:10.1073/pnas.1931005100.
- [21] E. Mabrouk, D. Cuvelier, F. Brochard-Wyart, P. Nassoy, M.-H. Li, Bursting of sensitive polymersomes induced by curling, *Proc. Natl. Acad. Sci.* 106 (2009) 7294–7298. doi:10.1073/pnas.0813157106.
- [22] L.J. Ignarro, *Nitric oxide: biology and pathobiology*, Academic press, 2000.
- [23] H. Ischiropoulos, J.S. Beckman, Oxidative stress and nitration in neurodegeneration: Cause, effect, or association?, *J. Clin. Invest.* 111 (2003) 163–169. doi:10.1172/JCI200317638.
- [24] C. Szabó, H. Ischiropoulos, R. Radi, Peroxynitrite: biochemistry, pathophysiology and development of therapeutics, *Nat. Rev. Drug Discov.* 6 (2007) 662–680. doi:10.1038/nrd2222.

Chapter 4: Nitric Oxide detection



4. Nitric Oxide detection

4.1. Introduction

Nitric oxide (NO) is a major chemical messenger in living organisms [1]. NO is involved in a wide range of immune defense and signaling mechanisms such as neural communication, antitumor activity, blood pressure regulation and non-specific immune defense [2]. Moreover several studies suggested that NO could play a key role in the apparition and the spread of a broad range of diseases such as neurodegenerative diseases, cardiovascular disease, diabetes and cancer [3] [4]. Therefore understanding the mechanism involved in NO production has been crucial to find new drugs and treat the previously cited diseases. NO is produced by NO synthase which has different and even opposite biological functions [5] [6] [7]. Its mechanism is not yet clearly understood in spite of numerous studies on NO synthase. Microreactors could encapsulate the enzyme in order to have a confined and a controlled environment. Controlling species release and concentration inside the microreactor and measuring the enzyme response could help to disentangle the complex reaction pathway of the enzyme. Monitoring NO gas production from the enzyme and detecting it under confocal microscopy can be performed with fluorescence techniques. NO production and detection are challenging due to NO reactivity towards biological species and oxygen. In order to develop tools for a NO synthase microreactor, firstly different methods are presented to obtain a reliable NO source, then fluorescent NO probes were studied to measure the enzyme activity and finally a molecular tool is presented in order to control the NO production directly inside the microreactor.

4.2. NO production

Nitric oxide is a colorless and odorless gas. NO is a free radical and thus has a high reactivity towards a wide range of components. This gas can react with itself to form the toxic and orange gas NO₂ and thus has to be used with cautious. Due to its high reactivity with oxygen, handling and storing NO gas is challenging. NO can be dissolved in deoxygenated water however if not frozen and kept under NO atmosphere the gas concentration in the solution will gradually decrease. However having a reliable source of NO and measuring exactly its concentration is a prerequisite to measure precisely fluorescent probe performance. To this end, a hemoglobin method to assess NO concentration in a solution is presented as well as three different ways to obtain standard NO solutions.

4.2.1. NO quantification based on hemoglobin absorption

4.2.1.1. Principle of hemoglobin quantification

Hemoglobin (Hb) is the iron-containing oxygen-transporting metalloprotein in red blood cells. This protein increases the maximum oxygen concentration in the blood and thus delivers oxygen efficiently to organs [8]. The oxygenated, ferrous (iron (II)) form of hemoglobin or oxyhemoglobin (HbO_2) reacts with nitric oxide to yield to the ferric form (iron (III)) called methemoglobin (MetHb) [9]. Hemoglobin absorbs in the UV visible spectral region and the two forms of hemoglobin, MetHb and HbO_2 have different absorption spectra (Figure 66).

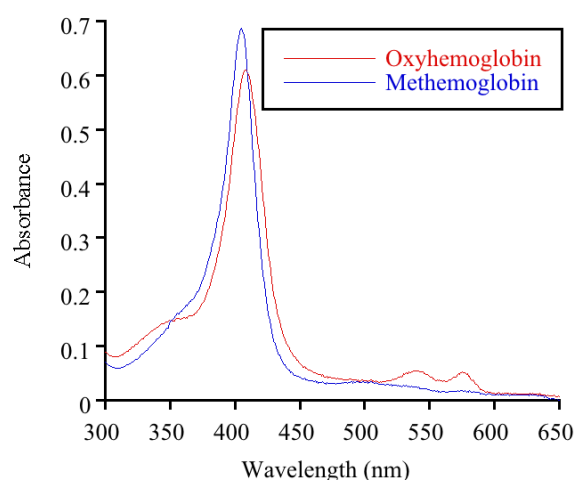


Figure 66: Electronic spectra of MetHb and HbO_2 in phosphate buffer (50 mM pH 7.4).

The difference between the two spectra can be used to measure the NO solution concentration [10]. The subtraction of the absorbances at 577 and 590 nm or 421 and 401 nm have molar attenuation coefficient of respectively 10 3000 and 77 200 $\text{M}^{-1}\cdot\text{cm}^{-1}$ [10]. Therefore small aliquots of NO solution with an unknown concentration was added to an oxyhemoglobin solution and HbO_2 was gradually converted into MetHb. The absorption spectra were recorded for each NO solution addition and the NO concentration was deduced from the obtained spectra.

4.2.1.2. Hemoglobin preparation

A prerequisite to obtain a precise measurement of the NO concentration is to convert all the hemoglobin into HbO_2 . Beforehand, the hemoglobin was fully oxygenated to get rid of the MetHb. To this end, 25 mg of Hb (Sigma-Aldrich, H25000) were dissolved in 1 mL of

phosphate buffer (50 mM pH 7.4). The mixture was gently mixed in order to avoid formation of bubbles that could damage Hb. An excess of sodium dithionite was then added in Hb solution to reduce the Hb into HbO₂. A slight color change was observed after reduction: from dark red to blood red. The sodium dithionite salt excess was removed by using sephadex column (G-25 in PD-10 Desalting Columns GE healthcare (n°17085101)). The samples were collected (2 drops per vial) and frozen if not use the same day.

4.2.1.3. Quantification method

The NO solution of unknown concentration (stock solution) was defrosted, kept on ice and used the same day. O₂ was removed from a 2 mL vial with septa caps and the stock NO solution was diluted 20 fold with degassed phosphate buffer (PB) (50 mM, pH 7.4) inside the vial. In order to avoid contamination of the NO stock solution with oxygen, a gas tight syringe previously rinsed 3 times with degassed PB was used. The diluted NO solution was kept on ice during all the measurement processes. In order to avoid O₂ contamination during sample collection, an inflated N₂ balloon connected with a needle to the NO diluted solution was used. The HbO₂ solution previously prepared was defrosted and diluted in PB. The final HbO₂ solution should have an absorption between 0.8 and 1 at 415 nm (optical path 10mm) and has a final volume of 3 mL. A gastight syringe (rinsed 3 times with degassed PB) was used to add 20 μL of diluted NO solution in the HbO₂ solution. The resulting solution was gently homogenized and left to rest 2 min before measuring the absorption. The absorption spectrum was recorded between 600 and 350 nm. The previous step was repeated until 200 μL were added. The gastight syringe needle was kept inside the septa cap of the diluted NO solution between measurements in order to avoid O₂ contamination. The gastight syringe was also rinsed with NO diluted solution before collecting 20 μL.

An example of the absorption data collected during the concentration measurement of an NO solution is presented in Figure 67.

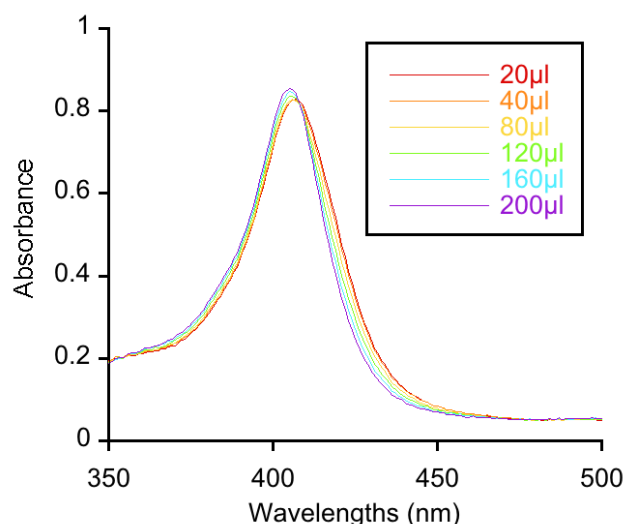


Figure 67: Electronic absorption spectra of successive additions of NO solutions in an HbO₂ solution.

NO addition gradually induced a shift of the absorption band maximum due to the conversion of HbO₂ into MetHb. The absorption at 421 and 401 nm were collected from the absorption spectra. From the subtraction of the two absorbances the concentrations of the MethHb (C(MetHb) produced were calculated *via* the molar attenuation coefficient of 77 200 M⁻¹cm⁻¹. Knowing that one NO reacts with one HbO₂ to give one MetHb; the quantity of NO added after each NO solution addition was deduced and the quantity of NO in the solution depending on the volume of NO diluted solution added was plotted (Figure 68).

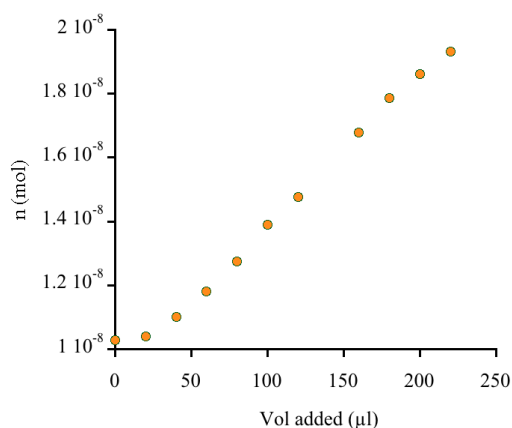


Figure 68: Quantity of methemoglobin produced versus NO diluted solution volume added. From this plot NO stock solution concentration can be deduced.

From the slope and taking into account the dilutions, the concentration found of this stock NO solution was 937 μM. For all the solution the concentration never exceeded 1 mM. In order to

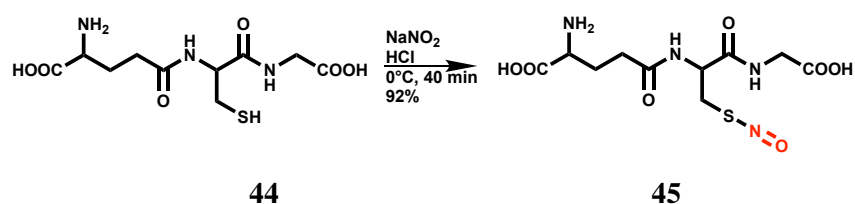
have the most accurate concentration during fluorescent probe calibration, the NO concentration measurement and the use the NO solution were performed the same day. Indeed the NO solution concentration decreased over time when defrosted.

4.2.2. S-Nitrosogluthatione

The first NO source tested was S-nitrosogluthatione (GSNO). This tripeptide can stabilize, stock and transport NO in mammals [11]. This molecule is based on glutathione, an antioxidant protein, on which NO form a stable bond with the sulfur of the cysteine. GSNO is a simple way to stock, produce, and is water soluble. The absorption band of the S-NO bond, allows efficient quantification of GSNO.

4.2.2.1. Synthesis of GSNO

S-nitrosogluthatione (GSNO) (**45**) was synthesized from commercially-available glutathione (**44**). To this end, glutathione was reacted with NaNO_2 in acidic conditions. The S-nitrosogluthatione can be destabilized and can release NO due to metal, oxygen traces or strong stirring. Thus in order to have a stable S-nitrosogluthatione, metal traces were removed from the glassware, ultrapure deoxygenated water was used, the reaction was performed at 0°C and the mixture was gently stirred. The mixture was precipitated in acetone and dried. The resulting pink powder of S-nitrosogluthatione was obtained in 92 % yield.



Scheme 34: General scheme of S-nitrosogluthatione synthesis from glutathione.

4.2.2.2. Quantification of GSNO produced

The reaction previously described does not lead to full conversion of GSH into GSNO. In order to calibrate precisely the fluorescence probe, the NO concentration has to be precisely known. To this end, the GSNO concentration was measured. GSNO absorbs in the UV spectral region,

contrary to GSH, thus GSNO concentration could be easily determined with a spectrophotometer. The bond between S and NO has an absorption band maximum at 334 nm with molar attenuation coefficient of $922 \text{ M}^{-1} \cdot \text{cm}^{-1}$. GSNO was dissolved in phosphate buffer (50 mM, pH 7.4) with a known concentration. The resulting solution absorption was measured and should be <1 at 334 nm (Figure 69). The results showed that 98 % of the glutathione was converted into GSNO.

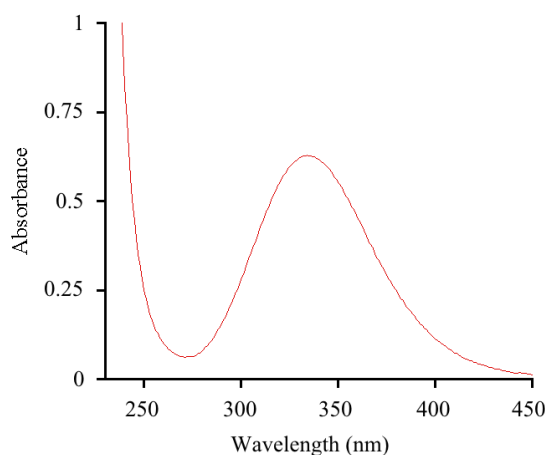


Figure 69: Electronic absorption spectrum of GSNO. The bond between S and NO absorbs at 334 nm.

4.2.2.3. NO Release from GSNO

Several methods have been studied in order to break the S-NO bond of GSNO and release nitric oxide [12]. CuSO_4 or ascorbic acid both induces NO release from GSNO. However while CuSO_4 was dissolved in phosphate buffer a blue precipitate appeared probably due to copper precipitation. Thus ascorbic acid was used inducing NO release. 1 mM of ascorbic acid was added to a solution of 1 mM of GSNO in phosphate buffer (50 mM, pH 7.4). The NO release was followed by spectrophotometry *via* the decrease of the S-NO bond absorption as shown in Figure 70. A spectrum was recorded every 5 min.

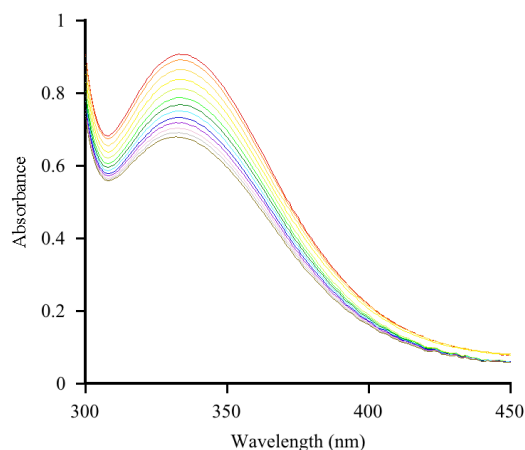


Figure 70: Electronic absorption spectra of GSNO (1 mM) in phosphate buffer (50 mM, pH 7.4) recorded every 5 min after acid ascorbic addition (1 mM).

The absorption decrease at 334 nm is correlated to the release of NO. After 1 hour, only 25 % of GSNO was converted into GSH. During the probe calibration, the probe concentration was 50 μ M. In the presence of 1 mM of ascorbic acid 10 min were necessary to release 50 μ M of NO and saturate the probe. In order to increase the NO release speed, several ascorbic acid concentrations were tested: 1 mM, 20 mM and 40 mM. The GSNO concentration was plotted for several ascorbic acid concentrations depending on the reaction time (Figure 71).

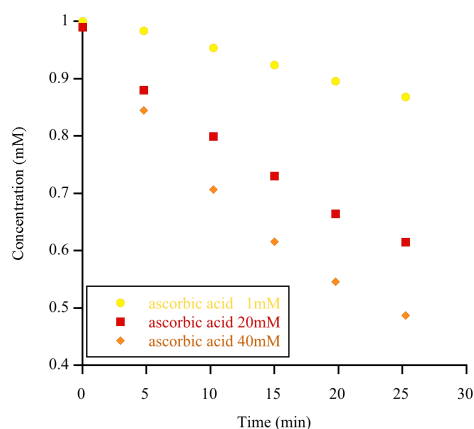


Figure 71: Concentration of GSNO depending on the reaction time measured by spectrophotometry, with 1 mM, 20 mM and 40 mM of ascorbic acid. GSNO concentration was initially 1 mM in phosphate buffer (50mM, pH 7.4).

The GSNO concentration decreased and NO release was faster for higher ascorbic acid concentration. In less than 2 minutes, 50 μ M of NO was released with 20 mM ascorbic acid. GSNO allows to have a fast release of NO in the presence of higher ascorbic acid concentration.

4.2.3. NO production from NaNO₂ and sulfuric acid

The second method used to obtain NO solution was to generate NO from sodium nitrite in acidic condition [13] (equation 1).



Before reaction, all apparatus and the solution were degassed with N₂ during 30 min due to NO sensitivity to oxygen. Then 2 M H₂SO₄ solution was slowly added drop by drop to a saturated NaNO₂ solution. Addition of H₂SO₄ in the NaNO₂ solution generated an orange gas. NO is a colorless gas, the orange color was due to the presence of undesired NO₂. In order to remove NO₂ the resulting gas was bubbled twice in a 30 % NaOH solution. NO₂ was converted into NO gas as follows (equation 2):



After bubbling in basic solution the gas was transparent showing the full conversion of NO₂ into NO. The resulting gas was finally bubbled into phosphate buffer (50 mM pH 7.4) in order to solubilize NO. The obtained solution was divided in small vials and frozen for later use. The final solution concentration was measured with the hemoglobin method described earlier (part 4.2.1). The concentration obtained was surprisingly low ($\approx 190 \mu\text{M}$). We hypothesized that the concentration obtained was due to NO solution stored under N₂ atmosphere. Due to the low concentration obtained, these NO solutions were not used for probe calibration. Effectively, the addition of NO solution would dilute the probe solution too much.

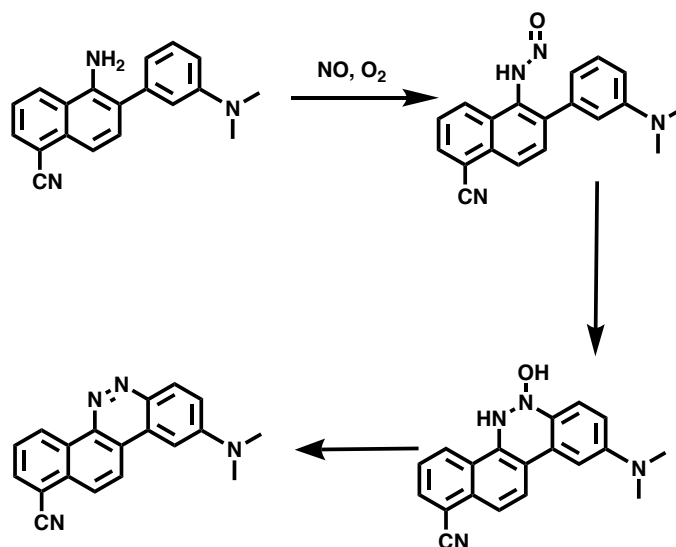
4.2.4. Nitric oxide from gas bottle

The last method used was the use of NO gas bottle. This method consists in bubbling gas from a bottle into a KOH solution (to remove nitrite) then in water solution for 5 to 30 min. With this method the NO concentration was higher than the previous method, up to 937 μM (30 min bubbling). However NO gas bottles are very expensive and we had only restricted access.

4.3. Nitric oxide fluorescent probes

4.3.1. Introduction on nitric oxide fluorescent probes

A major project goal was to study NO synthase. Monitoring the enzyme activity in situ, required to detect NO production. To this end, NO fluorescent probes were synthesized and studied. A wide range of NO probes have already been developed. The main family of NO probe used is based on o-phenylenediamine such as 4,5-diaminofluorescein [14] or 2,3-diamino-naphthalene [15]. The diamine group on the molecule quenches the probe fluorescent due to photoinduced electron transfer from the amines to the fluorophore. Nitric oxide reacts with the diamine to give the corresponding triazole which prevents the photoinduced electron transfer and restores the fluorescence [16]. However, these molecules have drawbacks such as high sensitivity to oxidation, H_2O_2 , NO_2 • NO_3^- [17] and to ascorbic acid [18]. A new mechanism for NO detection, was developed by Yang et al [19]. This mechanism was based on azo bond formation that creates a fluorescent molecule, as shown Scheme 35.



Scheme 35: Mechanism of azo-bond formation following NO capture.

The amine captures NO and forms a nitrosamine that then reacts with the aromatic ring. The azo bond is formed after water release. The newly formed azo bond increases the molecule conjugation length, which imparts fluorophore properties to the molecule. This new probe is not sensitive to pH, not toxic for the cell (under 100 μM). In addition, it reacts fast (80% of the signals complete in 20 s), and the molecule is chemically stable. However it suffers from one

drawback: this molecule is not soluble in water, all the measurements were performed in water:DMSO 80:20 (v/v).

In order to be able to detect NO in the inner medium of the microreactor and in its membrane, the molecule presented in the study described above was synthesized, modified to be water soluble, and their properties were studied.

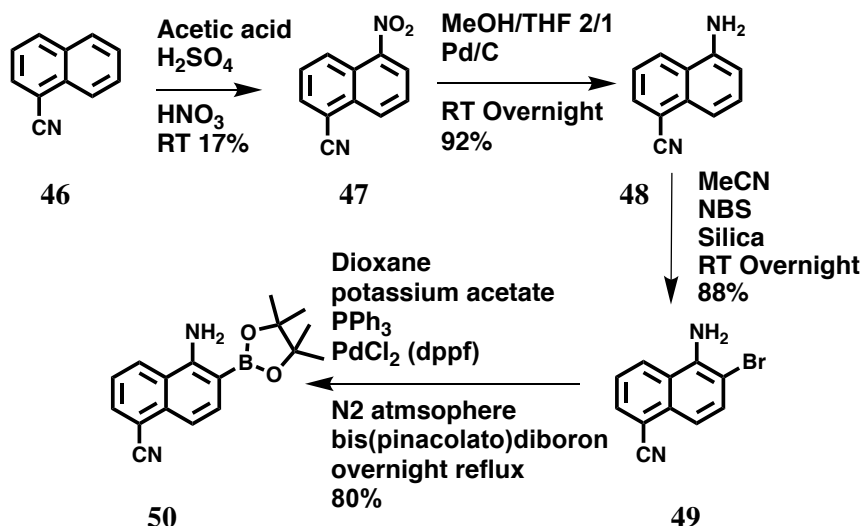
4.3.2. Synthesis of the hydrophilic and hydrophobic nitric oxide fluorescent probes

4.3.2.1. Hydrophobic probe synthesis

4.3.2.1.1. Naphthalene building block synthesis

The synthesis was performed in two steps. A naphthalene building block was designed in order to be used as building block for several molecules synthesized in this chapter. The synthesis protocol was adapted from a literature procedure [19] (Scheme 36).

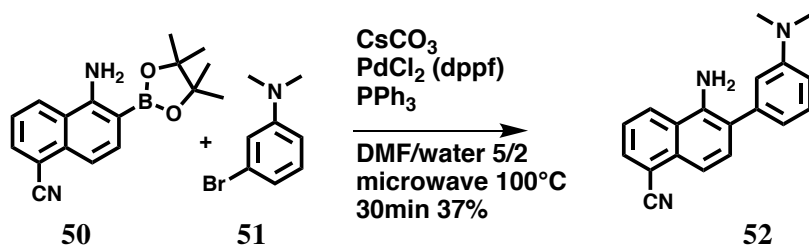
The commercially available 1-cyanonaphthalene (**46**) was reacted with nitric acid and sulfuric acid to give the 5-nitro-1-naphthalenecarbonitrile (**47**) in 17 % yield. The yield was low because naphthalenes nitrated 2 or 3 times were also obtained. The nitro group was then reduced into a primary amine with dihydrogen, catalyzed by palladium on carbon. The reaction was almost quantitative and gave the corresponding amine, 5-amino-1-naphthonitrile (**48**) in 92 % yield. **48** was then reacted with N-bromosuccinimide in order to brominate the naphthalene on position 6. 5-Amino-6-bromo-1-naphthalenecarbonitrile (**49**) was obtained in 88 % yield. **49** was then reacted with bis(pinacolato diboron) in order to be able to couple with other building blocks *via* a Suzuki-Miyaura reaction. The reaction mixture was degassed and then the coupling was catalyzed by palladium. The final product **50** was obtained in 80 % yield.



Scheme 36: Synthetic route of naphthalene building block.

4.3.2.1.2. Hydrophobic probe synthesis

The first building block **50** obtained was used for the synthesis of the next molecule. The hydrophobic molecule described in a previous study [19] was obtained in one step *via* a Suzuki-Miyaura reaction (Scheme 37).



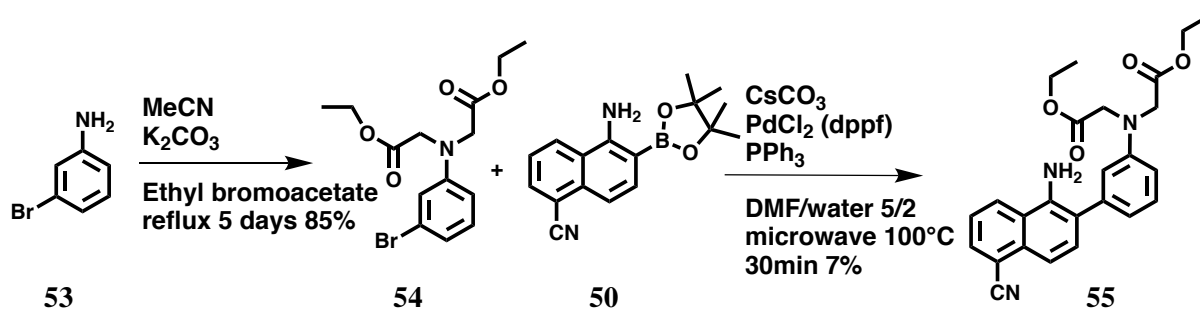
Scheme 37: Synthesis of the hydrophobic NO probe.

The commercially available 3-bromo-N,N-dimethylaniline was reacted with the previously synthesized naphthalene building block **50**. The final hydrophobic NO probe **52** was obtained in 37% yield.

4.3.2.2. Hydrophilic probe synthesis

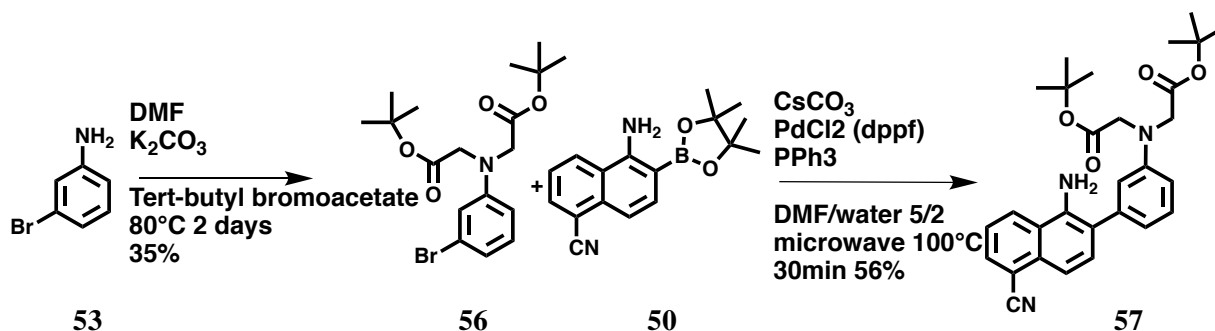
4.3.2.2.1. Carboxylic acid protecting group

The design of the hydrophilic molecule was inspired from the hydrophobic NO probe described earlier. Two carboxylic acid containing solubilizing groups were added on the molecule, replacing the two methyls of the dimethyl aniline to confer water solubility. To that end, the commercially-available 3-bromoaniline (**53**) was reacted with ethyl bromoacetate in order to alkylate the amine group. The corresponding tertiary amine (**54**) was obtained in 85 % yield. The modified bromoaniline **54** was then reacted with the naphthalene building block **50** via a Suzuki-Miyaura coupling to give the protected hydrophilic NO probe **55** in 7 % yield. This reaction had a particularly low yield and a significant amount of side product rendered the purification difficult. The quantity of **55** obtained was too low to perform the last step reaction. The cause of the low yield was thus investigated.



*Scheme 38: Synthetic route for precursor **55** of a hydrophilic NO probe.*

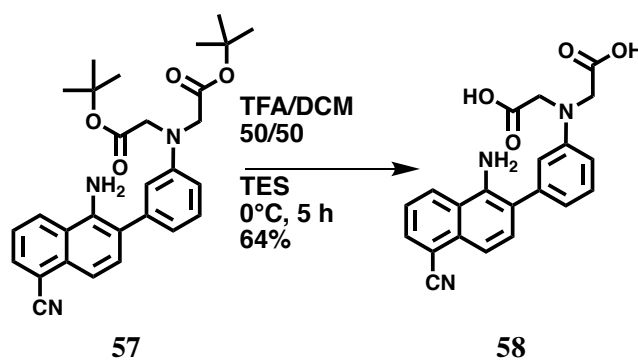
We hypothesized that the protecting groups of the carboxylic acid were degraded during the Suzuki-Miyaura coupling. Indeed the base $CsCO_3$ was added and the mixture was heated. These conditions were favorable for ester hydrolysis leading to a plethora of side products. The protecting group was thus changed to *tert*-butyl that is known to be less sensitive to hydrolysis [20]. To that end, 3-bromoaniline (**53**) was reacted with *tert*-butyl bromoacetate to give the desired *tert*-butyl protected carboxylic acid (**56**) in 35 % yield. **56** was then coupled with the modified naphthalene **50** to give protected hydrophilic NO probe **57**. The yield obtained with the new *tert*-butyl protecting group, was 8 times higher at 56 % yield. The side product quantity generated during the reaction decreased and thus purification was simpler.



Scheme 39: Synthesis route of the tert-butyl protected hydrophilic NO probe.

4.3.2.2.2. Carboxylic acid deprotection

Protecting group cleavage had to be optimized due to the high sensitivity of the product to degradation. Deprotection of **57** was first performed with a mixture 50/50, TFA/DCM (v/v). However, after 2 hours reaction the product was degraded. During the cleavage a tertbutyl carbocation was formed that could cause side reactions and product degradation. Thus TES was used as carbocation scavenger [21] and ^1H NMR showed product formation and no degradation. After a rapid screening, the experimental conditions of choice were: TFA/DCM (50:50 v/v) solution with 4 equivalents of TES at 0°C under argon atmosphere with a reaction time of 5 hours.



Scheme 40: Tert-butyl deprotection of the hydrophilic NO probe.

The final product **58** was also sensitive to the work-up conditions. **58** degraded rapidly in presence of concentrated acid. Therefore while evaporating DCM/TFA mixture, a large excess of DCM was added to co-evaporate and remove completely TFA. The final solid was then washed with diethyl ether three times to remove acid traces. The final hydrophilic NO probe (**58**) was obtained in 64 % yield.

4.3.3. Fluorescence properties of the nitric oxide probes

4.3.3.1. NO probe solution preparation method

The hydrophilic NO probe (**58**) was dissolved in phosphate buffer (50 mM, pH 7.4) at 500 μ M and this solution was used as a stock solution. In order to dissolve completely the probe, the mixture was sonicated during 15 min. The solid probe was fully soluble in water, showing that the two added solubilizing groups were effective. The stock solution was kept at -20°C. In order to use the probe, the stock solution was defrosted and sonicated for 15 min in case of solid precipitation during the solution freezing. The stock solution was diluted to obtain a hydrophilic probe solution of 50 μ M in PB. The same conditions were used to dissolve the hydrophobic probe solution **52** however instead of using PB as the solvent, a mixture of PB (50 mM and pH 7.4) 80 % and DMSO 20 % was used.

4.3.3.2. Calibration of the NO probe with GSNO as a NO source

In order to calibrate the fluorescence of the probe, GSNO **47** was first used as NO source. This tripeptide was easy to store and to use. To this end, three solutions were prepared separately in PB (50 mM, pH 7.4): a hydrophilic probe solution, an ascorbic acid solution and a GSNO solution (O_2 free and kept under an inert atmosphere). 50 equivalents of GSNO and 1000 equivalents of acid ascorbic were added to the probe solution. The final concentrations were 50 μ M for the probe, 1 mM for GSNO and 20 mM for the ascorbic acid. A large excess of GSNO was added in order to quickly saturate the probe and quickly obtain a fluorescence signal. 20 equivalents of ascorbic acid compared to GSNO were added in order to have fast NO release (in less than 2 min as shown part 4.2.2.3). The fluorescence was then monitored by spectrofluorimetry. After one hour measurement, no fluorescent appeared. We hypothesized that ascorbic acid or GNSO prevented the formation of the fluorescent form of the probe. Indeed a study showed that ascorbic acid prevents the formation of nitrosamine [1] a reaction intermediate of the fluorescent form of the probe (Scheme 35). GSNO could not therefore be used as a reliable source of NO in our case.

4.3.3.3. Calibration of the NO probe with NO from gas bottle as the NO source

NO solution from a NO gas bottle was finally used. After defrosting, the NO solution was kept on ice and used the same day. The NO solution was connected to an inflated N₂ balloon in order to avoid O₂ contamination. NO solution was collected with an anaerobic syringe and rinsed with deoxygenated PB before use. The anaerobic syringe needle was kept inside the vial during measurement to avoid O₂ contamination.

The NO concentration of the NO solution from the gas bottle was measured the same day. 0.1 equivalent of NO was added in 450 μ L of the probe solution (50 μ M). The solution was homogenized and left to react for 3 min in order to obtain almost complete reaction of NO with the probe. The excitation spectra and the emission spectra were then recorded. The emission wavelengths used for the excitation spectra was 530 nm for the hydrophilic probe and 550 nm for the hydrophobic probe. The excitation wavelengths used for the emission spectra were 416 nm for the hydrophilic probe and 440 nm for the hydrophobic probe. The parameters used for spectrophotometer are described in the experimental part. The process was repeated for 0.2 to 1 equivalent. The obtained emission and excitation spectra are shown in Figure 72.

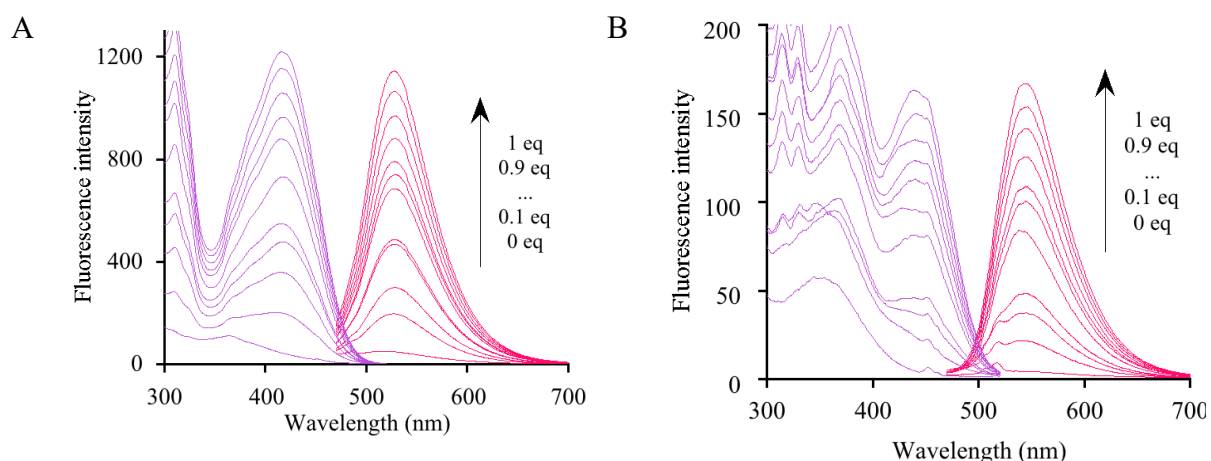


Figure 72: Excitation (purple) and emission (red) spectra of the (A) hydrophilic and (B) hydrophobic probe after addition of NO solution. Hydrophilic probe was solubilized in PB (50mM, pH 7.4) and the hydrophobic probe was solubilized in 80% PB (50mM, pH 7.4) and 20 % DMSO. The emission wavelengths used for the excitation spectra were 530 nm for the hydrophilic probe and 550 nm for the hydrophobic probe. The excitation wavelength used for the emission spectra were 416 nm for the hydrophilic probe and 440 nm for the hydrophobic probe.

Before NO addition the two probes showed minimal fluorescence. NO addition in the probe solution induced a fast increase of the emission band intensity centered at 530 nm for the hydrophilic probe and 550 nm for the hydrophobic probe. The excitation band intensity also increased fast with NO addition with a band centered at 416 nm for the hydrophilic probe and 440 nm for the hydrophobic probe. The fluorescence was induced by a higher conjugation of the molecule resulting from the azo bond formation and the planar form. The maximum emission wavelengths intensities, $\lambda_{em}=530\text{ nm}$, $\lambda_{ex}=416\text{ nm}$ and $\lambda_{em}=550\text{ nm}$, $\lambda_{ex}=440\text{ nm}$, for respectively the hydrophilic and hydrophobic dyes, were plotted depending on the concentration of NO added. The resulting graph is presented in Figure 73.

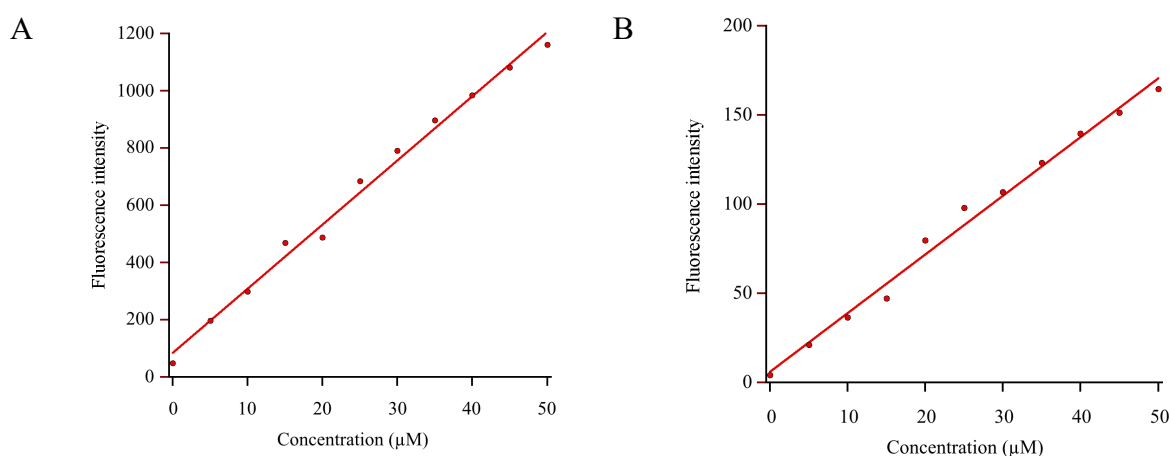


Figure 73: Maximum emission wavelengths intensity depending on the concentration of NO added of the (A) hydrophilic ($\lambda_{em}=530\text{ nm}$, $\lambda_{ex}=416\text{ nm}$) and (B) hydrophobic probe ($\lambda_{em}=550\text{ nm}$, $\lambda_{ex}=440\text{ nm}$). Hydrophilic probe was solubilized in PB (50mM, pH 7.4) and the hydrophobic probe was solubilized in 80% PB (50mM, pH 7.4) and 20 % DMSO. The emission wavelengths used for the hydrophilic probe were 530 and 550 nm for the hydrophobic probe.

The plots showed an excellent linear correlation with R^2 of 0.99 for the two probes that allow a quantitative measurement of NO concentration.

4.3.4. Conclusion

Understanding the mechanism of NO synthase and NO production has been crucial to find new drug and treat a broad range of disease such as neurodegenerative disease, cardiovascular disease, diabetes, cancer. To this end, monitoring NO gas production from the enzyme and detecting it under confocal microscopy could help to disentangle the complex reaction pathway of the enzyme. Two NO probes based on formation of an azo bond that induce fluorescence

have been studied. These probes have stable signal and high selectivity against other nitro compounds. The two probes were designed to have different solubility properties in order to detect NO in the membrane and in the inner medium of the microreactor. One probe with hydrophobic properties and another with hydrophilic properties. The probes were synthesized in 5 and 6 steps for respectively the hydrophobic and hydrophilic probes. Critical steps were encountered for the protection and deprotection of the carboxylic acid of the hydrophilic probe. *Tert*-butyl showed enough resistance for the synthesis conditions used contrary to ethyl group. TES was used as carbocation scavenger avoiding product degradation during the deprotection step for the hydrophilic molecule. In order to test the probes properties, several sources of NO were tested such as GSNO, NO from NaNO₂ or NO gas from bottle and the resulting NO concentration were measured *via* hemoglobin absorption. NO release from GSNO was triggered by ascorbic acid and the release kinetic was studied. However ascorbic acid prevented the formation of the fluorescent molecule and GSNO could not be used. NO from NaNO₂ gave low concentration solution therefore, NO solution from gas bottle was finally used. The NO detection of the probes was tested. Probes showed an increase of the fluorescent intensity ($\lambda_{em\ Max}= 530\text{ nm}$, $\lambda_{ex\ Max}=440\text{ nm}$ for the hydrophilic probe, $\lambda_{em\ Max}= 530\text{ nm}$, $\lambda_{ex\ Max}=440\text{ nm}$ for the hydrophilic probe) after addition of NO. The fluorescence intensity increase had an excellent linear correlation ($R^2 = 0.99$) depending on the NO quantity added allowing a quantitative measurement of NO in situ.

4.4. Control of the NO production in situ via a molecular tool

4.4.1. Feedback strategy presentation

NO is produced by NO synthase which has different and even opposite biological functions [1]. Its mechanism is not yet clearly understood in spite of numerous studies. Microreactors could encapsulate the enzyme in order to have a confined and controlled environment. Introducing reactants in a controlled manner directly in the microreactor while enzyme activity is monitored could help disentangle the complex reaction pathways. The goal aimed in this part was to be able to have fine control of the rate of NO production. One possibility explored to control the enzyme in situ was to use a feedback process. The strategy adopted to control enzyme activity was to use NO production to induce the release of a species that activates new enzymes leading to a higher NO production rate. Calcium can trigger the enzyme production of NO and calcium

trap have been widely studied thus the combination of calcium trap with NO probe could induce an efficient feedback process as shown in Figure 74.

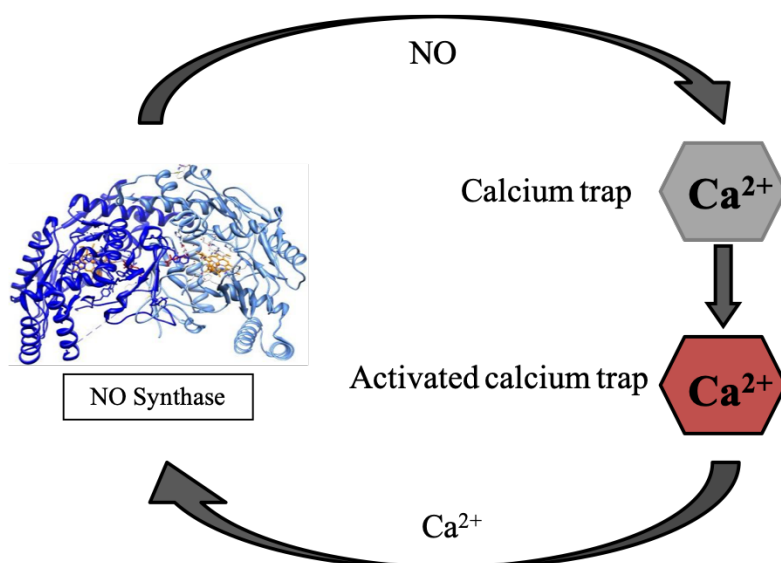
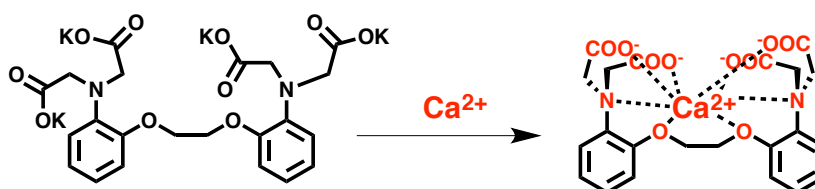


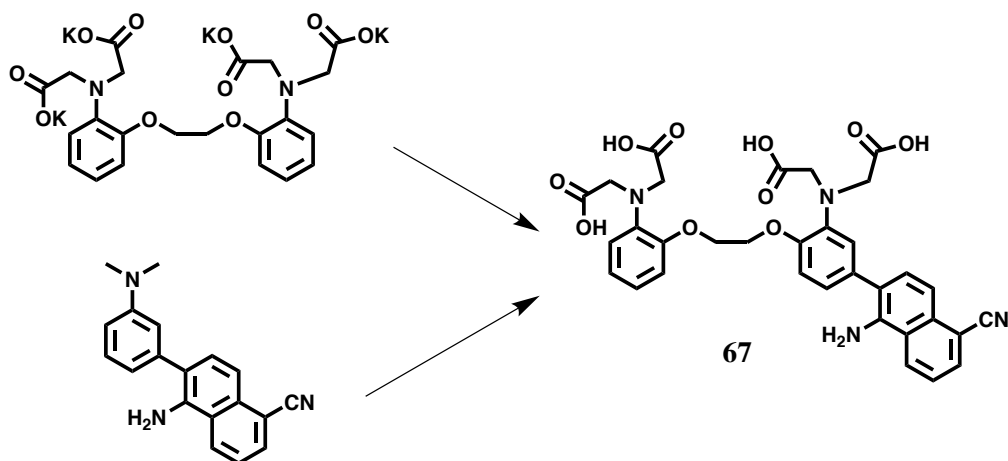
Figure 74: Schematic strategy of the feedback process to control NO production from NO synthase with Ca^{2+} .

NO production from NO synthase activates the calcium trap which release calcium inducing activation of other enzymes. BAPTA (1,2-Bis(2-Aminophenoxy)ethane-N,N,N',N'-tetraacetic acid) is an efficient calcium trap with a high selectivity against magnesium [22] (Scheme 41).



Scheme 41: BAPTA molecule which is an efficient calcium trap with a high selectivity against magnesium.

The affinity of BAPTA towards Ca^{2+} can be increased or decreased *via* electron withdrawing or releasing groups on the aromatic groups [22]. NO probe presented part 4.3.2 could provide a switchable electron-withdrawing group on the BAPTA as shown Scheme 42.



Scheme 42: Combination of BAPTA and NO probe to give a molecular tool to control NO production (BAPTA-NOp).

The combination of BAPTA and NO probe leading to BAPTA-NOp (**67**) could induce an autoactivation of the enzyme and allow to control the nitric oxide production. NO is produced by the enzyme (Figure 75 A) and react with **67** (Figure 75 B). Reaction between **67** and NO form an azo bond to give BAPTA-AZO (**70**) resulting in a higher conjugation than BAPTA-NOp. Due to the higher conjugation the cyano electron withdrawing group attract electron of the tertiary amine of the BAPTA resulting in a weaker complexation of calcium and its release (Figure 75 C). The released calcium activates other enzymes and produces even more nitric oxide (Figure 75 D).

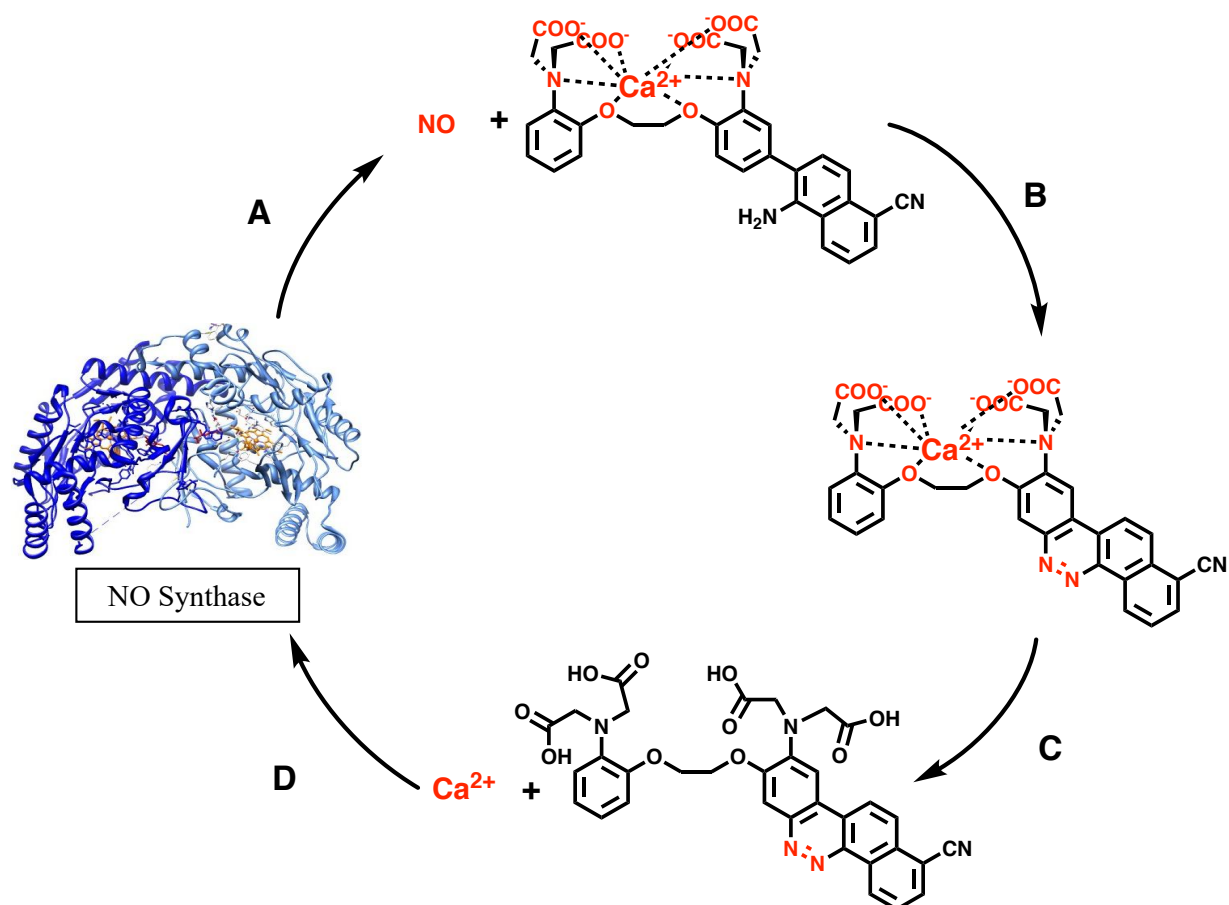


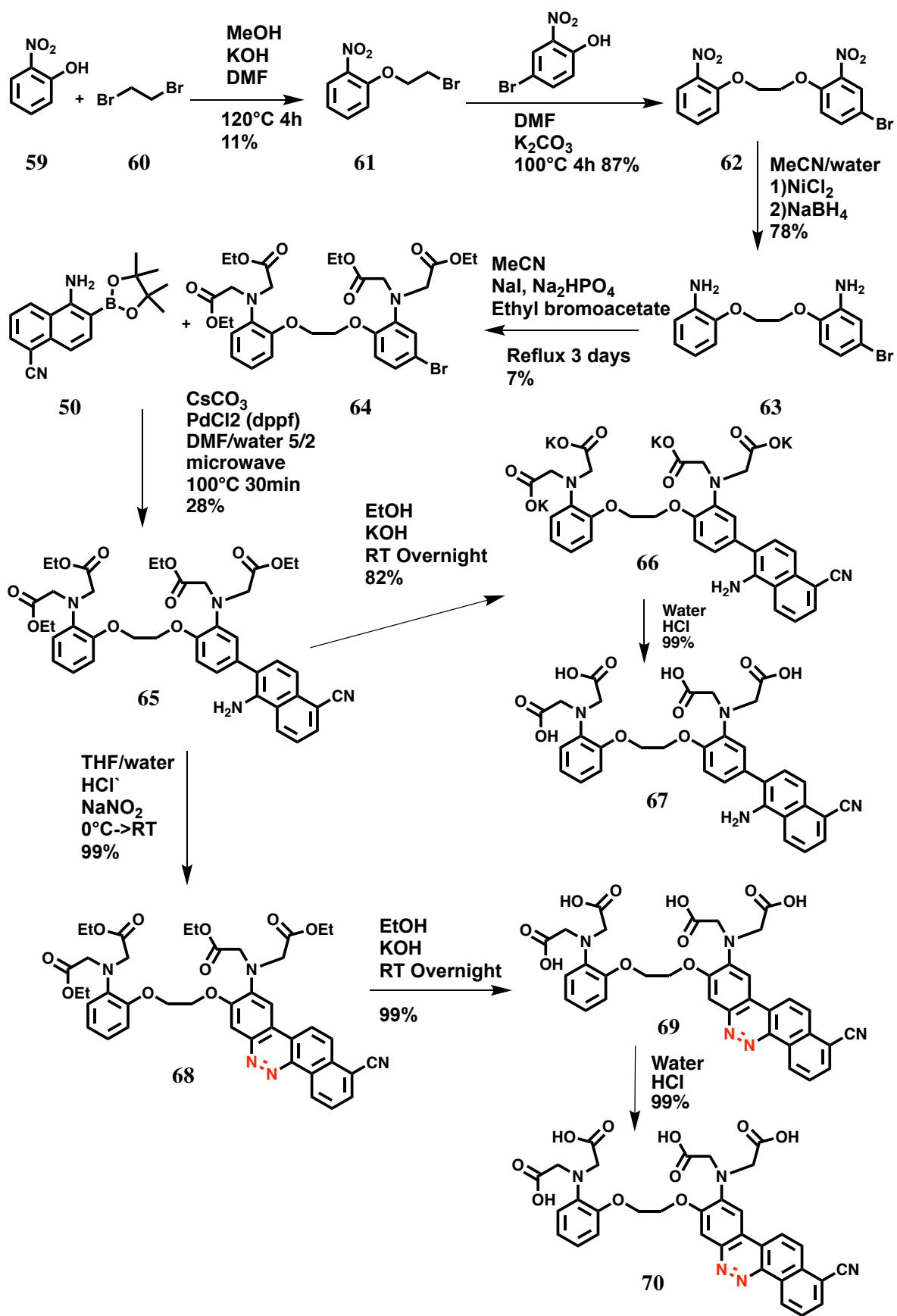
Figure 75: Expected feedback mechanism of BAPTA-NOp to control the NO production.

This enzyme autoactivation strategy was explored and in order to control the releasing effect of calcium due to azo-bond formation after reaction with NO, the complexation constant of BAPTA-NOp and BAPTA-AZO were measured.

4.4.2. BAPTA-NOp and BAPTA-AZO synthesis

The synthesis is described in Scheme 43. The commercially available 2-nitrophenol (**59**) was reacted with 1,2 dibromoethane (**60**) to form 1-(2-bromoethoxy)-2-nitrobenzene (**61**) in 11% yield. An excess of **60** was added in order to have only one addition of **59** per dibromoethane chain. **61** was then reacted with 4-bromo-2-nitrophenol to give 4-bromo-1-nitro-2-(2-(2-nitrophenoxy)ethoxy)-benzene (**62**) in 87 % yield. This reaction allowed introduction of a bromo substituent on the aromatic ring in order to have a non-symmetric molecule. The two nitro groups were then reduced into amine groups to give 4-bromo-1-amino-2-(2-(2-nitrophenoxy)ethoxy)-benzene (**63**) in 78 % yield. The two amine groups were then alkylated twice in order to graft the two protected carboxylic acids. To this end, **63** was reacted with ethyl

bromoacetate to give the corresponding alkylated amine (**64**) in 7 % yield. The low yield was probably due to the protecting group ethyl which was hydrolyzed during the reaction as shown previously (part 4.3.2.2.1). **64** was then coupled with the previously synthesized modified naphthalene **50** (part 4.3.2.1) *via* Suzuki-Miyaura reaction to give **65** in 28 % yield. The low yield was also probably due to the deprotection of the carboxylic acid. Azo bond form and the amine form, were synthesized in order to compare the two different calcium dissociation constants. To this end, **65** was nitrogenated to form the azo bond by reacting with NaNO₂ in acidic condition to give **68** in almost quantitative yield (99 %). During the reaction, yellow **65** turned red due to the higher conjugation of the molecule. The azo form molecule was obtained by deprotection of the carboxylic acid under basic condition to give the corresponding potassium salt **69** in almost quantitative yield (99 %). The corresponding protonated carboxylic acid was precipitated by adding hydrochloric acid to a water solution of the potassium salt **69** to give BAPTA-AZO **70** in almost quantitative yield (99 %). The amine form was obtained in the same manner by deprotection of the 4 carboxylic acids under basic condition to obtain the amine potassium salt form **66** in almost quantitative yield (99 %). And the corresponding protonated carboxylic acid was obtained by precipitation with acid to obtain the final amine form BAPTA-NOp **67** in almost quantitative yield (99 %).



Scheme 43: General scheme of the synthesis route of BAPTA-NOp and BAPTA-AZO.

4.4.3. Calcium constant Measurement of BAPTA-NOp and BAPTA-AZO

The effective dissociation constants (K_d) of the calcium complexes of **67** and **70** were determined in an aqueous buffer under pseudo-intracellular conditions (30 mM MOPS (3-[N-morpholino]propanesulfonic acid), 100 mM KCl at pH 7.2) by electronic absorption spectroscopy. The procedure for the K_d measurement is detailed in the experimental part. Briefly, BAPTA-NOp and BAPTA-AZO were dissolved in the pseudo intracellular buffer with a concentration between 1 and 10 μM . Several free Ca^{2+} concentrations were used with BAPTA-NO and BAPTA-AZO. The resulting absorption spectra were measured and the K_d could be deduced. In order to neutralize all the calcium impurities from the glassware and the water, EGTA was used to bind all the free Ca^{2+} . The free Ca^{2+} concentration in the calcium complex **67** and **70** solution was adjusted by mixing a solution of 10 mM of EGTA (without free Ca^{2+}) and of 10 mM CaEGTA (with a free Ca^{2+} concentration of 39 μM). The addition of these two solutions allowed to obtain concentrations between 0 and 39 μM as described by Tsien [22] and the resulting absorption spectra are shown Figure 76.

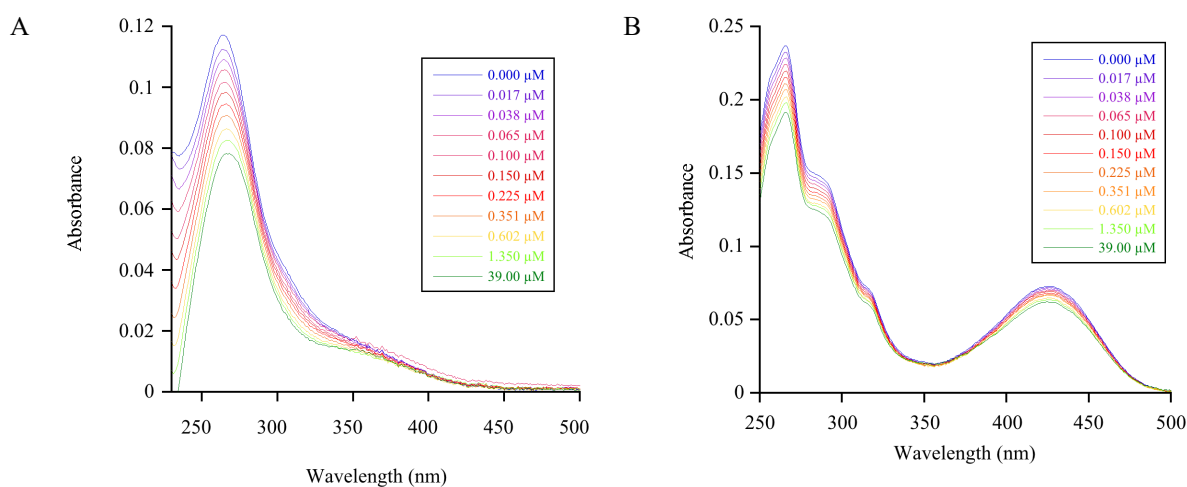


Figure 76: Electronic absorption spectra of A) BAPTA-NOp **67** and B) BAPTA-AZO **70** upon Ca^{2+} -addition in pseudo intracellular buffer.

The spectra of **67** and **70** showed differences in their absorption bands. The main absorption bands for both molecules were in the UV spectral region (263 nm for **67** and 268 nm for **70**) due to naphthalene and alkoxyanilino group. New absorption bands in UV-vis spectral region (288, 315 and 425 nm) appeared for **70** due to the azo bond and the higher conjugation of the molecule. The absorption spectra showed small decreases in the visible spectral region upon

Ca²⁺ addition. However, in the UV spectral region, the absorption spectra showed higher changes due to the alkoxyanilino groups which were directly involved in the complexation of calcium and absorb in the UV spectral region. The maximal changes for **67** were at 263 nm, and 268 nm for **70**. The spectral variation of these bands were used to measure the ground state dissociation constant K_d of both molecules with a Hill plot. To this end, the logarithm of the absorption changes ($\log[(A-A_{\min})/(A_{\max}-A)]$) was plotted over the logarithm of the free Ca²⁺ concentration and the fitting of the obtained graph showed linear correlation with R² = 0.99 for both molecule indicating a mono-binding (Figure 77). The linear fit slope gave the Hill coefficient describing cooperativity of Ca²⁺ on the BAPTA and the intercept give the logarithm of the dissociation constant K_d.

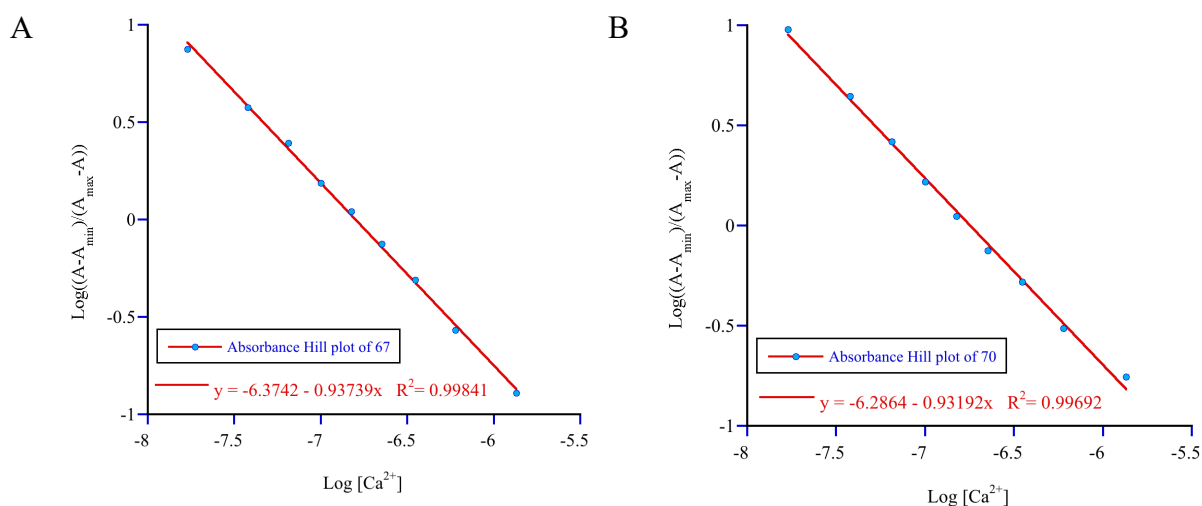


Figure 77: Hill plot for the spectral change of A) BAPTA-NOp **67** and B) BAPTA-AZO **70** in absorption at, respectively, 263 nm and 425 nm.

A Hill coefficient higher than unity indicates positively cooperative binding, a Hill coefficient lower than one indicates a negatively cooperative binding. For both molecules the slope is close to the unity indicating a non-cooperative binding. The dissociation constant K_d found for **67** was 0.42 μM and 0.52 μM for **70**. The K_d were in agreement with BAPTA family K_d (BAPTA K_d= 0.59 μM [23]). The K_d of **67** and **70** are relatively close. Azo bond formation does not induce a strong increase of the K_d which means that the BAPTA-AZO does not release calcium. Cyano group did not withdraw sufficiently enough the electrons of the alkoxyaniline to decrease the affinity of **70** with calcium. The cyano group might be too far or its withdrawing effect too weak to release calcium. The molecule cannot therefore be used for feedback process.

4.4.4. Fluorescent properties

The fluorescent properties of BAPTA-AZO were studied (Figure 78). BAPTA-NOp as expected did not have fluorescent properties. However, BAPTA-AZO showed fluorescent with a maximum emission band at 520 nm. Additionally, the maximum band shifted to 540 nm when Ca^{2+} was chelated to BAPTA. These properties could allow to measure simultaneously NO and Ca^{2+} concentration with the radiometric method [24].

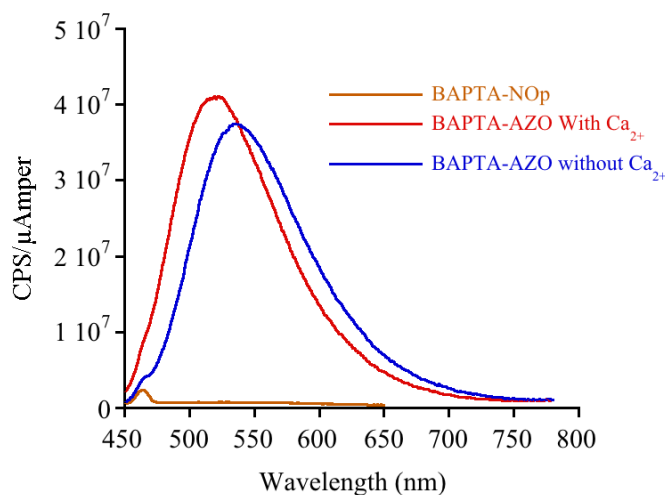


Figure 78: Fluorescent spectra of BAPTA-NOp, BAPTA-AZO with or without calcium in water at a concentration of 15 mM ($\lambda_{\text{ex}}=400$ nm).

4.4.5. Conclusion

The aim of this part was to autoactivate the NO synthase *via* a feedback process. We hypothesized that the combination of BAPTA and NO probe (BAPTA-NOp) could induce an autoactivation of the enzyme and could control the nitric oxide production. NO would be produced by the enzyme and react with BAPTA-NOp to give BAPTA-AZO. Due to the higher conjugation, the cyano electron withdrawing group would attract electron of the tertiary amine of the BAPTA resulting in a weaker complexation of calcium and its release. To test this hypothesis BAPTA-NOp and BAPTA-AZO have been synthesized in 10 steps and their dissociation constant K_d were measured. K_d found for BAPTA-NOp and BAPTA-AZO were respectively 0.42 μM and 0.52 μM . Their K_d were in agreement with BAPTA family K_d . However, the K_d of BAPTA-NOp and BAPTA-AZO are relatively close and BAPTA-AZO have a relatively low K_d which mean the AZO form does not release calcium and that the molecule cannot be used for feedback process.

4.5. Conclusion

Nitric oxide (NO) is a major chemical messenger in living organism. Several studies suggested that NO could play a key role in the apparition and the spread of a broad range of diseases. Understanding the mechanism involved in NO production by NO synthase has been crucial. NO synthase mechanism is not yet clearly understood and microreactor could encapsulate the enzyme in order to have a confined and controlled environment. Controlling species release and concentration inside the microreactor and measuring the enzyme response could help to disentangle the complex reaction pathway of the enzyme. In order to monitor NO gas production directly inside the microreactor, two NO probes have been studied. These probes are based on formation of an azo bond that induces fluorescence, resulting in stable signal and high selectivity against other nitro compounds. The two probes were designed to have different solubility properties (one hydrophobic another hydrophilic) in order to detect NO in the membrane and in the inner aqueous medium of the microreactor. The probes were synthesized in 5 and 6 steps. Critical steps were encountered for the protection and deprotection of the carboxylic acid of the hydrophilic probe. *Tert*-butyl proved to be an efficient protecting group with the conditions used and TES was used during the deprotection step avoiding hydrophilic probe degradation. In order to test the probes properties, several NO sources were tested such as GSNO, NO from NaNO₂ or NO as gas from a bottle and the resulting NO concentration were measured *via* hemoglobin absorption. NO release from GSNO was triggered by ascorbic acid and the release kinetics were studied. However, ascorbic acid prevents the formation of the fluorescent molecule and GSNO could not be used. NO from NaNO₂ gave low concentration solutions therefore NO solution from a gas bottle was finally used. The NO detection of the probes were tested. Probes showed an increase of the fluorescent intensity ($\lambda_{em\ max}= 530\ nm$, $\lambda_{ex\ max}=440\ nm$ for the hydrophilic probe, $\lambda_{em\ max}= 530\ nm$, $\lambda_{ex\ max}=440\ nm$ for the hydrophilic probe) after addition of NO. The fluorescence intensity was fitted and had an excellent linear correlation ($R^2 = 0.99$) depending on the NO quantity added allowing a quantitative measurement of NO. The probes are currently tested *in vitro* at the laboratory CITHEFOR (Lorraine University EA 3452).

In a second part, another molecular tool was synthesized in order to study NO synthase. Introducing reactants in a controlled manner directly in the microreactor could help monitor enzyme activity and information about enzyme mechanisms may be obtained. To this end, a molecular tool was designed to have fine control of the rate of NO production by a feedback process. We hypothesized that the combination of BAPTA and NO probe (BAPTA-NOp) could

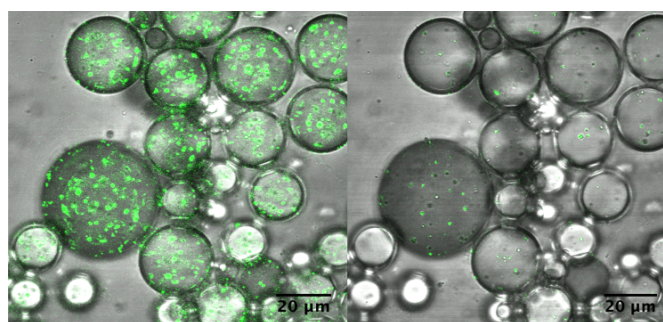
induce an autoactivation of the enzyme and could control the nitric oxide production. NO would be produced by the enzyme and react with BAPTA-NOp to give BAPTA-AZO. Due to the higher conjugation, the cyano electron withdrawing group would attract electron of the tertiary amine of the BAPTA resulting in a weaker complexation of calcium and its release. To test this hypothesis BAPTA-NOp and BAPTA-AZO have been synthesized in 10 steps and their dissociation constant K_d were measured. K_d found for BAPTA-NOp and BAPTA-AZO were, respectively, 0.42 μM and 0.52 μM . Their K_d values were in agreement with the BAPTA family K_d values. Unfortunately, the K_d of BAPTA-NOp and BAPTA-AZO are relatively close and BAPTA-AZO have a relatively low K_d which mean the AZO form does not release calcium and that the molecule cannot be used for the feedback process.

References

- [1] L.J. Ignarro, Nitric oxide: biology and pathobiology, Academic press, 2000.
- [2] J. Lincoln, C.H.V. Hoyle, G. Burnstock, Nitric Oxide in Health and Disease, Cambridge University Press, Cambridge, 1997. <http://discovery.ucl.ac.uk/186320/> (accessed March 20, 2019).
- [3] H. Ischiropoulos, J.S. Beckman, Oxidative stress and nitration in neurodegeneration: Cause, effect, or association?, *J. Clin. Invest.* 111 (2003) 163–169. doi:10.1172/JCI200317638.
- [4] C. Szabó, H. Ischiropoulos, R. Radi, Peroxynitrite: biochemistry, pathophysiology and development of therapeutics, *Nat. Rev. Drug Discov.* 6 (2007) 662–680. doi:10.1038/nrd2222.
- [5] W.C. Sessa, eNOS at a glance, *J. Cell Sci.* 117 (2004) 2427–2429. doi:10.1242/jcs.01165.
- [6] I.N. Mungrue, D.S. Bredt, nNOS at a glance: implications for brain and brawn, *J. Cell Sci.* 117 (2004) 2627–2629. doi:10.1242/jcs.01187.
- [7] C.J. Lowenstein, E. Padalko, iNOS (NOS2) at a glance, *J. Cell Sci.* 117 (2004) 2865–2867. doi:10.1242/jcs.01166.
- [8] R.E. Dickerson, I. Geis, Hemoglobin: Structure, Function, Evolution, and Pathology, Benjamin/Cummings Publishing Company, 1983.
- [9] T.H. Han, D.R. Hyduke, M.W. Vaughn, J.M. Fukuto, J.C. Liao, Nitric oxide reaction with red blood cells and hemoglobin under heterogeneous conditions, *Proc. Natl. Acad. Sci. U. S. A.* 99 (2002) 7763–7768. doi:10.1073/pnas.122118299.
- [10] M.E. Murphy, E. Noack, [24] Nitric oxide assay using hemoglobin method, in: *Methods Enzymol.*, Academic Press, 1994: pp. 240–250. doi:10.1016/S0076-6879(94)33027-1.
- [11] C.C. Chiueh, P. Rauhala, The redox pathway of S-nitrosoglutathione, glutathione and nitric oxide in cell to neuron communications, *Free Radic. Res.* 31 (1999) 641–650.
- [12] J.N. Smith, T.P. Dasgupta, Kinetics and mechanism of the decomposition of S-nitrosoglutathione by l-ascorbic acid and copper ions in aqueous solution to produce nitric oxide, *Nitric Oxide Biol. Chem.* 4 (2000) 57–66. doi:10.1006/niox.2000.0272.
- [13] K.-J. Huang, H. Wang, M. Ma, X. Zhang, H.-S. Zhang, Real-time imaging of nitric oxide production in living cells with 1,3,5,7-tetramethyl-2,6-dicarbethoxy-8-(3',4'-diaminophenyl)-difluoroboradiazas-indacene by invert fluorescence microscope, *Nitric Oxide.* 16 (2007) 36–43. doi:10.1016/j.niox.2006.05.003.
- [14] H. Kojima, K. Sakurai, K. Kikuchi, S. Kawahara, Y. Kirino, H. Nagoshi, Y. Hirata, T. Nagano, Development of a fluorescent indicator for nitric oxide based on the fluorescein chromophore, *Chem. Pharm. Bull. (Tokyo).* 46 (1998) 373–375.
- [15] A.M. Miles, Y. Chen, M.W. Owens, M.B. Grisham, Fluorometric Determination of Nitric Oxide, *Methods.* 7 (1995) 40–47. doi:10.1006/meth.1995.1006.
- [16] E.W. Miller, C.J. Chang, Fluorescent probes for nitric oxide and hydrogen peroxide in cell signaling, *Curr. Opin. Chem. Biol.* 11 (2007) 620–625. doi:10.1016/j.cbpa.2007.09.018.
- [17] D. Jourdeuil, Increased nitric oxide-dependent nitrosylation of 4, 5-diaminofluorescein by oxidants: implications for the measurement of intracellular nitric oxide, *Free Radic. Biol. Med.* 33 (2002) 676–684.
- [18] X. Zhang, W.-S. Kim, N. Hatcher, K. Potgieter, L.L. Moroz, R. Gillette, J.V. Sweedler, Interfering with nitric oxide measurements 4, 5-diaminofluorescein reacts with dehydroascorbic acid and ascorbic acid, *J. Biol. Chem.* 277 (2002) 48472–48478.
- [19] Y. Yang, S.K. Seidlits, M.M. Adams, V.M. Lynch, C.E. Schmidt, E.V. Anslyn, J.B. Shear, A Highly Selective Low-Background Fluorescent Imaging Agent for Nitric Oxide, *J. Am. Chem.*

-
- Soc. 132 (2010) 13114–13116. doi:10.1021/ja1040013.
- [20] P.G.M. Wuts, T.W. Greene, *Greene's Protective Groups in Organic Synthesis*, John Wiley & Sons, 2006.
- [21] A. Mehta, R. Jaouhari, T.J. Benson, K.T. Douglas, Improved efficiency and selectivity in peptide synthesis: Use of triethylsilane as a carbocation scavenger in deprotection of t-butyl esters and t-butoxycarbonyl-protected sites, *Tetrahedron Lett.* 33 (1992) 5441–5444. doi:10.1016/S0040-4039(00)79116-7.
- [22] R.Y. Tsien, New calcium indicators and buffers with high selectivity against magnesium and protons: design, synthesis, and properties of prototype structures, *Biochemistry.* 19 (1980) 2396–2404. doi:10.1021/bi00552a018.
- [23] R. Pethig, M. Kuhn, R. Payne, E. Adler, T.-H. Chen, L.F. Jaffe, On the dissociation constants of BAPTA-type calcium buffers, *Cell Calcium.* 10 (1989) 491–498.
- [24] S. Wang, H. Ding, Y. Wang, C. Fan, G. Liu, S. Pu, A colorimetric and ratiometric fluorescent sensor for sequentially detecting Cu²⁺ and arginine based on a coumarin–rhodamine B derivative and its application for bioimaging, *RSC Adv.* 9 (2019) 6643–6649. doi:10.1039/C8RA09943J.

Chapter 5: Investigation of species release in microreactors



5. Investigation of species release in microreactors

5.1. Introduction

Cells are extraordinary bio-machines [1] that can process complex synthesis with a high level of control. As an example, synthesis of complex molecules, intricate processes or cascade biochemical reactions can be performed in cells. In addition, toxic species can be synthesized without damaging cells and incompatible species can coexist in the same medium due to compartmentalization [2]. Biochemical reactions can be performed with a high level of control in space and time. Mimicking some cellular functions would afford access to these complex processes. To achieve this goal, scientists have been interested in designing microreactors in order to mimic the simplest cellular functions such as enzyme synthesis of molecules in a confined space [3]. However to the best of our knowledge most microreactor reaction initiation steps are limited to species diffusion through the microreactor membrane [4][5][6][7]. In order to have a control on the initiation step and to start an enzymatic reaction at a specific location and time, the controlled reactant release in the microreactor was explored. This work aims to lay the foundation for temporal and spatial control of enzyme function by controlling substrate release. The previous chapter discussed the development of the requisite tools and strategies to develop a synthetic cell microreactor. In particular, methods were proposed to destabilize nanopolymersomes and release species via light excitation. In this chapter, on-going work into implementing this release method to start enzymatic reactions in a microreactor is presented.

5.2. Controlled species release in space and time inside a microreactor

5.2.1. Controlled destabilization of nanopolymersomes inside a microreactor

5.2.1.1. *Photosensitive polymersome encapsulation in a microreactor*

Nanopolymersomes were formed by nanoprecipitation, using the PEG₄₃-coumarin-*b*-PTMC₈₁ block copolymer described in part 2.5. The obtained nanopolymersomes had a diameter of 320 nm and a monomodal distribution with a PDI of 0.11. To prepare giant vesicles using an emulsion-centrifugation method, PEO_{1.3}-*b*-PBut_{2.5} was dissolved in toluene at a concentration

of 3 mg/mL. 4 μL of the nanopolymeromes solution were added to 400 μL of toluene solution. The solution was vigorously hand shaken for 25 seconds in order to form the emulsion in toluene that was stabilized by the copolymer: the obtained mixture comprised nanopolymeromes encapsulated in a $\text{PEO}_{1.3}\text{-}b\text{-PBut}_{2.5}$ emulsion. The resulting emulsion was observed by confocal microscopy as shown Figure 79.

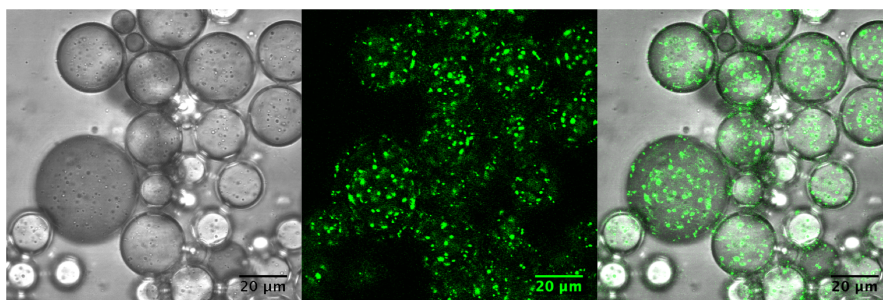


Figure 79: Confocal observation of a water emulsion stabilized by $\text{PEO}_{1.3}\text{-}b\text{-PBut}_{2.5}$ containing light-sensitive $\text{PEG}_{43}\text{-coumarin-}b\text{-PTMC}_{81}$ nanopolymeromes (green channel, $\lambda_{\text{ex}} = 405 \text{ nm}$, 50 mW, 3% emission range of coumarin, 485 nm).

The emulsion droplets were around 20 μm in size. The nanopolymeromes were readily visible due to fluorescent coumarin moiety covalently inserted between PEG and PTMC. The nanopolymeromes were freely moving inside the emulsion droplet due to Brownian motion showing the successful encapsulation of the nanopolymeromes inside the emulsion droplet microreactor without any aggregation. In addition, one can clearly see that all the microreactors contained homogeneous distribution of nanopolymeromes.

5.2.1.2. Temporal control of nanopolymeromes destabilization in a microreactor.

The previously formed microreactors were irradiated at 405 nm 80% 50 mW for 2 min under confocal microscopy and the number of nanopolymeromes was monitored. The resulting irradiated microreactors are shown Figure 80.

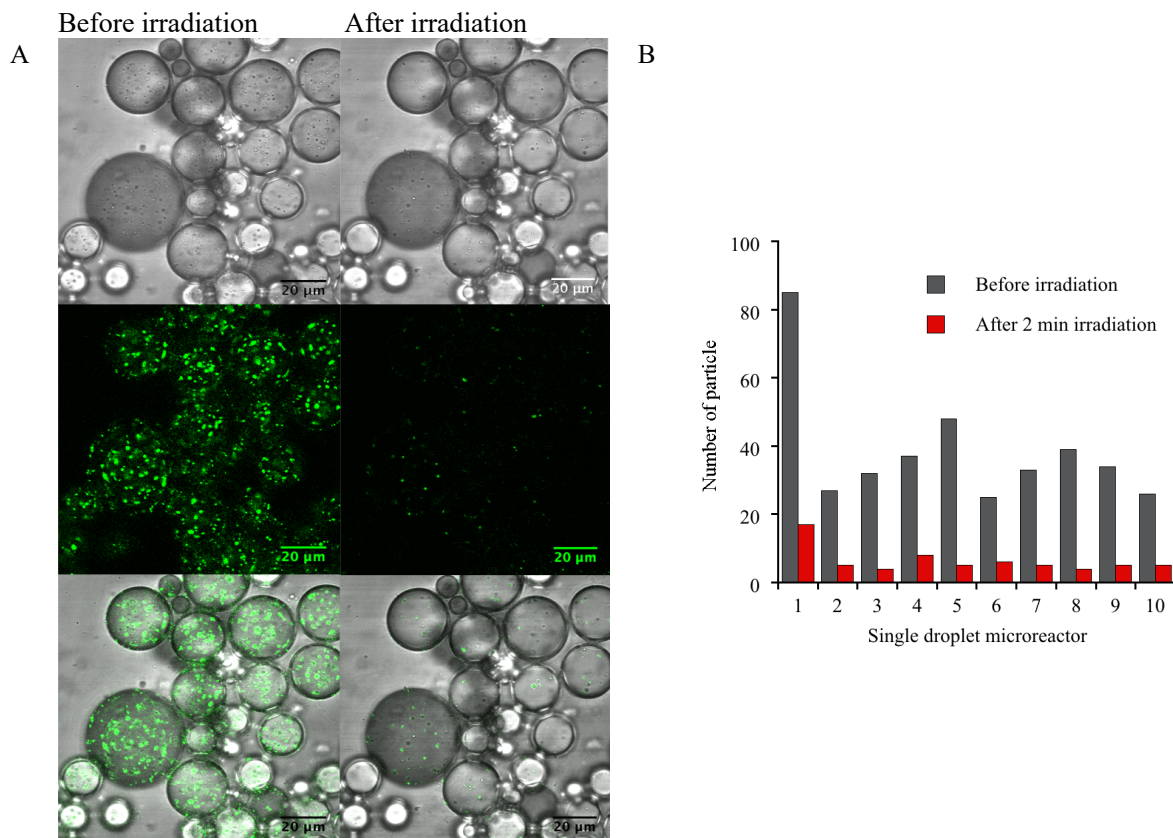


Figure 80: A) Confocal observation of water emulsion stabilized by $PEO_{1.3}$ - b - $PBut_{2.5}$ containing light-sensitive PEG_{43} -coumarin- b - $PTMC_{81}$ nanopolymersomes irradiated 2 min at 405 nm 80% 50 mW (green channel, $\lambda_{ex} = 405$ nm, 50 mW, 3% emission range of coumarin, 485 nm). B) Quantitative measure of the irradiation effect, the nanopolymersomes were counted on the transmission image for each emulsion droplet before and after irradiation.

After 2 min irradiation, the coumarin fluorescence was bleached and the number of particles decreased in each microreactor. In order to have a quantitative measure of the irradiation effect, the nanopolymersomes were counted on the transmission image for each emulsion droplet (Figure 80 B). On average the number of particles decreased by 83% with a standard deviation of 4.5%. The average was calculated from 10 emulsion droplets. The quantitative measure showed that 405 nm irradiation had a significant and homogenous destabilization effect on the nanopolymersomes. Confocal fluorescence microscopy observation confirmed the scattered light intensity decrease measured by DLS (part 2.7.6). These results revealed that destabilization of nanopolymersomes can be induced directly inside the microreactor with temporal control.

5.2.1.3. Spatial control of nanopolymerome destabilization in a microreactor.

In order to assess the spatial control of nanopolymerome destabilization, a proportion of the microreactors were irradiated and the resulting images obtained by confocal microscopy are shown in Figure 81. In the region below the red dashed line the microreactors were irradiated during 2 min at 405 nm (50 mW, 80%), while in the region above the red dashed line the emulsion droplets were not irradiated.

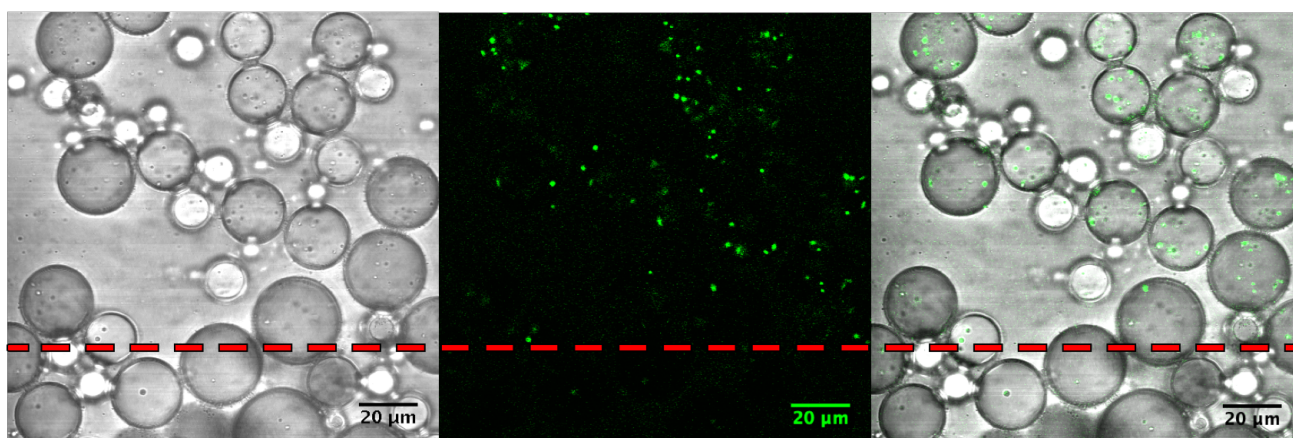


Figure 81: Confocal observation of water emulsion stabilized by PEO_{1.3}-b-PBut_{2.5} containing light-sensitive PEG₄₃-coumarin-b-PTMC₈₁ nanopolymeromes (green channel, $\lambda_{ex} = 405$ nm, 50 mW, 3% emission range of coumarin, 485 nm). Under the red dashed line emulsion droplet were irradiated 2 min at 405 nm (80% 50 mW). Above the red dashed line emulsion droplets were not irradiated.

The images clearly showed that the microreactors located in the irradiated zone had a lower number of nanopolymeromes. Above the dashed line, the microreactors contained on average 11.2 nanopolymeromes and under the dashed line the microreactors contained on average 1.4 nanopolymeromes. This difference corresponded to a decrease of 87% that is consistent with the results presented in part 5.2.1.2. These results showed that destabilization of nanopolymeromes can be induced at a specific location.

5.2.2. Species release inside the microreactor

5.2.2.1. Strategy

In order to measure the release properties of the PEG₄₃-coumarin-*b*-PTMC₈₁ nanopolymersomes in a microreactor, fluorescein was used as the encapsulated species due to its hydrophilicity and its self-quenching properties at high concentration (Figure 83). The strategy was to encapsulate fluorescein at a quenched concentration inside the nanopolymersomes (F-Nano). Considering that the F-Nano were not fluorescent due the quenched dye, it was anticipated that fluorescein release would dilute the dye and thus induce a fluorescence increase of the microreactor inner medium, as schematically depicted on Figure 82. A similar strategy was previously reported in our group to measure the release efficiency of nano-objects [8] [9].

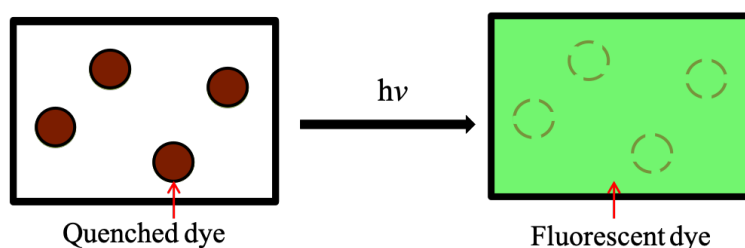


Figure 82: Schematic representation of the strategy used to study the nanoparticle release.

Fluorescein fluorescence was measured at different concentrations in order to estimate a suitable concentration to have maximum light absorption and high fluorescence quenching (Figure 83). While right angle fluorescence detection of the homogenous solution is not perfectly representative of that of microdomains in polymersome solutions, concentrations around 0.1M show minimal fluorescence, and in principle a maximal enhancement upon polymersome bursting. Therefore the fluorescein concentration chosen inside the F-Nano was 80 mM to minimize initial emission.

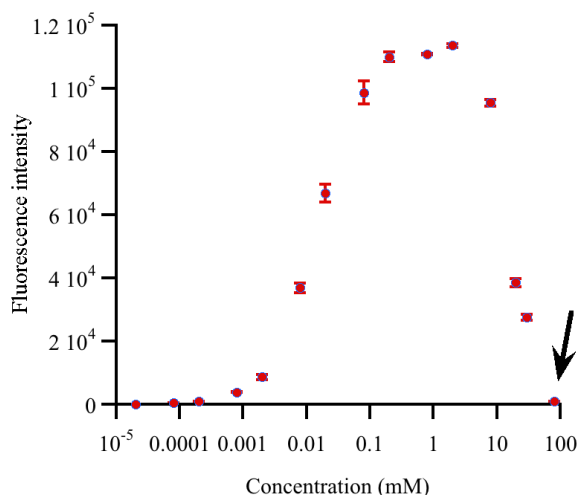


Figure 83: Fluorescein fluorescence in water at different concentrations. The black arrow indicated the chosen quenched concentration.

5.2.2.2. Fluorescein encapsulation method

Nanopolymersomes containing fluorescein (F-Nano) were formed by nanoprecipitation with PEG₄₃-coumarin-*b*-PTMC₈₁ block copolymer. Nanoprecipitation was performed with a syringe pump. 2.7 mL of 80 mM fluorescein solution was added during 15 s into 300 μ L of DMSO containing the copolymer at 10 mg/mL. During the water addition the mixture was stirred at 500 tr/min in a 5 mL brown glass vial. To remove DMSO the particle suspension was dialyzed 3 times again 5 L of deionized water with a 3.5 kDa membrane during 2 hours. In order to remove the fluorescein in the outer medium, F-Nano were purified by size exclusion chromatography with sephadex G-100 gel column (15 cm). The obtained particles had monomodal distribution with a PDI of 0.13 and diameter of 312 nm.

5.2.2.3. Measurement of the amount of loaded fluorescein

In order to measure the quantity of loaded fluorescein in the F-Nano, the destabilization of PEG₄₃-coumarin-*b*-PTMC₈₁ nanoparticles was studied *via* DMSO addition. The fully destabilized nanoparticles would release all their fluorescein content and the final fluorescein concentration could be measured. The stability of nanoparticles upon addition of DMSO was monitored by DLS at 90° *via* the decrease of the scattered light intensity, and the results are presented in Figure 84. The nanopolymersomes were also diluted with water to be able to compare the scattered light intensity change between stable and destabilized particles.

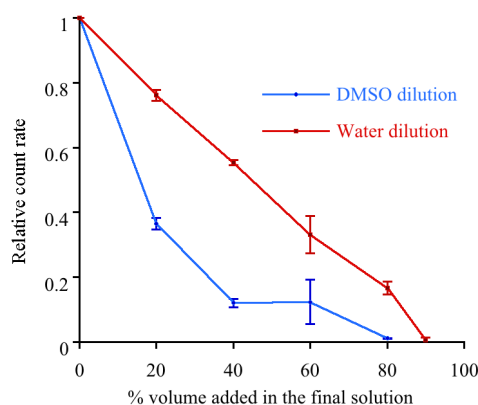


Figure 84: Relative count rate of PEG₄₃-coumarin-b-PTMC₈₁ nanopolyersomes depending on the volume of water or DMSO percentage added in the solution.

Water addition induced a linear decrease of the scattered light intensity, however DMSO addition induced a fast decrease of the scattered light intensity. 80% of DMSO addition decreased the signal intensity to almost zero indicating a total particle destabilization. This DMSO percentage was used to fully destabilize nanopolyersomes and to measure the total amount of encapsulated fluorescein. To this end the fluorescence intensity of fluorescein in DMSO:water 80:20 (v:v) was measured (Figure 85, fluorimeter parameters described in the experimental part).

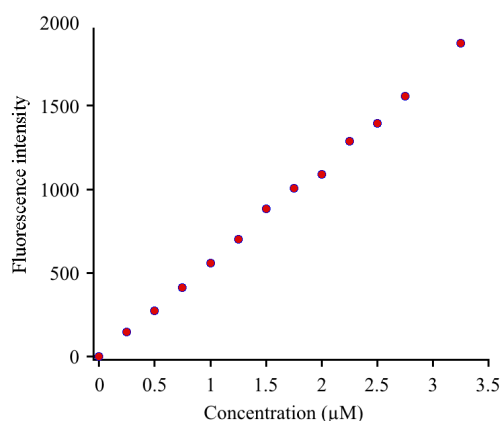


Figure 85: Calibration curve of fluorescein in a DMSO:water 80:20 (v:v) mixture ($\lambda_{ex}=460\text{ nm}$, $\lambda_{em}=520\text{ nm}$)

A linear correlation was obtained for the fluorescence depending on the fluorescein concentration allowing a precise measurement of the fluorescein encapsulated in the nanopolyersomes. To this end the F-Nano were destabilized by adding 80% of DMSO by volume and the fluorescence of the resulting DMSO:water solution obtained was 1.03 µM. This concentration allowed to deduce the initial fluorescein concentration in the whole solution

volume taking into account the dilution (dilution by 5): 5.1 μM . This concentration is not the concentration inside nanopolymersomes but rather the theoretical maximum concentration that could be obtained if all the fluorescein was released from the nanopolymersomes, this concentration being large enough to be measured in confocal experiments.

5.2.2.4. Release inside a pseudo-microreactor

The F-Nano were thus encapsulated inside emulsion droplets stabilized by $\text{PEO}_{1.3}\text{-}b\text{-PBut}_{2.5}$ in the same way as described in part 5.2.1.1. The resulting microreactors were irradiated for 10 s at 405 nm (50 mW, 80%). The images obtained by confocal imaging are presented in Figure 86 A. The fluorescence intensity in the inner medium was measured for 7 emulsion droplets microreactors (Figure 86 B).

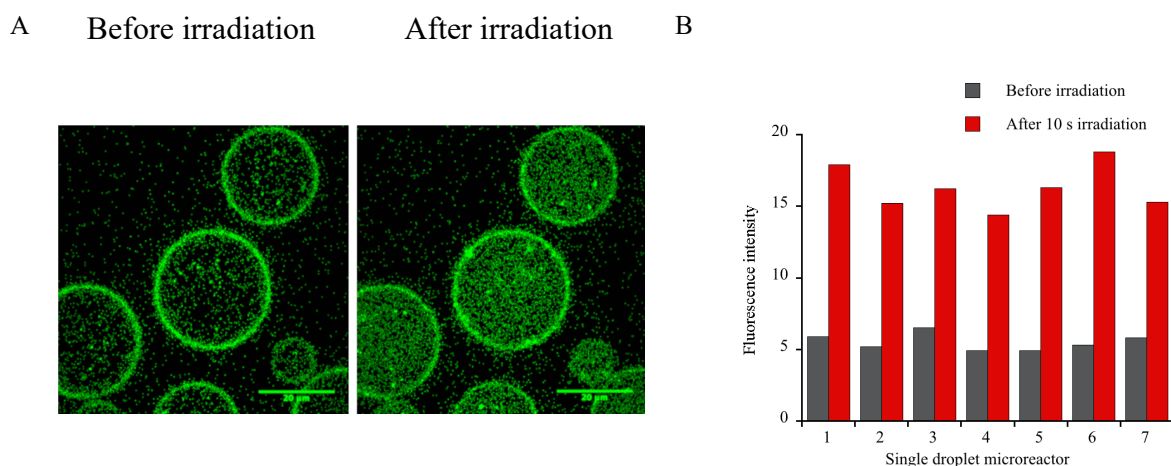


Figure 86: A) Confocal observation of water emulsion stabilized by $\text{PEO}_{1.3}\text{-}b\text{-PBut}_{2.5}$ containing $\text{PEG}_{43}\text{-coumarin-}b\text{-PTMC}_{81}$ polymersomes before and after 10 s irradiation at 405 nm 80% 50 mW. Fluorescein was encapsulated in the polymersomes (scale bar 20 μm , green channel $\lambda_{\text{ex}}=488$ nm, 40 mW, 10%, emission range of fluorescein, 520 nm). B) Fluorescence intensity (arbitrary unit) measured in the inner medium of 7 emulsion droplets before and after 10 s irradiation at 405 nm 80% 50 mW.

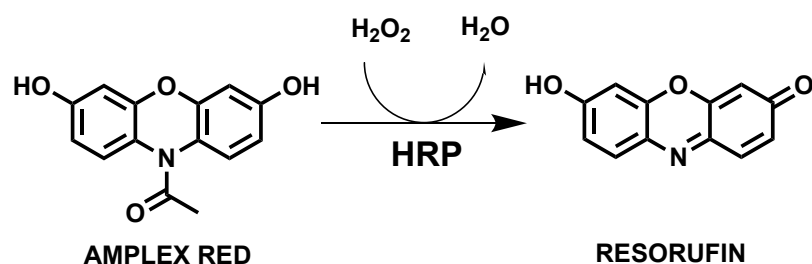
Before irradiation, fluorescence was observed at the interface between the toluene and water phase and the individual nanopolymersomes were fluorescent. These observations showed that certain amount of fluorescein leaked during nanopolymersomes and emulsion droplet formation. Several methods could be considered to avoid fluorescein leakage such as, decrease the dialysis time or equilibrate the osmotic pressure between the inner and the outer medium. Nevertheless, one can clearly see that after irradiating at 405 nm for 10 s the fluorescence

diffused in the whole volume of the inner medium (Figure 86 A), showing that the fluorescein was released from the F-Nano. As a control, the emulsion was irradiated at 488 nm 40mW, 100% and 633 nm 10 mW 100%. No fluorescence diffusion was observed, confirming that the observed release resulted from F-nano destabilization due to specific irradiation at the wavelength of coumarin.

5.3. Enzyme activity inside a microreactor

5.3.1. Study of the horseradish peroxidase enzymatic reaction.

In order to study the control of the enzymatic reaction inducing by the release of reactants from the PEG₄₃-coumarin-*b*-PTMC₈₁ polymersomes inside a microreactor, several enzymes were tested. Horseradish peroxidase (HRP) is a commonly used enzyme for H₂O₂ detection [10]. This reaction is convenient for confocal microscopy due to the production of a fluorescent molecule (resorufin) from a non-fluorescent Amplex[®] red (AR) (Scheme 44).



Scheme 44: HRP enzymatic conversion of the non-fluorescent Amplex[®] Red into the fluorescent resorufin.

This enzymatic reaction is quantitative, one equivalent of H₂O₂ giving one equivalent of resorufin. This enzyme was studied and tested for encapsulation in polymersome microreactors made of PEO_{1.3}-*b*-PBut_{2.5}.

5.3.1.1. Calibration of the fluorescence under confocal microscopy

The first step was to assess the linear correlation between the H₂O₂ concentration and the fluorescence intensity under the confocal microscopy. The conditions used for HRP reaction were optimized and are described in the experimental part. Briefly, several solutions of HRP, AR and H₂O₂ in PBS (pH 7.4) were prepared. HRP and AR concentrations remained constant for all the solutions (respectively 0.4 U/mL and 50 μM) and H₂O₂ concentration varied between 0 and 37 μM. AR is sensitive to light and can form resorufin without H₂O₂ [11] thus solutions

had to be freshly prepared and protected from light. The resulting solutions were observed under confocal microscopy and the fluorescence intensity was measured for each solution as shown in Figure 87.

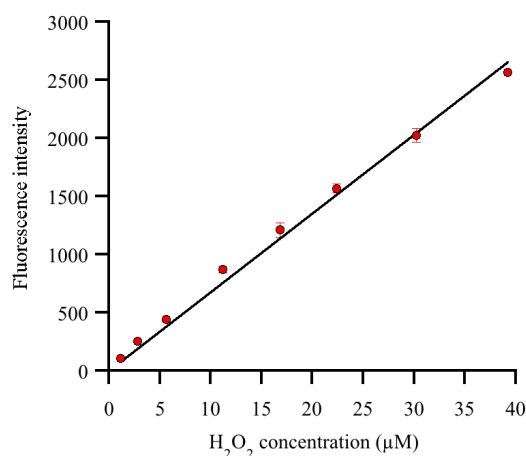


Figure 87: Fluorescence intensity (arbitrary unit) observed under confocal microscopy depending on the H₂O₂ concentration (AR, 20% 514nm 6% emission range 549-688 nm).

The resorufin fluorescence measured under confocal microscopy has a linear correlation with H₂O₂ concentration. R² found was 0.99 showing that the H₂O₂ concentration can be determined precisely for bulk solution under confocal microscopy and HRP enzymatic activity can theoretically be monitored in these conditions.

5.3.1.2. Encapsulation with emulsion centrifugation technique

A linear correlation was obtained for the resorufin in a bulk solution. The fluorescence intensity of resorufin inside polymersomes, was assessed. To this end HRP, AR and H₂O₂ in PBS solutions were prepared in the same way as described in part 5.3.1.1. The solutions were loaded with the emulsion centrifugation technique described in part 3.4. The resulting confocal microscopy images of PEO_{1.3}-*b*-PBut_{2.5} polymersomes that were obtained are presented in Figure 88.

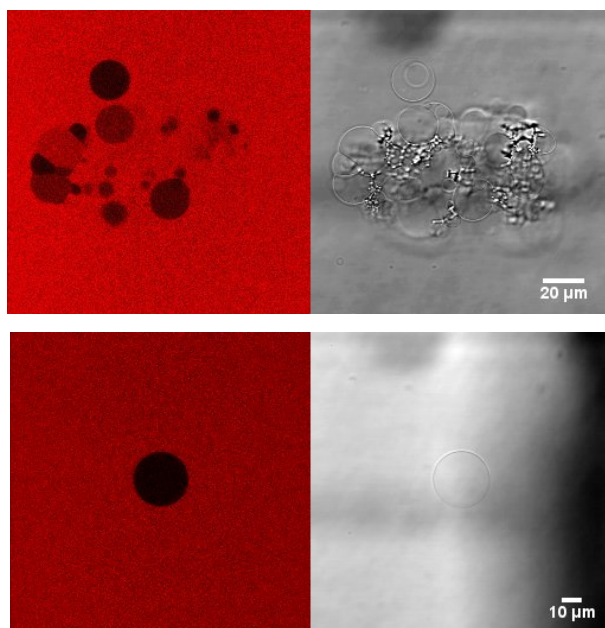


Figure 88: HRP, AR and H₂O₂ in PBS solution loaded in PEO_{1.3}-b-PBut_{2.5} polymersomes.

Surprisingly, the obtained vesicles were not fluorescent and even more surprisingly the fluorescence observed was in the outer medium (reverse encapsulation). The conditions used to encapsulate the HRP, AR and H₂O₂ fluorescent mixture were screened to find the cause of such reverse encapsulation, and it was found that PBS seemed to interfere with the encapsulation process. Indeed, Resorufin was encapsulated with and without PBS. In the first case the fluorescence was observed in the outer medium and not in the inner medium (Figure 88). In the second case the fluorescence was observed in the inner medium and not in the outer medium (Figure 89).

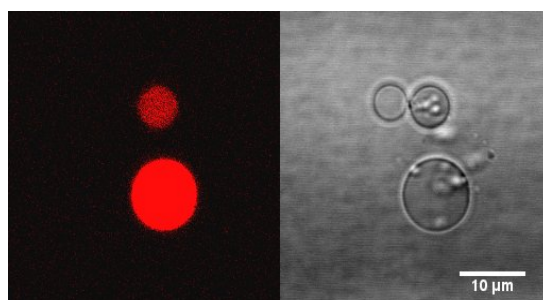


Figure 89: Resorufin without PBS encapsulated in PEO_{1.3}-b-PBut_{2.5} polymersomes.

PBS seemed to induce an increase of the permeation of the polymersomes. Due to a lack of time the reason of the reverse encapsulation was not investigated further. However, we can deduce that the emulsion centrifugation technique was not compatible with encapsulation of

the HRP enzymatic reaction. Indeed, stable pH and thus buffer is required to obtain precise and stable fluorescent intensity of resorufin [12]. We suggest that microfluidic techniques could be tested to encapsulate the HRP enzymatic reaction.

5.4. Conclusion

Multicompartmentalization is one of the key parameters that allow living cells to synthesize toxic species without damaging cells and incompatible species to coexist in the same medium [1] [2]. Biochemical reactions can be performed with a high level of control in space and time due to the cell compartments and the release of species in a control manner.

Scientists have been interested in designing microreactors that could mimic the simplest cellular functions and control [3]. However, to the best of our knowledge most microreactor reaction initiation steps are limited to species diffusion through the microreactor membrane [4][5][6][7]. In order to have a control on the initiation step and to start an enzymatic reaction at a specific location and time, the controlled reactant release in the microreactor via light sensitive multicompartment was explored. The previous chapters discussed the development of the requisite tools and strategies to develop a synthetic cell microreactor. In particular, methods were proposed to destabilize nanopolymersomes and release species via light excitation. In this chapter, on-going work into implementing this release method to start enzymatic reactions in a microreactor is presented.

References

- [1] B. Alberts, A. Johnson, J. Lewis, M. Raff, K. Roberts, P. Walter, *Molecular Biology of the Cell*, 4th ed., Garland Science, 2002.
- [2] S.M. Adl, A.G.B. Simpson, C.E. Lane, J. Lukeš, D. Bass, S.S. Bowser, M.W. Brown, F. Burki, M. Dunthorn, V. Hampl, A. Heiss, M. Hoppenrath, E. Lara, L. Le Gall, D.H. Lynn, H. McManus, E.A.D. Mitchell, S.E. Mozley-Stanridge, L.W. Parfrey, J. Pawlowski, S. Rueckert, L. Shadwick, L. Shadwick, C.L. Schoch, A. Smirnov, F.W. Spiegel, The revised classification of eukaryotes, *J. Eukaryot. Microbiol.* 59 (2012) 429–493. doi:10.1111/j.1550-7408.2012.00644.x.
- [3] Y. Tu, F. Peng, A. Adawy, Y. Men, L.K.E.A. Abdelmohsen, D.A. Wilson, Mimicking the Cell: Bio-Inspired Functions of Supramolecular Assemblies, *Chem. Rev.* 116 (2016) 2023–2078. doi:10.1021/acs.chemrev.5b00344.
- [4] R.J.R.W. Peters, M. Marguet, S. Marais, M.W. Fraaije, J.C.M. van Hest, S. Lecommandoux, Cascade Reactions in Multicompartmentalized Polymersomes, *Angew. Chem. Int. Ed.* 53 (2014) 146–150. doi:10.1002/anie.201308141.
- [5] S.F.M. van Dongen, M. Nallani, J.J.L.M. Cornelissen, R.J.M. Nolte, J.C.M. van Hest, A Three-Enzyme Cascade Reaction through Positional Assembly of Enzymes in a Polymersome Nanoreactor, *Chem. – Eur. J.* 15 (2009) 1107–1114. doi:10.1002/chem.200802114.
- [6] D.M. Vriezema, P.M.L. Garcia, N. Sancho Oltra, N.S. Hatzakis, S.M. Kuiper, R.J.M. Nolte, A.E. Rowan, J.C.M. van Hest, Positional Assembly of Enzymes in Polymersome Nanoreactors for Cascade Reactions, *Angew. Chem.* 119 (2007) 7522–7526. doi:10.1002/ange.200701125.
- [7] Y. Elani, R.V. Law, O. Ces, Vesicle-based artificial cells as chemical microreactors with spatially segregated reaction pathways, *Nat. Commun.* 5 (2014) 5305. doi:10.1038/ncomms6305.
- [8] A. Peyret, E. Ibarboure, N. Pippa, S. Lecommandoux, Liposomes in Polymersomes: Multicompartment System with Temperature-Triggered Release, *Langmuir.* 33 (2017) 7079–7085. doi:10.1021/acs.langmuir.7b00655.
- [9] O. Rifaie-Graham, S. Ulrich, N.F.B. Galensowske, S. Balog, M. Chami, D. Rentsch, J.R. Hemmer, J.R. de Alaniz, L.F. Boesel, N. Bruns, Wavelength-Selective Light-Responsive DASA-Functionalized Polymersome Nanoreactors, *J. Am. Chem. Soc.* (2018). doi:10.1021/jacs.8b04511.
- [10] V. Mishin, J.P. Gray, D.E. Heck, D.L. Laskin, J.D. Laskin, Application of the Amplex Red/Horseradish Peroxidase Assay to Measure Hydrogen Peroxide Generation by Recombinant Microsomal Enzymes, *Free Radic. Biol. Med.* 48 (2010) 1485–1491. doi:10.1016/j.freeradbiomed.2010.02.030.
- [11] B. Zhao, F.A. Summers, R.P. Mason, Photooxidation of Amplex red to resorufin: Implications of exposing the Amplex red assay to light, *Free Radic. Biol. Med.* 53 (2012) 1080–1087. doi:10.1016/j.freeradbiomed.2012.06.034.
- [12] V. Towne, M. Will, B. Oswald, Q. Zhao, Complexities in horseradish peroxidase-catalyzed oxidation of dihydroxyphenoxazine derivatives: appropriate ranges for pH values and hydrogen peroxide concentrations in quantitative analysis, *Anal. Biochem.* 334 (2004) 290–296. doi:10.1016/j.ab.2004.07.037.

General conclusion

Controlling species release was performed *via* light sensitive nanopolymersomes. In a first step, several non-light sensitive PEG₄₅-*b*-PTMC with different PTMC length were synthesized in order to find the appropriate hydrophilic ratio to form stable polymersomes. PEG₄₅-*b*-PTMC₈₁, with a hydrophilic ratio of 19%, self-assembled into well-defined polymersomes. Then, a 1st generation of light sensitive copolymer PEG₄₃-coumarin-*b*-PTMC₈₁ based on a photocleavable coumarin linker was synthesized (Figure 9).

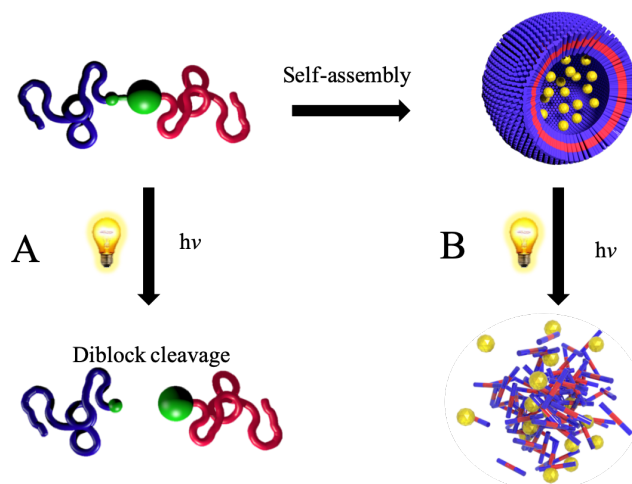


Figure 91: Strategy used to control reactant release temporally and spatially via light-sensitive polymersomes (B), comprising photodegradable diblock copolymers (A).

To this end, the coumarin light-sensitive linker was first synthesized with two grafting groups (carboxylic acid and alkyne group), in order to be able to graft one hydrophilic and one hydrophobic polymer. The PEG₄₅ chain-end was modified into an amine in order to be grafted on the carboxylic acid of the coumarin. Trimethylene carbonate (TMC) was polymerized to form poly(trimethylene carbonate) PTMC with an azide chain-end. The key parameter to obtain a low dispersity (1.05) was the initiator 3-azido-1-propanol purification. PEG₄₅-NH₂ and PTMC₈₁-N₃ were successively grafted onto the coumarin linker to give the 1st generation of light sensitive amphiphilic block copolymer PEG₄₅-coumarin-*b*-PTMC₈₁. The copolymer had a narrow dispersity of 1.05.

This copolymer self-assembled into well-defined polymersomes with a hydrodynamic diameter of 120 nm and a narrow dispersity (PDI \approx 0.1). UV irradiation of polymersomes induced no change in the morphology or the particle sizes. DLS at 90° showed particles were either partly destabilized or lost partly their mass after irradiation (30% signal loss after 2.5 hours irradiation). However, most nanoparticles (70%) were not destabilized by irradiation. The stability of the polymersomes could be explained by coumarin dimerization, favoured by self-

assembly, that prevents PEG release. In order to improve the destabilization efficiency, a new copolymer design was synthesized and analyzed.

A 2nd design of a light sensitive copolymer based on a photocleavable coumarin linker was implemented. The first generation of light sensitive particles was not fully destabilized and dimerization was suspected to improve particle stability. Indeed, dimerization prevents PEG release and thus improves particle stability. In order to improve PEG release from particles and thus favour particle destabilization, copolymer design was modified in two different ways. The cleavage efficiency was improved by changing the leaving group. The quantum yield obtained by irradiation at 365 nm (0.012) was greater than the one of the 1st generation (0.0034). The PEG could be more efficiently cleaved before it could dimerize. The second modification was the polymer position on the coumarin. Therefore only PEG was released instead of PEG-coumarin that induces a more efficient escape of the PEG.

In order to synthesize the 2nd generation of PEG₄₃-coumarin-*b*-PTMC₈₁, a coumarin-based light-sensitive linker was first synthesized with two different functional groups (hydroxyl and alkyne group), in order to be able to selectively graft one hydrophilic and one hydrophobic polymer. The PEG₄₃ chain-end was transformed into an isocyanate in order to be conjugated on the hydroxyl of the coumarin. PEG₄₃-NCO and PTMC₈₁-N₃ were successively grafted on the coumarin linker to give the 2nd generation of light sensitive amphiphilic block copolymer PEG₄₃-coumarin-*b*-PTMC₈₁. The copolymer obtained had a narrow dispersity of 1.04.

Light scattering measurements showed that the copolymer could self-assemble into well-defined particles with a hydrodynamic radius of 150 nm and a narrow dispersity (PDI \approx 0.1). Cryo-TEM showed polymersomes and polymersome aggregates. Polymersome irradiation induced change in the polymersome morphology. After irradiation the remaining particles had a ratio Rg/Rh that decreased suggesting particle densification. The polymersome solution was irradiated for 150 min and the scattered light intensity decreased up to 71%, suggesting particle destabilization and aggregation. The light scattering measurements were confirmed by cryo-TEM. The images obtained showed undefined aggregates and round particle aggregates. These results showed that a light-sensitive copolymer was successfully synthesized that could self-assemble into polymersomes, which were destabilized upon UV irradiation.

Controlling species release was also performed *via* another mechanism: destabilization of polymersomes induced by intra-polymersome osmotic pressure change. The fast osmotic pressure increase in the internal medium of polymersomes could not be compensated fast enough by water flow, resulting in polymersome rupture and species release. Osmotic pressure increase was controlled *via* a light sensitive cleavable molecule.

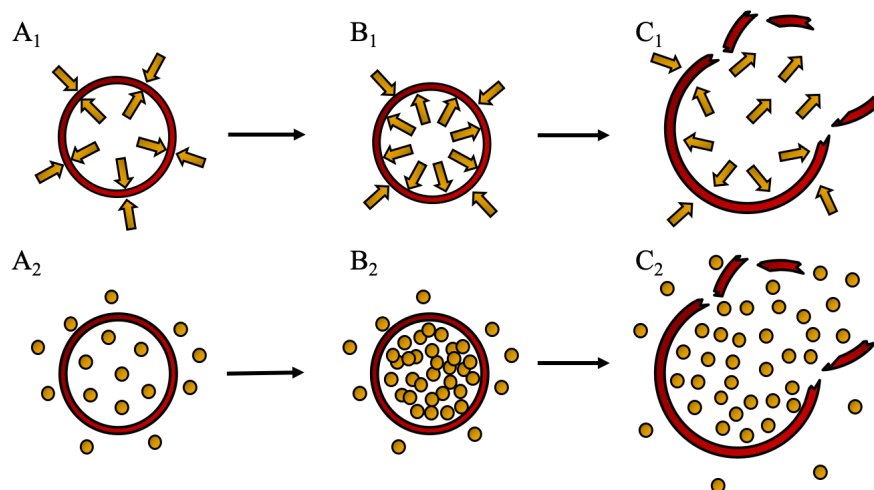


Figure 92: Strategy used to induce polymersome bursting. GUVs are stable while osmotic pressure is the same in the inner and outer medium (A1). Osmotic pressure increase (B1) was used to induce polymersome rupture (C1). Control of the molecular concentration leads to control of the osmotic pressure. Increase of the molecular concentration in the GUV (A1 to B2) leads to osmotic pressure increase and polymersome rupture (C2).

Two molecules with two different cleavage mechanisms were studied: coumarin heterolytic cleavage and N-alkyl-4-picolinium-thioxanthone (NAP-th) based on mediated electron transfer. NAP-th was easily synthesized in 2 steps, its water solubility was the limiting parameter and the maximal solubility concentration found was 1 mM. Several methods were tested to increase its water solubility, such as changing the counter ion or adding a hydrophilic group, without increasing the water solubility. The quantum yield measured in the presence of the mediator triethanol amine was 0.16. This value showed that the cleavage was very efficient.

Modified coumarin was also successfully synthesized in 6 steps, two hydrophilic groups were added to increase the solubility of the molecule and 10 mM of the molecule was readily solubilized in water. The measured photochemical quantum yield was 0.016 on irradiating at 365 nm and 0.029 for 405 nm. The cleavage was less efficient than NAP-th, however its solubility was higher. One hour of irradiation at 365 nm induced 87 % cleavage of the molecule.

This cleavage released diethyl amine that can be used to increase the solution pH. Indeed, after only 10 min irradiation the pH increased from 4.5 to 6.5.

The second step consisted in encapsulating both molecules inside the polymersome made of PEO_{1,3}-*b*-PBut_{2,5} *via* an emulsion-centrifugation technique. Modified coumarin was encapsulated inside polymersome with a concentration of 10 mM and NAP-th of 1 mM. Irradiation at 405 nm induced fast polymersome bursting for both molecules. These systems inducing fast and efficient release could be used to initiate reaction of microreactors and thus to have a precise control in space and time for the design of artificial cellular systems.

In order to monitor NO gas production directly inside the microreactor, two NO probes were studied. These probes are based on formation of an azo-bond that induces fluorescence, resulting in stable signal and high selectivity against other nitro compounds. The two probes were designed to have different solubility properties (one hydrophobic and the other hydrophilic) in order to detect NO in the membrane and in the inner aqueous medium of the microreactor. The probes were synthesized in 5 and 6 steps (Figure 80).

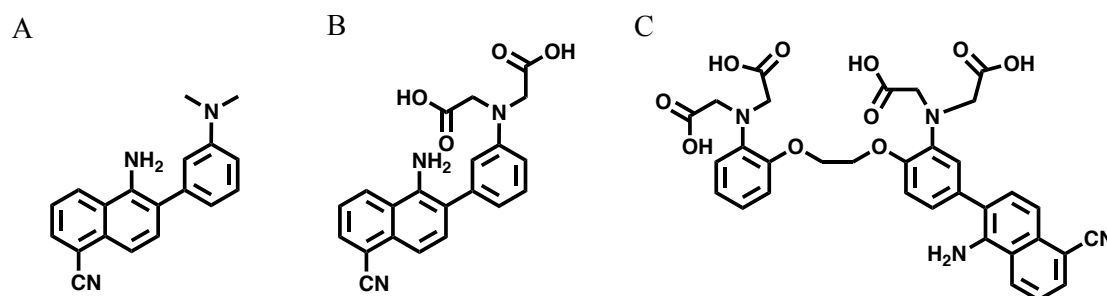


Figure 93: A) NO hydrophobic fluorescent probe B) NO hydrophilic fluorescent probe C) BAPTA-NOp

Critical steps were encountered for the protection and deprotection of the carboxylic acid of the hydrophilic probe. *Tert*-butyl proved to be an efficient protecting group with the conditions used and TES was used during the deprotection step avoiding hydrophilic probe degradation. In order to test the probes properties, several NO sources were tested such as GSNO, NO from NaNO₂ or NO as gas from a bottle and the resulting NO concentration were measured *via* hemoglobin absorption. NO release from GSNO was triggered by ascorbic acid and the release kinetics was studied. However, ascorbic acid prevents the formation of the fluorescent molecule and GSNO could not be used. NO from NaNO₂ gave low concentration solutions therefore NO solution from a gas bottle was finally used.

The NO detection of the probes was tested. Probes showed an increase of the fluorescent intensity ($\lambda_{em\ max}= 530\ nm$, $\lambda_{ex\ max}=440\ nm$ for the hydrophilic probe, $\lambda_{em\ max}= 530\ nm$, $\lambda_{ex\ max}=440\ nm$ for the hydrophilic probe) after addition of NO. The fluorescence intensity was fitted and had an excellent linear correlation ($R^2 = 0.99$) depending on the NO quantity added allowing a quantitative measurement of NO. The probes are currently tested *in vitro* at the laboratory CITHEFOR (Lorraine University EA 3452).

In a second part, another molecular tool was synthesized in order to study NO synthase. Introducing reactants in a controlled manner directly in the microreactor could help monitor enzyme activity and information about enzyme mechanisms may be obtained. To this end, a molecular tool was designed to have fine control of the rate of NO production by a feedback process. We hypothesized that the combination of BAPTA and NO probe (BAPTA-NOp) could induce an autoactivation of the enzyme and could control the nitric oxide production. NO would be produced by the enzyme and react with BAPTA-NOp to give BAPTA-AZO. Due to the higher conjugation, the cyano electron withdrawing group would attract electron of the tertiary amine of the BAPTA resulting in a weaker complexation of calcium and its release. To test this hypothesis BAPTA-NOp and BAPTA-AZO have been synthesized in 10 steps and their dissociation constant K_d were measured. K_d found for BAPTA-NOp and BAPTA-AZO were respectively $0.42\ \mu M$ and $0.52\ \mu M$. Their K_d values were in agreement with the BAPTA family K_d values. Unfortunately, the K_d of BAPTA-NOp and BAPTA-AZO are relatively close and BAPTA-AZO have a relatively low K_d which mean the AZO form does not release calcium and that the molecule cannot be used for the feedback process.

Finally, in order to ensure control on the initiation step and to start an enzymatic reaction at a specific location and time, the release of reactant in a controlled manner in the microreactor was explored. PEG₄₃-coumarin-*b*-PTMC₈₁ nanopolymersomes were successfully encapsulated inside emulsion droplet microreactors stabilized by PEO_{1.3}-*b*-PBut_{2.5} copolymers and observed under confocal microscopy. The irradiation at 405 nm induced an efficient destabilization of the nanopolymersomes inside the microreactor. 2 min irradiation induced a decrease of 83% of the number of nanoparticles (Figure 80).

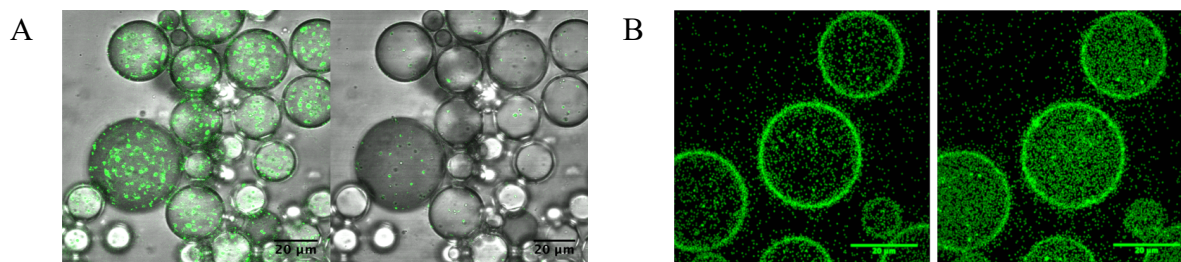


Figure 94: Confocal observation of water emulsion stabilized by $PEO_{1.3}$ - b - $PBut_{2.5}$ containing light-sensitive PEG_{43} -coumarin- b - $PTMC_{81}$ nanopolymersomes irradiated 2 min at 405 nm 80% 50 mW (green channel, $\lambda_{ex} = 405$ nm, 50 mW, 3% emission range of coumarin, 485 nm). B) Confocal observation of water emulsion stabilized by $PEO_{1.3}$ - b - $PBut_{2.5}$ containing PEG_{43} -coumarin- b - $PTMC_{81}$ polymersomes before and after 10 s irradiation at 405 nm 80% 50 mW. Fluorescein was encapsulated in the polymersomes (scale bar 20 μ m, green channel λ_{ex} =488 nm, 40 mW, 10% , emission range of fluorescein, 520 nm).

In order to study the release from the PEG_{43} -coumarin- b - $PTMC_{81}$ nanopolymersomes, quenched fluorescein was encapsulated to obtain nanopolymersomes containing fluorescein (F-Nano). In order to measure the fluorescein quantity encapsulated in the nanopolymersomes, 80% by volume of DMSO was added to fully destabilize the particles and release the fluorescein. The theoretical maximum fluorescein concentration that the nanopolymersomes could release was 5.1 μ M. The F-Nano polymersomes were then loaded in emulsion droplets microreactor stabilized by $PEO_{1.3}$ - b - $PBut_{2.5}$. The resulting emulsion was irradiated for 10 s resulting in the diffusion of the fluorescence in the whole medium, showing that fluorescein was released from F-Nano inside the microreactor.

Building a microreactor that could mimic some cellular basic function and develop an operational synthetic cell is a real challenge. There is still a long way to go to obtain a versatile artificial cell. However, we believe the tools developed during this PhD work will help getting closer to a rudimentary robust artificial cell. NO synthase is a complex enzyme that requires several substrates and particular conditions. In the first instance the tools developed here could be used to build a controllable microreactor by microfluidics containing well known enzyme such as HRP or GOX.

The life fundamental building blocks are well known, however we are far from understanding how these building blocks interact, self-organize, exchange information and process. Pertinent information about how cells function is anticipated, from both successful and unsuccessful implementations of artificial cells.

Experimental Part

7. Experimental Part

Solvents and chemical products

Commercially-available products were purchased from Sigma Aldrich, Acros Chemicals, Lancaster and Fluka and were used as received. The dried solvents were obtained as follows: toluene and diethyl ether was distilled over sodium; acetonitrile and dichloromethane were distilled over calcium hydride and dimethylformamide (DMF) was stored over molecular sieves. Deuterated solvents for NMR analysis were bought from Sigma-Aldrich and Eurisotop. Deionized water was obtained by purification over an ion exchange column and a membrane filter of 0.45 μm (MSI, Micron separation, Inc.). Solvents for spectroscopy without the addition of stabilizing agents or other absorbing material were used as received.

Thin layer chromatography and silica columns

Thin layer chromatography was performed on silica gel 60 F254 sheets on aluminium produced by Merck. Spots on the TLC plate were observed under UV light (254 nm / 365 nm). When appropriate for non-chromophoric compounds an appropriate staining agent was employed.

Nuclear magnetic resonance spectroscopy (NMR)

^1H and ^{13}C NMR were performed on:

AVANCE400: AVANCE III HD 400 spectrometer operating at 400.2 MHz and 100.7 MHz for ^1H and ^{13}C respectively.

Temperature: 298K

Probe: 5 mm Bruker multinuclear z-gradient direct probe.

PRODIGY 400: AVANCE NEO 400 BRUKER spectrometer operating at 400.3 MHz and 100.7 MHz for ^1H and ^{13}C respectively.

Temperature: 298K

Probe: 5 mm Bruker multinuclear z-gradient direct cryoprobe-head.

Chemical shifts are reported in ppm (δ) and are referenced to the NMR solvent (CDCl_3 , D_2O , MeOD, CD_3CN , DMSO) residual peak. Abbreviations used are s = singlet, d = doublet, t = triplet, q = quartet, dd = doublet of doublets, dt = doublet of triplets, m = multiplet and br=broad. The coupling constants (J) are reported in Hertz (Hz).

Size Exclusion Chromatography in THF

Polymer molar masses were determined by Size Exclusion Chromatography (SEC) using tetrahydrofuran (THF) as the eluent. Measurements in THF were performed on an Ultimate 3000 system from ThermoScientific equipped with diode array detector DAD. The system also includes a multi-angle light scattering detector MALS and differential refractive index detector dRI from Wyatt technology. Polymers were separated on three G2000, G3000 and G4000 TOSOH HXL gel columns (300 x 7.8 mm) (exclusion limits from 1000 Da to 400 000 Da) at a flowrate of 1 mL/min. Column temperature was held at 40°C. An Easivial kit of Polystyrene from Agilent was used as the standard (Mn from 162 to 364 000Da).

Mass spectrometry

Mass spectra are measured by the “Centre d’Etude Structurale et d’Analyse des Molecules Organique” (CESAMO) at the university of Bordeaux. The measurements were carried out on a QStar Elite mass spectrometer (Applied Biosystems). The instrument is equipped with an electrospray ionisation (ESI) source and the spectra were recorded in either positive or negative ionisation mode. The electrospray needle was maintained at 5000 V and operated at room temperature. Samples were introduced by injection through a 20 µL sample lip into a 4500 µL/min flow of methanol from the LC pump. Alternatively field desorption (FD) was used as ionization mode on a time of flight (TOF) mass spectrometer (Accu TOF GCv). The FD-emitter voltage was 10 kV and 1 – 2 µL of sample solution was deposited on a 13 µm emitter wire and inserted into the machine.

Electronic absorption spectroscopy (UV-Vis)

Electronic absorption spectra have been measured on a Varian UV-Vis-NIR spectrophotometer Cary 5000. The wavelengths observed ranged from 200 – 800 nm. Sample solutions were measured in matched quartz cells with a pathlength of 10 mm. Before each measurement a baseline of pure solvent was been taken and was subtracted from the measured spectra.

Fluorescence spectroscopy

Fluorescence measurements were performed on spectrofluorometer JASCO FP-8500 with a Xe arc lamp with shielded lamp housing (150 W). The photometric system was a radio-photometer

system using monochromatic light to monitor the intensity output of the Xe lamp. Measures were performed in quartz cells with a pathlength of 10 mm at 20°C.

Parameters used for emission et excitation spectra measurements:

Mode	Emission	Mode	Excitation
Ex bandwidth	2.5 nm	Ex bandwidth	2.5 nm
Em bandwidth	2.5 nm	Em bandwidth	2.5 nm
Response	1 sec	Response	1 sec
Sensitivity	High	Sensitivity	High
Measurement range	470 - 700 nm	Measurement range	300 – 520 nm
Data interval	0.5 nm	Data interval	0.5 nm
Ex wavelength	416.0 nm	Em wavelength	535.0 nm
Scan speed	200 nm/min	Scan speed	200 nm/min
No. of accumulations	3	No. Of accumulations	3
Auto gain	Off	Auto gain	Off
Shutter control	Open only for measurement	Shutter control	Open only for measurement
Light source	Xe lamp	Light source	Xe lamp
Filter	Stop scan for exchanging filter	Filter	Stop scan for exchanging filter
Blank correction	Off	Blank correction	Off
Temperature	20°C	Temperature	20°C

UV lamp

Irradiation experiments were carried out with a Hamamatsu Lightningcure LC8 200 W Mercury-Xenon lamp. A filter (A9616-05) was used centering the light emission at 365 nm as shown Figure 95. Samples were placed at 1 cm from the light guide output and irradiated for a defined time.

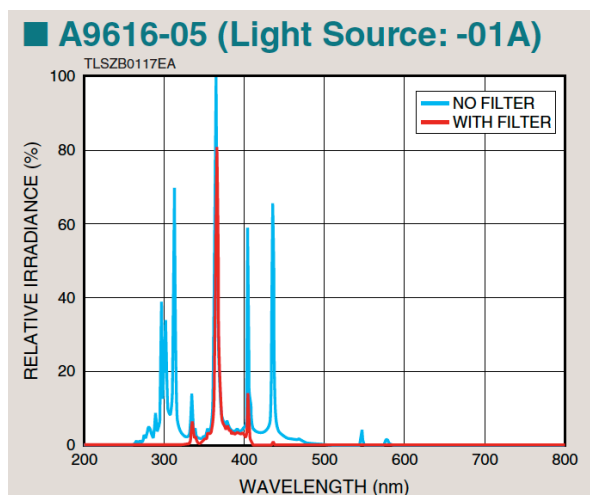


Figure 95: Emission spectra of the UV lamp with and without the filter A9616-05.

TEM and Cryo TEM

TEM images were taken from a Hitachi H7650 at the Bordeaux Imaging Center. CRYO-TEM Images were taken by Jean Michel Guigner at Institut de minéralogie, de physique des matériaux et de cosmochimie UMR 7590 - Sorbonne Université/CNRS/MNHN/IRD.

Photochemical quantum yield

Montalti M., Credi A., Prodi L., Gandolfi M. T., *Handbook of photochemistry*, Taylor and Francis p601-604. ($\phi_{\text{Fe}^{2+}} = 1.21$ at 365.6 nm)

Photochemical quantum yields have been determined according to a standard procedure using a ferrioxalate actinometer. A solution of potassium ferrioxalate (0.012 M) in H_2SO_4 (0.05 M) and a solution of phenanthroline (0.1 %) in H_2SO_4 (0.5 M) buffered with sodium acetate trihydrate (225 g/L) has been prepared. Ferrioxalate can be used as an actinometer up to 500 nm. The “micro-version” of the initial method by Hatchard and Parker and described by Fisher has been used. Under irradiation the ferrioxalate is decomposing according to the following equation.



After irradiating a solution of ferrioxalate (3 ml) for a certain time, a solution of phenanthroline (0.5 ml) is added, which forms a tris-phenanthroline complex only with the Fe^{2+} ions ($\epsilon = 11100 \text{ cm}^{-1}\text{M}^{-1}$ at 510 nm) The absorption is compared to a non-irradiated reference solution which is kept in the dark and the difference between the two is noted and gives ΔA . The molar amount of Fe^{2+} is given the following equation.

$$\text{moles } Fe^{2+} = \frac{V \times \Delta A}{l \times \epsilon_{510}}$$

Where V is the total volume (3.5 ml) l is the optical path of cell and ϵ_{510} is the extinction coefficient of the $Fe(\text{phen})^{2+}$ complex. Thus, the photons absorbed by the solution per time unit ($Nh\nu/t$) is:

$$Nh\nu/t = \frac{V \times \Delta A}{l \times \epsilon_{510}}$$

Where ϕ_λ is the quantum yield for the formation of Fe^{2+} , t is the irradiation time F is the fraction of photons absorbed by the ferrioxalate solution ($F = 1 - 10^{-A}$). If the irradiated solution is sufficiently concentrated the F factor can be omitted. Upon irradiation of the sample solution the it needs to be taken in account that the spectroscopical change should not surpass 10 % to obtain a reliable value for the photochemical quantum yield. The concentration of the light induced change C_i (isomerisation or photocleavage) can be calculated as follows:

$$C_i = \frac{\Delta A}{\epsilon - \epsilon_{product}}$$

ϵ is the extinction coefficient of the starting material and $\epsilon_{product}$ is the extinction coefficient of the photoproduct. The photochemical quantum yield is then calculated as shown in the following equation.

$$\phi_\lambda = \frac{C_i \times V_s}{\left(\frac{Nh\nu}{t}\right) \times t}$$

Here V_s is the irradiated volume of the sample and t stands for the irradiation time of the sample.

Calcium titration

Two calcium calibration stock solutions have been prepared, one containing 10 mM EGTA (0 μM Ca^{2+} -buffer) and another with 10 mM CaEGTA (39 μM Ca^{2+} -buffer). In addition both buffers were charged with 100 mM KCl and 30 mM 3-(N-Morpholino)-propanesulfonic acid (MOPS) adjusted at pH 7.2. In both buffers an equivalent amount of Ca^{2+} -binding probe was dissolved with a final concentration between 1-10 μM . In order to determine the K_d both fluorescence and electronic absorption spectra have been taken after having adjusted the free Ca^{2+} concentration to 0.017 μM , 0.038 μM , 0.065 μM , 0.100 μM , 0.150 μM , 0.225 μM , 0.35 μM , 1.35 μM and 39 μM . Therefore 2 mL of the 0 μM Ca^{2+} -sample was placed in a cuvette and the spectra were recorded. 200 μL of the sample was discarded and replaced with 200 μL of the 39 μM Ca^{2+} -sample. In that fashion a concentration of 0.017 μM Ca^{2+} can be obtained without changing the concentration of the analyte. The aforementioned Ca^{2+} concentrations were then adjusted by discarding 250, 222, 250, 286, 333, 400, 500, 667 and 1000 μL and replacing the removed volume with an equivalent volume of the 39 μM Ca^{2+} sample. For the calculation of the free Ca^{2+} -concentration a constant room temperature of 21 $^\circ\text{C}$ was assumed. The spectral change at a certain wavelength is then introduced into Hill plot which is the logarithm of $(A-A_{\text{min}})/(A_{\text{max}}-A)$ where A is the absorption at a certain wavelength plotted over the logarithm of the free Ca^{2+} concentration as obtained from the Ca^{2+} -buffers. A schematic representation of the obtained graph is shown in figure 83.

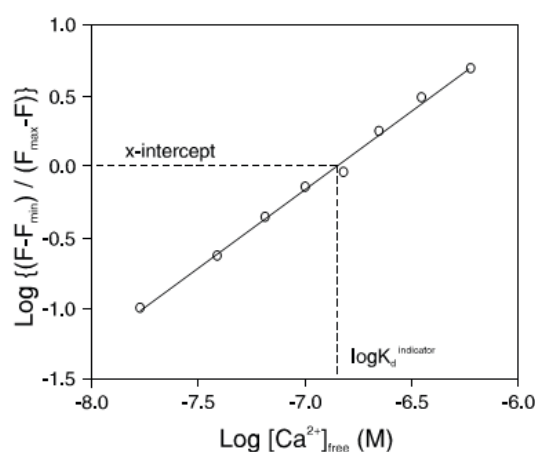


Figure 96: Schematic representation of the Hill plot obtained from a Ca^{2+} titration.

The x-intercept in this graph gives the logarithm of the K_d as shown in figure 83.

Preparation of vesicles *via* emulsion centrifugation technique.

30 μL of glucose 380 mM was added at the bottom of a 2 mL plastic eppendorf. 30 μL of a PBut_{2.5}-*b*-PEO_{1.3} (3 mg/mL) toluene solution was added gently on the glucose phase. The two phases solution was allowed to stabilize 30 min in order to form a stable copolymer leaflet at the interface. A sucrose solution was prepared with a concentration that equilibrates the osmotic pressure with the glucose solution depending on the other components. 5 μL of a sucrose solution was poured in 500 μL of PEO_{1.3}-*b*-PBut_{2.5} (3 mg/mL) toluene solution. The solution was vigorously hand shaken for 25 seconds in order to form the sucrose emulsion in toluene that was stabilized by the copolymer. 75 μL of the emulsion was poured quickly and gently in the toluene phase of the first vial containing the glucose phase. Quickly the resulting emulsion in toluene was centrifuged (3 min, 500 g, room temperature) on top of the glucose solution. The toluene of the centrifuge solution was partly removed, 80 μL of glucose (380 mM) solution was gently added. The solution was again centrifuged (3 min at 500 g room temperature). All the toluene was removed. On the bottom of the vial, a pellet of polymersomes is visible. After toluene removal, the solution was left to rest for few hours until all the polymersomes were dispersed and the aggregates at the bottom disappeared.

Confocal microscopy

Laser scanning confocal microscopy images were acquired on an inverted Leica TCS SP5 microscope equipped with an HCX PL APO 63 \AA ~, NA 1.4 oil immersion objective in fluorescence mode. Samples (≈ 20 μL) were injected in a homemade chamber that was sealed to prevent evaporation. The laser outputs were controlled via the Acousto-Optical Tunable filter (AOTF) and the two collection windows using the Acousto-Optical Beam Splitter (AOBS) and photomultipliers (PMT).

HRP Amplex Red H₂O₂ solution preparation

Three solutions were prepared in PBS: Amplex Red 1 mM (with 10% DMSO for solubilization) HRP 4 U/mL and H₂O₂ 100 μM. The solution were then prepared as follows:

H₂O₂ (μM)	1	5	15	25	35	45
HRP (U/ML)	0,4	0,4	0,4	0,4	0,4	0,4
AR (μM)	50	50	50	50	50	50
V H₂O₂ (μL)	1	5	15	25	35	45
V HRP (μL)	10	10	10	10	10	10
V AR (μL)	5	5	5	5	5	5
V PBS (μL)	84	80	70	60	50	40
V TOT	100	100	100	100	100	100

Dynamic light scattering

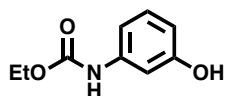
The measurements were performed on a Malvern ZetaSizer Nano ZS instrument with detection at 90°. Samples were analyzed at 25°C. Three measurements were performed for each sample. The particle size distribution was determined using a NNLS analysis fit with a quadratic weighting scheme. Z-average hydrodynamic diameters and polydispersity indexes (PDI) were derived through the cumulant method.

R_g and R_h measurements

Dynamic light scattering (DLS) experiments were performed using an ALV/CGS3 compact goniometer equipped with an ALV/LSE-5004 light scattering electronics and an ALV-7004 multi tau digital correlator with pseudo-cross correlation detection. The light source was a 22 mW He-Ne laser operating at λ=632.8 nm. The measurements were carried out at 25°C. At least three measurements of 60 sec were performed. The distribution of relaxation times was obtained by applying the Contin method and the hydrodynamic radii derived through application of the Stokes Einstein equation.

Synthesis

2



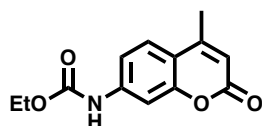
3-Aminophenol (**1**) (15.3 g, 1eq) was dissolved in ethyl acetate (50 mL). The mixture was heated to reflux for 30 min. Ethyl chloroformate was added dropwise over a 1 hour period. The reaction mixture was allowed to cool to RT. A precipitate was formed, which was removed by filtration and washed with ethyl acetate (3 x 30 mL). The combined filtrate was evaporated under reduced pressure to obtain 12.4 g (98% yield) of the product (**2**) as a white powder.

^1H NMR (400 MHz, CDCl_3) δ (ppm) 7.38 (br. s, 1H), 7.13 (t, $J=8.1$ Hz, 1H), 6.75 (br. s, 1H), 6.63 (dd, $J=1.2$ Hz, $J=8.1$ Hz, 1H), 6.58 (dd, $J=8.1$ Hz, $J=2.3$ Hz, 1H), 4.23 (q, $J=7.1$ Hz, 2H), 1.31 (t, $J=7.1$ Hz, 3H),

^{13}C NMR (400 MHz, CDCl_3) δ (ppm) 157.1, 154.2, 138.9, 130.1, 110.85, 110.5, 106.1, 61.8, 14.6.

HRMS (ESI): Calculated $m/z = 204.0631$ for $\text{C}_9\text{H}_{11}\text{NO}_3\text{Na}$; found $m/z = 204.0628$ $[\text{M}+\text{Na}]^+$

3



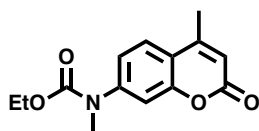
A solution of ethyl (3-hydroxyphenyl)carbamate (**2**) (12.3 g, 1.0 eq) in EtOAc was suspended in 100 mL of 70% H_2SO_4 . The resulting solution was stirred at RT for 3 hours. The mixture was poured on ice, giving a white precipitate that was recrystallized from EtOH. 9.5 g of coumarin derivative (**3**) was obtained (54% yield).

^1H NMR (400 MHz, CDCl_3) δ (ppm) 7.52 (d, $J=8.6$ Hz, 1H), 7.47 (d, $J=2.0$ Hz, 1H), 7.41 (d, $J=8.6$ Hz, 1H), 7.08 (s, 1H), 6.18 (d, $J=1.0$ Hz, 1H), 4.27 (q, $J=7.1$ Hz, 2H), 2.4 (d, $J=1.0$ Hz, 3H), 1.33 (t, $J=7.1$ Hz, 3H),

^{13}C NMR (400 MHz, CDCl_3) δ (ppm) 161.4, 154.6, 153.2, 152.5, 141.8, 125.5, 115.5, 114.5, 113.2, 106.0, 61.9, 18.7, 14.6.

HRMS (ESI): Calculated $m/z = 270.0737$ for $\text{C}_{13}\text{H}_{13}\text{NO}_4\text{Na}$; found $m/z = 270.0724$ $[\text{M}+\text{Na}]^+$

4



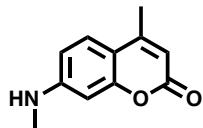
9.5 g (1.0 eq) of **3** was dissolved in 250 mL of THF. 1.0 g of NaH (1.05 eq) was slowly added and the mixture was stirred for 30 min at RT. 6.0 g of MeI (1.1 eq) was then added and the reaction mixture was stirred for 24 hours. The solvent was evaporated, water was added and the white precipitate was filtered, dried and recrystallized in EtOH. 5.5 g of **4** was obtained (54% yield).

^1H NMR (400 MHz, CDCl_3) δ (ppm) 7.54 (d, $J = 8.6$ Hz, 1H), 7.29 (dd, $J = 8.6$ Hz, $J = 2.1$ Hz, 1H), 7.24 (d, $J = 2.1$ Hz, 1H), 6.24 (d, $J = 1.1$ Hz, 1H), 4.22 (q, $J = 7.1$ Hz, 2H), 3.36 (s, 3H), 2.42 (d, $J = 1.1$ Hz, 3H), 1.28 (t, $J = 7.1$ Hz, 3H).

^{13}C NMR (400 MHz, CDCl_3) δ (ppm) 160.9, 155.2, 153.9, 152.1, 146.6, 124.7, 121.0, 117.2, 114.4, 112.9, 62.4, 37.2, 18.7, 14.6.

HRMS (ESI): Calculated $m/z = 284.08933$ for $\text{C}_{14}\text{H}_{15}\text{NO}_4\text{Na}$; found $m/z = 284.0887$ [$\text{M}+\text{Na}$] $^+$

5

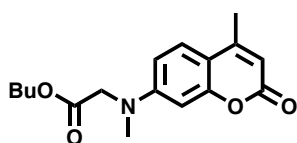


5.0 g (1.0 eq) of **4** was suspended in a mixture of 14 mL of $\text{H}_2\text{SO}_4/\text{AcOH}$ (1/1, v/v). The suspension was heated to 125°C for 2 hours. The mixture was left to cool to RT then the solution was poured on 100 mL of ice and pH was increased to 9 with 1N NaOH solution. The brown precipitate was filtered, dried and recrystallized from EtOH. 3.3 g of **5** was obtained (91% yield).

^1H NMR (400 MHz, CDCl_3) δ (ppm) 7.35 (d, $J = 8.6$ Hz, 1H), 6.51 (dd, $J = 8.6$ Hz, $J = 2.3$ Hz, 1H), 6.44 (d, $J = 2.3$ Hz, 1H), 5.97 (d, $J = 1.0$ Hz, 1H), 4.34 (s, 1H), 2.9 (s, 3H), 2.34 (d, $J = 1.0$ Hz, 3H).

^{13}C NMR (400 MHz, CDCl_3) δ (ppm) 162.1, 156.1, 153.1, 152.6, 125.6, 110.6, 110.2, 109.5, 97.9, 30.4, 18.7

HRMS (ESI): Calculated $m/z = 212.0681$ for $\text{C}_{11}\text{H}_{11}\text{NO}_2\text{Na}$; found $m/z = 212.0688$ [$\text{M}+\text{Na}$] $^+$

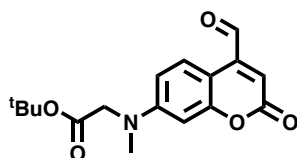
6

5 (3.2 g, 1.0 eq) was dissolved in DMF (30 mL). BrCH₂CO₂^tBu (3.8 g, 1.1 eq) and K₂CO₃ (2.9 g, 1.2 eq) were then added and the mixture was heated to 100°C for 12 hours. The solution was then concentrated and water was added, resulting in precipitation. The precipitate was filtered and the product was purified by silica column chromatography (Cyclohexane/ EtOAc ; 3/1 to 1/1, v/v) to obtain 1.8 g of **6** (yield 34%).

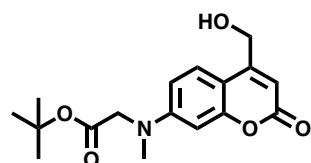
¹H NMR (400 MHz, CDCl₃) δ (ppm) 7.40 (d, *J* = 8.9 Hz, 1H), 6.58 (dd, *J* = 2.5 Hz, *J* = 8.9 Hz, 1H), 6.5 (d, *J* = 2.6 Hz, 1H), 5.98 (d, *J* = 1.1 Hz, 1H), 4 (s, 2H), 3.11 (s, 3H), 2.34 (d, *J* = 1.1 Hz, 3H), 1.43 (s, 9 H).

¹³C NMR (400 MHz, CDCl₃) δ (ppm): 169.1, 162.1, 155.7, 152.9, 152.0, 125.6, 110.6, 110.0, 108.9, 98.8, 82.4, 55.0, 39.9, 28.2, 18.6.

HRMS (ESI): Calculated *m/z* = 304.1543 for C₁₇H₂₂NO₄ ; found *m/z* = 304.1539 [M+H]⁺

7

6 (1.7 g, 1.0 eq) was suspended in p-xylene (80 mL) with Se₂O₃ (3.6 g, 3 eq). The mixture was refluxed under vigorous stirring under an argon atmosphere during 24 hours. The mixture was filtered and concentrated under reduced pressure. The dark brown oil (**7**) was used in the next reaction without further purification.

8

7 (1.8 g, 1.0 eq) was dissolved in MeOH (100 mL) and NaBH₄ (0.43 g, 2.0 eq) was carefully added into the solution. The mixture was stirred 3 hours at RT. The solution was concentrated and carefully neutralized with 1M HCl solution, diluted with water and extracted with EtOAc. The organic phase was washed with water, dried with MgSO₄ and the solvent was removed

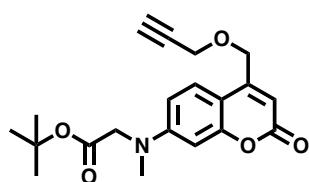
under reduced pressure. The product was purified by silica column chromatography (Cyclohexane/ EtOAc ; 7/3 to 4/6, v/v) to obtain 0.94 g of **8** (yield 52%).

¹H NMR (400 MHz, CDCl₃) δ (ppm) 7.32 (d, *J* = 8.88 Hz, 1H), 6.56 (dd, *J* = 8.90 Hz, *J* = 2.58 Hz, 1H), 6.51 (d, *J* = 2.56 Hz, 1H), 6.31 (s, 1H), 4.81 (d, *J* = 1.24 Hz, 2H), 4.0 (s, 2H), 3.12 (s, 3H), 1.44 (s, 9H).

¹³C NMR (400 MHz, CDCl₃) δ (ppm) 169.2, 162.4, 155.8, 154.6, 152.0, 124.4, 109.1, 107.8, 106.8, 99.0, 82.5, 61.0, 55.0, 39.9, 28.2

HRMS (ESI): Calculated *m/z* = 320.1492 for C₁₇H₂₂NO₅; found *m/z* = 320.1489 [M+H]⁺

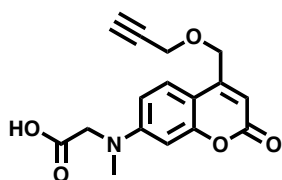
9



8 (0.67 g, 1 eq) was dissolved in dry DMF under inert conditions, NaH (0.10 g, 2.0 eq) was added and the mixture was stirred for 30 min. Propargyl bromide (0.75 g, 3 eq) was added, the mixture was heated at 60 °C and was stirred for 24 hours. Water was then added and the mixture was extracted with EtOAc (4x15 mL), the organic phase was washed with brine, dried over MgSO₄ and concentrated under reduced pressure. The crude product was purified by silica column chromatography (Cyclohexane/ EtOAc; 8/2 to 6/4, v/v) to obtain 233 mg of **9** (yield 31%).

¹H NMR (400 MHz, DMSO) δ (ppm) 7.37 (d, *J* = 8.8 Hz, 1H), 6.36 (m, 3H), 5.25 (d, *J* = 1.4 Hz, 2H), 4.94 (d, *J* = 2.4 Hz, 2H), 4.20 (s, 2H), 3.65 (t, *J* = 2.3 Hz, 1H), 3.04 (s, 9H).

10



9 (175 mg, 1.0 eq) was dissolved in of DCM (20 mL), TFA (20 mL) was then added and the reaction mixture was stirred for 2 hours at RT. The solvent was removed under reduced pressure, the solid was washed 3 times with diethyl ether and dried under reduced pressure. The solid was recrystallized in EtOH. 125 mg of **10** was obtained (82% yield)

^1H NMR (400 MHz, DMSO) δ (ppm) 7.36 (d, J = 8.8 Hz, 1H), 6.36 (m, 3H), 5.25 (d, J = 1.3 Hz, 2H), 4.95 (d, J = 2.4 Hz, 2H), 4.22 (s, 2H), 3.64 (t, J = 2.3 Hz, 1H), 3.05 (s, 3H).

HRMS (ESI): Calculated m/z = 300.0877 for $\text{C}_{16}\text{H}_{14}\text{NO}_5$; found m/z = 300.0875 [M-H] $^-$

12

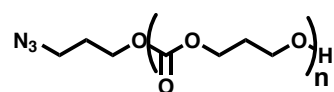


Prior to the reaction 3-bromo-1-propanol was purified by silica column chromatography (Cyclohexane/ EtOAc; 4/1, v/v. TLC staining: phosphomolybdic acid). The purified 3-bromo-1-propanol (1g, 1.0 eq) and sodium azide (795 mg.) were then dissolved in a mixture of acetone (120 mL) and water (20 mL) and the resulting solution was refluxed overnight. Acetone was then removed under reduced pressure, 10 mL of water were added and the mixture was extracted with diethyl ether (3 x 10 mL). The organic layers collected were dried over MgSO_4 and, after removal of the solvent under reduced pressure, 3-azido-1-propanol was isolated as a colourless oil **12**. The oil was dried on CaH_2 overnight and then cryo-distilled under reduced pressure.

^1H NMR (400 MHz, CDCl_3) δ (ppm) 3.70 (t, J = 6.0 Hz, 2H), 3.41 (t, J = 6.6 Hz, 2H), 2.36 (br, 1H), 1.80 (m, J = 6.3 Hz, 2H).

D. Quémener, T.P. Davis, C. Barner-Kowollik, M.H. Stenzel, RAFT and click chemistry: A versatile approach to well-defined block copolymers, Chem. Commun. 0 (2006) 5051–5053. doi:10.1039/B611224B.

13



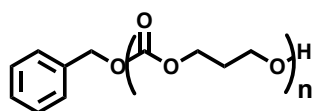
In a glovebox, dry 3-azido-1-propanol **12** (19.6 mg, 1.0 eq), dry DBU (29.6mg, 1.0 eq), dry N' -[3,5-bis(trifluoromethyl)phenyl]- N -cyclohexylthiourea (93.4 mg, 1.3 eq) and dry TMC (2.0 g, 101 eq) were dissolved in dry CH_2Cl_2 (2.5 mL) under inert atmosphere. After 3 hours, acetic acid (35 mg) was added to the mixture. The resulting copolymer was precipitated 3 times in diethyl ether at 0°C . 1.51g of N_3 -PTMC **13** was obtained (80% conversion).

^1H NMR (400 MHz, CDCl_3) δ (ppm) 4.22 (t, J = 6.2 Hz, 322H), 3.72 (t, J = 6.0 Hz, 2H), 3.42 (t, J = 6.6 Hz, 2H), 2.04 (m, J = 6.3 Hz, 161H).

^{13}C NMR (101 MHz, CDCl_3) δ (ppm) 28.0, 64.3, 154.9.

SEC (RI): M_w (Đ) 12600 g mol^{-1} (1.05).

14

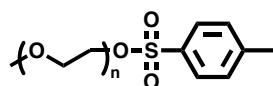


In a glovebox, dry benzyl alcohol (21.0 mg, 1.0 eq), dry DBU (29.6mg, 1.0 eq), dry N'-[3,5-bis(trifluoromethyl)phenyl]-N-cyclohexylthiourea (93.4 mg, 1.3 eq) and dry TMC (2.0 g, 101 eq) were dissolved in dry CH₂Cl₂ (2.5 mL) under inert atmosphere. After 3 hours, acetic acid (35 mg) was added to the mixture. The resulting copolymer was precipitated 3 times in diethyl ether at 0°C. 1.54 g of benzyl-PTMC **14** was obtained (80% conversion).

¹H NMR (400 MHz, CDCl₃) δ 7.25-7.39 (m, 5H), 5.16 (s, 2H), 4.24 (t, *J* = 6.3 Hz, 330H), 3.74 (t, *J* = 6.0 Hz, 1H), 2.05 (t, *J* = 6.3 Hz, 165H).

SEC (RI): M_w (Đ) 13000 g mol⁻¹ (1.04).

16



Poly(ethylene glycol) methyl ether (2000 g/mol, 2.0 g, 1.0 eq), triethylamine (202 mg, 2.0 eq), trimethyl amine (5.9 mg, 0.1 eq) were dissolved in DCM (5 mL). p-toluenesulfonyl chloride was then added carefully (285 mg, 1.5 eq) in DCM. The final mixture was stirred overnight at RT. DCM was partially removed and the resulting polymer was precipitated 3 times in 15 mL of diethyl ether. 1.4 g of tosylated PEG₄₅ **16** was obtained (65% yield).

¹H NMR (300 MHz, DMSO) δ (ppm) 7.78 (d, *J* = 8.3 Hz, 2H), 7.48 (d, *J* = 8.1 Hz, 2H), 4.11 (t, *J* = 4.4, Hz, 2H), 3.50 (s, 183H), 3.24 (s, 3H), 2.42 (s, 3H).

¹³C NMR (400 MHz, CDCl₃) δ (ppm) 70.6.

HRMS (ESI): Calculated *m/z* = 1882.0205 for C₈₄H₁₆₂NaO₄₁S; found *m/z* = 1882.0269 [M+Na]⁺

17



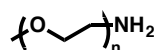
16 (1.4 g) was dissolved in EtOH (20 mL) and sodium azide (91 mg, 2.0 eq) was added to the mixture. The reaction mixture was refluxed overnight, and then diluted with water (100 mL). Ethanol was removed from the mixture under reduced pressure. The aqueous layer was extracted with DCM (3x20 mL). The organic layer was dried over MgSO₄ and concentrated

under reduced pressure. The resulting mixture was precipitated in diethyl ether 3 times. 1.26 g of PEG₄₅-azide **17** was obtained (90% yield).

¹H NMR (400 MHz, DMSO) δ 3.51 (s, 178H), 3.24 (s, 3H).

P.A. Ledin, N. Kolishetti, G.-J. Boons, Multifunctionalization of polymers by strain-promoted cycloadditions, *Macromolecules*. 46 (2013) 7759–7768.

18



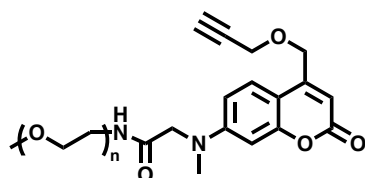
To a solution methyl-PEG₄₅-azide (**17**) (1.0 g, 1.0 eq) in 100 mL MeOH, PPh₃ was added (0.39 g, 3 eq). The reaction mixture was refluxed overnight under an argon atmosphere and then cooled down to RT. The solvent was removed under reduced pressure. The resulting polymer was precipitated 3 times in diethyl ether (15 mL). PEG amine **18** (0.90 g) was obtained (58% yield).

¹H NMR (400 MHz, CDCl₃) δ (ppm) 3.62 (s, 176H), 3.36 (s, 3H), 2.90 (t, *J* = 5.2 Hz, 2H).

¹³C NMR (400 MHz, CDCl₃) δ (ppm) 41.6, 59.0, 70.6

HRMS (ESI): Calculated *m/z* = 1705.0456 for C₇₇H₁₅₈N; found *m/z* = 1705.0434 [M+Na]⁺

19

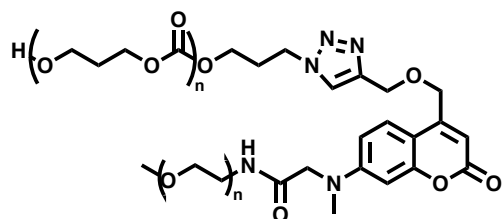


Under an inert atmosphere DMAP (68 mg, 3 eq), EDCI (88 mg, 3 eq) and coumarin derivative **10** (85 mg, 1.5 eq) were dissolved in dry DCM (2 mL). The mixture was stirred for 15 min at RT. PEG-NH₂ (376 mg, 1.0 eq) was then added to the mixture and the reaction was stirred at RT overnight. Water (5 mL) and DCM (5 mL) were then added and the reaction mixture was extracted with DCM (4x15 mL). The organic phase was washed with water then brine and dried over MgSO₄ and concentrated. The resulting polymer was purified by silica column chromatography (DCM/ MeOH; 95/5, v/v). 120 mg of PEG-coumarin **19** was obtained (28% yield).

¹H NMR (400 MHz, CDCl₃) δ 7.30 (d, *J* = 8.8 Hz, 1H), 6.94 (br, 1H), 6.36 (m, 3H), 5.23 (d, *J* = 1.4 Hz, 2H), 4.78 (d, *J* = 2.3 Hz, 2H), 4.00 (s, 2H), 3.64 (s, 237H), 3.38 (s, 4H), 3.14 (s, 3H), 2.63 (t, *J* = 2.3 Hz, 1H).

SEC (RI): M_w (Đ) 30970 g mol⁻¹ (1.03).

20

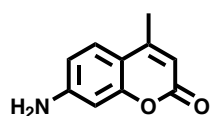


PEG₄₅-coumarin **19** (64 mg, 1.0 eq), PTMC-N₃ **13** (224 mg, 1.0 eq) and sodium ascorbate (8.7 mg, 2.0 eq) were dissolved in dry DMSO (3 mL). Pentahydrate copper sulphate (28 mg, 4 eq) was then added and the reaction was left under stirring overnight at 30°C. Water (1 mL) was added to the reaction mixture and the solution was dialysed (3.5 kDa) against water EGTA mixture for the two first dialysis and against water for the next 3. The resulting copolymer was lyophilized and 165 mg of PEG₄₅-coumarin-*b*-PTMC₈₁ (57% yield).

¹H NMR (400 MHz, CDCl₃) δ 7.75 (s, 1H), 7.27 (d, *J* = 8.8 Hz, 1H), 6.74 (s, 1H), 6.51 (d, *J* = 2.0 Hz, 1H), 6.34 (dd, *J* = 8.8 Hz, *J* = 2.1 Hz, 1H), 6.28 (s, 1H), 5.30 (s, 2H), 5.16 (d, *J* = 1.4 Hz, 2H), 4.24 (t, *J* = 6.3 Hz, 363H), 3.99 (s, 2H), 3.64 (s, 207H), 3.38 (s, 3H), 3.15 (s, 3H), 2.05 (m, *J* = 6.3 Hz, 177H).

SEC (RI): M_w (Đ) 15810 g mol⁻¹ (1.05).

21

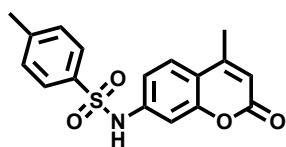


Ethyl acetoacetate (45.8 mmol, 1eq) was added to a mixture of 3-aminophenol (45.8 mmol, 1eq) and Y(NO₃)₃·6H₂O (4.58 mmol, 0.1 eq) in a 100 mL round bottom flask. The reaction mixture was stirred at 90°C for 2 hours. Then the solid product was suspended in water. The resulting crude product was filtered and recrystallized in EtOH to give a yellow/green crystalline powder (50% yield).

¹H NMR (DMSO, 300 MHz) δ (ppm): 7.41 (d, 1H), 6.57 (dd, 1H), 6.41 (d, 1H), 6.12 (s, 2H), 5.91 (s, 1H), 3.35 (s, 1H), 2.31 (s, 3H).

B. Karami, M. Kiani, Synthesis of the Coumarins via Pechmann Method in the Presence of Environmentally Friendly Y(NO₃)₃·6H₂O, J. Chin. Chem. Soc. 61 (2014) 213–216. doi:10.1002/jccs.201200610.

22



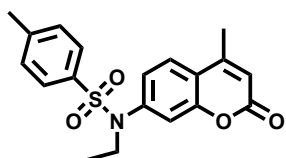
7-Amino-4-methylcoumarin (9.6 g, 1.0 eq) was dissolved in CH₂Cl₂ (10 mL). The reaction mixture was cooled down to 0°C. p-Toluenesulfonyl chloride (15.7 g, 1.5 eq) in pyridine (32 mL) was slowly added to the solution. The reaction mixture was stirred overnight at RT. The pyridine was removed under reduced pressure and a thick oil was obtained. The oil was diluted in ethanol (10 mL) and then poured into deionized water. The obtained solid was filtered, rinsed several times with water and rinsed with a minimum volume of ethanol and dried under vacuum overnight to obtain 14.0 g of **22** (78% yield).

¹H NMR (300 MHz, DMSO) δ (ppm) 10.91 (s, 1H), 7.74 (d, *J* = 8.0 Hz, 2H), 7.63 (d, *J* = 8.6 Hz, 1H), 7.37 (d, *J* = 7.9 Hz, 2H), 7.10 (, *J* = 8.6 Hz, 1H), 7.03 (s, 1H), 6.23 (s, 1H), 3.32 (s, 1H), 2.33 (s, 6H).

¹³C NMR (300 MHz, DMSO) δ (ppm) 159.7, 153.6, 153.0, 143.8, 141.4, 136.2, 130.0, 126.7, 126.6, 115.2, 114.6, 112.5, 105.0, 21.1, 17.9

HRMS (FD⁺): Calculated *m/z* = 329.0722 for C₁₇H₁₅NO₄S ; found *m/z* = 329.0730 [M]⁺

23



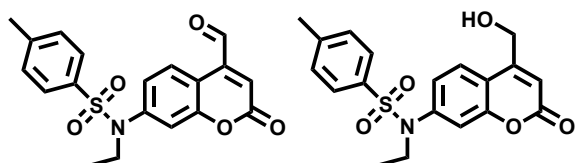
K₂CO₃ (8.8 g, 1.5 eq), NaI (0.64g, 0.1 eq), bromoethane (64 ml, 20 eq), **22** (14 g, 1.0 eq) and TBAB (1.38 g, 0.1 eq) were dissolved in 400 mL of acetonitrile. The reaction mixture was refluxed for 6 hours. After cooling down to RT, the solvent was removed under reduced pressure and a solid was obtained. The solid was dissolved in CH₂Cl₂ and the organic phase was washed 3 times with water. The organic phase was dried with MgSO₄ and evaporated under reduced pressure. The solid was recrystallized in EtOH to obtain 10.2 g of **23** (67% yield).

¹H NMR (400 MHz, CDCl₃) δ (ppm) 7.58 (d, *J* = 8.5 Hz, 1H), 7.47 (d, *J* = 8.3 Hz, 2H), 7.24 (m, 3H), 6.87 (d, *J* = 2.1 Hz, 1H), 6.28 (d, *J* = 1.2 Hz, 1H), 3.62 (q, *J* = 7.1 Hz, 2H), 2.44 (m, 6H), 1.09 (t, *J* = 7.1 Hz, 3H)

^{13}C NMR (400 MHz, CDCl_3) δ (ppm) 160.51, 153.7, 152.0, 144.1, 142.4, 134.9, 129.8, 127.6, 125.6, 125.0, 119.3, 115.5, 115.3, 45.4, 18.8, 14.0

HRMS (ESI): Calculated $m/z = 358.1113$ for $\text{C}_{19}\text{H}_{20}\text{NO}_4\text{S}$; found $m/z = 358.1108$ $[\text{M}+\text{H}]^+$

24/25



23 (5.1 g) was suspended in *p*-xylene (250 mL) with Se_2O_3 (3.2 g, 2.0 eq). The mixture was refluxed under vigorous stirring under argon atmosphere during 24 hours. The mixture was filtered and concentrated under reduced pressure. The dark brown oil **24** was used in the next reaction without further purification.

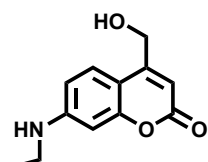
24 (5.1 g, 1.0 eq) was dissolved in 125 mL MeOH and NaBH_4 (1.04 g, 2.0 eq) was carefully added into the solution. The mixture was stirred 3 hours at RT. The solution was concentrated to remove methanol and carefully neutralized with 1M HCl solution, diluted with water and extracted with CH_2Cl_2 . The organic phase was washed with water and brine, dried with MgSO_4 and the solvent was removed under reduced pressure. The product was purified by silica column chromatography (Cyclohexane/ EtOAc; 1/1, v/v) to obtain 3.4 g of **25** (yield 66%).

^1H NMR (300 MHz, DMSO) δ (ppm) 7.48 (m, 3H), 7.26 (d, $J = 7.10$ Hz, 2H), 7.18 (dd, $J = 8.5$ Hz, $J = 2.1$ Hz, 1H), 6.92 (d, $J = 2.1$ Hz, 1H), 6.62 (t, $J = 1.5$ Hz, 1H), 4.89 (d, $J = 1.6$ Hz, 2H), 3.62 (q, $J = 7.1$ Hz, 2H), 2.43 (s, $J = \text{Hz}$, 3H), 1.09 (t, $J = 7.1$ Hz, 3H)

^{13}C NMR (300 MHz, DMSO) δ (ppm) 160.84, 153.8, 153.8, 144.2, 142.4, 134.8, 129.9, 127.6, 125.6, 123.89, 116.7, 115.8, 112.3, 77.4, 60.7, 45.4, 21.7, 13.97

HRMS (ESI): Calculated $m/z = 374.1062$ for $\text{C}_{19}\text{H}_{20}\text{NO}_5\text{S}$; found $m/z = 305.1057$ $[\text{M}+\text{H}]^+$

26



25 (3.4 g, 1.0 eq) was dissolved in concentrated sulfuric acid (25 mL). The mixture was stirred at 0°C for 1 hour. The solution was then poured carefully into water and neutralized with saturated sodium bicarbonate solution. The aqueous phase was washed 3 times with EtOAc.

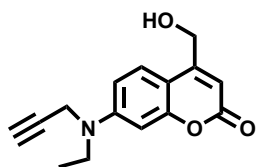
The organic phase was dried with MgSO₄ and the solvent was removed under reduced pressure. The product was purified by silica column chromatography (Cyclohexane/ EtOAc: 1/1, v/v) to obtain 340 mg of **26** (yield 17%).

¹H NMR (300 MHz, DMSO) δ (ppm) 7.36 (d, *J* = 8.8 Hz, 1H), 6.60 (d, *J* = 5.1 Hz, 1H), 6.56 (dd, *J* = 8.8 Hz, *J* = 2.2 Hz, 1H), 6.39 (d, *J* = 2.2 Hz, 1H), 6.05 (s, 1H), 5.48 (t, *J* = 5.6 Hz, 1H), 4.65 (dd, *J* = 5.5 Hz, *J* = 1.2 Hz, 2H), 3.11 (m, 2H), 1.17 (t, *J* = 7.2 Hz, 3H)

¹³C NMR (300 MHz, DMSO) δ (ppm) 161.12, 157.05, 155.69, 152.24, 124.75, 110.15, 106.06, 103.60, 96.18, 59.04, 36.97, 14.01

HRMS (ESI): Calculated *m/z* = 218.0823 for C₁₂H₁₂NO₃; found *m/z* = 218.0812 [M-H]⁻

27



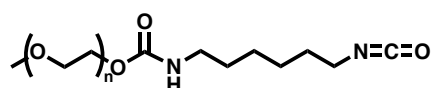
K₂CO₃ (239 mg, 1.5 eq), NaI (17.5 mg, 0.1 eq), 1-bromo-2-butyne (4.22 ml, 20 eq), **26** (253 mg, 1.0 eq) and TBAB (37.6 mg, 0.1 eq) were dissolved in acetone (15 mL). The reaction mixture was reflux for 6 hours. After cooling down to RT, the solvent was removed under reduced pressure and a solid was obtained. The solid was dissolved in CH₂Cl₂ and the organic phase was washed 3 times with water. The organic phase was dried with MgSO₄ and evaporated under reduced pressure. The product was purified by silica column chromatography (Cyclohexane/ EtOAc; 1/1, v/v) to obtain 105 mg of **27** (35% yield).

¹H NMR (300 MHz, DMSO) δ 7.49 (d, *J* = 9.3 Hz, 1H), 6.78 (dd, *J* = 2.6, 9.0 Hz, 1H), 6.67 (d, *J* = 2.5 Hz, 1H), 6.13 (t, *J* = 1.4 Hz, 1H), 5.53 (t, *J* = 5.4 Hz, 1H), 4.69 (d, *J* = 4.1 Hz, 1H), 4.22 (d, *J* = 2.3 Hz, 1H), 3.52 (q, *J* = 7.0 Hz, 1H), 3.18 (t, *J* = 2.3 Hz, 1H), 1.15 (t, *J* = 7.0 Hz, 1H).

¹³C NMR (400 MHz, DMSO) δ 161.4, 157.3, 155.6, 150.5, 125.4, 110.1, 107.4, 105.4, 99.0, 80.9, 74.9, 59.5, 45.7, 12.5

HRMS (ESI): Calculated *m/z* = 256.09682 for C₁₅H₁₄NO₃; found *m/z* = 256.0977 [M-H]⁻

30



HDMI (3.7 mL, 10.0 eq) and DBTL (210 μ L, 0.1 eq) were dissolved in 5 mL of CH_2Cl_2 under inert conditions. Monomethyl poly(ethylene glycol)₄₃ (4.0 g, 1.0 eq) was dissolved in 5 mL of CH_2Cl_2 under inert condition and the resulting solution was added dropwise in the HDMI solution during 2 hours. The solution was stirred for 3 hours at RT. The solvent was then removed and the resulting solid was precipitated 3 times in dry diethyl ether to obtain 4.0 g of **30** (93% yield).

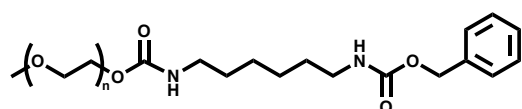
^1H NMR (400 MHz, CDCl_3) δ 4.87 (s, 1H), 4.18 (t, $J = 4.4$ Hz, 2H), 3.61 (s, 172H), 3.35 (s, 3H), 3.28 (m, 2H), 3.13 (m, 2H), 1.63-1.27 (m, 8H).

^{13}C NMR (101 MHz, CDCl_3) δ 70.5, 63.8, 59.0, 42.8, 31.1, 26.2, 26.1, 25.9.

Infrared: isocyanate (2271 cm^{-1}) and carbamate groups (1718 cm^{-1}).

SEC (RI): M_w ($\text{\textcircled{D}}$) 2961 g mol^{-1} (1.06).

31



PEG₄₃-HDMI **30** (500 mg, 1.2 eq) benzyl alcohol (22 μ l, 1.0 eq) and DBTL (2.7 μ L, 0.1 eq) were dissolved in 5 mL of CH_2Cl_2 under inert atmosphere. The solution was stirred for 5 hours at RT. The solvent was removed and the resulting solid was precipitated 3 times in diethyl ether to obtain 380 mg of **31** (93% yield).

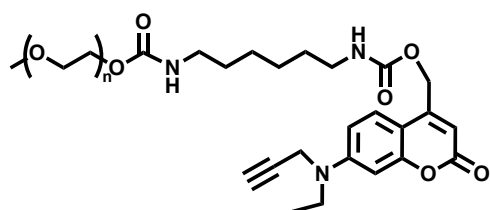
^1H NMR (400 MHz, CDCl_3) δ 7.34-7.26 (m, 5H), 5.07 (s, 2H), 4.86 (br, 2H), 4.18 (t, $J = 4.4$ Hz, 2H), 3.62 (s, 175H), 3.36 (s, 3H), 3.19-3.14 (m, 4H), 1.47 (br, 5H), 1.31 (br, 5H).

^{13}C NMR (101 MHz, CDCl_3) δ 128.5, 70.6, 59.0, 29.8, 26.2.

Infrared: carbamate groups (1718 cm^{-1})

SEC (RI): M_w ($\text{\textcircled{D}}$) 3080 g mol^{-1} (1.06).

32



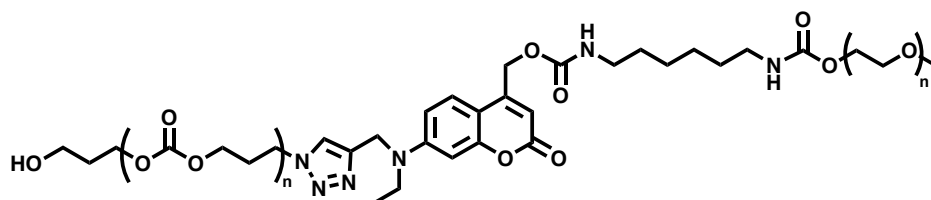
PEG₄₃-HDMI **30** (308 mg, 1.2 eq), **27** (33 mg, 1.0 eq) and DBTL (1.5 μ L, 0.1 eq) were dissolved in CH₂Cl₂ (2 mL) under an inert atmosphere. The solution was stirred for 5 hours at RT. The solvent was removed and the resulting solid was precipitated 3 times in diethyl ether. The product was then purified by silica column chromatography (DCM/ MeOH: 99/1 to 92/8, v/v) to obtain 165 mg of PEG₄₃-Coumarin **32** (41% yield).

¹H NMR (400 MHz, DMSO) δ 7.51 (d, J = 8.9 Hz, 1H), 7.17 (t, J = 5.4 Hz, 1H), 7.06 (br, 1H), 6.81 (dd, J = 2.3, 9.0 Hz, 1H), 6.69 (d, J = 2.4 Hz, 1H), 6.03 (s, 1H), 5.23 (s, 2H), 4.23 (d, J = 1.8 Hz, 2H), 4.03 (t, J = 4.6 Hz, 4H), 3.51 (s, 364H), 3.24 (s, 6H), 3.18 (t, J = 2.2 Hz, 1H), 3.01 (m, 2H), 2.94 (m, 6H), 1.39 (q, J = 6.7 Hz, 6H), 1.23 (br, 14H), 1.15 (t, J = 7.0 Hz, 3H).

¹³C NMR (101 MHz, DMSO) δ 70.2.

SEC (RI): M_w (Đ) 3097 g mol⁻¹ (1.06).

33



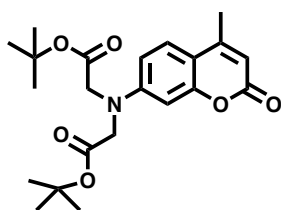
PEG₄₃-coumarin **32** (150 mg, 1.0 eq), PTMC-N₃ **13** (619 mg, 1.2 eq) and sodium ascorbate (20 mg, 2.0 eq) were dissolved in dry DMSO (2 mL). Pentahydrate copper sulphate (64.4 mg, 4 eq) was then added and the reaction was left under stirring overnight at 30°C. The copolymer was purified by silica column chromatography (DCM/MeOH ; 96/4 to 94:6, v/v). 313 mg of PEG₄₃-coumarin-*b*-PTMC₈₁ **33** (47% yield) was obtained.

¹H NMR (400 MHz, DMSO) δ 8.03 (s, 1H), 6.81 (d, J = 9.1 Hz, 1H), 6.69 (d, J = 2.2 Hz, 1H), 5.97 (s, 2H), 5.20 (s, 2H), 4.64 (s, 2H), 4.53 (t, J = 5.2 Hz, 1H), 4.39 (t, J = 7.1 Hz, 2H), 4.13 (t, J = 6.3 Hz, 358H), 3.50 (s, 167H), 3.24 (s, 3H), 3.06-2.88 (m, 4H), 1.44-1.19 (m, 10H), 1.14 (t, J = 7.0 Hz, 3H).

¹³C NMR (101 MHz, DMSO) δ 154.8, 70.2, 64.7, 28.0.

SEC (RI): M_w (Đ) 15170 g mol⁻¹ (1.04).

34

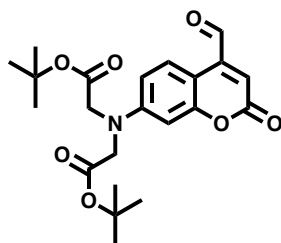


21 (22.8 mmol, 1eq) was dissolved in acetonitrile (120 mL) tert-butylbromoacetate (114 mmol, 5 eq), NaI (45.4 mmol, 2eq) and DIPEA (91 mmol, 4eq) were then added to the solution. The resulting mixture was heated at reflux for 3 days. The solvent was then removed under reduced pressure and the residue was dissolved in EtOAc (100 mL). The solution was washed with water and brine and dried with MgSO₄. The product was purified by silica column chromatography (Cyclohexane/ EtOAc; 5/1, v/v) to obtain **34** (25% yield).

¹H NMR (DMSO, 300 MHz) δ (ppm): 7.57 (d, 1H), 6.58 (dd, 1H), 6.43 (d, 1H), 6.05 (d, 1H), 4.19 (s, 4H), 2.36 (d, 3H), 1.43 (s, 18H).

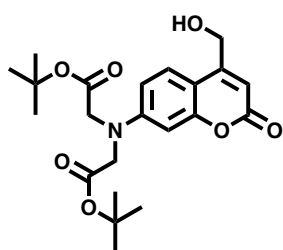
W.A. Velema, J.P. van der Berg, W. Szymanski, A.J.M. Driessen, B.L. Feringa, Orthogonal Control of Antibacterial Activity with Light, ACS Chem. Biol. 9 (2014) 1969–1974. doi:10.1021/cb500313f.

35



34 (5.45 mmol, 1eq) was suspended in p-xylene (50 mL) with Se₂O₃ (10.9 mmol, 3 eq). The mixture was refluxed under vigorous stirring under an argon atmosphere during 24 hours. The mixture was filtered and concentrated under reduced pressure. The dark brown oil **35** was used in the next reaction without further purification.

36

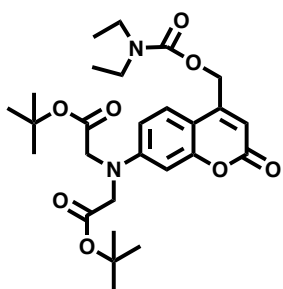


34 (4.8 mmol, 1.0 eq) was dissolved in a mixture of MeOH (50 mL) and THF (50 mL). The mixture was cooled on ice and NaBH₄ (7.2 mmol, 1.5 eq) was carefully added into the solution. The mixture was stirred 3 hours at RT. The solution was concentrated and carefully neutralized with 1M HCl solution, diluted with water and extracted with EtOAc. The organic phase was washed with water, brine, dried with MgSO₄ and the solvent was removed under reduced pressure. The product was purified by silica column chromatography (Cyclohexane/ EtOAc; 4/1, v/v) to obtain **36** (52% yield).

¹H NMR (DMSO, 300 MHz) δ (ppm): 7.50 (d, 1H), 6.55 (dd, 1H), 6.45 (d, 1H), 6.16 (s, 1H), 5.56 (t, 1H), 4.70 (d, 2H), 4.19 (s, 4H), 1.43 (s, 18H).

W.A. Velema, J.P. van der Berg, W. Szymanski, A.J.M. Driessen, B.L. Feringa, Orthogonal Control of Antibacterial Activity with Light, ACS Chem. Biol. 9 (2014) 1969–1974. doi:10.1021/cb500313f.

37



Diethylcarbamoyl chloride (0.5 mL, excess) was added to a solution of compound **34** (0.24 mmol, 1.0 eq) in pyridine (3 mL) at RT. The mixture was heated to 90°C for 48 hours under a nitrogen atmosphere. The reaction mixture was then cooled down to RT, 5 mL of 1N HCl was added and the mixture was extracted with EtOAc. The combined organic layers were washed with saturated NaHCO₃ solution and concentrated.

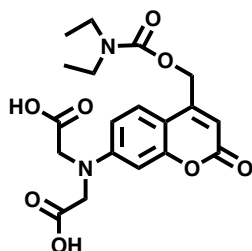
The product was purified by silica column chromatography (Cyclohexane/ EtOAc; 5/1, v/v) to obtain **37** (40% yield).

^1H NMR (CDCl_3 , 400 MHz) δ (ppm): 7.40 (d, 1H), 6.54 (m, 2H), 6.24 (s, 1H), 5.29 (d, 2H), 4.09 (s, 4H), 3.38 (q, 4H), 1.52 (s, 18H), 1.2 (t, 6H).

^{13}C NMR (CDCl_3 , 400 MHz) δ (ppm): 167.9, 160.7, 154.6, 153.8, 150.2, 149.5, 123.5, 108.1, 107.3, 106.8, 98.2, 81.5, 61.1, 53.3, 41.2, 40.4, 28.7, 27.1, 13.1, 13.4.

HRMS (ESI): Calculated $m/z = 541.2520$ for $\text{C}_{27}\text{H}_{38}\text{N}_2\text{O}_8\text{Na}$; found $m/z = 541.2504$ $[\text{M}+\text{Na}]^+$

38



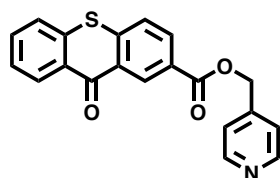
37 (0.058 mmol, 1eq) was dissolved in THF (0.5 mL). 0.13 mL of a KOH solution in water (100 mg in 1mL; 4 eq) was added to the mixture. The resulting solution was stirred at RT overnight. The solvents were removed under reduced pressure and the residue was dissolved in a minimum volume of water. HCl solution was added until all the solid precipitated. Product **37** was obtained in 40% yield.

^1H NMR (DMSO, 600 MHz, 60°C) δ (ppm): 7.53 (d, 1H), 6.64 (dd, 1H), 6.5 (d, 1H), 6.01 (s, 1H), 5.28 (s, 2H), 4.22 (s, 4H), 3.31 (q, 4H), 1.12 (t, 6H).

^{13}C NMR (MeOD, 400 MHz) δ (ppm): 175.8, 162.3, 155.6, 155.2, 152.0, 150.7, 125.0, 109.0, 107.7, 106.4, 98.0, 62.1, 56.3, 41.9, 41.3, 13.0, 12.2.

HRMS (ESI): Calculated $m/z = 405.39$ for $\text{C}_{19}\text{H}_{21}\text{N}_2\text{O}_8$; found $m/z = 405.13$ $[\text{M}-\text{H}]^-$

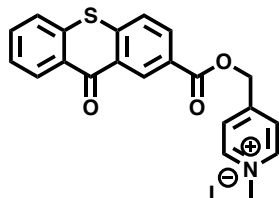
40



Under an inert atmosphere, DMAP (122 mg, 1.0 eq), EDCl.HCl (191 mg, 1.0 eq) and 2-carboxy thioxanthone **39** (256 mg, 1.0 eq) were dissolved in MeCN (10 mL). The mixture was stirred for 15 min at RT. 4-Pyridine methanol (164 mg, 1.5 eq) was then added to the mixture and the reaction was refluxed overnight. The solvent was removed under reduced pressure. The residue was purified by silica column chromatography (Cyclohexane/ EtOAc; 1/1, v/v). 196 mg of **40** was obtained (56% yield).

^1H NMR (300 MHz, CDCl_3) δ 9.32 (d, $J = 1.6$ Hz, 1H), 8.64 (m, $J = 3.0$ Hz, 3H), 8.28 (dd, $J = 2.0, 8.5$ Hz, 1H), 7.68 (m, $J = 2.1$ Hz, 2H), 7.57 (m, $J = 3.2$ Hz, 2H), 7.38 (d, $J = 5.3$ Hz, 2H), 5.44 (s, 2H).

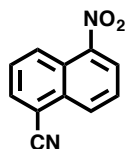
41



40 (103 mg, 1.0 eq) was dissolved in 3 mL of MeOH. MeI (0.2 mL, 10.0 eq) was added to the solution and the mixture was refluxed for 4 days. The mixture was cooled to RT, the precipitate was filtrated and washed with DCM (5x5mL). The solid was dried under reduced pressure to obtain **41** (32% yield).

^1H NMR (300 MHz, DMSO) δ 9.10 (d, $J = 1.6$ Hz, 1H), 9.00 (d, $J = 6.6$ Hz, 2H), 8.50 (dd, $J = 1.3, 8.4$ Hz, 1H), 8.37 (dd, $J = 2.0, 8.5$ Hz, 1H), 8.23 (d, $J = 6.7$ Hz, 2H), 8.09 (d, $J = 8.4$ Hz, 1H), 7.94 (d, $J = 8.1$ Hz, 2H), 7.86 (m, 1H), 7.67 (m, 1H), 5.76 (s, 2H), 4.36 (s, 3H).

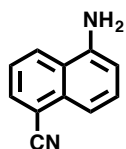
47



1-Naphthalenecarbonitrile (10 g, 0.065 mol) was solubilized in acetic acid (80 mL). Sulfuric acid (30 mL) and nitric acid (4.74 mL, 0.069 mol) are slowly added. The reaction mixture heated to 60°C for 2h. The mixture was poured on ice then the reaction mixture was filtered and recrystallized in ethanol then filtered again. 3.33g (yield = 16.8%) was obtained.

^1H NMR (300 MHz, DMSO) δ (ppm): 8.63 (d, $J = 8.8$ Hz, 1H), 8.48 (d, $J = 3.4$ Hz, 1H), 8.45 (d, $J = 2.7$ Hz, 1H), 8.37 (d, $J = 7.2$ Hz, 1H), 7.99-7.90 (m, 2H).

48

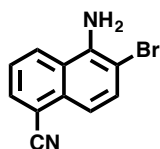


5-Nitronaphthalene-1-carbonitrile (3.33 g, 16.8 mmol) was dissolved in methanol (100 mL) and THF (50 mL). Pd/C (50 mg) was added, the flask placed under hydrogen atmosphere and

stirred overnight at RT. The reaction mixture was filtered over celite and solvent removal yielded 2.8 g (yield = 99%) of product.

^1H NMR (300 MHz, DMSO) δ (ppm): 8.45 (d, J = 8.6 Hz, 1H), 8.02 (d, J = 8.2 Hz, 1H), 7.50-7.43 (m, 2H), 7.25 (d, J = 8.2 Hz, 1H), 6.81 (d, J = 8.6 Hz, 1H), 6.15 (s, 2H).

49



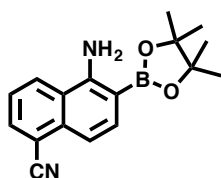
5-Aminonaphthalene-1-carbonitrile (2.80 g, 16.6 mmol) was dissolved in acetonitrile (200 mL) then NBS (2.96 g, 16.6 mmol) and silica (70 mg) were added. The reaction was stirred overnight at RT. The product was purified by chromatography (cyclohexane/ethyl acetate; 4:1, v/v) and 1.77 g (yield = 43 %) of **49** was obtained.

^1H NMR (300 MHz, CDCl_3) δ (ppm): 8.61 (d, J = 8.7 Hz, 1H), 8.11 (d, J = 7.2 Hz, 1H), 7.72 (d, J = 8.8 Hz, 1H), 7.59 (t, J = 7.2 Hz, 1H), 7.24 (d, J = 8.8 Hz, 1H), 6.34 (s, 2H).

^{13}C NMR (400 MHz, DMSO) δ (ppm): 142.7, 133.2, 133.08, 131.9, 128.5, 124.2, 122.3, 117.8, 112.4, 108.8, 102.5.

HRMS (EI): Calculated m/z = 245.98005 for $\text{C}_{11}\text{H}_7\text{N}_2\text{Br}$; m/z = 245.97926 $[\text{M}]^+$

50



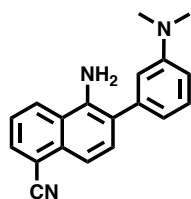
5-Amino-6-bromonaphthalene-1-carbonitrile (1.77 g, 7.16 mmol) was dissolved in dioxane (30 mL) with potassium acetate (2.14 g, 21.8 mmol), bis(pinacolato)diboron (3.64g, 14.3 mmol) and triphenylphosphine (0.188 g, 0.716 mmol). The reaction mixture was degassed under N_2 during 30 min and $\text{PdCl}_2(\text{dppf})$ (0.315 g, 0.43 mmol) was added. The reaction was stirred overnight at reflux. The product was filtered on silica with ethyl acetate and purified by chromatography (cyclohexane/EtOAc; 4:1, v/v). 0.873 g (yield = 49%) was obtained.

^1H NMR (300 MHz, CDCl_3) δ (ppm): 8.06 (d, $J = 8.56$ Hz, 1H), 7.87-7.80 (m, 2H), 7.49 (d, $J = 8.42$ Hz, 1H), 7.41 (d, $J = 7.20$ Hz, 1H), 1.37 (s, 12H).

^{13}C NMR (300 MHz, CDCl_3) δ (ppm): 151.5, 135.5, 135.4, 133.5, 126.6, 123.2, 122.4, 118.2, 113.3, 110.268, 83.9, 83.1, 26.9, 24.9, 24.5, 17.4.

HRMS (ESI): Calculated $m/z = 317.1417$ for $\text{C}_{17}\text{H}_{19}\text{BrN}_2\text{O}_2\text{Na}$; $m/z = 317.1431$ $[\text{M}+\text{Na}]^+$

52

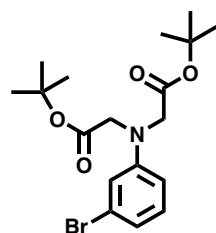


Modified naphthalene **50** (96 mg, 1.3 eq), 3-bromo-*N,N*-dimethyl aniline **51** (50 mg, 1.0 eq), triphenyl phosphine (4.1 mg, 0.2 eq) and caesium carbonate (253 mg, 3.1 eq) were fully dissolved in a mixture of DMF and water (respectively 5 and 2 mL). The solution was degassed by bubbling N_2 for 30 min. PdCl_2 (dppf) (33 mg, 0.16 eq) was then added under an inert atmosphere. The solution was heated at 100°C for 30 min via microwave. Water (10 mL) was added to the mixture and the aqueous phase was washed with ethyl acetate (3x15 mL). The solvent was removed under reduced pressure. The crude product was purified by silica column chromatography (Cyclohexane/ EtOAc; 6:1 to 3:1, v/v) and recrystallized in EtOH to obtain 94 mg of **52** (37% yield).

^1H NMR (400 MHz, CDCl_3) δ 8.12 (d, $J = 8.6$ Hz, 1H), 7.73 (dd, $J = 0.7, 8.5$ Hz, 1H), 7.50 (m, 2H), 7.38 (dd, $J = 7.9, 8.0$ Hz, 1H), 6.84 (s, 3H), 4.46 (s, 2H), 3.01 (s, 6H).

Y. Yang, S.K. Seidlits, M.M. Adams, V.M. Lynch, C.E. Schmidt, E.V. Anslyn, J.B. Shear, A Highly Selective Low-Background Fluorescent Imaging Agent for Nitric Oxide, *J. Am. Chem. Soc.* 132 (2010) 13114–13116. doi:10.1021/ja1040013.

56



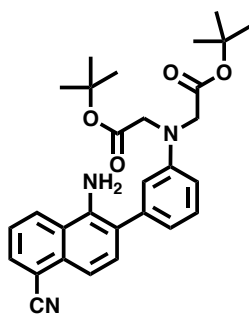
K_2CO_3 (1.88 g, 1.2 eq) was added to a solution of 3-bromoaniline **33** (1.27 mL 1.0 eq) in DMF (15 mL). Tert-butyl bromoacetate (4 mL, 2.4 eq) was then added to the mixture. The reaction

mixture was stirred for 2 days at 80°C. The solvent was removed under reduced pressure and the residue was diluted with EtOAc (40 mL), washed with saturated solution of NaHCO₃ (20 mL) and water (20 mL). The organic phase was collected, dried with MgSO₄ and the solvent was evaporated under reduced pressure. The crude product was purified by silica column chromatography (Cyclohexane/ Toluene; 5:5 to 67:3, v/v then Cyclohexane/ EtOAc; 95:5 to 90:10, v/v) to obtain 1.6 g of **56** (35% yield).

¹H NMR (400 MHz, CDCl₃) δ 6.98 (t, *J* = 8.1 Hz, 1H), 6.80 (ddd, *J* = 0.7, 1.7, 7.9 Hz, 1H), 6.65 (t, *J* = 2.2 Hz, 1H), 6.43 (ddd, *J* = 0.7, 2.7, 8.5 Hz, 1H), 3.91 (s, 4H), 1.40 (s, 18H).

¹³C NMR (101 MHz, CDCl₃) δ 169.7, 149.3, 130.4, 123.3, 120.7, 115.4, 111.0, 82.0, 54.5, 28.1.

57

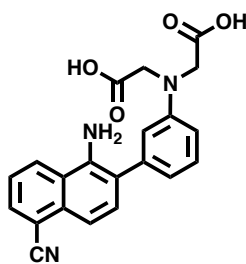


Modified naphthalene **50** (147 mg, 1.0 eq), **56** (200 mg, 1.0 eq), triphenyl phosphine (26.2 mg, 0.2 eq) and caesium carbonate (488 mg, 3 eq) were fully dissolved in a mixture of DMF and water (respectively 5 and 2ml). The solution was degassed by bubbling N₂ for 30 min. PdCl₂ (dppf) (41 mg, 0.16 eq) was then added under inert atmosphere. The solution was heated at 100°C for 30 min via microwave. Water (10 mL) was added to the mixture and the aqueous phase was washed with ethyl acetate (3x15 mL). The solvent was removed under reduced pressure. The crude product was purified by silica column chromatography (Cyclohexane/ EtOAc; 6:1 to 5:1, v/v) to obtain 135 mg of **57** (56% yield).

¹H NMR (400 MHz, CDCl₃) δ 8.13 (d, *J* = 8.6 Hz, 1H), 7.89 (dd, *J* = 0.8, 7.1 Hz, 1H), 7.72 (d, *J* = 8.6 Hz, 1H), 7.47-7.52 (m, 2H), 7.34 (t, *J* = 7.9 Hz, 1H), 6.88 (d, *J* = 7.6 Hz, 1H), 6.67 (s, 1H), 6.63 (dd, *J* = 2.5, 8.1 Hz, 1H), 4.06 (s, 4H), 1.47 (s, 18H).

¹³C NMR (101 MHz, CDCl₃) δ 170.0, 148.6, 139.7, 132.7, 132.3, 131.3, 130.0, 126.7, 123.9, 123.3, 118.8, 118.2, 115.3, 113.2, 111.6, 110.5, 81.9, 77.2, 60.4, 54.4, 28.1

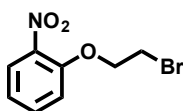
HRMS (ESI): Calculated *m/z* = 510.2363 for C₂₉H₃₃N₃O₄Na; found *m/z* = 510.2381 [M+Na]⁺

58

57 (30 mg, 1.0 eq) and triethylsilane (28.6 mg, 4 eq) were dissolved in DCM (1 mL) under an inert atmosphere. The reaction mixture was then cool down to 0°C and 1 mL of TFA was added to the reaction mixture. The solution was stirred during 4h30 min at 0°C. DCM (20 mL) was then added to the solution and the solvent was removed under reduced pressure without heating. The resulting solid was washed three times with diethyl ether to obtain 15 mg of **58** (65% yield). ¹H NMR (400 MHz, MeOD) δ 8.28 (d, *J* = 8.6 Hz, 1H), 7.84 (dd, *J* = 1.1, 7.2 Hz, 1H), 7.49 (dd, *J* = 0.8, 8.5 Hz, 1H), 7.44 (dd, *J* = 7.2, 8.6 Hz, 1H), 7.37 (d, *J* = 8.5 Hz, 1H), 7.27 (d, *J* = 15.8 Hz, 1H), 6.78 (d, *J* = 6.6 Hz, 1H), 6.59 (m, 2H), 4.16 (s, 4H).

¹³C NMR (101 MHz, MeOD) δ 149.5, 141.5, 141.1, 134.0, 133.7, 132.5, 131.1, 129.0, 125.5, 125.0, 124.8, 119.9, 119.1, 115.4, 114.0, 112.4, 110.9, 54.5, 28.3.

HRMS (ESI): Calculated *m/z* = 374.1146 for C₂₁H₁₆N₃O₄; found *m/z* = 374.1141 [M-H]⁻

61

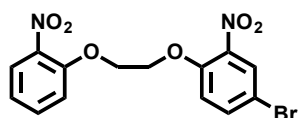
2-Nitrophenol (20 g, 143.8 mmol) was solubilized in hot MeOH (100 mL). A solution of KOH (8.0 g, 143.8 mmol) in MeOH was added and a precipitate was formed. The solvent was evaporated and the solid was dissolved in DMF (40 mL). 1,2-dibromoethane (48.8 g, 580 mmol) was added and the reaction mixture and heated to 120 °C for 4 h. After cooling, the reaction mixture was filtered and the precipitate was washed with DCM and a small volume of water. The organic phase was washed three times with NaOH_{aq.} (4 g/L) and three times with brine. The organic phase was dried over MgSO₄, filtered and evaporated. The crude product was purified by column chromatography (Cyclohexane/ EtOAc; 10:1 to 4:1, v/v) to obtain 3.8 g (11 % yield) of the product.

^1H NMR (300 MHz, CDCl_3) δ (ppm): 7.85-7.06 (m, 4H), 4.42 (t, $J = 6.4$ Hz, 2H), 3.67 (t, $J = 6.5$ Hz, 2H).

HRMS (FI+): Calculated $m/z = 244.9687$ for $\text{C}_8\text{H}_8\text{BrNO}_3$; $m/z = 244.969$ $[\text{M}]^+$

R.Y. Tsien, New calcium indicators and buffers with high selectivity against magnesium and protons: design, synthesis, and properties of prototype structures, *Biochemistry*. 19 (1980) 2396–2404. doi:10.1021/bi00552a018.

62



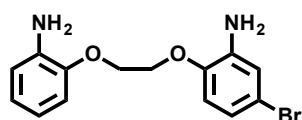
61 (1.6 g, 7.2 mmol), 1-(2-bromoethoxy)-2-nitrobenzene (1.8 g, 7.2 mmol) and carbonate potassium (3.0 g, 21.9 mmol) were dissolved in DMF (16 mL). Then the reaction was stirred for 4h at 100°C . DMF was evaporated and the product was recrystallized in EtOH. 2.4 g (yield = 87%) was obtained.

^1H NMR (600 MHz, CDCl_3) δ (ppm): 8.10 (d, $J = 2.5$ Hz, 1H), 7.86-7.81 (t, $J = 7.8$ Hz, 2H), 7.65 (t, $J = 7.5$ Hz, 1H), 7.42 (m, 2H), 7.14 (t, $J = 8.1$ Hz, 1H), 4.53 (m, 4H).

^{13}C NMR (600 MHz, CDCl_3) δ (ppm): 150.7, 150.1, 140.3, 139.7, 136.5, 134.2, 127.0, 124.8, 120.9, 117.7, 115.5, 111.4, 68.3, 67.9.

HRMS (ESI): Calculated $m/z = 404.9701$ for $\text{C}_{14}\text{H}_{11}\text{N}_2\text{O}_6\text{BrNa}$; $m/z = 404.9692$ $[\text{M}+\text{Na}]^+$

63



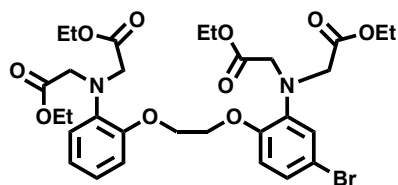
62 (2.42 g, 6.31 mmol) was dissolved in a mixture of MeCN/ H_2O (30:3, v/v). NiCl_2 (0.340 g, 2.6 mmol) was added and the solution mixture was stirred 3 min. NaBH_4 (1.92 g; 50.8 mmol) was added and the solution mixture was stirred 15 min. Then water (50 mL) was added. The product was extracted with DCM, filtered on silica and evaporated. 1.62 g of **63** (yield = 79.4%) was obtained.

^1H NMR (600 MHz, CDCl_3) δ (ppm): 6.86-6.68 (m, 7H), 4.34 (m, 4H), 3.79 (s, 4H).

^{13}C NMR (600 MHz, CDCl_3) δ (ppm): 146.1, 145.2, 138.3, 136.7, 122.0, 120.5, 118.4, 117.6, 115.4, 114.1, 113.7, 112.5, 67.7, 67.2.

HRMS (ESI): Calculated = 345.0222 for $\text{C}_{14}\text{H}_{15}\text{N}_2\text{O}_2\text{BrNa}$; $m/z = 345.0209$ $[\text{M}+\text{Na}]^+$

64



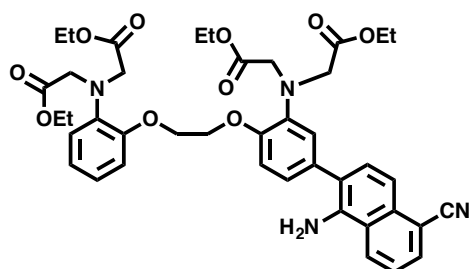
4-Bromo-1-amino-2-(2-(2-nitrophenoxy)ethoxy)-benzene (1.62g, 4.0 mmol) was dissolved in dry acetonitrile (20 ml) under argon. NaI (0.242g; 1.6 mmol), Na₂HPO₄·12H₂O (7.2 g, 20.1 mmol) and ethyl bromoacetate (3.36g, 20.1mmol) were added then the reaction mixture was stirred at reflux for 5 days. The product was extracted with ethyl acetate and water. The product was purified by chromatography (cyclohexane/ EtOAc; 4:1 to 2:1, v/v) 0.218 g of product was obtained (yield = 6.5%).

¹H NMR (300 MHz, CDCl₃) δ (ppm): 7.00 (dd, J = 2.30 Hz, J = 8.57 Hz, 1H), 6.9-6.8 (m, 5H), 6.72 (d, J = 8.61 Hz, 1H), 4.2 (s, 4H), 4.1 (d, J = 6.53 Hz, 8H), 4.0 (q, J = 7.15 Hz, 8H), 1.2-1.1 (m, 12H).

¹³C NMR (300 MHz, CDCl₃) δ (ppm): 171.5, 171.0, 150.1, 149.4, 140.7, 139.3, 124.4, 122.0, 121.7, 121.5, 118.8, 114.2, 113.5, 113.0, 67.3, 66.8, 60.9, 60.7, 53.3, 53.3, 13.9, 13.9.

HRMS (ESI): Calculated = 689.1656 for C₂₈H₃₉N₂O₁₀BrNa; m/z = 689.1680 [M+Na]⁺

65



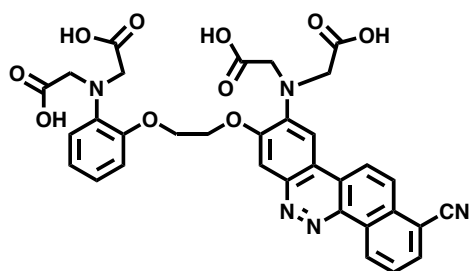
5-Amino-6-(4,4,5,5-tétraméthyl-1,2,3-dioxaborolan-2-yl)-1-naphtalene-1-carbonitrile (155 mg, 0.53 mmol), bromo-BAPTA (238 mg, 0.36 mmol) cesium carbonate (362 mg, 1.1 mmol) and triphenylphosphine (18.7 mg, 0.071 mmol) were dissolved in a mix DMF/water (7.5 mL/ 3 mL) then degassed with N₂. [1,1'-Bis(diphenylphosphino)ferrocene]dichloropalladium(II) (Pd(dppf)Cl₂) (39.1 mg, 0.053 mmol) was added. The reaction mixture was heated 30 min at 100°C in a microwave oven. The product was extracted with EtOAc and purified by chromatography (DCM/MeOH; 97:3 to 95:5, v/v). 75.5 mg of **65** were obtained (yield= 28%).

and the resulting mixture was slowly added to the solution. The reaction mixture was stirred overnight at RT. The product was purified by column (cyclohexane/ ethyl acetate, 1:1, v/v). 50 mg of the product was obtained (98.8% yield).

^1H NMR (600 MHz, CDCl_3) δ (ppm): 10.00 (d, $J = 8.4$ Hz, 1H), 8.47 (d, $J = 8.9$ Hz, 1H), 8.42 (d, $J = 9.4$ Hz, 1H), 8.12 (d, $J = 7.3$ Hz, 1H), 8.0 (s, 1H), 7.9 (dd, $J = 8.2$ Hz, $J = 7.5$ Hz, 1H), 7.7 (s, 1H), 6.95-6.89 (m, 3H), 6.86 (dd, $J = 7.6$ Hz, $J = 1.8$ Hz, 1H), 4.6 (m, 2H), 4.44 (s, 4H), 4.41 (m, 2H), 4.17 (s, 4H), 4.12 (q, $J = 7.1$ Hz, 4H), 4.04 (q, $J = 7.2$ Hz, 4H), 1.20 (t, $J = 7.1$ Hz, 6H), 1.11 (t, $J = 7.1$ Hz, 6H).

^{13}C NMR (600 MHz, CDCl_3) δ (ppm): 171.6, 170.8, 153.2, 150.3, 145.2, 145.1, 140.9, 139.8, 133.8, 132.2, 131.6, 129.6, 128.1, 127.7, 124.9, 122.4, 122.1, 121.9, 119.5, 119.4, 117.8, 117.7, 113.7, 110.4, 110.0, 105.8, 68.1, 66.9, 61.6, 60.9, 54.3, 53.7, 30.4, 29.8, 14.2, 14.2.

70



9-Ester-(BAPTA)-dibenzo[*c,h*]cinnoline-1-carbonitrile (30 mg ; 0.039 mmol) was dissolved in ethanol (1.5 mL), then water (1 mL) containing KOH (100 mg ; 1.8 mmol) was added. The mixture was stirred at RT overnight. The solvent was partially evaporated under reduced pressure to remove ethanol and neutralized with diluted HCl (1M). A solid precipitated and the HCl was added until there was no more solid precipitation. The solid was filtered and dried overnight. 25.1 mg of the final product was obtained (yield = 98.1%).

^1H NMR (600 MHz, DMSO) δ (ppm): 12.58 (br, 3H), 9.91 (d, $J = 8.3$ Hz, 1H), 8.88 (d, $J = 9.4$ Hz, 1H), 8.40-8.46 (m, 2H), 8.02-8.10 (m, 2H), 7.8 (s, 1H), 7.02 (dd, $J = 4.7$ Hz, 1H), 6.86 (t, $J = 4.6$ Hz, 2H), 6.73 (dd, $J = 4.8$ Hz, 1H), 4.59 (br, 2H), 4.44 (s, 4H), 4.38 (br, 2H), 4.05 (s, 4H).

^{13}C NMR (300 MHz, MeOD) δ (ppm): 176.5, 173.78, 155.1, 151.6, 147.1, 142.0, 140.1, 139.3, 135.2, 131.8, 130.0, 129.4, 129.2, 128.3, 123.5, 122.3, 121.4, 120.0, 119.8, 119.1, 117.7, 113.9, 110.8, 106.8, 104.8, 70.0, 67.6, 58.8, 55.8, 55.5, 18.4.

HRMS (FD⁺): Calculated = 654.1836 for $\text{C}_{33}\text{H}_{28}\text{N}_5\text{O}_{10}$; $m/z = 654.185$ [M+H]⁺

Nitric oxide (NO) has been identified as an important chemical messenger in cells and living organisms. Understanding the mechanism involved in NO production by NO-synthase is of fundamental importance. Mimicking basic cell functions by encapsulating NO-synthase in a controlled and confined cell like environment, could help provide information about the enzyme. Polymersomes resulting from the self-assembly of amphiphilic block copolymers were used as the synthetic cell like microreactor. To this end, three major challenges were addressed in this thesis: (1) controlling species release and concentration inside the microreactor, (2) measuring the enzyme response by NO detection and (3) controlling enzymatic reactions in space and time inside a microreactor. Light was used as the exogenous stimulus to induce release; its application is instantaneous, non-invasive and easy to control spatially and temporally. Two different ways to release species via light excitation were explored. The first strategy involves destabilization of nanopolymersomes by block separation, induced by copolymer photocleavage. The second strategy was to induce fast osmotic pressure increase of the polymersomes internal medium, resulting in bursting and species release. In order to monitor NO production by NO-synthase in different parts of the microreactor, hydrophobic and hydrophilic fluorescent NO probes have been synthesized and studied showing excellent correlation with NO concentration. The release of species inside microreactor was finally achieved in order to control enzymatic reaction.

Key words: Photosensitivity, polymersomes, protocell, enzyme, fluorescent probe

Le monoxyde d'azote (NO), un neurotransmetteur important en biologie, a attiré l'attention ces dernières années pour son rôle majeur joué dans l'apparition d'une myriade de maladies telles que certains cancers, diabètes etc. Comprendre les mécanismes biologiques liés à la production du NO pourrait aboutir à la découverte de nouveaux moyens thérapeutiques. Cependant, le fonctionnement de l'enzyme qui produit le monoxyde d'azote, la NO-Synthase, n'est pas complètement élucidé. Dans ce but, des approches biomimétiques peuvent apporter une solution. Les microréacteurs ou proto-cellules, enveloppes imitant sommairement la compartimentation cellulaire sont un outil de choix, permettant de répliquer un environnement contrôlé où les concentrations et distances de réactions sont proches d'une cellule, permettant ainsi d'étudier le fonctionnement de la NO-Synthase. Cette thèse présente trois problématiques qui ont pour but de développer un tel microréacteur encapsulant la NO-Synthase : (1) la libération contrôlée d'espèces réactives déclenchée par un stimulus lumineux, (2) le suivi de l'activité de l'enzyme par des sondes fluorescentes et (3) le contrôle de la réaction enzymatique dans l'espace et dans le temps. Deux systèmes ont été étudiés pour libérer de manière contrôlée des espèces: la première consiste à déstabiliser des nano polymersomes par photo-clivage du copolymère qui le constitue. Le deuxième système est basé sur une rapide augmentation de la pression osmotique par irradiation à l'intérieur des polymersomes, induisant un éclatement de ceux-ci et la libération d'espèces encapsulées. La deuxième problématique abordée est le suivi de l'activité enzymatique au moyen de sondes hydrophobes et hydrophiles fluorescentes qui détectent le monoxyde d'azote à différents endroits du microréacteur. Le dernier point abordé est l'étude des microréacteurs et la libération contrôlée en leur sein.

Mots clefs : Photosensible, polymersomes, cellule artificielle, enzyme, sonde fluorescente

Résumé

Résumé

L'oxyde nitrique (NO) est un important messenger chimique dans l'organisme vivant. Le NO est impliqué dans un large éventail de mécanismes de défense immunitaire et de signalisation biologiques telles que la communication neuronale, l'activité antitumorale, la régulation de la tension artérielle et la défense immunitaire non spécifique. De plus, plusieurs études suggèrent que le NO pourrait jouer un rôle clé dans l'apparition et la propagation d'un large éventail de maladies telles que les maladies neurodégénératives, les maladies cardiovasculaires, le diabète et le cancer. Il est donc crucial de mieux comprendre les mécanismes impliqués dans la production de NO, et ainsi développer des pistes pour l'élaboration de nouveaux médicaments et traiter les maladies précédemment citées. Le NO est produit par la NO synthase, une enzyme pouvant avoir des fonctions biologiques opposées. Son fonctionnement n'est pas encore bien compris malgré les nombreuses études sur la NO synthase. L'utilisation de microréacteurs pour encapsuler et étudier l'enzyme permettrait d'obtenir un environnement confiné et contrôlé mimant celui de la cellule. Cependant, dans la plupart des microréacteurs qui ont été développés dans la littérature, les réactions biochimiques sont induites simplement par le mélange des différents composants ou dépendent des propriétés de diffusion à travers les membranes des microréacteurs. L'étude de la cinétique de ces réactions complexes est donc très difficile, voire impossible.

Dans ce contexte, trois enjeux majeurs ont été abordés dans cette thèse : le contrôle de la libération et de la concentration des espèces réactives à l'intérieur du microréacteur, la mesure de la réponse enzymatique par la détection du NO et la libération contrôlée dans l'espace et dans le temps d'espèces au sein des microréacteurs.

Pour résumer, nous avons décidé de développer un microréacteur compartimenté et sensible à la lumière pour étudier le comportement complexe du NOS (Figure 1).

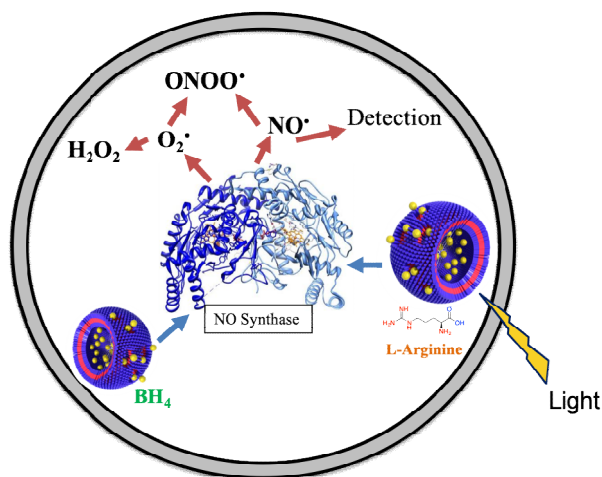


Figure 1: Représentation schématique de la cellule synthétique pour étudier l'activité de la NO synthase, basée sur l'encapsulation de nanopolymersomes photosensibles. La modulation des substrats enzymatiques et des cofacteurs (L-Arg, BH4) peut être contrôlée par photoactivation.

Le contrôle de la libération des espèces a été effectué par l'intermédiaire de nanopolymersomes photosensibles. Dans un premier temps, plusieurs PEG₄₅-*b*-PTMC avec différentes longueurs de poly(triméthylène carbonate) PTMC ont été synthétisés afin de trouver le rapport hydrophile/hydrophobe permettant de former des polymersomes stables. Le PEG₄₅-*b*-PTMC₈₁, avec un rapport hydrophile/hydrophobe de 19%, s'auto-assemble en polymersomes avec une polydispersité faible. Dans un second temps, une 1^{ère} génération d'un copolymère photosensible a été synthétisé : le PEG₄₃-coumarine-*b*-PTMC₈₁ dont la photosensibilité est basé sur une molécule de liaison : la coumarine photoclivable (Figure 2).

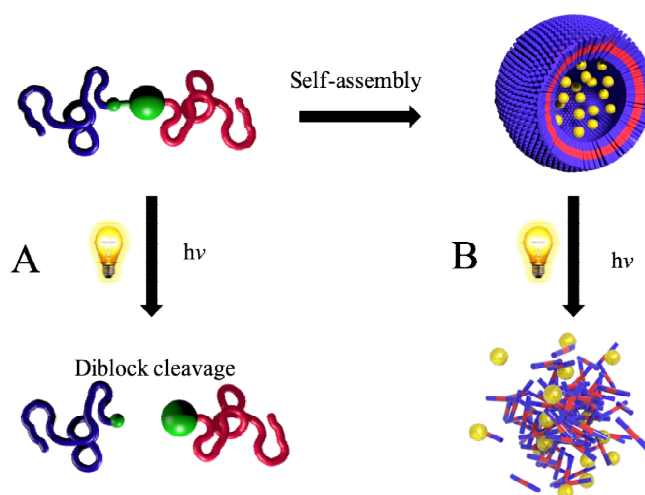


Figure 2: Stratégie utilisée pour contrôler la libération des réactifs dans le temps et dans l'espace par l'intermédiaire de polymersomes photosensibles (B), à l'aide des copolymères photodégradables (A).

La coumarine photosensible a d'abord été synthétisée avec un groupe acide carboxylique et un groupe alcyne aux deux extrémités, afin de pouvoir greffer un polymère hydrophile et un polymère hydrophobe. L'extrémité de la chaîne d'un PEG₄₃ a été modifiée en une amine afin de pouvoir le lier à l'acide carboxylique de la coumarine. Le bloc hydrophobe a été par la suite synthétisé. Le triméthylène carbonate (TMC) a été polymérisé pour former du PTMC avec une extrémité de chaîne azotée. Le paramètre clé pour obtenir une faible dispersité (1,05) était une purification poussée de l'initiateur 3-azido-1-propanol. PEG₄₃-NH₂ et PTMC₈₁-N₃ ont été greffés successivement sur la molécule de liaison coumarine pour donner le copolymère amphiphile photosensible de 1^{ère} génération PEG₄₅-coumarine-*b*-PTMC₈₁. Le copolymère a été obtenu avec une dispersité faible de 1,05.

Les mesures de diffusion de la lumière ont montré que le copolymère pouvait s'auto-assembler en particules bien définies avec un rayon hydrodynamique de 150 nm et une polydispersité faible (PDI \approx 0.1). La cryo TEM a montré que ces particules étaient des polymersomes.

Les polymersomes ont ensuite été irradiés sous UV (365 nm) n'entraînant pas de modification de leur morphologie ou de leur taille. La mesure de la diffusion de la lumière a montré que les particules étaient partiellement déstabilisées ou perdaient partiellement leur masse après irradiation (30% de perte de signal après 2,5 heures d'irradiation).

Cependant, la plupart des nanoparticules (70 %) n'ont pas été déstabilisées par l'irradiation. La stabilité des polymersomes pourrait s'expliquer par la dimérisation de la coumarine, elle-même favorisée par l'auto-assemblage empêchant la libération du PEG. Afin d'améliorer l'efficacité de déstabilisation des nanoparticules, un nouveau copolymère a été synthétisée et analysée.

La première génération de particules photosensibles n'était pas complètement déstabilisée et il a été supposé que la dimérisation, empêchant la libération du PEG, améliorait la stabilité des particules. Afin de favoriser la libération du PEG, la conception du copolymère a été modifiée de deux façons différentes. L'efficacité du clivage a été améliorée en changeant le groupe partant. Le rendement quantique obtenu par irradiation à 365 nm (0,012) était supérieur à celui de la 1^{ère} génération (0,0034). Le PEG est libéré plus efficacement avant de dimériser. La deuxième modification était la position des polymères sur la coumarine. En effet, avec le deuxième copolymère, seul le PEG est libéré au lieu du PEG-coumarine induisant une libération plus efficace du PEG.

Afin de synthétiser la 2^{ème} génération de PEG₄₃-coumarine-*b*-PTMC₈₁, la coumarine photosensible a été synthétisée avec un groupe hydroxyle et un groupe alcyne aux deux

extrémités, afin de pouvoir greffer un polymère hydrophile et un polymère hydrophobe. L'extrémité de la chaîne PEG₄₃ a ensuite été modifiée en isocyanate afin de pouvoir le lier au groupe hydroxyle de la coumarine. PEG₄₃-NCO et PTMC₈₁-N₃ ont été greffés successivement sur la molécule de liaison coumarine pour donner le copolymère amphiphile photosensible de 2^{ème} génération PEG₄₃-coumarine-*b*-PTMC₈₁ (Figure 3).

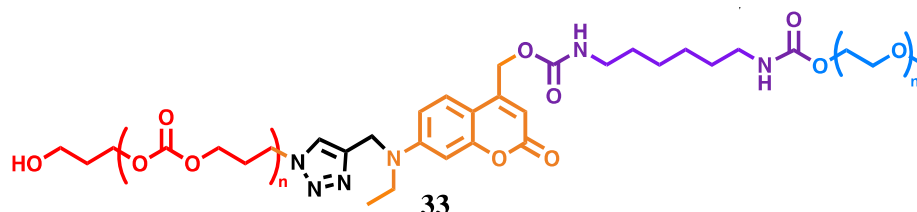


*Figure 3 : Structure chimique du copolymère PEG₄₃-coumarine-*b*-PTMC₈₁ photosensible.*

Le copolymère a été obtenu avec une dispersité faible de 1,04. Les mesures de diffusion de la lumière ont montré que le copolymère pouvait s'auto-assembler en particules bien définies avec un rayon hydrodynamique de 150 nm et une polydispersité faible (PDI \approx 0.1). Les observations par cryo-TEM ont montré des polymersomes et des agrégats de polymersomes. L'irradiation des polymersomes a induit un changement de leur morphologie. Après irradiation, le rapport Rg/Rh des particules restantes a diminué, ce qui suggère une densification des particules. La solution de polymersomes a été irradiée pendant 150 minutes et l'intensité de la lumière diffusée a diminué de 71%, suggérant une déstabilisation et une agrégation des particules. Les mesures de diffusion de la lumière ont été confirmées par cryo-TEM. Les images obtenues ont montré une majorité d'agrégats indéfinis après irradiation des polymersomes. Cette partie a présenté la synthèse d'un copolymère photosensible, son auto-assemblage en polymersomes, et la photosensibilité des particules formées par irradiation UV.

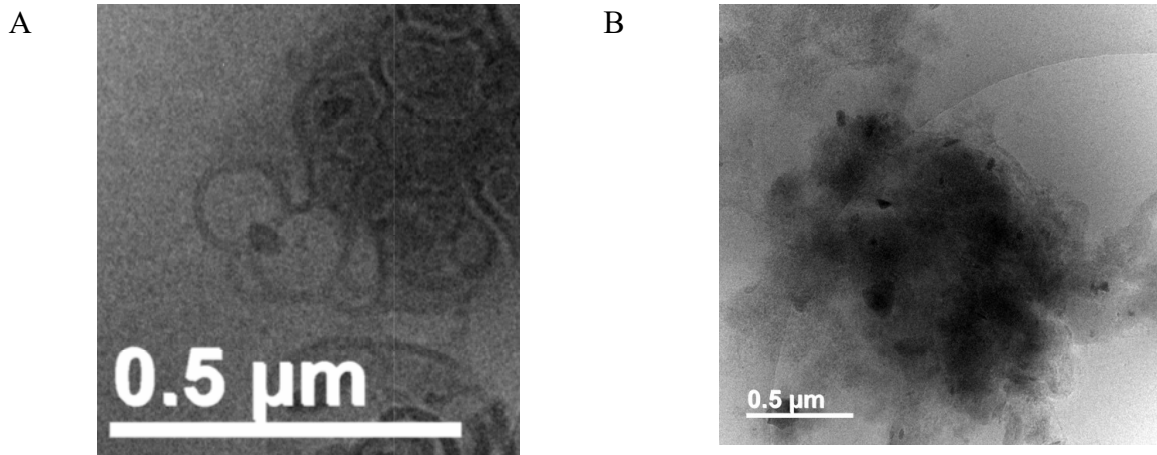


Figure 4 : Images cryo-TEM de polymersomes de PEG_{43} -coumarine- b - $PTMC_{81}$ A) avant et B) après irradiation

Une deuxième voie a été explorée pour contrôler la libération d'espèces par irradiation : le changement de pression osmotique dans les polymersomes induisant leur déstabilisation. L'augmentation rapide de la pression osmotique dans le milieu interne des polymersomes n'a pas pu être équilibré assez rapidement avec l'eau, ce qui a entraîné la rupture des polymersomes et la libération des espèces. L'augmentation de la pression osmotique a été contrôlée par des molécules clivables sensibles à la lumière.

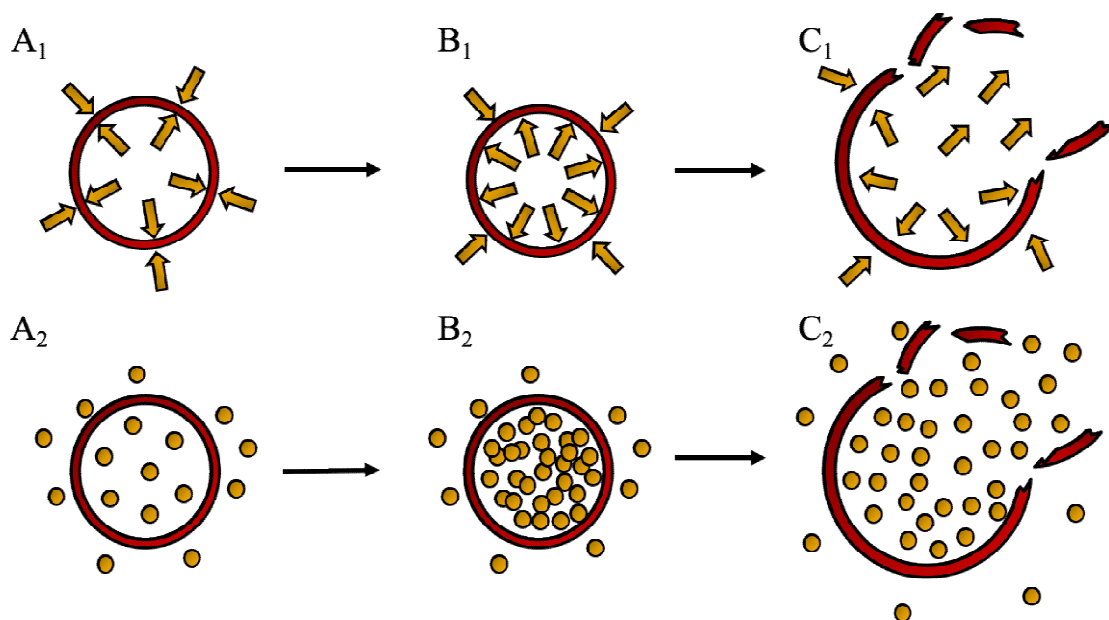


Figure 5: Stratégie utilisée pour induire l'éclatement des polymersomes. Les polymersomes sont stables lorsque la pression osmotique est la même dans le milieu interne et externe (A1). L'augmentation de pression osmotique (B1) a été utilisée pour induire la rupture du polymère (C1). Le contrôle de la concentration moléculaire permet de contrôler la pression osmotique.

L'augmentation de la concentration des espèces présentes dans le polymersomes (A2, B2) entraîne une augmentation de la pression osmotique et une rupture des polymersomes (C2).

Deux molécules ayant deux mécanismes de clivage différents ont été étudiées : le clivage hétérolytique de la coumarine et le transfert d'électrons à médiation basée sur le N-alkyl-4-picolinium-thioxanthone (NAP-th).

Le NAP-th a été facilement synthétisé en 2 étapes, sa solubilité dans l'eau était le paramètre limitant et la concentration maximale de solubilité trouvée était de 1 mM. Plusieurs méthodes ont été testées pour augmenter sa solubilité dans l'eau, comme le changement du contre ion ou l'ajout d'un groupe hydrophile, mais sans permettre d'augmenter significativement la solubilité dans l'eau. Le rendement quantique mesuré en présence du médiateur triéthanolamine était de 0,16. Cette valeur a montré que le clivage était très efficace.

La coumarine modifiée a également été synthétisée avec succès en 6 étapes, deux groupes hydrophiles ont été ajoutés pour augmenter la solubilité de la molécule qui a pu être facilement mise en solution dans l'eau à des concentrations de l'ordre de 10 mM. Le rendement quantique mesuré était de 0,016 pour une illumination à 365 nm et de 0,029 pour 405 nm. Le clivage était moins efficace que le NAP-th, mais sa solubilité était meilleure. Une irradiation d'une heure à 365 nm a induit un clivage de la molécule de 87 %. Ce clivage a libéré une base : de la diéthylamine qui a pu être utilisé pour augmenter le pH de la solution. En effet, après seulement 10 minutes d'irradiation, le pH est passé de 4,5 à 6,5.

La deuxième étape a consisté à encapsuler les deux molécules à l'intérieur du polymersomes de PEO_{1,3}-b-PBut_{2,5} par la technique d'émulsion-centrifugation. La coumarine modifiée a été encapsulée dans un polymersome avec une concentration de 10 mM et NAP-th a été encapsulé avec une concentration de 1 mM. L'irradiation à 405 nm sous microscope confocal a provoqué l'éclatement rapide des polymersomes contenant les deux molécules. Ces systèmes induisant une libération rapide et efficace pourraient être utilisés pour initier une réaction dans les microréacteurs et ainsi avoir un contrôle précis dans l'espace et le temps de systèmes cellulaires artificiels.

Afin de suivre la production de NO directement à l'intérieur du microréacteur, deux sondes à NO ont été étudiées. Ces sondes sont basées sur la formation d'une liaison azoïque induisant une fluorescence de la molécule, résultant en un signal stable et une sélectivité élevée par rapport aux autres composés nitro. Les deux sondes ont été conçues pour avoir des propriétés de solubilité différentes (l'une hydrophobe, l'autre hydrophile) afin de détecter le

NO dans la membrane et dans le milieu aqueux interne du microréacteur. Les sondes ont été synthétisées en 5 et 6 étapes (Figure 6 A,B).

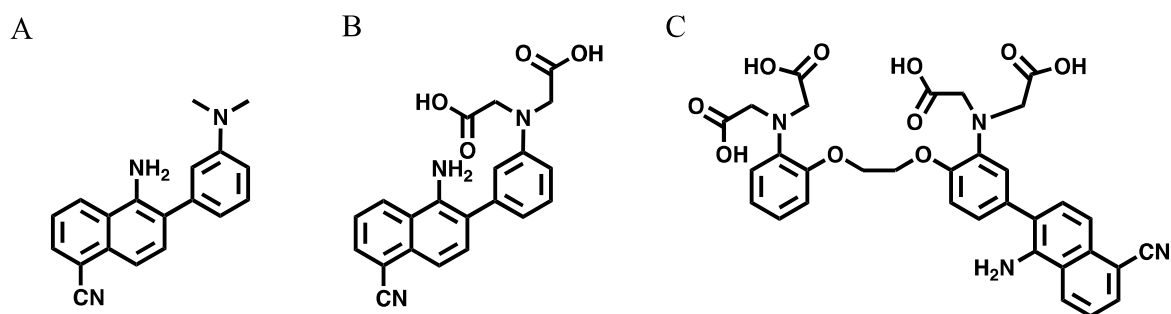


Figure 6: A) Sonde de NO fluorescente hydrophobe B) sonde fluorescente hydrophile de NO C) BAPTA-NOp

Des étapes critiques ont été rencontrées pour la protection et la déprotection de l'acide carboxylique de la sonde hydrophile. Le tert-butyle s'est avéré être un groupe protecteur efficace dans les conditions utilisées et le TES a permis d'éviter la dégradation de la sonde hydrophile pendant l'étape de déprotection. Afin de tester les propriétés des sondes, plusieurs sources de NO ont été testées comme le GSNO, le NO provenant NaNO₂ ou le NO gazeux provenant d'une bouteille. La concentration de NO obtenue a été mesurée grâce à l'absorption de l'hémoglobine. La libération de NO par le GSNO grâce à l'acide ascorbique et sa cinétique de libération a été étudiée. Cependant, l'acide ascorbique empêche la formation de la molécule fluorescente et le GSNO n'a pu être utilisé. Le NO de NaNO₂ a donné des solutions de faible concentration, c'est pourquoi a finalement été utilisée, la solution de NO provenant d'une bouteille de gaz. La détection du NO par les sondes a été testée. Les sondes ont montré une augmentation de l'intensité de fluorescence ($\lambda_{em\ max} = 530\ nm$, $\lambda_{ex\ max} = 440\ nm$ pour la sonde hydrophile, ($\lambda_{em\ max} = 530\ nm$, $\lambda_{ex\ max} = 440\ nm$ pour la sonde hydrophile) après addition de NO. L'intensité de fluorescence obtenue a une excellente corrélation linéaire ($R^2 = 0,99$) en fonction de la quantité de NO ajoutée permettant une mesure précise et quantitative de la concentration de NO (Figure 7 **Erreur ! Source du renvoi introuvable.**). Les sondes sont actuellement testées in vitro au laboratoire CITHEFOR (Université de Lorraine EA 3452).

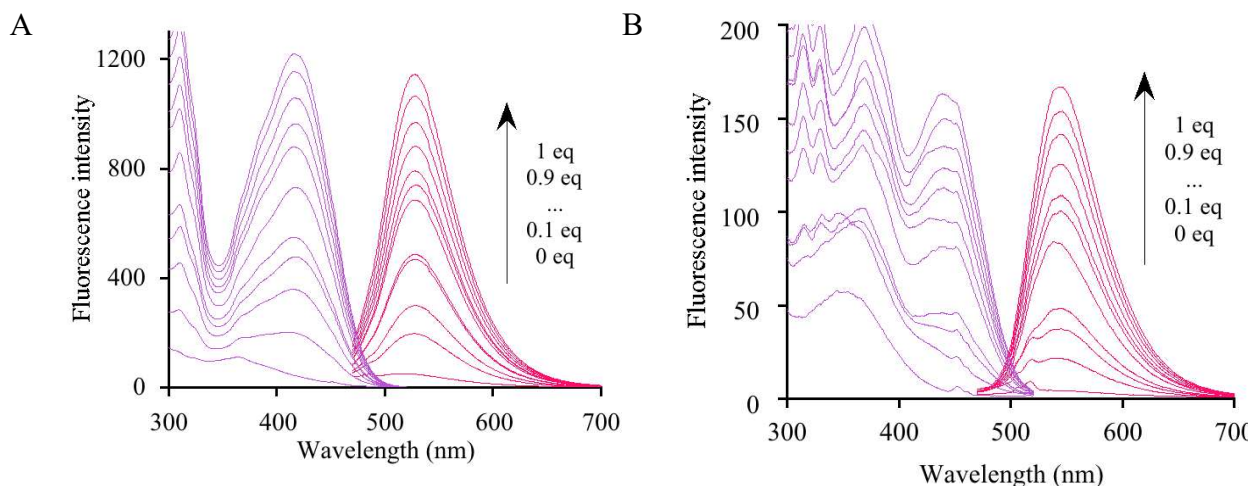


Figure 7: Spectre d'excitation (violet) et d'émission (rouge) de la sonde (A) hydrophile et (B) hydrophobe après addition d'une solution de NO. La sonde hydrophile a été solubilisée dans du tampon phosphate (50mM, pH 7.4) et la sonde hydrophobe a été solubilisée dans 80% tampon phosphate (50mM, pH 7.4) et 20% de DMSO. Les longueurs d'onde d'émission utilisées pour les spectres d'excitation étaient de 530 nm pour la sonde hydrophile et de 550 nm pour la sonde hydrophobe. La longueur d'onde d'excitation utilisée pour les spectres d'émission était de 416 nm pour la sonde hydrophile et de 440 nm pour la sonde hydrophobe.

Dans une deuxième partie, un autre outil moléculaire a été synthétisé afin d'étudier la NO synthase. L'introduction contrôlée de réactifs directement dans le microréacteur pourrait aider à suivre l'activité enzymatique et des informations sur le mécanisme de l'enzyme pourrait être obtenues. À cette fin, un outil moléculaire a été conçu pour contrôler avec précision le taux de production de NO par un processus de rétroaction. Nous avons émis l'hypothèse que la combinaison de la sonde BAPTA et de la sonde NO (BAPTA-NOp) pourrait induire une auto-activation de l'enzyme et pourrait contrôler la production d'oxyde nitrique. NO serait produit par l'enzyme et réagirait avec BAPTA-NOp pour donner BAPTA-AZO. En raison de la conjugaison plus élevée, le groupe cyano attracteur d'électrons attirerait les électrons de l'amine tertiaire du BAPTA, ce qui entraînerait une complexation plus faible du calcium et sa libération. Pour vérifier cette hypothèse, BAPTA-NOp et BAPTA-AZO ont été synthétisés en 10 étapes et leurs constantes de dissociation K_d ont été mesurées. Le K_d de BAPTA-NOp et de BAPTA-AZO étaient respectivement de 0,42 μM et 0,52 μM . Les valeurs des K_d étaient en accord avec les valeurs des K_d des BAPTA. Cependant, le K_d de BAPTA-NOp et BAPTA-AZO sont relativement proches et le K_d de BAPTA-AZO est relativement faible, ce qui signifie que la forme AZO ne libère pas de calcium et que la molécule ne peut être utilisée pour le processus de rétroaction.

Finalem^{ent}, afin d'assurer le contrôle de l'étape d'initiation et de déclencher une réaction enzymatique à un endroit et à un moment précis, la libération contrôlée de réactifs dans des microréacteurs a été étudiée. Les nanopolymersomes PEG₄₃-coumarine-*b*-PTMC₈₁ ont été encapsulés avec succès dans des microréacteurs composé d'émulsion d'eau stabilisés par des copolymères PEO_{1,3}-*b*-PBut_{2,5} et observés sous microscope confocal. L'irradiation à 405 nm a induit une déstabilisation efficace des nanopolymersomes à l'intérieur du microréacteur. Une irradiation de 2 min a induit une diminution de 83% du nombre de nanoparticules (Figure 8**Erreur ! Source du renvoi introuvable.**).

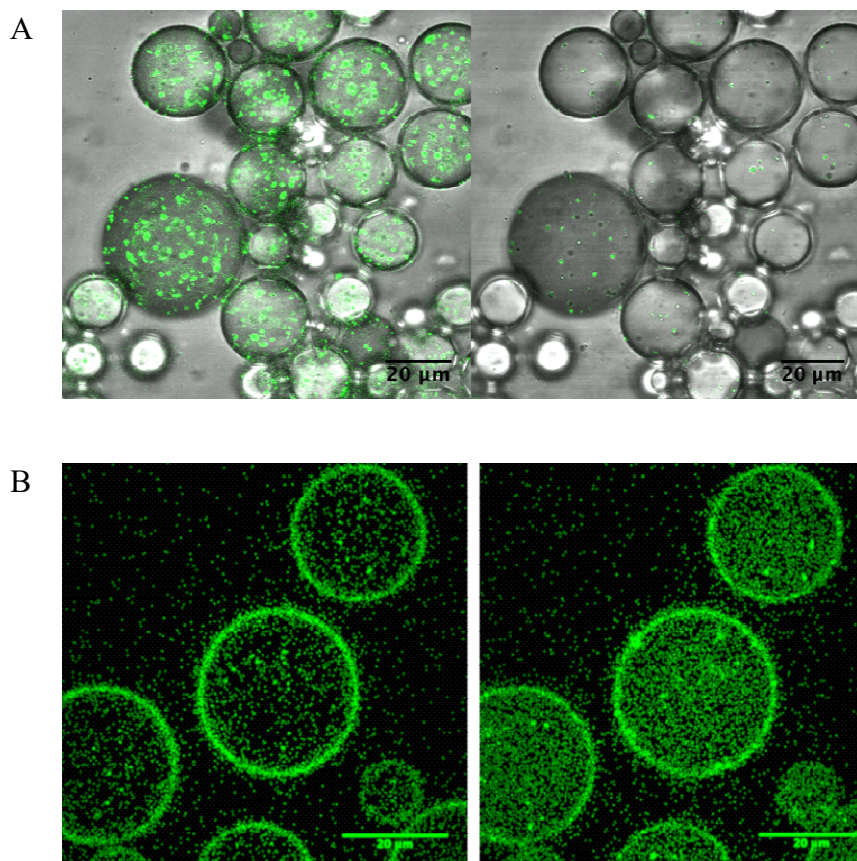


Figure 8: A) Observation en microscopie confocale d'une émulsion aqueuse stabilisée par $PEO_{1.3}$ - b - $PBut_{2.5}$ contenant des nanopolymersomes PEG_{43} -coumarin- b - $PTMC_{81}$ photosensibles irradiés 2 min à 405 nm (80%, 50 mW) (canal vert, λ_{ex} = 405 nm, 50 mW, 3% observation dans la gamme d'émission de la coumarine, 485 nm). B) Observation confocale d'une émulsion aqueuse stabilisée par $PEO_{1.3}$ - b - $PBut_{2.5}$ contenant des polymersomes PEG_{43} -coumarin- b - $PTMC_{81}$ avant et après une irradiation de 10 s à 405 nm (80%, 50 mW). La fluorescéine a été encapsulée dans les polymersomes (barre d'échelle 20 μ m, canal vert λ_{ex} = 488 nm, 40 mW, 10%, observation dans la gamme d'émission de la fluorescéine, 520 nm).

Afin d'étudier la libération des nanopolymersomes PEG_{43} -coumarine- b - $PTMC_{81}$, de la fluorescéine a été encapsulé dans les nanopolymersomes (F-Nano). Afin de mesurer la quantité de fluorescéine encapsulée dans les nanopolymersomes, 80% en volume de DMSO a été ajouté à une solution de particules pour déstabiliser complètement les nanopolymersomes et libérer la fluorescéine. La concentration maximale théorique de fluorescéine que les nanopolymersomes pouvaient libérer était de 5,1 μ M. Les F-Nano ont ensuite été encapsulés dans des gouttes d'émulsion stabilisées par du $PEO_{1.3}$ - b - $PBut_{2.5}$ formant ainsi un microreacteur. Les microreacteurs obtenus ont été irradiés pendant 10 s, entraînant la libération de la fluorescéine des F-Nano dans le microreacteur.

La construction de microréacteurs capables d'imiter certaines fonctions cellulaires de base et de développer une cellule synthétique opérationnelle représente l'un des projets les plus difficiles de ce siècle. Il reste encore un long chemin à parcourir pour obtenir une cellule artificielle polyvalente permettant de reproduire certaines fonctions biologiques ou d'étudier le fonctionnement d'enzymes complexes. Cependant, les outils développés dans le cadre de ce travail de thèse visaient à aider à se rapprocher un peu plus d'une cellule artificielle fonctionnelle. La NO synthase est une enzyme complexe qui nécessite plusieurs substrats et des conditions particulières. Dans un premier temps, les outils développés ici pourraient être utilisés pour construire des microréacteurs contrôlables contenant des enzymes bien connues telles que HRP ou GOX grâce à la microfluidique.

Les éléments fondamentaux à la base de la vie sont bien connus, mais nous sommes loin de comprendre comment ces éléments interagissent, s'auto-organisent, et échangent des informations. Les questions fondamentales concernant l'apparition de la vie pourront ainsi être posées par les échecs et les succès de la construction d'une cellule artificielle.